Molecular analysis of the *Axin1* and *Axin2* genes in hepatocellular carcinoma models

Matthew Zverev

PhD Thesis

Cardiff School of Biosciences

2023

Ysgoloriaethau Sgiliau Economi Gwybodaeth
Knowledge Economy Skills Scholarships

UNDEB EWROPEAIDD
EUROPEAN UNION

Llywodraeth Cymru
Welsh Government

Cronfa Gymdeithasol Ewrop
European Social Fund

Acknowledgments

Firstly, I would like to thank my supervisor Prof. Trevor Dale for all the guidance and support he has provided during the progress of this thesis. I would also like to thank KESS2 and Cellesce for funding my PhD project, without their support this research would not have been possible.

I am grateful for the invaluable technical support provided by numerous individuals, without whom the research presented here would not have been feasible. Specifically, I would like to express my appreciation to Derek Scarborough and Mark Isaac for their exceptional histological services and to Mark Bishop for his assistance with FACS.

I am also grateful to everyone who I have worked with at 3rd Floor East “Escalation Office” who have made it such a great environment to do my PhD in, especially the cheeky pint or two after work. In particular, I would like to thank current and past members of the Dale lab including: Eider Valle-Encinas for aiding in teaching me organoid culture and Carmen Velasco-Martinez for all her support during the crazy covid times. In particular, I would like to thank Anika Offergeld who not only taught me ES cell culture but despite no longer being a group member always had time to discuss the Axin project. I have been fortunate to supervise several great undergraduate students including Safiah Afifi, Aaron Handley, Loren Waters and Caitlin Alder.

On a more personal note, I would like to thank my friends and family for their support and encouragement since my move to Cardiff. Lastly, to Elisa, thank you for everything. Without you I’m not sure I would have got to the end of this endeavour.

Contents

Table of Contents

List of Figures

List of Tables

Abbreviations

Symbols

°C	Degrees Celsius
μg	Micrograms
μl	Microlitres
μm	Micrometres
μM	Micromolar

A

AFP	α-Fetoprotein
Ah	Aryl hydrocarbon
AhCreER^T	Aryl Hydrocarbon Cre recombinase Estrogen Receptor transgene
Alb	Albumin
APC	Adenomatous Polyposis Coli
Axin	Axis Inhibitor

B

BD	Bile duct
BEC	Biliary epithelial cells
BNF	β-naphthoflavone
bp	Base Pairs
BrdU	Bromodeoxyuridine (5-bromo-2'-deoxyuridine)
BSA	Bovine Serum Albumin

C

CCl4	Carbon tetrachloride
CDE	choline-deficient, ethionine- supplemented
cDNA	Complementary Deoxyribonucleic Acid
CHIR	CHIR99021 GSK-3 inhibitor
CIN	Chromosomal instability
c-Myc	Cellular Myelocytomatosis oncogene
CRC	Colorectal Cancer
Cre	Causes recombination
CreER^T	Cre eostrogen receptor fusion protein
CRISPR	Clustered regularly interspaced palindromic repeats
CT	Cycle time
CV	Central vein

D

DAB	3,3' diaminobenzidine
DAX	Double Axin deleted
DIX	Dishevelled and Axin domain
DM	Differentiation media
DMSO	Dimethyl sulfoxide
DNA	Deoxyribonucleic acid
DNase	Deoxyribonuclease
dNTP	Deoxynucelotid triphosphate
DR	Ductal reaction
DSB	Double strand break
Dvl	Dishevelled

E

ECL	Electro-chemoluminiscence
ECM	Extra cellular matrix
EGF	Epidermal growth factor
EM	Expansion media
EMT	Epithelial-mesenchymal transition
EtOH	Ethanol

F

FBS	Fetal bovine serum
FGF	Fibroblast growth factor
fl	Flox (allele containing loxp site)
FLP	Flippase
FRT	FLP recognition target
Fzd	Frizzled

G

gDNA	Genomic DNA

GEMMs	Genetically engineered mouse models
GFP	Green Fluorescent Protein
GI	Gastrointestinal
GS	Glutamine Synthetase
GSK-3	Glycogen synthetase kinase 3
H	
H&E	Haematoxylin and Eosin
HBV	Hepatitis B virus
HCC	Hepatocellular Carcinoma
HCV	Hepatitis C virus
HGF	Hepatocyte growth factor
HPC	Hepatic progenitor cell
HSC	Hepatic stellate cell
HSEC	Hepatic sinusoidal epithelial cell
I	
IF	Immunofluorescence
IHC	Immunohistochemistry
iPSCs	Induced pluripotent stem cells
ISCs	Intestinal stem cells
K	
Kb	Kilo base
Krt7	Cytokeratin 7
Krt8	Cytokeratin 8
Krt19	Cytokeratin 19
L	
LEF	Lymphoid enhancing factor
Lgr5	Leucin rich repeat containing G protein coupled receptor 5
loxp	Locus of crossover of bacteriophage P1
LRP	Lipoprotein Receptor-related Protein
LSECs	liver sinusoidal endothelial cells
M	
MAB	Monoclonal antibody
MCD	methionine and choline-deficient
mES cells	Mouse embryonic stem cells
Min	Multiple Intestinal Neoplasia
MMTV	Mouse Mammary Tumour Virus
mRNA	messenger RNA
N	
NASH	Non-alcoholic steatohepatitis
NAFLD	Non-alcoholic fatty liver disease
NGS	Normal goat serum
NRS	Normal rabbit serum
O	
O/N	Overnight
P	
PBS	Phosphate Buffered Saline
PCP	Planar cell polarity
PCR	Polymerase chain reaction
PDX	Patient derived xerograph
PH	Primary hepatocyte
PHx	Partial hepatectomy
PI	Propidium iodide
PS	Portal space
Q	
qPCR	Quantative PCR
R	

RGS	Regulator of G Protein signalling
RNA	Ribonucleic acid
Rnf43	Ring Finger 43
ROS	Reactive oxygen species
Rspo	R-spondin
RT	Room temperature
RT-qPCR	Reverse Transcription qPCR

S

SDS	Sodium Dodecyl Sulphate
sFRP	secreted Fzd-related proteins

T

TAA	Thioacetamide
Taq	DNA polymerase from Thermus aquaticus
TBS	Tris buffered saline
TBS/T	TBS with Tween20
TCF	T-cell factor

U

UV	Ultraviolet

V

V	Volts
VLDL	Very low-density lipoprotein

W

Wnt	Wingless type murine mammary tumour virus Integration site family
WT	Wild type
W/V	Weight per volume

X

x g	times gravity
X-gal	5-Bromo-4-Chloro-3-indolyl-β-D-Galactopyranoside

Z

Znrf3	Zinc and Ring Finger

Summary

Aberrant Wnt/β-catenin signalling is frequently implicated in hepatocellular carcinoma (HCC) pathogenesis. AXIN1, a key component of the β-catenin destruction complex, plays a critical role in regulating Wnt/β-catenin signalling. Mutations of *AXIN1* in HCC form a highly proliferative subset of tumours that are genomically unstable and clinically aggressive but lack a clear Wnt/β-catenin transcriptional signature.

A previous study in this lab showed that conditional deletion of *Axin1* in the liver led to the late onset emergence of HCC that shared many similarities to those observed in the human disease. One possible explanation for the lack of a clear strong Wnt/β-catenin signature is that the Axin1 homologue, Axin2, which is also a Wnt/β-Catenin transcriptional target, partially rescues Axin1 loss. Utilizing a floxed *Axin2* allele developed in this lab, this doctoral thesis aims to investigate the role of Axin1 and Axin2 using *in vivo* and *in vitro* liver models. The results in this thesis show that the loss of Axin2 exacerbated Axin1 dependent tumourigenesis. Surprisingly and by contrast with the loss of APC or mutation of β-catenin, combined acute loss of Axin1 and Axin2 did not activate hepatic Wnt/β-catenin signalling. Instead, additional deletion of Axin2 appeared to attenuate some of the effects of Axin1 deletion. This brought into question whether the Axin alleles used were truly null and led us to attempt to generate definitive Axin nulls in ES cells. Additionally, we used bile duct derived liver (BD) organoids to study the deletion of Axin *in vitro* to study specific cellular and molecular processes in a controlled environment in which deletion can be observed in real time. When grown in BD organoid differentiation conditions that promote hepatocyte and biliary differentiation, Axin deletion induced significant increases in Wnt/β-catenin signalling, particularly in double *Axin1* and *Axin2* deleted organoids. The data obtained from this study provides valuable insights into the context dependent functional significance of Axin1 and Axin2 function that has implication for using Axin regulators as therapeutic targets in HCC.

Chapter 1: Introduction

1.1 Hepatocellular Carcinoma

1.1.1 Etymology, surveillance, and therapeutic strategies

Hepatocellular carcinoma (HCC) accounts for 75-85% of liver cancers and imposes a considerable global health burden. It ranks sixth among the most common cancers and fourth in cancer-related mortality. HCC usually develops in the context of an underlying chronic liver disease. Most new cases are diagnosed in Eastern and South-eastern Asia, which is attributed to the high prevalence of chronic hepatitis B (HBV) and hepatitis C (HCV) infection. While liver cancer incidence is relatively lower in Europe and North America, there has been an increase in cases over the past decade due to an increase in lifestyle risk factors such as obesity, smoking, and alcoholic liver disease (Sung et al. 2021). HCC typically presents at an advanced stage with a poor prognosis. However, screening programs in high-risk populations can facilitate early detection of tumours, which are more amenable to curative therapies. In combination with ultrasound imaging, alpha-fetoprotein (AFP) is the most established and frequently used serological biomarker for surveillance of primary liver cancer however, AFP presents challenges in terms of sensitivity and specificity at different threshold levels (Trevisani et al. 2001). However, tracking changes in serum AFP levels over time, was able to correctly identify 74.3 % of patients with chronic liver disease who went on to develop HCC while also accurately recognising 72.9 % of patients with chronic liver disease who did not (Hughes et al. 2021).

Treatment options for HCC are based on the Barcelona Clinic Liver Cancer (BCLC) staging classification (Figure 1.1) and is used to classify HCC into five subclasses based on various factors such as tumour burden, underlying liver function, vascular invasion, or underlying comorbidities (Reig et al. 2022). Treatment success rates are significantly influenced by the stage at which the cancer is detected. Unfortunately, only a minority of patients are candidates for curative surgical treatment due to the asymptomatic nature of HCC and late diagnosis (Yang et al. 2019). Transarterial chemoembolization (TACE) is the primary treatment option for intermediate-stage liver cancer patients who are not suitable for surgery and has a median survival of around 30 months (Galle et al. 2018). In advanced cases of HCC,

conventional chemotherapy is generally ineffective, with response rates of less than 10% and median survival of 10 months (Deng et al. 2015). To better understand HCC prognosis, there has been a focus on identifying novel key targets by increasing our understanding of the genetic alterations and signalling pathways involved in hepatocarcinogenesis.

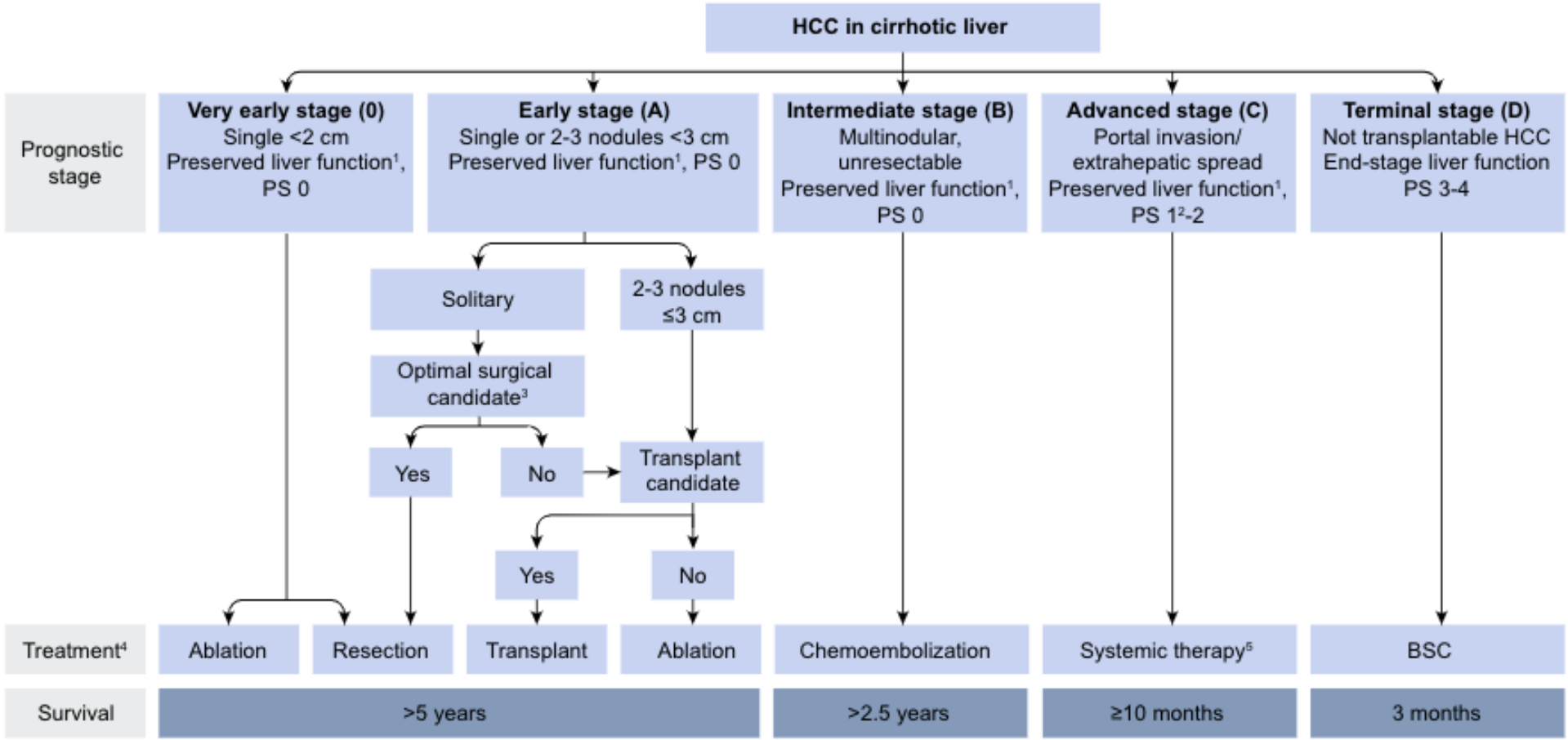

Figure 1.1 Modified BCLC staging and treatment strategy
The 5-stage classification system of BCLC determines the first-line treatment recommendation and prognosis. Median survival for each tumour stage is estimated based on available scientific evidence. BSC, best supportive care. Figure from (Galle et al. 2018)

1.1.2 HCC risk factors

A primary cause of altered liver function is excessive alcohol consumption. Chronic alcohol abuse can damage liver cells and causes changes to the immune system that results in chronic inflammation, leading to alcoholic liver disease. Initially, the liver may be able to repair itself, but over time, scar tissue can build up, leading to cirrhosis, creating an environment favouring HCC development. Alcohol consumption also promotes liver carcinogenesis through the formation of acetaldehyde and reactive oxygen species (ROS) (Ganne-Carrié and Nahon 2019).

Aflatoxin is a toxin produced by certain strains of the fungi Aspergillus, which can grow on seed crops. The ingestion of aflatoxin can result in a codon 249 mutation in the p53 tumour suppressor gene, making an individual more susceptible to developing HCC (Gouas et al. 2009).

Viral hepatitis infection leads to immune activation and an inflammatory response which causes cellular damage and death. The outcome of a viral infection, whether it becomes an acute or chronic disease, depends on various factors such as the strength of the immune response, the types of immune cells involved, and the virus's ability to evade the body's defences (Lefkowitch 2021). The long-term presence of the virus in liver cells causes several cycles of inflammation, injury, and healing, ultimately resulting in the formation of scar tissue or fibrosis which can eventually lead to HCC (Wong 2014).

Non-alcoholic fatty liver disease (NAFLD) is another condition that can cause altered liver function. This condition occurs when excess fat accumulates in the liver, causing inflammation and damage to liver cells. NAFLD is associated with obesity, type 2 diabetes, and high cholesterol levels. In its early stages, NAFLD may not cause any noticeable symptoms, but as the disease progresses, it can lead to liver damage, cirrhosis, and liver failure (Benedict and Zhang 2017).

1.1.3 Inflammation and HCC

Chronic inflammation stands out as a key element in the risk factors associated with HCC. The connection between cancer and chronic inflammation is evident in the development of various cancers, including liver, oesophageal, stomach, and colon cancers (Zhao et al. 2021). Inflammatory processes induce cell damage, creating a

cytokine-rich microenvironment that supports cell replication, angiogenesis, and tissue repair.

Hepatocarcinogenesis is intricately linked to chronic liver damage, with 80% - 90% prevalence of cirrhosis in HCC patients (Fattovich et al. 2004). The progression from mild to severe liver inflammation involves hepatic fibrosis, cirrhosis, and ultimately hepatocarcinogenesis. In response to signals from damaged hepatocytes, inflammatory cells (including macrophages, neutrophils, and lymphocytes) release pro-inflammatory cytokines such as Interleukin-1β (IL-1β), Interferon-gamma (IFN-γ), and Tumour Necrosis Factor α (TNFα), establishing a pro-inflammatory microenvironment that exacerbates hepatocellular damage (Wen et al. 2012).

Persistent infiltration of inflammatory cells, coupled with continuous parenchymal damage, triggers a wound-healing response leading to fibrosis. Hepatic stellate cells (HSC) transdifferentiate into myofibroblasts, expressing α-smooth muscle actin (α-SMA) and migrating to the site of liver injury (Jiang & Török 2013). Myofibroblasts contribute to fibrogenesis by producing extensive extracellular matrix (ECM) molecules, particularly collagen type I/III, driving capillarization of sinusoids—a feature in the pathogenesis of small HCC (Higashi et al. 2017; Kin et al. 1994).

The fibrotic liver microenvironment becomes enriched with ECM and pro-inflammatory factors. Notably, ECM proteins like fibronectin and vitronectin, binding hepatocyte growth factor, form complexes promoting endothelial cell migration and proliferation (Rahman et al. 2005). Simultaneously, the fibrotic ECM acts as a source of damage-associated molecular patterns (DAMPs), potent local pro-inflammatory factors that disrupt normal homeostatic signalling, amplifying liver inflammation, genotoxic stress, and replicative stress on hepatocytes (Frevert et al. 2018).

Oxidative stress, resulting from increased production of free radicals and peroxides, contributes to tissue damage, fibrogenesis and DNA damage. Toxic metabolites like acetaldehyde can bind to DNA, inducing genomic alterations. Inhibition of DNA-repair enzymes exacerbates these alterations, culminating in abnormal DNA accumulation and neoplastic transformation (Sadasivam et al. 2022). Cirrhosis, the most advanced stage of liver fibrosis, involves irreversible changes in tissue architecture, leading to reduced blood flow, tissue hypoxia, portal hypertension, and an increased risk of liver failure. The cirrhotic environment fosters the accumulation of genetic and epigenetic mutations, promoting dysplastic foci formation and eventual malignant transformation into HCC (Zanotti et al. 2022).

1.1.4 Aryl hydrocarbon receptor and its role in the immunology of HCC

The Aryl hydrocarbon receptor (AHR), belonging to the evolutionarily conserved Per-Arnt-Sim (PAS) superfamily and serving as a ligand-activated transcription factor, was initially known for its involvement in xenobiotic metabolism, regulating cellular responses to aromatic hydrocarbons. Upon ligand binding, AHR undergoes conformational changes, translocates to the nucleus, and forms a heterodimer with the AHR nuclear translocator (ARNT) (Haidar et al. 2021). This complex binds to specific DNA sequences called xenobiotic response elements (XREs), regulating the transcription of target genes in various biological processes (Denison et al. 2011). However, beyond xenobiotic metabolism, recent evidence emphasizes AHR's substantial role in immune system regulation. Studies indicate AHR's impact on immune cell development, differentiation, and function, with expression observed in T cells, B cells, dendritic cells, and macrophages (Stockinger et al. 2014).

AHR activation has been linked to the differentiation of regulatory T cells (Tregs), fostering an anti-inflammatory environment, and maintaining immune homeostasis. Additionally, AHR signalling influences macrophage polarization, determining their pro-inflammatory or anti-inflammatory profiles in response to environmental cues (Quintana et al. 2008). Research demonstrates that treating wild-type mice with the high-affinity ligand TCDD (dioxin) induces liver inflammation and fibrosis (Lamb et al., 2016). In the context of AHR-dependent immune regulation in the liver, a noteworthy observation is the constitutive production of tolerogenic AHR ligands, specifically kynurenines, by the hepatocyte-specific enzyme tryptophan-2,3-dioxygenase (TDO2) within the liver (Stone et al. 2013). Activation of AHR by kynurenines induces immunosuppression in both T cells and antigen-presenting cells (APCs) (Quintana et al. 2008). Additionally, in response to lipopolysaccharide (LPS) challenge, the induction of kynurenine-producing indoleamine 2,3-dioxygenase 1 (IDO1) in hepatic stellate cells (HSCs) leads to enhanced AHR signalling in thymus-derived natural Tregs. This, in turn, induces the upregulation of Foxp3, epigenetic stabilization, expansion, and an enhanced suppressive capacity (Kumar et al. 2017). These endogenous AHR ligands strongly contribute to tumour immune escape. Elevated AHR expression, along with increased kynurenine production, results in sustained AHR activation, perpetuating a pro-tumorigenic immunosuppressive microenvironment.

1.1.5 Mutational landscape of HCC

Cancer has long been established as a multistep process in which various functional capabilities are acquired by the cancer cells at different stages of tumour pathogenesis. These capabilities are the result of accumulated genetic and epigenetic defects in the cells (Hanahan 2022). Genomic analysis has played a crucial role in identifying the main drivers responsible for the initiation and progression of HCC. In HCC the multi-step pathophysiological process, involves various factors working together to inflict cellular harm, causing chronic liver inflammation, necrosis, and anomalous hepatocyte regeneration. These factors collectively contribute to the formation of cirrhosis, which advances to dysplastic nodules, early HCC, and eventually advanced HCC (West et al. 2017; Villanueva 2019).

TERT promotor mutations have been found to be the earliest and the most common changes driving the transformation of premalignant lesions into HCC (Nault et al. 2014). HBV DNA can integrate into various regions of the host genome, and it has been found that in between 50-85% of HCC cases associated with chronic HBV infection, the virus integrates into the promoter region of the TERT gene leading to the overexpression of TERT (Péneau et al. 2022).

Driver mutations are also commonly found in genes regulating cell cycle control and in the Wnt/β-catenin signalling pathway (Table 1.1). Disruptions to the p53/cell cycle signalling pathway occur in over 50% of cases. Tumours with TP53 mutations are typically associated with more aggressive HCC subtypes, often characterized by HBV infection and genomic instability (Campani et al. 2023). The Wnt/β-catenin pathway is among the most activated oncogenic pathways in HCC. The most common changes are mutation of CTNNB1 in exon 3 (11-37%) or inactivation of AXIN1 (5-15%; Table 1.1). These mutations are usually found in a mutually exclusive manner (Zucman-Rossi et al. 2007). Several studies (Lee et al. 2006; Boyault et al. 2007; Chiang et al. 2008; Hoshida et al. 2009; Abitbol et al. 2018) places CTNNB1 and AXIN1 mutant HCCs into two distinct classes; non-proliferative and proliferative respectively (Figure 1.2). The non-proliferative classification of HCC is associated with better histological differentiation, lower levels of AFP, chromosomal stability and a less aggressive phenotype that relates to an improved clinical outcome. Conversely, the proliferative class of HCC relates to poor cell differentiation, chromosomal instability, more aggressive tumours, high levels of serum AFP and a poorer clinical outcome.

HCC tumours show high degrees of genomic instability, resulting in recurrent chromosomal abnormalities and gene fusions (Katoh et al. 2006). Chromosomal instability (CIN) has been found to be prevalent in HCC, facilitating tumour heterogeneity, drug resistance, immune system evasion, and ultimately promoting HCC progression.

Pathway(s)	Gene(s)	Alteration	Frequency in HCC
Telomere maintenance	*TERT*	Promoter mutation	54–60%
		Amplification	5–6%
Cell cycle control	*TP53*	Mutation or deletion	12–48%
	RB1	Mutation or deletion	3–8%
	CCND1	Amplification	7%
	CDKN2A	Mutation or deletion	2–12%
WNT–β-catenin signalling	*CTNNB1*	Mutation	11–37%
	AXIN1	Mutation or deletion	5–15%
Oxidative stress	*NFE2L2*	Mutation	3–6%
	KEAP1	Mutation	2–8%
Epigenetic and chromatin remodelling	*ARID1A*	Mutation or deletion	4–7%
	ARID2	Mutation	3–18%
	KMT2A (*MLL1*), *KMT2B* (*MLL4*), *KMT2C* (*MLL3*) and *KMT2D* (*MLL2*)	Mutation	2–6%
AKT–mTOR–MAPK signalling	*RPS6KA3*	Mutation	2–9%
	TSC1 and *TSC2*	Mutation or deletion	3–8%
	PTEN	Mutation or deletion	1–3%
	FGF3, *FGF4* and *FGF19*	Amplification	4–6%
	PI3KCA	Mutation	0–2%
Angiogenesis	*VEGFA*	Amplification	3–7%

Table 1.1 Molecular aberrations most commonly found in HCC
Table from (Llovet et al. 2016)

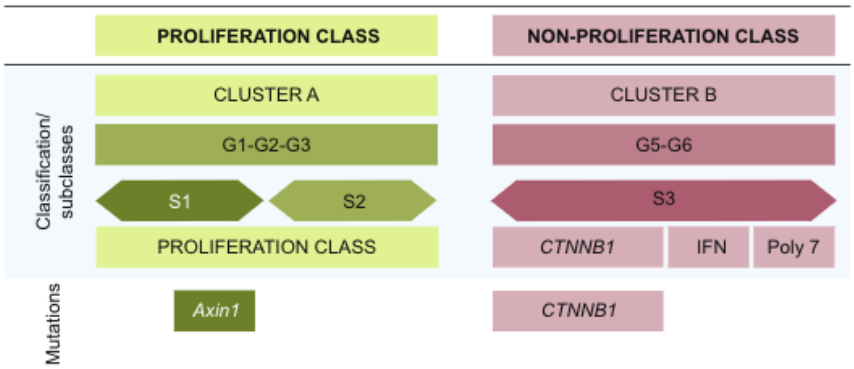

Figure 1.2 Summary of HCC classification
Summary of studies placing HCC into 2 distinct classes with AXIN1 and CTNNB1 mutations being found to be in the separate classes. Modified from (Abitbol et al. 2018)

1.2 Wnt pathway

The Wnt signalling pathway is highly conserved across species, from invertebrates to mammals and is involved in regulating various cellular processes, including development, growth, differentiation, and maintenance in many tissues (Wiese et al. 2018). The systems that Wnt signalling regulates during development include gastrulation and mesoderm formation, establishment of the primary body axis, neural tube formation, limb development, organogenesis, and placenta formation (Knöfler et al. 2019; Royle et al. 2021; Rim et al. 2022). In the adult, Wnt signalling is involved in the maintenance of multiple tissues, particularly where tissues maintain a stem cell population where the local activation of Wnt signalling is a key feature of stem cell niches. This including skin and hair follicles, the skeletal, nervous, cardiovascular, immune, and digestive systems (Rosso and Inestrosa 2013; Steinhart and Angers 2018; Haseeb et al. 2019). This has been best studied in the intestine where the proliferation and multipotency of intestinal epithelial stem cells depend on the maintenance and regulation of Wnt pathway activity (Krausova and Korinek 2014).

The importance of the Wnt pathway is demonstrated by the fact that mutations or dysregulation of Wnt pathway components can lead to developmental defects, cancer and other diseases in humans and other animals (Nusse and Clevers 2017). In normal liver cells, the Wnt pathway is tightly regulated (Russell and Monga 2018), but in HCC, dysregulation of this pathway can lead to uncontrolled cell growth and proliferation. The Wnt signalling pathway can be broadly categorized into β-catenin-dependent (canonical) and β-catenin-independent (non-canonical) pathways. The non-canonical pathway is further divided into planar cell polarity (PCP) and the Wnt/Ca2+ pathways. The best studied is the Wnt/β-catenin pathway.

1.2.1 Wnt/β-catenin signalling

The Wnt pathway is named after Wnt ligand proteins that are a family of secreted cysteine-rich glycoprotein ligands. There are 19 human Wnt genes. Wnts are secreted through a pathway that involves lipid modification and secretion by proteins including Porcupine (PORCN), a transmembrane O-acyltransferase that palmitoylates Wnt and Wntless, a protein that regulates Wnt secretion (Mikels and Nusse 2006). Following secretion, Wnt ligands bind to a range of transmembrane receptors (van

Amerongen 2012). In the case of canonical Wnt/β-catenin signalling, the key receptors include 7-transmembrane Frizzled (Fzd) receptors and lipoprotein receptor-related protein (LRP) 5/6 co-receptors (Agostino and Pohl 2020). The Wnt/Fzd/LRP receptor complex activates intracellular signalling to control levels of the pathway's primary effector β-catenin via the action of the β-catenin destruction complex.

In the absence of Wnt ligands, a β-catenin destruction complex is formed (Figure 1.3A). Axin1 and adenomatous polyposis coli (APC) bind the kinases glycogen synthase kinase 3 (GSK3) and casein kinase 1α (CK1α). CK1α phosphorylates Ser45 in β-catenin after which GSK3 adds phosphate groups to Thr41, Ser37 and Ser33 (Stamos and Weis 2013). The ubiquitin ligase β-TrCP binds to the phosphorylated β-catenin, inducing ubiquitination which targets β-catenin for proteasomal degradation. The pathway is activated when Wnt proteins bind to lipoprotein receptor-related protein (LRP5/6) and Fzd receptors on the plasma membrane. The Wnt/Frizzled/LRP complex recruits the protein Dishevelled (Dsh) which in turn binds to and recruits Axin to the cell membrane. GSK-3 at the cell membrane (likely GSK-3 that is directly associated with Axin) phosphorylates the intracellular tail of Lrp6 forming a phosphorylated sequence that strongly inhibits GSK-3 catalytic activity by competitive inhibition (Gammons et al. 2016; Liu et al. 2022). As a result of receptor recruitment, Dishevelled binding and GSK-3 inhibition, β-catenin turnover by the Axin-associated destruction complex is prevented. This allows β-catenin levels to accumulate in the cytoplasm and translocate to the nucleus where it acts as a transcriptional activator in a complex with members of the TCF family of DNA binding proteins (Nusse and Clevers 2017).

There are multiple mechanisms whereby Wnt signalling can be modulated (Liu et al. 2022). Of particular relevance to liver biology and later experiments in this report, R-spondin ligands have been shown to enhance Wnt/β-catenin signalling by modulating cell surface levels of the Fzd receptor (ter Steege and Bakker 2021). R-spondin binds Lgr5/6 receptors and to inhibit the action of Rnf43 and Znrf3, two transmembrane E3 ligases that would otherwise function to eliminate Wnt receptors from the cell surface (Figure 1.3B). The net outcome of Rspo1/Rspo2 binding is an increase in Fzd receptors and stronger responses to endogenous Wnt ligands (de Lau et al. 2014).

The Wnt pathway plays a critical role in regulating the balance between proliferation and differentiation and deregulation of the Wnt signalling pathway can have significant consequences for homeostasis and has been linked to various

diseases. Aberrant activation or inhibition of Wnt/β-catenin signalling, impacting proliferation, repair, survival and differentiation has been linked to heart diseases such as atherosclerosis and cardiac fibrosis, lung diseases such as chronic obstructive pulmonary disease and idiopathic pulmonary fibrosis, nervous system disease such as Parkinson's and Alzheimer's, osteoporosis and osteogenesis dysregulation, and liver disease such as liver fibrosis and cholestasis (Liu et al. 2022). Dysregulation of components of the Wnt/β-catenin pathway has also been implicated in cancer.

A

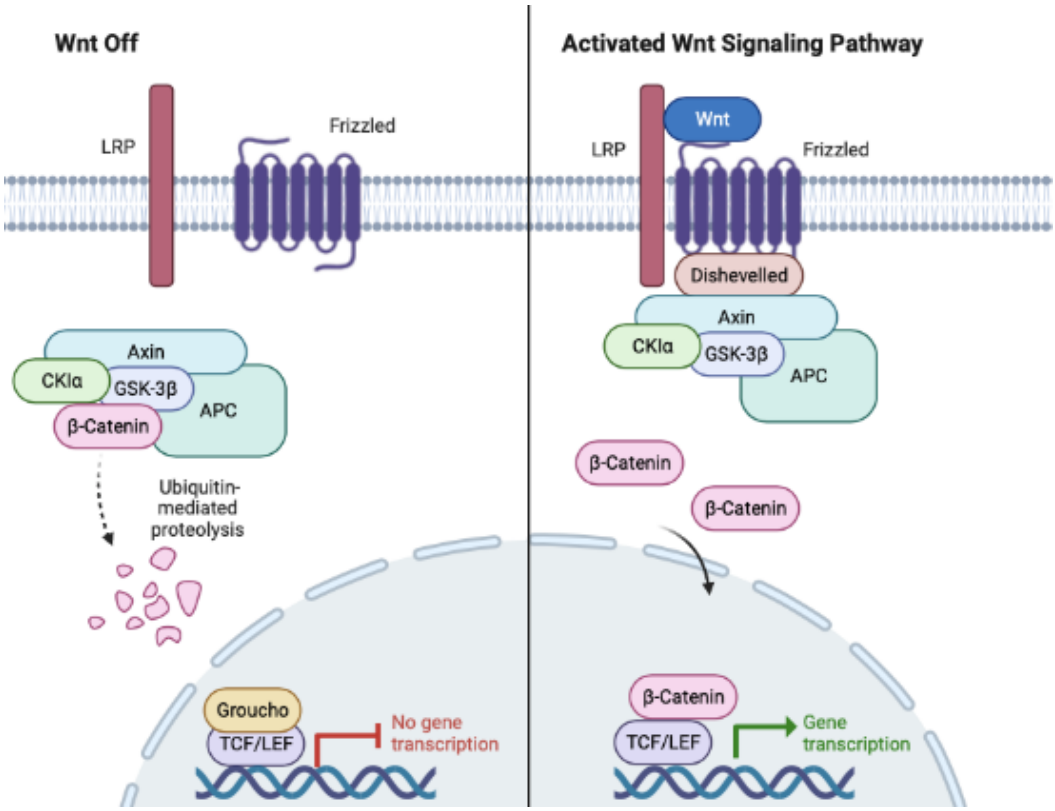

B

Figure 1.3 Wnt/β-catenin signalling.
(A) In the Wnt off state a complex containing Axin, APC, CK1 and GSK3 phosphorylates β-catenin, resulting in its ubitiquination by β-TrCP, marking it for proteasomal degradation. In the presence of Wnt ligand, the receptor complex of Frizzled and LRP5/6 recruits Axin and other parts of the destruction complex, disrupting the degradation of β-catenin allowing it to accumulate and serve as an activator of TCF dependent transcription of Wnt target genes. Image created using Biorender. **(B)** Cell surface interactions between R-spondins and LGR5 family members potentiate Wnt signalling. Transmembrane molecules ZNRF3 and RNF43 negatively regulate Wnt signalling by inducing turnover of FZD molecules through their E3 ubiquitin ligase activity. R-spondin binding to ZNRF3 is believed to diminish its activity, increasing Wnt signalling by increasing the availability of FZD receptors. Figure adapted from (Zhong and Virshup 2020).

1.2.2 Dysregulation of the Wnt pathway in cancer

Dysregulation of the Wnt pathway is a common occurrence in various cancer types. Several mechanisms of dysregulation have been identified, including mutations in the pathway's components, aberrant expression of ligands, alterations in receptor expression, dysregulation of Wnt antagonists, and changes in crosstalk with other signalling pathways (Bugter et al. 2021; Parsons et al. 2021). The most common integrating consequence in dysregulation is the de-repression of Wnt/β-catenin signalling. However, there is some data to suggest that other branches of the pathway can drive tumourigenesis (Nusse and Clevers 2017). Dysregulation of Wnt/β-catenin signalling in cancer spans components that function at the cell surface through to nuclear transcription factors (Liu et al. 2022).

One of the earliest components found to be mis-regulated was the overexpression of Wnt1 (Int-1) following integration of the Mouse Mammary Tumour Virus (MMTV) which induced breast cancer (Nusse and Varmus 1982). Mutations in genes encoding Fzds are rare in tumours however hypermethylation of Fzd genes in various types of cancer including acute myeloid leukaemia, breast cancer, glioblastoma multiforme and ovarian cancer have been reported (Sun et al. 2021). Overexpression of Lrp6 has been identified in multiple cancer types, including breast cancer (Ma et al. 2017). *RNF43* truncating mutations have been found to interfere with β-catenin turnover by selectively trapping CK1 and AXIN1 at the plasma membrane, driving oncogenic β-catenin mediated transcription despite Wnt receptor downregulation (Spit et al. 2020).

Mutations of the 'gatekeeper' tumour suppressor gene *APC*, particularly in familial colorectal cancer (CRC) predisposition syndromes such as familial adenomatous polyposis (FAP) has long been established as a vital initial stage in the development of colorectal cancer (Kinzler and Vogelstein 1996). Early studies showed that mutations in *APC* in colorectal cancers activated Wnt signalling (Morin et al. 1997). Activating mutations of *CTNNB1* are less common in CRC (Yaeger et al. 2018) however, as stated earlier, they were found in 11-37 % of HCC, and were found to be highly prevalent in endometroid endometrial carcinoma (Liu et al. 2014). Interestingly, in the mouse liver, overexpression of β-catenin alone did not induce tumourigenesis (Harada et al. 2002). However, later studies showed that combinations of β-catenin activation with coactivation of Akt, Yap1 or Myc were able to do so (Stauffer et al. 2011;

Tao et al. 2014; Bisso et al. 2020). Deletions of *AXIN1* are a common genetic alteration in a subset of medulloblastomas (Dahmen et al. 2001) and nonsense *AXIN2* mutations have been shown to cause oligodontia and a predisposition to CRC (Lammi et al. 2004).

Mutations of Transcription factor 7-like 2 (*TCF7L2*), a member of the TCF family, have been observed in a range of different tumour types, including colon, breast, lung, and prostate cancer (Zhang et al. 2018). TCF7L2 has been shown to act as a tumour suppressor in some contexts, while promoting tumour growth in others. Findings in a study by (Wenzel et al. 2020) suggested that TCF7L2 played a role in suppressing the migration and invasion of colorectal cancer cells. The precise reasons why different mutations of components in the WNT pathway exhibit specificity for particular tissues is unclear.

The aberrant activation of the Wnt/β-catenin signalling pathway in cancer is a common theme that is often associated with the acquisition of a stem cell-like fate. The capacity of differentiated cells to induce cancerous changes once they regain stem cell characteristics is recognised as an established hallmark of cancer (Hanahan 2022). The intestinal epithelium is one of the most studied systems in which the role of Wnt/β-catenin signalling in cancer and stem cell biology has been extensively investigated (Ramadan et al. 2022). The prevailing belief is that tumour initiation is often caused by mutations that occur in long-lived intestinal stem cells (ISCs) (Barker et al. 2009). Non-canonical WNT/PCP signalling in cancer is less well studied but is increasingly being shown to be important (Corda and Sala 2017). Mutations of *Axin1* and *β-catenin* in HCC have been assumed to be linked to Wnt pathway deregulation. However, Axin function has been linked to cellular processes and signalling that extends beyond classical Wnt/β-catenin signalling.

1.2.3 Axin, interaction partners and modulation.

Axin was initially identified as a negative regulator of Wnt signalling during the characterization of the mouse Fused locus (Zeng et al. 1997). Mutant alleles of this locus resulted in embryonic lethality and axis duplication. Axin-like, Axil (later Axin2 or Conductin) an Axin1 homolog, was discovered in yeast two-hybrid experiments (Yamamoto et al. 1998). Axin1 has two isoforms, Axin1 isoform-a and the shorter Axin1 isoform-b due to exon 8 being alternatively spliced (Zeng et al. 1997), and likewise, Axin2 also has two isoforms resulting from exon 6 being alternatively spliced (Li et al.

2015). Both Axins contain multiple functional domains (Figure 1.4A). These include the tankyrase binding motif, the conserved N-terminal RGS domain that binds APC, GSK3β and β-catenin binding motifs, and the C-terminal DIX domain which mediates homomeric complex formation, as well as binding to other DIX domain-containing proteins, most notably proteins of the dishevelled family (Morrone et al. 2012; Pronobis et al. 2015; Yamanishi et al. 2019). The DIX domain of Axin has been shown to be important in mediating β-catenin degradation as specific point mutations interfere with Axin oligomerisation, which is key to an effective destruction complex (Fiedler et al. 2011).

In vivo studies, in which an Axin2 cDNA was inserted into the Axin1 locus, showed that both Axins are functionally equivalent and act to inhibit Wnt signalling by acting as a scaffolding protein in the formation of the β-catenin destruction complex (Chia and Costantini 2005). A crucial difference is that Axin1 is constitutively and ubiquitously expressed, whereas the Axin2 promoter contains binding sites for TCF-factors and is a Wnt/β-catenin pathway target. Axin2 is thought to act in a negative feedback loop to modulate Wnt/β-catenin pathway activity in a tissue specific and developmental manner (Lustig et al. 2002a). In the study by Bernkopf (Bernkopf et al. 2015), suggests that the DIX domain of Axin2 results in less efficient binding with Dvl2, thus allowing it to remain active in the destruction complex despite upstream inhibition signals. The differences in Axin1 versus Axin2 gene expression may explain why Axin1 knockout results in embryonic lethality at e9.5, while mice carrying the homozygous ConductinlacZ allele (also known as Axin2lacZ or Axin2tm1Wbm), which is presumed to be null, only show mild skull abnormalities (Yu et al. 2005).

Axin2 has been shown to be regulated at the transcriptional level with three alternative 5′-untranslated regions (UTRs). The 5′-UTRs influence the amount of Axin2 protein expressed within different cell types (Hughes and Brady 2005). Stability of AXIN have been shown to be modulated by tankyrase, a poly(ADP-ribose) polymerase (Callow et al. 2011). AXIN is bound and subjected to PARylation by tankyrase, which in turn, triggers the activation of the PAR-dependent E3 ubiquitin ligase RNF146, which ubiquitylates AXIN, tankyrase, and itself. As a result, the whole complex is marked for degradation by the proteasome.

The Wnt/β-catenin destruction complex is beginning to be considered as a biomolecular condensate (Schaefer and Peifer 2019). Recently it has been shown that Axin undergoes phase separation (Nong et al. 2021). Mediated by Axin's ability to form

homo-oligomers via the DIX domain (Faux et al. 2008), the condensates that form through phase separation of Axin are thought to facilitate the rapid and efficient assembly of the Wnt/β-catenin destruction complex by concentrating the component proteins and promoting their interactions. AXIN has been thought to be the concentration limiting component of the β-catenin destruction complex (Lee et al. 2003). However, more recent data suggests that levels of Axin may be expressed at similar to that of APC (Kitazawa et al. 2017; Schaefer et al. 2018).

As a scaffolding protein, Axin has been found to interact with proteins in diverse signalling pathways other than Wnt/β-catenin including TGF-β signalling, JNK signalling and Hippo pathway (Figure 1.4B). The NCBI website notes 183 interacting partners for Axin1 and 74 for Axin2.

The TGF-β signalling pathway plays a crucial role in regulating many aspects of cellular behaviour, including cell growth, proliferation, differentiation, and apoptosis. Axin regulates the effects of Smad3 by enhancing TGF-β-receptor-mediated activation (Furuhashi et al. 2001). However, in the absence of TGF-β stimulation, Smad3 has the ability to associate with Axin and glycogen synthase kinase (GSK)-3β, forming a complex. This complex induces the phosphorylation of Smad3 by GSK-3β, leading to Smad3's degradation (Guo et al. 2008). Additionally, Axin has been shown to facilitate the assembly of a complex consisting of Smad7 and the E3 ubiquitin ligase RNF111 (Arkadia), which leads to the degradation of Smad7 (Liu et al. 2006). This suggests that Axin's role in TGF-β signalling may be pleiotropic and context dependant.

MEKK1 and MEKK4 competitively bind with distinct regions of Axin1 to induce JNK activation, which is critical for apoptotic signalling (Luo et al. 2003). In a study by (Rui et al. 2002), JNK activation via Axin required sumoylation at the C-terminal. Using an immunokinase assay and deletions of the Axin C-terminal transfected into 293T cells, showed that the removal of these sites greatly reduced Axin's ability to activate JNK but had no effect on Wnt signalling. This suggests that Axin can work independently in both pathways.

Hippo signalling is involved in regulating cell growth and differentiation. YAP, a transcriptional co-activator, plays a crucial role in the Hippo signalling pathway and has been suggested to interact with Axin, and recruits the E3 ubiquitin ligase β-TrCP to the β-catenin destruction complex (Azzolin et al. 2014). In the study by (Abitbol et al. 2018), AXIN1/Axin1 mutant HCC in humans and mouse models were highly enriched with an oncogenic Yap and Notch signature.

The formation of a complex comprising AXIN, AMPK, and LKB1 has been suggested to lead to the activation of AMPK, a critical sensor of the cellular-energy status that is involved in protecting cells against stress induced by low nutrient levels (Zhang et al. 2013). Axin has also been found to interact with HIPK2, (homeodomain-interacting protein kinase-2), facilitating phosphorylation of the tumour suppressor protein p53, which in turn promotes transcription of target genes that are essential for maintaining genomic stability and preventing cancer development (Rui et al. 2004). This interaction was also found to be vital for the induction of apoptosis following DNA damage (Li et al. 2009). Specifically, Axin has been shown to bind to Pirh2, a ubiquitin ligase that regulates the stability of multiple proteins involved in DNA damage response, as well as histone acetyltransferases Tip60 and p300, that regulate gene expression in response to DNA damage. These interactions suggest that Axin may play a broader role in the regulation of DNA damage response pathways beyond its well-characterized role in Wnt signalling.

Axin and APC2 have also been demonstrated to play a crucial role in maintaining mitotic fidelity (Poulton et al. 2013). Both proteins are required for proper chromosomal separation during cell division, as well as for fine-tuning cytoskeletal rearrangements. The loss of either protein can lead to an increased frequency of chromosome segregation errors and ultimately, genomic instability. A dominant-negative form of Axin1 as well as siRNA knockdown of Axin1 was able to trigger macropynocytosis (a type of endocytosis) in the absence of Wnt ligand in cultured cells thus promoting increased nutrient uptake (Tejeda-Muñoz et al. 2019).

Axin is a highly versatile scaffolding protein that interacts with multiple proteins and signalling pathways, highlighting its potential importance in facilitating signal integration and crosstalk. These interactions suggest that Axin plays a central role in coordinating cellular responses to a variety of stimuli, including those involved in development, as well as those that maintain cellular homeostasis throughout life. This is underscored by the phenotypes associated with Axin loss of function, which include defects in development, and mitotic fidelity. Furthermore, Axin polymorphisms have been associated with osteoporosis (Cui et al. 2022) and congenital heart disease (Crauciuc et al. 2020). For Axin's role in HCC to be better understood and exploited for therapeutic benefit, the contribution of its various functions will need to be better understood in the liver.

A

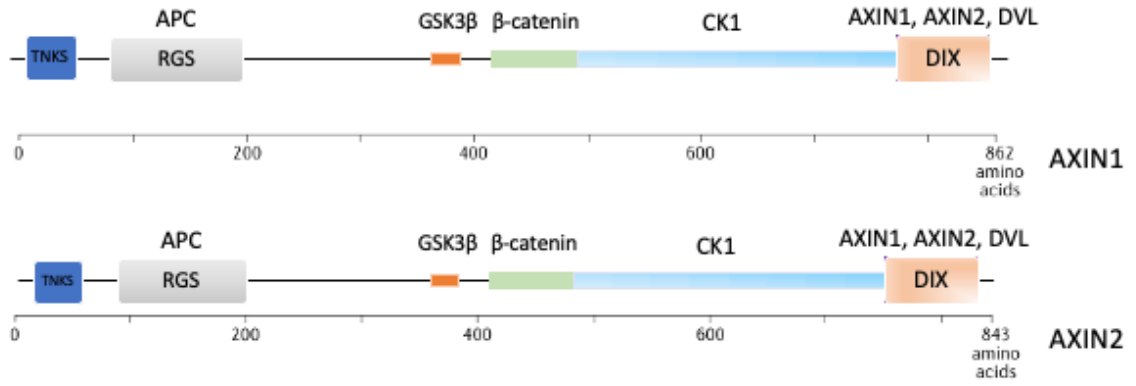

B

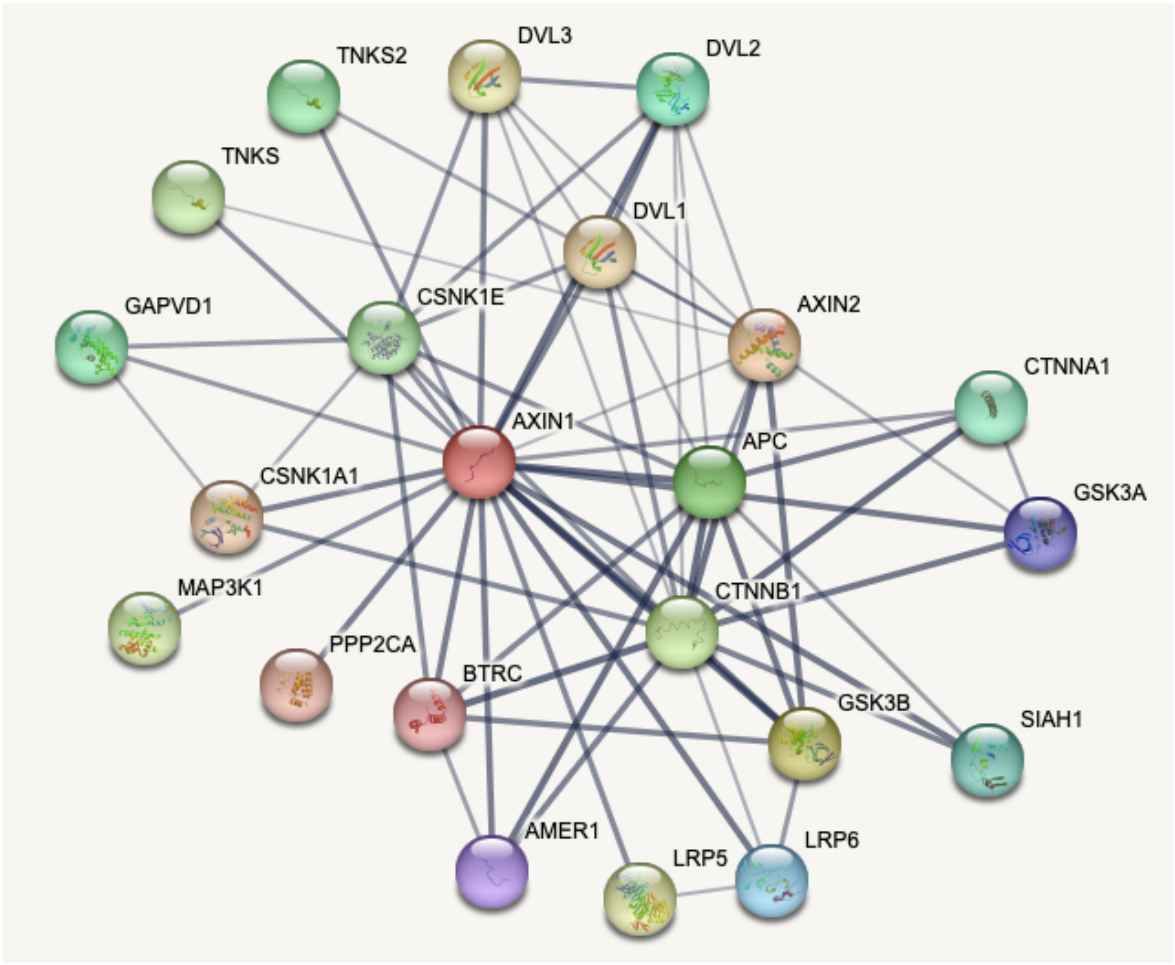

Figure 1.4 Axin functional domains and interaction partners
(A) Schematic representation of Axin1 (top) and Axin2 (bottom) proteins and the location of their major binding regions; RGS domain, DIX domain and TNKS, GSK3, β-Catenin and CK1 binding regions. Adapted from (Bugter et al. 2021). **(B)** Top 20 protein interaction partners of Axin1 and Axin2 created using string-db.org based on a confidence score of the interaction to be true.

1.3 The Wnt pathway in liver homeostasis

1.3.1 Anatomy and function of the liver

The liver is a major organ with diverse functions, playing a central role in nutrient and vitamin metabolism, while also detoxifying and eliminating toxins and drugs. The liver synthesizes biologically important proteins, including those involved in blood clotting, and produces bile for lipid digestion and absorption. Additionally, the liver contributes to immune function through its Kupffer cells.

Accounting for 3-5% of body mass, the liver is subdivided into two main (left and right) and two accessory (caudate and quadrate) lobes. Blood supply is delivered by the portal vein and hepatic artery meaning that the liver receives a unique mix of oxygen and nutrient-rich blood. This blood flow is directed through a network of heavily fenestrated hepatic sinusoidal endothelial cells (HSECs) that line the hepatocytes, ensuring efficient delivery of oxygen and nutrients to the liver cells. The blood is directed to the central vein (CV), which serves as the draining point for the liver's lobules. The luminal side of the sinusoids contains the liver's macrophages (the Kupffer cells). Hepatic stellate cells (HSCs) occupy the space of Disse, situated between the HSECs and the hepatocytes. Bile produced by hepatocytes is secreted into bile canaliculi, which are the spaces between hepatocytes formed by tight junctions. From there, bile enters intrahepatic bile ducts formed by cholangiocytes (ductal cells or biliary epithelial cells), flows into the extrahepatic bile ducts, and finally empties into the duodenum (Trefts et al. 2017).

The hepatic lobule is a functional unit of the liver, consisting of a hexagonal-shaped structure with portal tracts at the corners and the central vein at the centre. The portal tracts contain the branches of the hepatic artery, portal vein, and bile duct and known as the portal triad (Figure 1.5A). Hepatocytes make up around 60% of the liver cell composition and are the functional cells of the liver, are arranged in plates radiating outward from the central vein (Ben-Moshe and Itzkovitz 2019). Their functions or metabolic activities are not uniform but rather exhibit a gradient of specialization from the portal triad to the central vein (Figure 1.5B). The pericentral or zone 3 surrounds the central vein and has a lower oxygen tension, which results in decreased oxidative metabolism and increased reliance on glycolysis. The periportal or zone 1, located adjacent to the portal triad, has a higher oxygen tension and is responsible for gluconeogenesis, glycogen synthesis, and urea production. This zone also contains a

higher density of bile canaliculi for bile secretion. The intermediate zone between the periportal and pericentral regions (zone 2) contains a mixture of the functions of the other two zones. Lobular blood flow patterns may be responsible for at least part of this zonation however, the Wnt/β-catenin pathway has also been shown to play a crucial role.

In the steady-state liver, pericentral hepatocytes exhibit co-expression of Lgr5 and Axin2 (Planas-Paz et al. 2016). Numerous stem cells found in tissues, such as the intestine (intestinal stem cells; ISCs), express Lgr5 and Axin2 and rely on Wnt/β-catenin signalling for maintaining homeostasis and during proliferation following damage (Barker et al. 2007). In the study by (Wang et al. 2015), lineage tracing of Axin2 positive cells suggested they have the potential to replenish all hepatocytes across the liver lobule during normal renewal, flowing from the central to the portal vein. The use of TertCreERT2/+ mice with a Rosa26LSL-Tomato/+ reporter to trace telomerase expressing hepatocytes in the study by Lin et al (Lin et al. 2018) showed these cells as the source of new hepatocytes, producing distributed clonal clusters. The size of these clusters was disputed by using a Rosa26-Rainbow Cre reporter allele and lineage-tracing strategy in the study by Chen et al (Chen et al. 2020) which showed much smaller clusters. More recent studies using Axin2 lineage tracing point to there being no zonal dominance during homeostasis (Sun et al. 2020; May et al. 2023). These observations are also consistent with Lgr5 lineage tracing experiments (Planas-Paz et al. 2016; Ang et al. 2019) and therefore suggests that homeostatic turnover of the hepatocellular compartment is contributed to by hepatocytes distributed throughout the parenchyma. It has been suggested that the observations seen by Wang were a result of the disruption of one Axin2 allele using the CreERT2 cassette used in the lineage tracing experiment(May et al. 2023) and the larger cluster size in the Lin study was possibly due to the bias in proliferation of Tert expressing hepatocytes (Sarin et al. 2005).

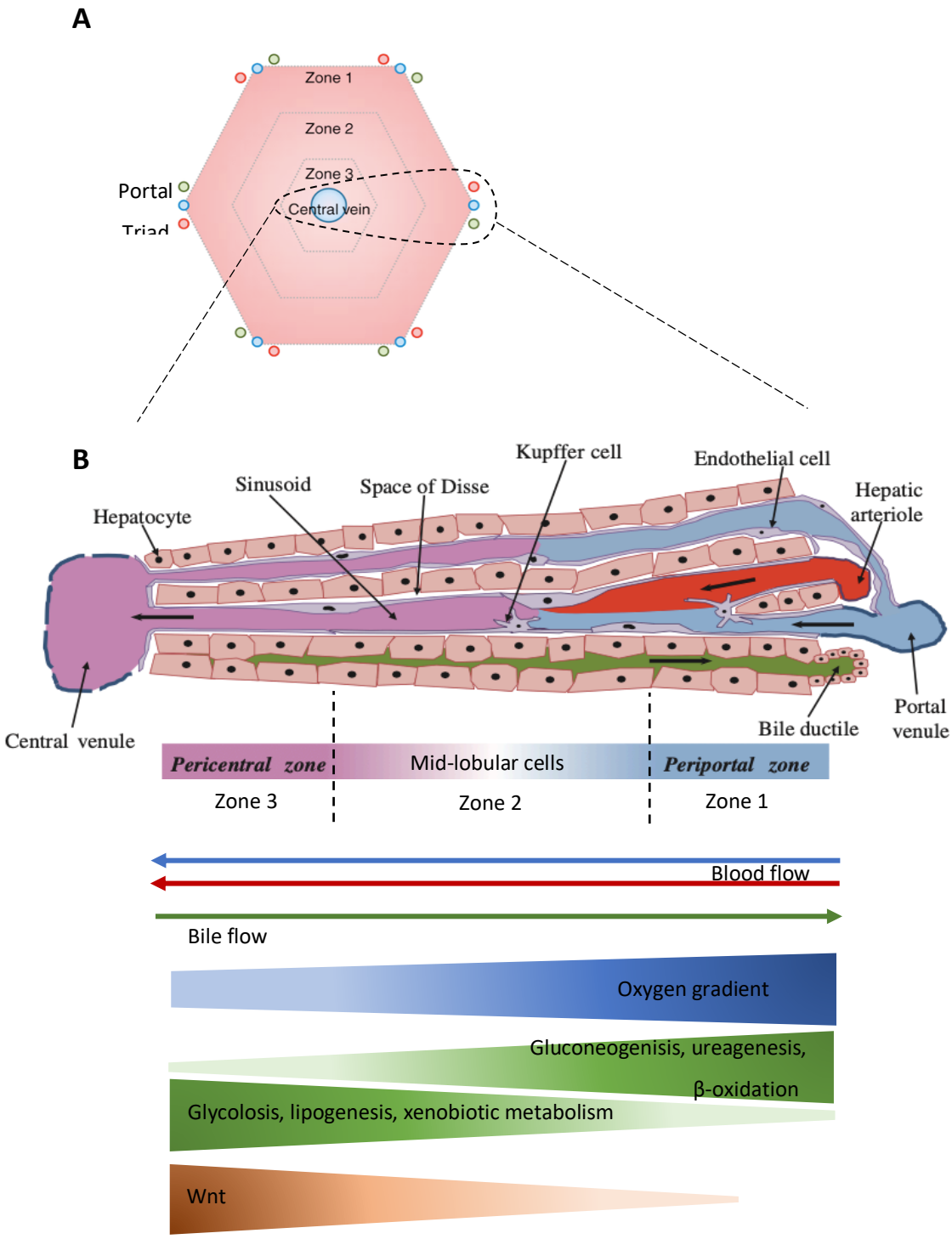

Figure 1.5 Anatomy of the liver lobule and liver zonation
(A) Hepatic lobule, the main building block of the liver showing a central vein in the center of a hepatic lobule connected to the portal tracts which includes the hepatic artery, portal vein and bile duct known as the portal triad. **(B)** Blood flows from the hepatic arteriole and portal venule to the central vein, passing through sinusoids lined with epithelial cells and cords of hepatocytes. Kupfer cells are liver macrophages and located within the lumen of the sinusoids. Bile produced by hepatocytes is secreted into bile canaliculi and flows towards the bile duct. Hepatocytes differ in their functions depending on location and are divided into three different metabolic zones. Figures adapted from (Trefts et al. 2017)

1.3.2 Liver zonation and Wnt/β-catenin

Oxygen, nutrients, and hormones gradients are formed by the blood flow from the portal veins and hepatic arteries situated at the corners of the lobules towards the central veins that drain them (Figure 1.5B). In an inverse manner, the Wnt morphogens Wnt2 and Wnt9b, and Wnt agonist Rspo3 are secreted from the central vein, creating a gradient of Wnt/β-catenin activity (Rocha et al. 2015; Preziosi et al. 2018). This creates hepatocytes that are not homogeneous but rather hepatocytes that show regional division across the liver lobule into different functional zones termed 'liver zonation'. This allows efficient and specialized metabolic processes to occur for optimised liver function. Perturbations of liver zonation are linked with driving hepatic pathophysiology (Martini et al. 2023).

Studies have shown that Wnt/β-catenin signalling is important in maintaining liver zonation (Benhamouche et al. 2006; Reed et al. 2008; Burke et al. 2009). Wnt/β-catenin pathway is active in the pericentral zone (Zone 3) of the liver owing to the secretion of Wnt ligands and Wnt agonists by central vein endothelial cells (Rocha et al. 2015; Preziosi et al. 2018). This regulates the expression of genes involved in bile acid metabolism and detoxification. Notably the expression of glutamine synthetase (GS) is restricted to the first couple of layers of hepatocytes surrounding the central vein. In contrast, the Wnt/β-catenin pathway is suppressed by Apc expression in the periportal zone (Zone 1). Here, hepatocytes express the enzyme phosphoenolpyruvate carboxykinase (PEPCK) for gluconeogenesis, and carbamoyl-phosphate synthetase 1 (CPS1), an enzyme involved in the urea cycle. CPS1 is expressed periportally but is absent in the first to second cell layer surrounding the central vein.

Early evidence of the significance of Wnt/β-catenin signalling in the establishment of liver metabolic zonation came from studies on mice where Apc was selectively inactivated in the liver (Benhamouche et al. 2006). The authors initially demonstrated that the localization of active β-catenin and Apc proteins was complementary, with active dephosphorylated β-catenin predominantly expressed in the pericentral zone, while Apc was predominantly expressed in the periportal zone. Conditional hepatic deletion of the negative Wnt/β-catenin regulator Apc led to increased proliferation, severe hepatomegaly, and ultimately death by day 10-15 post induction. They observed a shift in hepatocyte phenotype from periportal to pericentral,

as evidenced by the expression of GS throughout the liver from the central vein to the portal triad. The loss of Apc also resulted in the upregulation of additional genes and proteins (such as Glt1, Oat, Lect2, Axin2 and Rnase4) that are normally only expressed in pericentral hepatocytes. Conversely, periportal-specific markers such as Arginase1, Cps1, Glutaminase2, and Pepck1 were downregulated in the Apc knock-out mice. When blocking hepatocyte β-catenin by inhibiting Wnt signalling using an adenoviral vector expressing the Wnt antagonist, Dickkopf 1 (Dkk1), there was an observed decrease in pericentral gene expression pattern and an increase in periportal markers. These results were further confirmed in the study by (Burke et al. 2009), who also showed that the loss of Apc resulted in the expression of nuclear β-catenin and GS in most hepatocytes, regardless of their location within the liver. Deletion of β-catenin, on the other hand, resulted in a loss of GS expression and a complementary increase in Cps1 expression. Deletion of c-Myc did not appear to affect liver zonation suggesting that the metabolic zonation of the liver is dependent on β-catenin but independent of c-Myc. In the later study by (Planas-Paz et al. 2016), the authors suggested that the RSPO-LGR4/5-ZNRF3/RNF43 signalling module is also involved in regulating the spatiotemporal distribution of Wnt/β-catenin activity within the liver and plays a key role in controlling metabolic liver zonation.

Interestingly, conditional deletion of Axin1 did not alter zonation as marked by GS expression in the mouse liver (Feng et al. 2012; Abitbol et al. 2018). A possible explanation raised at the time was that Axin2 acts in a functional compensatory manner and that loss of both Axin1 and Axin2 should result in a strong “Wnt ON” phenotype and increase levels of GS expression in the liver as seen with APC deletion or β-catenin activation (Benhamouche et al. 2006; Miyoshi et al. 2009).

1.4 Liver injury and repair

It has long been known that the liver shows remarkable regenerative properties and that mature hepatocytes have stem-cell-like self-renewal capacity as shown by serial transplantation (Overturf et al. 1997). Although liver cells have low turnover rates during homeostasis, they possess remarkable regenerative abilities following damage. Repair strategies in the liver depend on the type and extent of the damage caused and can be broadly categorized as hepatocyte mediated and liver progenitor cell (LPC) mediated regeneration (So et al. 2020).

Hepatocyte mediated regeneration is the most common form of liver repair and involves the replication of mature hepatocytes. Recent studies provide evidence that all hepatocytes, regardless of their lobular position or ploidy status, possess comparable homeostatic and reparative capabilities of the liver parenchyma (Chen et al. 2020; Matsumoto et al. 2020; Sun et al. 2020).

Biliary epithelial cells (BECs) form the bile ducts responsible for the excretion of bile, as well as smaller ductules and canals of Hering, which are important for the collection of bile (Boyer 2013). BECs have been shown to play a critical role in liver regeneration. BECs are able to establish an auxiliary biliary system in response to injury in a process known as a ductular reaction (DR) (Kamimoto et al. 2016). This reaction is crucial for the regeneration of the liver following injury, as it allows for the formation of new bile ducts and the expansion of the existing ones.

In chronic liver disease, the proliferation of hepatocytes can be impaired, and as a result, the liver can be forced to regenerate through the proliferation and differentiation of LPCs (sometimes termed oval cells or hepatic progenitor cells) into hepatocytes and cholangiocytes instead. The exact location and identity of LPCs is yet to be resolved.

Raven et al conducted a study in which they induced liver injury in CK19 tdTomato mice using adeno-associated virus (AAV8) p21 hepatotropic virus. They found that the liver was repopulated with td-tomato-positive hepatocytes derived from cholangiocytes (Raven et al. 2017). This suggests the existence of a liver stem progenitor cell with bipotential properties within the cholangiocyte compartment, that is capable of regenerating both injured bile ducts and liver parenchyma.

Lineage-tracing studies have identified hepatocytes as another potential source of liver progenitor cells (LPCs). In a study conducted by the Grompe group, hepatocyte-derived progenitors were distinct from their biliary-derived counterparts based on RNA-sequencing, ultrastructural analysis, and *in vitro* progenitor assays. The study also found that human hepatocytes in chimeric mice could give rise to biliary progenitors *in vivo*. However, after the liver injury was resolved, these hepatocyte derived LPCs reverted back to hepatocytes (Tarlow et al. 2014). These findings suggest that hepatocytes can differentiate into LPCs under conditions of chronic liver injury and contribute to the LPC pool.

1.4.1 Acute injury models

Partial hepatectomy (PHx) is a very commonly employed model for studying acute liver injury and regeneration in rodents (Michalopoulos and Bhushan 2021). The procedure involves the surgical removal of up to 2/3rds of the adult liver. The remaining liver is able to grow back by increasing the number of cells and hepatocyte size to compensate. It has allowed insights into the signalling mechanisms involved in hepatic regeneration (Michalopoulos 2010). PHx induces the rapid activation of more than 100 genes that are not typically expressed in a healthy liver (Taub 2004). These genes are involved in preparing hepatocytes for cell cycle entry and coordinating the necessary adjustments for cell proliferation.

The Wnt/β-catenin pathway plays a crucial role in liver regeneration by promoting the proliferation of hepatocytes and the expansion of liver progenitor cells (Monga 2014). A study in 2001 by Monga (Monga et al. 2001) first identified β-catenin's involvement in liver regeneration following PHx. After PHx in rats, there is a rapid 2.5 increase in protein levels of β-catenin within the first five minutes. However, this activation is followed by decrease in Wnt-1 and increases of APC and Axin protein levels, which results in a decrease in total β-catenin protein, suggesting tight regulation of Wnt/β-catenin signalling during early rat liver regeneration. In a follow-up study (Sodhi et al. 2005), when β-catenin expression was knocked down during PH, there was a significant reduction in hepatocyte proliferation, resulting in a lower liver weight to body weight ratio. Additionally, the animals with β-catenin knockdown displayed decreased levels of the cell-cycle markers PCNA and Ki67. This observation was validated in mice using Albumin Cre for hepatocyte-specific conditional knockout of β-catenin. Mice that undergo partial hepatectomy with conditional β-catenin knock-out show slower liver regeneration than normal which was linked to reduced expression of multiple cyclins (Tan et al. 2006). Conversely, hepatocyte specific expression of ser45-mutant β-catenin, a stable form of β-catenin, resulted in accelerated liver regeneration that was associated with increased PCNA positive hepatocytes and increases in CyclinD1 (Nejak-Bowen et al. 2010).

In addition to the Wnt/β-catenin pathway, signalling pathways such as Hedgehog (Ochoa et al. 2010) and TGF-β (Karkampouna et al. 2012), and various growth factors, cytokines and signalling molecules such as HGF, EGF, TNFα, IL-6, norepinephrine, oestrogens, complement components, bile acids, and serotonin are involved in the regeneration of the liver (Michalopoulos and Bhushan 2021).

Understanding the molecular and cellular mechanisms underlying liver regeneration is critical for developing new therapies for liver diseases.

1.4.2 Chronic injury models

Chronic liver disease is a major risk factor for the development of HCC. Around 90% of HCC cases are believed to arise in the context of chronic liver disease (Llovet et al. 2021). Several models are available to understand the complex mechanisms underlying the development of HCC in the setting of chronic liver disease.

CCl_4 can be used in acute or chronic exposure settings (Ravichandra and Schwabe 2021). Upon repeated administration, CCl4 causes liver injury that progressively leads to fibrosis. CCl4 is metabolically activated in hepatocytes by P450 cytochromes, primarily CYP2E1 which is expressed pericentrally, resulting in the formation of trichloromethyl ($CCl3\bullet$), trichloromethyl peroxy, ($CCl3OO\bullet$) radicals that induce hepatocyte death through lipid peroxidation(Xu et al. 2017). The resulting injury and death of hepatocytes stimulate the activation and/or recruitment of resident and bone marrow-derived macrophages, which secrete pro-inflammatory and pro-fibrotic molecules, promoting the activation and proliferation of HSCs (Higashi et al. 2017).

The methionine and choline deficient (MCD) is a model of non-alcoholic steatohepatitis (NASH). Methionine and choline are indispensable for hepatic mitochondrial β-oxidation and very low-density lipoprotein (VLDL) synthesis (Macfarlane et al. 2011). The diet leads to rapid development of steatohepatitis, accompanied by immune cell infiltration and the development of severe hepatic inflammation in mice, resulting in pronounced fibrosis within eight weeks of initiating the diet. However, despite the severe liver damage, mice challenged with the MCD diet do not exhibit any indications of insulin resistance or obesity during the study period (Rinella and Green 2004). In fact, they experience significant weight loss, and decreased serum triglyceride and cholesterol levels which is the inverse seen in human NASH (Liu et al. 2013).

The DDC liver fibrosis model utilizes a diet that contains a porphyrinogen called 3,5-diethoxycarbonyl-1,4-dihydrocollidine. Accumulation of protoporphyrin in the liver leads to the formation of porphyrin plugs in small bile ducts, which obstructs the ducts and damages biliary epithelia(Fickert et al. 2007). This, in turn, leads to liver injury and ductular reaction, ultimately resulting in periportal liver fibrosis in as little as 2-3 weeks.

The model is reversible when animals are placed on a regular chow diet for a sufficient amount of time (Ravichandra and Schwabe 2021).

Thioacetamide (TAA) itself is not toxic to the liver however, hepatocytes located in both zone 1 and zone 3 have the capability to metabolize TAA to form toxic TAA-S-oxide (TAA-SO) and then to TAA-S,S-oxide (TAA-SO2), which triggers the generation of reactive oxygen species (ROS) (Wallace et al. 2015). Continued exposure to TAA can result in hepatocyte necrosis, which in turn leads to fibrosis then cirrhosis and increases the incidence of cholangiocarcinoma and HCC (Rekha et al. 2008).

Due to host species restriction, human hepatotropic pathogens such as HBV and HCV are limited to infecting only humans and chimpanzees. However, to facilitate *in vivo* infection and disease modelling, various transgenic, humanized mice created by engrafting the liver of immunodeficient mice with human hepatocytes, hydrodynamic injection, and viral vector-mediated transfection, and have been developed (Burm et al. 2018; Du et al. 2021).

These experimental models allow the induction of chronic liver injury and HCC in some cases. Each model has distinct characteristics that imitate various causes and patterns of disease progression but lack the specific mutational drivers that are often observed such as Axin1 inactivation.

1.5 Axin and the Wnt pathway in HCC

Components of Wnt/β-catenin pathway are mutated in a range of cancers including colon cancer, leukaemia, breast cancer and melanoma (Zhan et al. 2017). The Wnt/β-catenin pathway is essential for normal liver development and homeostasis, but its dysregulation has also been linked to the development and progression of HCC accounting for around 30-45% of cases (Figure 1.6A). The majority of Wnt/β-catenin mutations in HCC are activating CTNNB1 mutations in exon 3. As previously mentioned, CTNNB1 mutations are associated with a specific subgroup of HCC tumours that exhibit well-differentiated features and low proliferation rates. By contrast, inactivating mutations of AXIN1 occur in approximately 8-10% of HCC cases and are linked to a distinct subgroup of tumours that are characterised by higher rates of proliferation and chromosomal instability (Calderaro et al. 2017). Truncating AXIN1 mutations, accounting for 76% of AXIN1 mutations in HCC, are located across the gene (Figure 1.6B) and are frequently associated with the loss of heterozygosity (LOH) of the second allele. By contrast, 53% of HCC with Axin2 gene alteration show

amplification, with somatic AXIN2 mutations being less common, accounting for 2% of HCC cases (Figure 1.6C) and are not commonly associated with LOF. However, studies by Marvin et al, suggested that nonsynonymous point mutations in AXIN2 may generate dominant-negative alleles (Marvin et al. 2011). Surprisingly, APC mutations are detected in as low as 1.6% of cases of HCC (Guichard et al. 2012).

Although AXIN1 has been identified as a critical negative regulator of the Wnt/β-catenin pathway, there is still controversy surrounding whether loss of function mutations in AXIN1 in the liver result in the activation of the pathway as seen with Apc loss. Loss of Apc in the mouse liver shows stabilisation and nuclear translocation of β-catenin, resulting in strong activation of β-catenin dependent signalling and disruption of liver zonation (Colnot et al. 2004). Loss of Axin was hypothesised to replicate this phenotype. In an early study by Zucman Rossi (Zucman-Rossi et al. 2007), activating CTNNB1 (β-catenin) mutations were shown to be linked to expression of the β-catenin/TCF target gene glutamine synthetase (GS) in HCCs, while tumours with AXIN1 inactivating mutations showed no induction. AXIN1 mutations were also suggested to be linked to lower levels of β-catenin-dependent transcription compared to activated β-catenin mutations in cell lines (Zucman-Rossi et al. 2007). Deletion of Axin1 in mouse liver in the Dale lab was able to recapitulate this phenotype (Feng et al. 2012). Axin1 deleted livers had been found to activate only a subset of Wnt target genes; Axin2, c-Myc and CyclinD1. They observed an acute increase in proliferation and late onset HCC without a clear Wnt-activated phenotype such as effects on Wnt-regulated markers of zonation GS and CPS1 or nuclear accumulation of β-catenin. Subtle deregulation of the Wnt/β-catenin has been evidenced to alter stem cell function and fitness (Young et al. 2018) and it has been suggested that the threshold of β-catenin activation necessary to induce HCC may be lower than that for intestinal tumourigenesis (Buchert et al. 2010). Thus, the low level of Wnt/β-catenin activation following Axin1 deletion is sufficient to result in tumourigenesis. More recent research has indicated to AXIN1 deficiency inducing HCC without activation of β-catenin in 80% of cases and an alternative targeting and deletion of Axin1 did not result in a β-catenin program but did lead to tumourigenesis (Abitbol et al. 2018). Interestingly, β-catenin was shown to still be required for hepatocarcinogenesis in an Axin1 deleted and c-Met activated model of HCC (Qiao et al. 2019).

As a direct target of Wnt/β-catenin activation, Axin2 may act to compensate the loss of Axin1 to control the levels of β-catenin in the cytoplasm. Although Axin2 is seen

as a tumour suppressor as it acts to negatively regulate canonical Wnt pathway activation, elevated Axin2 expression acts as a potent promoter of colorectal carcinoma by up-regulating Snail1 and inducing epithelial-mesenchymal transition (EMT) and metastasis (Wu et al. 2012). More recently, it has been suggested that the Axin2-Snail axis is an unfavourable prognostic marker for oral squamous cell carcinoma (OSCC) and that high expression promotes active desmoplastic reactions and bone invasion in OSCC by activating cancer associated fibroblasts (An et al. 2020).

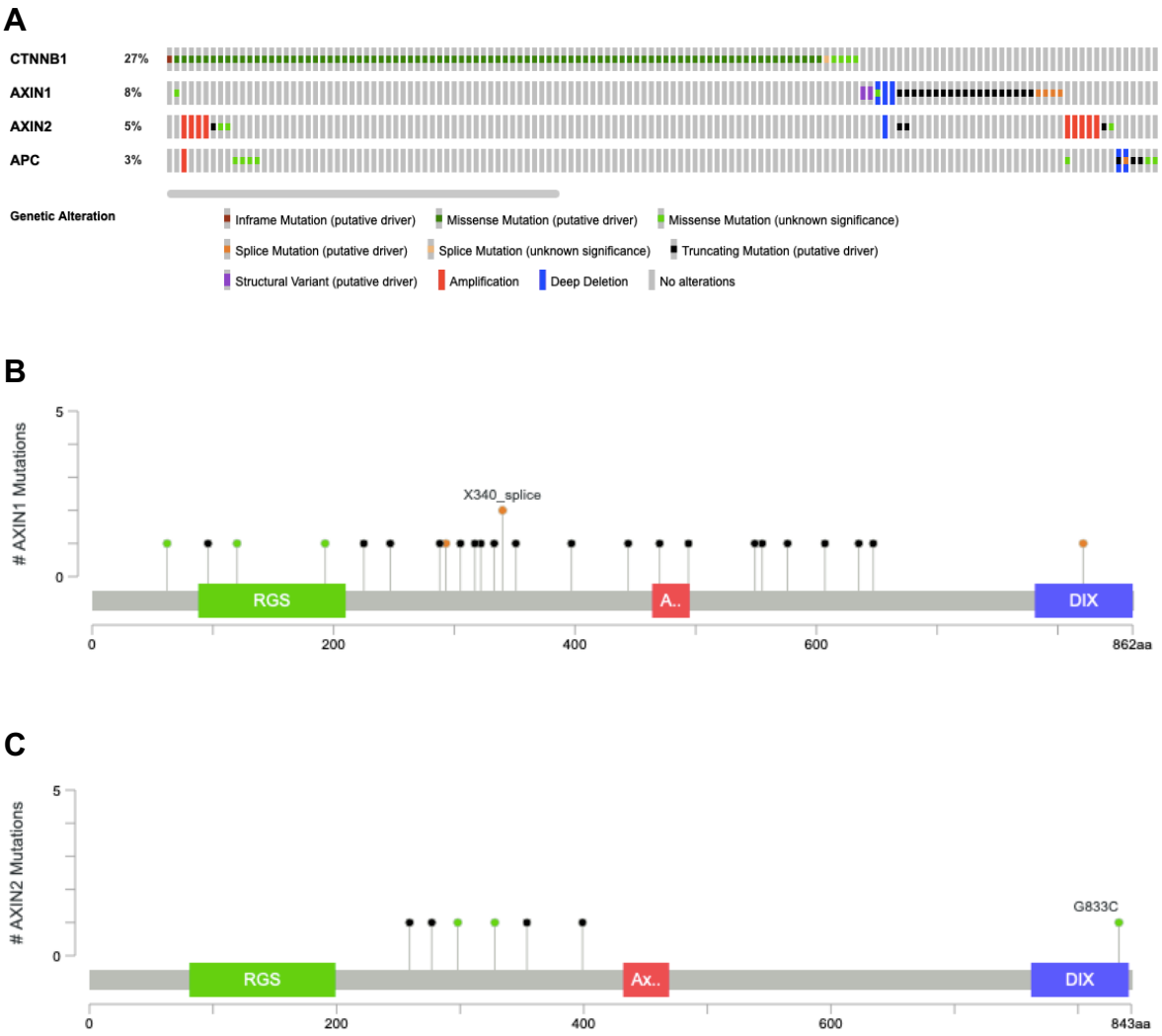

Figure 1.6 Wnt/β-Catenin pathway mutations in HCC
(A) Panel showing mutations and frequency of Wnt/β-Catenin pathway components in HCC. Majority of CTNNB1 and AXIN1 mutations are mutually exclusive with Log2 odds ratio of <-3 and p-value <0.001. Log2 odds ratio for Axin1 and Axin2 mutations equals 1.353 and a p-value of 0.155 for a tendency for co-occurrence. **(B,C)** Axin1 and Axin2 mutation locations in HCC. Green - missense mutation, black – truncating mutation, orange – splice. Data from Liver Hepatocellular Carcinoma (TCGA, PanCancer Atlas) from 353 samples and images generated using cBioPortal.

1.6 Pre-clinical models of HCC

The use of mouse models has played a crucial role in uncovering the molecular processes involved in HCC and has helped identify possible targets for therapy. To create these models, diverse techniques have been employed. As already discussed, chemo-toxic agents and special diets have been used to mimic the effects of environmental exposure to carcinogenic chemicals. The use of genetic modification techniques in mice has allowed the study of oncogenes and tumour suppressor genes that are implicated in the development of HCC.

1.6.1 *In vivo* models

Genetically engineered mouse models (GEMMs) have become an essential tool for studying cancer. They allow the manipulation of specific genes in mice and study how the molecular mechanisms of these changes affect the development and progression of cancer (Kersten et al. 2017). GEMMs can be generated through the use of various genetic engineering techniques, such as knockout or knock-in of specific genes, overexpression or conditional expression of oncogenes, and inducible or tissue-specific gene targeting.

Constitutive gene deletion has limitations due to the crucial role that many genes play in embryonic development. Consequently, if an important regulator of development is lost or activated constitutively, its function in adult tissues cannot be studied effectively. This is especially significant in cancer, where tumour suppressors and oncogenes are essential for normal development. A further limitation is related to the gene being lost across the entire organism, which makes it challenging to investigate the effects of gene loss in a specific tissue if inactivation causes significant complications in other areas of the organism. Finally, targeting a gene in all cells of the organism can conceal the effects of gene loss in specific cell types, as well as impact the interaction between different cell types.

To achieve temporal control over gene loss or activation, one of the most commonly used genetic engineering techniques in the generation of GEMMs is the Cre-lox system. The Cre-lox system utilizes the bacteriophage P1 Cre recombinase enzyme to selectively excise or invert (depending on the loxP site orientation) genes or DNA sequences in a controlled manner (Sauer and Henderson 1988). The Cre recombinase recognizes and binds to specific DNA sequences called loxP sites, which

are typically 34 base pairs in length and contain a core 13 bp sequence that is essential for recombination. The Cre recombinase then catalyses the recombination of the two loxP sites, resulting in the excision or inversion of the DNA segment flanked by the loxP sites (Kim et al. 2018). The Cre-loxP system can also be used for inducing the expression of oncogenes in a constitutively activated state. This involves placing a transcriptional stop-cassette flanked by loxP sites before the target gene. When expression is required, Cre recombinase is used to remove the loxP flanked region, thus eliminating the stop-cassette and allowing gene expression to proceed.

In combination with the Cre-lox system, the use of tissue-specific promoters such as Villin for the intestine, allows spatial control (Madison et al. 2002). An inducible promoter such as AhCre is able to combine temporal control and some tissue specificity. AhCre utilizes the regulatory elements present in the cytochrome P4501A1 gene (Cyp1A1). Under normal physiological conditions Cyp1A1 is not transcribed. However, when certain lipophilic xenobiotics (such as β-naphthoflavone) interact with the cytoplasmic aryl hydrocarbon receptor, it translocates to the nucleus, binds to the Cyp1A1 promoter, and initiates transcription of Cyp1A1 in the gastrointestinal tract with very high efficiency, particularly in the liver (Ireland et al. 2004). For more stringent control to overcome undesired expression, AhCre can be post-translationally regulated using a fusion protein between the recombinase and a mutated ligand binding domain of the human oestrogen receptor (ER). This fusion protein selectively binds to the oestrogen antagonist tamoxifen, rather than endogenous oestrogen. When tamoxifen is absent, the fusion Cre-ER protein remains in the cytoplasm and cannot access loxP sites. Binding of tamoxifen to the ER domain of the fusion protein reveals a nuclear localization signal and allows for the transport of Cre recombinase to the nucleus. Once in the nucleus, Cre recombinase can recognize and recombine the loxP sites (Kemp et al. 2004).

The patient-derived xenograft (PDX) model involves the transplantation of patient-derived tumour cells into immunocompromised mice such as non-obese diabetic/severe combined immunodeficiency (NOD/SCID) and athymic Balb/c nude mice (Okada et al. 2019). PDX tumours have been shown to recapitulate the molecular and histological characteristics of the original patient tumours (Shi et al. 2020). These models can be used to evaluate the efficacy of new drugs and treatments for HCC, providing a more accurate representation of clinical outcomes compared to traditional cell line models. However, PDX models can be time-consuming and expensive to

establish. The engraftment rate can vary, making it difficult to establish reliable models for all patients. Furthermore, PDX models may not fully capture the complex tumour microenvironment and immune response seen in patients (Abdolahi et al. 2022), limiting their utility.

CRISPR (Clustered Regularly Interspaced Short Palindromic Repeats) is a bacterial defence system that helps to protect bacteria from invading viruses. The system consists of two main components: the Cas enzyme and a guide RNA molecule. The establishment of Cas9 cleavage reactions in a laboratory setting and the proof of creating programmable double-strand breaks (DSBs) using custom spacer sequences led to the rapid development of a method for carrying out targeted mutation and insertion in mammalian cells and animal models, revolutionising the field of gene-editing (Jinek et al. 2012).

1.6.2 *In vitro* models of the liver

In vitro models range from simplistic 2D monolayers to more complex 3D models that resemble the tumour microenvironment. HCC cell lines are a valuable preclinical model, commonly used in drug discovery and cancer research. They offer insights into cellular signalling pathways, metabolism, proliferation, invasion, responses to chemotherapy or radiotherapy, drug resistance, as well as the molecular mechanisms of tumour growth and metastasis (Mirabelli et al. 2019). HCC cell lines can provide a reliable and reproducible model that is convenient to use. However, 2D cell lines have several limitations. 2D cultured cells are constrained to a flat morphology on a rigid surface, affecting cell polarity, normal cellular functions like signalling, proliferation, migration, and apoptosis. Furthermore, the constituents of the extracellular matrix (ECM) and cell-cell and cell-ECM interactions are negatively impacted under 2D conditions (Saydé et al. 2021). Additionally, 2D cell lines have a tendency to deviate from *in vivo* responses due to genetic drift after long-term culture (Quevedo et al. 2020) and thus limit their predictive value.

Primary human hepatocytes are traditionally seen as the “gold standard” for hepatic *in vitro* culture in pharmacological and toxicological research as they reflect the metabolism and functionality of the *in vivo* liver (Vinken 2021). However, acquisition and the long-term culture, maintenance and expansion of definitive hepatocyte cultures that retain functionality has proven to be challenging (Kaur et al. 2023). Early interventions such as collagen sandwich culture of hepatocytes by providing cell-ECM

interaction, has been shown to improve retention of hepatic functions, such as albumin secretion and cytochrome P-450 activities and maintain these functions for an extended period of over four weeks (Dunn et al. 1992). The morphology, cell assembly, and formation of bile canaliculi in sandwich cultures of primary human hepatocytes (PHH) are affected by the choice of ECM. Culturing PHH in a sandwich configuration with collagen as an underlay result in a tissue architecture that closely resembles *in vivo* trabecular cell arrangement. When overlaid with collagen, these cultures exhibit abundant bile canaliculi formation. In contrast, PHH cultured on a layer of Matrigel and overlaid with collagen display the most branched and stable bile canaliculi network (Deharde et al. 2016). Culturing primary hepatocytes (PH) in hydrogels in the form of hepatocyte spheroids promotes the upregulation of hepatic phenotype and gene expression. This approach enables the development of proper hepatocyte polarity and significantly enhances the lifespan and predictive capabilities of PH cultures (Chang and Hughes-Fulford 2014). Despite these advances, primary hepatocyte culture in sandwich cultures is dependent on primary tissue as a source of cells.

Induced pluripotent stem cells (iPSCs) can be differentiated into any cell type of the human body offering a unique opportunity to generate unlimited hepatocytes that maintain stable genomic, transcriptional, and epigenetic profiles for disease modelling (Tapia and Schöler 2016). However, the process of generating iPSCs and differentiating them into hepatocytes can be time-consuming and expensive. iPSC-derived hepatocytes can be heterogeneous in terms of their phenotype, gene expression, and functionality and may exhibit an immature phenotype, with lower levels of cytochrome P450 activity, reduced expression of some liver-specific genes such as Albumin, or an increase in the expression of the foetal liver marker AFP compared to primary hepatocytes (Corbett and Duncan 2019).

3D culture techniques have advanced to enable the development of liver organoids from adult tissue, offering a novel approach to overcome some of the limitations of traditional cell cultures. Organoids are cultures of primary cells, typically derived from stem cells, which are encouraged to differentiate into the specific cell types that make up the organ of interest and can grow into a mini-version of the organ *in vitro* (Hofer and Lutolf 2021). The recent explosion of research using organoids has been driven by the ability the generate and maintain long-term cultures from both normal and diseased tissues in 3D culture in Matrigel. Early work in the field focused

on small intestinal organoids where the role of Lgr5+ stem cells was defined. More recently, organoids have been established from multiple tissues including cancers.

Mouse bile duct (BD) organoids were first established in the Clever's laboratory by Meritxel Huch (Huch et al. 2013) using Lgr5+ cells derived from the liver's biliary epithelium using an Rspo1 containing medium. The organoids formed were cystic and hollow in shape and could be differentiated towards a hepatocyte like fate via the inhibition of TGFβ and Notch. In a subsequent study (Huch et al. 2015) BD organoids were established from human liver ductal cells. Human BD organoids were able to be differentiated towards a functional like hepatocyte fate *in vitro* and could be engrafted *in vivo* into the liver of CCl4 treated Balb/c nude mice. In their study, Broutier et al. demonstrated that 'tumoroids' derived from HCC, cholangiocarcinoma (CC) and a mixed HCC-CC subtypes of primary liver cancer preserved the histological architecture of the original tumour. Furthermore, these tumoroids retained expression of characteristic markers of the original tumours, such as AFP and HepPar1 for HCC and KRT19 and EpCAM for CC, even after being cultured for more than three months. These tumoroids, which were genetically stable and derived from individual patients, were also able to be utilized to assess the effectiveness of various drugs (Broutier et al. 2017).

Concurrent research published by (Hu et al. 2018; Peng et al. 2018) was able to establish PH organoids derived from mature hepatocyte cells from mouse and human sources. The morphology of these PH organoids was very distinct from the BD organoids, appearing as dense clumps of cells described as a "bunch of grapes" structure. The Hu protocol partly relied on the activation of the Wnt/β-catenin pathway with the addition of RSPO1 conditioned media. However, expansion of their mouse hepatocyte and human hepatocyte organoids slowed down after 2-3 months. The majority of the work instead relied on the culture of fetal liver cell derived organoids. The Peng protocol was only used on mouse primary hepatocytes to establish organoids, but they were able to be maintained long-term. A key component identified and used in their media was the cytokine TNFα. TNFα is released by liver and spleen macrophages, which is important during liver regeneration following partial hepatectomy (Michalopoulos and Bhushan 2021). The organoids were also able to be differentiated towards a periportal or pericentral phenotype using HGF/EGF or Wnt based media respectively. A drawback of the PH organoids in the Peng media was their slow growth, requiring up to 3 weeks in culture before passage. It is therefore

possible that the combination of the Hu media, that facilitates rapid growth and the Peng, media that allows organoids to be maintained long term will provide more optimal conditions for future research purposes.

1.7 Axin deletion

AhCre mediated deletion of Axin1 in the liver resulted in hepatocellular carcinoma in 5/9 mice, one year post induction (Feng et al. 2012). It is noteworthy that this tumour formation was not attributed to augmented levels of nuclear β-Catenin or modifications in liver zonation, which are commonly observed in mutants of other constituents of the canonical Wnt pathway such as APC (Colnot et al. 2004). Instead, there was an activation of a transcriptional program related to regulators of G2/M cell cycle and cytokinesis, along with increased proliferation, hepatomegaly, and an enlargement of hepatocyte cell volume. It is possible that any of the known β-catenin independent functions, or other still unknown mechanisms involving Axin1 might contribute to the phenotype of Axin1 loss in the liver. The simplest explanation however could be the partial rescue of Axin1 loss by the homologue Axin2, which is a transcriptional target of Wnt/β-catenin signalling. Axin2 may play a role in preventing the overall derepression of zonal Wnt targets but is not sufficient to restore Axin1's anti-proliferative functions. A thorough investigation of the conditional deletion of Axin2 or the combined conditional deletion of Axin1 and Axin2 in the liver has not been conducted thus far. There have been no documented reports of embryonic lethality associated with Axin2 mutations and a constitutive Axin2 mutant is available (Lustig et al. 2002b). The $Axin2^{lacZ}$ allele (also referred to as $Conductin^{lacZ}$ or Axin2tm1Wbm/J), contains a lacZ gene integrated in-frame with the native start codon of Axin2, replacing most of exon 2 and presumed to be null. The gene product of lacZ, β-Galactosidase, serves as a reliable indicator of Axin2 expression and, consequently, Wnt signalling activity. A conditional Axin2 allele was developed in this lab by Gui Jie Feng using similar methodology as for Axin1. Homologous recombination was used to target the ATG start codon containing exon 2 of the Axin2 gene with a construct containing exon 2 flanked by loxP sites. A Neomycin resistance cassette was eliminated by Flp-mediated recombination, resulting in an allele containing exon 2 flanked by loxP sites and a residual FRT site. When active Cre recombinase is present, the loxP flanked exon can be excised, leading to the loss of the start codon of Axin2 and subsequently, any Axin2 protein. Experiments using the embryonically active CMV-Cre resulted in

lethality in Axin2$^{\Delta/\Delta}$ embryos at E9.5 and was considered to be a more severe form of the Axin2$^{lacZ/lacZ}$ allele that was suggested to be a result of β-catenin/TCF pathway activation (Offergeld 2015 PhD Thesis).

Despite both constitutive and conditional constructs involving a change in exon 2 (lacZ insertion in Axin2^{lacZ} and removal of a loxP-flanked exon 2 in Axin2$^{\Delta/\Delta}$), they exhibit distinct characteristics. The Axin2^{lacZ} allele is commonly referred to as an Axin2 null allele in the literature, even though there is no published evidence supporting or disproving this claim. Until concrete evidence of a truncated Axin2 protein's presence or absence is discovered in any of the Axin2 lines, the true null identity remains unknown. Conducting a complete knockout of the entire coding region of Axin2 could assist in clarifying the phenotype.

Anika Offergeld conducted a study utilizing ES cells to investigate the effects of single and double Axin mutations. The research findings revealed that ES cells with single Axin mutations exhibited predominantly normal phenotypic characteristics. However, in ES cells with double Axin mutations, a slight upregulation of Wnt target genes was observed, while cell proliferation rates remained unaffected. In contrast, during the differentiation process into embryoid bodies, multiple indicators of the Wnt pathway exhibited an increase, accompanied by the activation of a gene expression profile associated with G2/M and the cell cycle. These alterations were accompanied by impaired differentiation.

This thesis will use both the conditional Axin alleles to investigate how Axin1 and Axin2 contribute to the development of HCC (Figure 1.7) The approach will involve a combination of mouse genetic models and organoids.

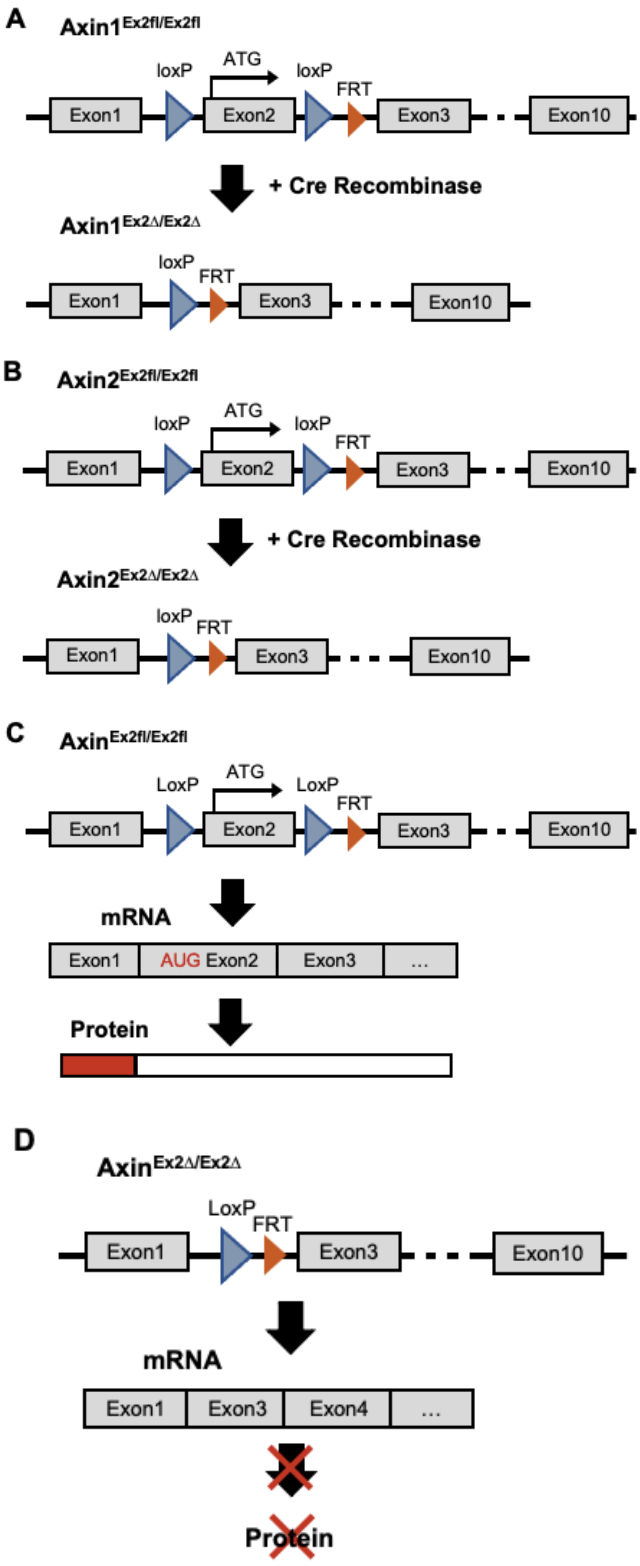

Figure 1.7 Schematic of Axin deletion
(A) loxP sites flank exon 2 of Axin1 (Axin1Ex2fl/ Ex2fl). **(B)** loxP sites flank exon 2 of Axin2 (Axin2Ex2fl/ Ex2fl). In the presence of Cre recombinase the loxP flanked exon is removed (AxinEx2Δ/ Ex2Δ). **(C)** Exon 2 of both Axin1 and Axin2 contains the ATG sequence responsible for the translation start. **(D)** The prediction is that Axin proteins cannot be made from the floxed out gene (AxinEx2Δ/Ex2Δ).

1.8 Aims and objectives

HCC is one of the most common forms of liver cancer and is associated with high mortality rates. AXIN1 mutations have been identified in a subset of HCC cases characterized as proliferative and with a particularly unfavourable prognosis (Rebouissou and Nault 2020). In contrast to the removal of Apc or the activation of β-catenin mutations, the absence of Axin1 in hepatocytes and tumours resulted in minimal or no significant upregulation of typical WNT target genes (Feng et al. 2012; Abitbol et al. 2018). The Axin1 homologue, Axin2, may act to compensate aspects of the loss of Axin1 to control the levels of β-catenin.

The principal aim of this thesis was to further examine the function that Axin1 and Axin2 play in the context of the development of HCC. Additionally, I aimed to optimise culture conditions for liver organoids to develop a more accurate *in vitro* drug response assay.

The objectives of this thesis were to establish an *in vivo* mouse model to study the role of Axin1 and Axin2 in liver homeostasis and the development of HCC. Secondly, an *in vitro* model will be developed to elucidate the role of Axin1 and Axin2 in a different context and, in the differentiation in liver bile duct organoids. Additionally, published, and optimised hepatocyte specific media conditions will be used concurrently on normal, and tumour derived hepatic cell sources to assess which best permits the retention of hepatic functions and tumour characteristics. Chapter 3 focuses on the *in vivo* analyses using short term and long-term cohorts of Cre-lox mediated deletion of Axin1 and or Axin2. Chapter 4 focuses on efforts at developing additional Axin alleles using CRISPR/Cas9 and Chapter 5 focuses on the development and use of PDX, human PH, mouse PH and BD derived organoid systems.

Chapter 2: Materials and Methods

2.1 Experimental Animals

2.1.1 Animal husbandry

Experiments in this thesis were performed in murine models (Mus musculus). Animals were housed according to UK Home Office Regulations and experiments were carried out under valid personal and project licenses. All animals used in experiments were reported in accordance with NC3R(UK) ARRIVE guidelines. Mice were given access to the Harlan standard diet (Special Diets Service UK, expanded diet) and water ad libitum and maintained on a 12:12 hour light dark schedule. Mice were housed using standard facilities and maintained on a mixed outbred background.

2.1.2 Breeding

Mice of 6 weeks and older of known genotype were bred mainly in trios of one male and two females. Pups were weaned at approximately 4 weeks old or when feeding independently. Pups were sexed and separated at weaning.

2.1.3 Identification

Upon reaching weaning age of 3-4 weeks old, the animals were sexed and then separated. Ear clipping was utilized as a method of animal marking for identification. The ear punch obtained from this procedure served as the source for DNA extraction and subsequent genotyping (detailed below).

2.1.4 Transgenic constructs and animals used in this project

A number of transgenic mouse lines were utilized in this research. These included mice with inducible tissue-specific transgenes that drive the expression of Cre recombinase, as well as loxP-targeted native alleles and reporter constructs. The transgenic line, AhCreERT, expresses a fusion protein of Cre recombinase with a mutated oestrogen receptor, providing enhanced control over Cre recombinase activation in the gastrointestinal (GI) tract (Kemp et al. 2004). ROSA-lacZ A floxed stop cassette is inserted between a lacZ gene and the ubiquitous ROSA26 promoter. In the presence of Cre recombinase the stop cassette is removed and the lacZ reporter is expressed. The Axin1 allele with loxP sites flanking exon 2 as described in (Feng et al. 2012). The

Axin2 allele with loxP sites flanking exon 2 as described in (Offergeld 2015 PhD Thesis). Additionally, the Apc transgene with loxP sites positioned within the introns surrounding exon 14 was generated by (Shibata et al. 1997).

2.1.5 Study design

Both male and female mice were used for the different timepoint studies. Mice were randomly allocated to the day 6, 1 month and ageing studies. Recombination of the floxed Axin1 and Axin2 alleles was carried out as described in section 2.1.6 on mice aged approximately 10 weeks of age then used for analysis at specified timepoints. Control animals used were age matched and were AhCreER^{T} positive unless otherwise stated. A priori power calculations were not carried out. Scoring of immunohistochemical analysis (Ki67 counts, nuclei size etc.) was blinded.

2.1.6 Combined injection of β-naphthoflavone and Tamoxifen

To activate recombinase expression and activity in mice carrying the AhCreER transgene, a combination of β-naphthoflavone (BNF) and Tamoxifen treatment was administered. Powdered BNF and Tamoxifen were added to corn oil to create a 10 mg/ml solution. The mixture was heated to 80 °C while vigorously stirring until complete dissolution. Solution was then aliquoted to amber bottles and stored at -20 °C. Recombinase induction involved administering four daily intraperitoneal (IP) injections of the combined BNF and Tamoxifen solution at a dose of 80 mg/kg. Injections were performed using 1 ml syringe (BD Plastipak) and 25G needle (BD Microlance 3).

2.1.7 Injection of 5-Bromo-2-deoxyuridine

Where indicated, experimental animals received an excess of 5-Bromo-2-deoxyuridine (BrdU; Amersham Biosciences). Animals were injected IP with 200 μl BrdU reagent 2 hours prior to harvesting.

2.1.8 PCR genotyping

Mice were genotyped by PCR using DNA extracted from ear punches used for identification at weaning age. Ear or tail biopsies were additionally taken at time of death to confirm genotype.

2.1.9 DNA extraction

Samples were thawed then digested in 250 μl cell lysis buffer (Qiagen) containing 5 μl proteinase K solution (Roche) overnight at 37 °C with agitation. The following day, samples were cooled to room temperature and 100 μl of protein precipitation solution (Qiagen) was added. The samples were briefly mixed by inversion and insoluble debris and protein were pelleted by centrifugation at 13,000 x g for 10 minutes at room temperature. The DNA was precipitated by adding the supernatant to 250 μl of isopropanol (ThermoFisher Scientific) in a DNase free Eppendorf. The solution was mixed by inversion and DNA was pelleted by centrifugation at 13,000 x g for 15 minutes. The supernatant was discarded, and the pellet was washed with 70% ethanol. The DNA was pelleted by centrifugation at 13,000 x g for 10 minutes and supernatant discarded. The pellet was air dried for 30 minutes at room temperature and resuspended in 250 μl of DNase/RNase free water (Ambion). gDNA was stored at room temperature or at 4°C for long-term storage.

2.1.10 PCR protocol

PCR was performed in 8 well 0.2 ml PCR SnapStrip tubes (Anachem). 3 µl gDNA was added to 47 µl PCR mix (detailed in Table 2.1). PCR mix with 3 µl DNase/RNase free water was run alongside the samples as a negative control. PCR reactions were performed in a T3000 Thermal Cycler (Biometra). Primer sequences and specific cycling conditions can be found in Table 2.2.

2.1.11 Visualisation of PCR products

PCR products were visualised by agarose gel electrophoresis. Before loading, reactions were mixed with 5µl of DNA loading dye (50% Glycerol (Sigma), 50% distilled water, 0.1% (w/v) Bromophenol Blue (Sigma)). PCR products were run on 2% (w/v) (4% for Ah Responder) agarose (Bioline) Tris Borate EDTA (TBE) (National Diagnostics) gels with Safeview Nucleic Acid Stain (NBS Bio). Samples were run alongside a molecular ladder (NEB) of appropriate size at 110 V until the desired bands were sufficiently separated. DNA bands on the gel were visualized using a GelDoc UV transilluminator (BioIRad).

Table 2.1 Genotyping PCR Master Mix

Component	Volume (ml)
gDNA	3
PCR grade water	Up to 50
5X Colorless GoTaq® Flexi Buffer (Promega)	10
MgCl2 (25 mM)	5
dNTPs (25mM; dATP, dCTP, dGTP, dTTP)	0.4
Primers (10 mM) (Sigma)	1 of each primer
GoTaq® G2 Hot Start Taq (Promega)	0.2

Table 2.2 Genotyping PCR primer sequences, cycling conditions and product size

PCR	Forward Primer (5' - 3')	Reverse Primer (5' - 3')	PCR Program	Expected Products
Cre	TGA CCG TAC ACC AAA ATT TG	ATT GCC CCT GTT TCA CTA TC	95°C 3mins, (95°C 30sec, 55°C 30sec, 72°C 1min) x35, 72°C 5mins	1000 bp
LacZ	CTG GCG TTA CCC AAC TTA AT	ATA ACT GCC GTC ACT CCA AC	95°C 3mins, (95°C 30sec, 55°C 30sec, 72°C 1min) x35, 72°C 5mins	500 bp
Ah Responder	AGG TTC CCT GGG ACT TGT TT	TCA CCA AAC CCT CCA TCA GT	94°C 5mins, (94°C 20sec, 57°C 20sec, 72°C 30sec), x30, 72°C 5mins	Responder: 196 bp Non-Responder: 178 bp
Axin1 - To check for LoxP sites flanking exon 2	CCT CAA GTA GAC GGT ACA ACG AAG GCA GAG	CTG TGC AGG AGC TCT ACT AAG CCT CTA CAC	95°C 2min30sec, (95°C 45sec, 60°C 45sec, 72°C 1min) x35, 72°C 10mins	Floxed: 531 bp WT: 383 bp
Axin1 KO - To test for loss of exon 2	CTC TGA ATG TGG ACT GTG TCC TTC CAT CAC	GCT GTG CAG GAG CTC TAC TAA GCC TCT A	95°C 2min30sec, (95°C 45sec, 57°C 45sec, 72°C 1min), x35, 72°C 10mins	KO: 402 bp Floxed: 2190 bp WT: 2042 bp
Axin1 3FL - To test for 3rd LoxP site after exon 10	ATA GCT GTC TCT TGC CTG CC	AGT GGT GTT CTC AGG TGC TG	95°C 2min30sec, (95°C 45sec, 60°C 45sec, 72°C 1min) x35, 72°C 10mins	WT: 509 bp undigested / 509 bp +Pst1 digest 3FL: 509 bp undigested / 395 and 114 bp + Pst1 digest
Axin1 3KO - To test for complete KO of Axin1	CAC TTG GTC GAG CTA AGC CA	GCT GTA GCC ATT GGG ACA CT	95°C 2min30sec, (95°C 45sec, 61°C 45sec, 72°C 1min) x35, 72°C 10mins	KO: 532 bp undigested 387 and 145 bp with Pst1 digest

Axin2 - To check for LoxP sites flanking exon 2	CCT GGA AGA TGA GCT AGC TTT GCA GAT GTC	CAA AAC TCA GTT GCA GTC GCT AGC AGT TCC	95°C 2min30sec, (95°C 45sec, 57°C 45sec, 72°C 1min) x35, 72°C 10mins	Floxed: 643 bp WT: 505 bp
Axin2 KO - To test for loss of exon 2	CTT GCG TGT TCT GGT TGT CGT GGG AGT	TAG CAG TGG AAT GAC CTC TTC CCA AAC TGG	95°C 2min30sec, (95°C 45sec, 60°C 45sec, 72°C 1min) x35, 72°C 10mins	KO: 504 bp Floxed: 1995 bp WT: 1854 bp
Axin2 3FL - To test for 3rd LoxP site after exon 10	TGT CAG CCT CAT CTT TGG	GGG AAC ACA CGA CTT AGC	95°C 2min30sec, (95°C 45sec, 57°C 45sec, 72°C 1min) x35, 72°C 10mins	WT: 465 bp undigested / 465 bp +Pst1 digest 3FL: 513 bp undigested / 377 and 136 bp + Pst1 digest
Axin2 3KO - To test for complete KO of Axin2	TTT AGG CAA CAT CAT CGG G	GGA CCA CGC TGT CAA ATG	95°C 2min30sec, (95°C 45sec, 61°C 45sec, 72°C 1min) x35, 72°C 10mins	562 bp undigested 426 and 138 bp with Pst1 digest
Apc	GTT CTG TAT CAT GGA AAG ATA GGT GGT C	CAC TCA AAA CGC TTT TGA GGG TTG ATT C	95°C 3mins, (95°C 30sec 60°C 30sec, 72°C 1min) x30, 72°C 5mins	Floxed = 314 bp WT = 226 bp

2.2 Tissue harvesting and processing

2.2.1 Dissection

Following a schedule 1 approved method of culling (cervical dislocation), animals were dissected using a micro-dissection kit. The mouse was sprayed with 70% EtOH (ethanol) and the skin and muscle wall of the abdomen cut through to open the abdominal cavity. Upon dissection, tissue samples were removed and placed in appropriate fixatives as quickly as possible. In general, other than liver, samples of the following tissues were also taken routinely for fixation: small and large intestine, spleen, pancreas, kidney, lung. Prior to fixation, small and large intestines were flushed well with water to remove debris from the intestinal lumen. Intestines were cut opened longitudinally, rolled from end-to-end and secured with a needle.

2.2.2 Formalin tissue fixation

Dissected out tissues were incubated in formalin for 24 hrs at 4°C then stored in 70% EtOH at 4°C until paraffin embedding.

2.2.3 Dehydration of tissue

Fixed tissues were removed from 70% EtOH, arranged in histocasettes and processed using an automatic processor (Leica TP1050). Samples were dehydrated in increasing concentrations of ethanol (70% for 1 hour, 95% for 1 hour, 100% 2 x 1 hour 30 min, 100% for 2 hours), Xylene 2 x 1 hour and paraffin 1 x 1 hour and 2 x 2 hours. After dehydration, samples were embedded in paraffin wax.

2.2.4 Tissue sectioning

Paraffin blocks were sectioned on a microtome (Leica RM2135) at a thickness of 5 μm. Sections were then floated onto poly-L-lysine (PLL) coated slides (Polysine, Thermo Fisher) and baked for 24 hours at 58 °C before use.

2.2.5 Fresh tissue preservation

Small samples of liver were removed and completely covered by OCT – Optimal Cutting Temperature cryoprotectant medium (R. A. Lamb) and frozen on dry ice. Samples were frozen on cork discs (R. A. Lamb) and wrapped in aluminium foil. Frozen samples were stored at -80 °C until required.

2.3 Tissue preservation for protein, RNA and DNA extraction

2.3.1 For DNA extraction

Liver samples intended for DNA extraction were removed and placed into a clean Eppendorf tube. Samples were then kept on ice until being transferred to a freezer at -20°C for storage. DNA extraction was then usually performed within 2 weeks.

2.3.2 For RNA extraction

Liver intended for RNA extraction was removed quickly and immersed into an Eppendorf tube containing RNAlater (Sigma). Samples were frozen on dry ice and then stored at -80 °C.

2.3.3 For protein extraction

Liver samples intended for future protein extraction were removed as quickly as possible to prevent protein degradation. Tissue was placed in an Eppendorf tube fitted with a locking lid. Samples were then quickly immersed in liquid nitrogen (LN2) to snap freeze tissue. After removal, samples were stored at -80°C until needed.

2.4 Genomic qPCR and qRT-PCR

2.4.1 DNA extraction for genomic qPCR

DNA extraction for use in genomic qPCR experiments was carried using the QIAamp DNA kit (Qiagen) according to manufacturer's instruction.

2.4.2 RNA extraction for RT-qPCR

Liver pieces were removed from storage in RNAlater (Sigma) and placed in 1ml Trizol reagent (Invitrogen) in screw-cap tubes containing 1.4mm ceramic beads (Lysing Matrix D tubes, MP Biomedical). Tissue samples were then homogenised using the FastPrep-24 5G Lysis System (MP Biomedical) running the mouse liver program. Tubes were then centrifuged at 10,000 x g for 10 mins at 4°C to pellet cell debris and the ceramic beads. Supernatants were pipetted into clean 1.5 ml Eppendorf tubes and 200 μl ice cold chloroform was added to each tube and shaken well. Tubes were kept on ice for 10 minutes with frequent agitation. The samples were then centrifuged for 15 minutes at 13000 x g at 4°C, and the aqueous phase of the supernatant carefully

pipetted into fresh Eppendorf tubes. 700 µl isopropanol was added to tubes and they were incubated at -20°C O/N for optimal RNA precipitation. The samples were then centrifuged for 15 minutes at 13000 x g at RT to pellet RNA. The supernatant was carefully aspirated from the pellet. The pellets were washed twice with 500 µl pre-chilled 70% EtOH and air dried for 5-10 minutes then resuspended in 50 µl DNase/RNase free water (Ambion) and incubated for 10 minutes at 65°C with gentle agitation if needed. Extracted RNA was quantified using the NanoDrop 1000.

2.4.3 DNase treatment

RNA samples were treated with DNase to remove any contaminant DNA using the TURBO DNA-free™ Kit (Invitrogen) according to manufacturer's instructions.

2.4.4 cDNA synthesis

Reverse transcription of RNA was performed using SuperScript™ IV Reverse Transcriptase (Invitrogen) according to manufacturer's instructions.

2.4.5 qPCR and RT-qPCR reactions

RT-qPCR or genomic qPCR was run in triplicate in MicroAmp fast optical 96 or 384-well reaction plates (Applied Biosystems) on a QuantStudio 7 Flex RT PCR system (Applied Biosystems) using SensiFAST SYBR Hi-ROX Mix (Bioline). Each well was made up of 10 µl SYBR, 2 µl of cDNA (diluted 1:5), 0.8 µl of each primer (10 mM) and 6.4 µl nuclease free H2O. The plate was sealed and centrifuged for 1 min at 1,000 x g. Full RT-qPCR primer sequences are listed in (Table 2.3). Thermocycler conditions were set to 95 °C for 20 s followed by 40 cycles of 95 °C denaturation for 1 sec and 60 °C annealing for 20 sec. RT-qPCR reactions for all cDNA samples were run with primers for the housekeeping gene β2 microglobulin (B2M) in order to normalise the expression levels of target genes. Genomic DNA samples were normalized to the single copy gene *ApoB*. The data were collected automatically using the StepOne Software. Samples were only analysed if they had a single peak in the melting curve and the triplicate repeats were within 1 CT value of each other. Data was then analysed using the 2-ΔΔCT method (Livak and Schmittgen 2001).

Primers were taken from (Feng et al. 2012) or from Primer Bank Database (https://pga.mgh.harvard.edu/primerbank/). In silico analysis of primer specificity was run using UCSC Genome Browser online tool before use (https://genome.ucsc.edu/).

Table 2.3 Mouse primer sequences used for RT-qPCR

Gene	Forward Primer 5'-3'	Reverse Primer 5'-3'
Afp	CTTCCCTCATCCTCCTGCTAC	ACAAACTGGGTAAAGGTGATGG
Albumin	TGCTTTTTCCAGGGGTGTGTT	TTACTTCCTGCACTAATTTGGCA
Apob	CACGTGGGCTCCAGCATT	TCACCAGTCATTTCTGCCTTTG
Ass1	CACGGGAAAGGGGAATGACC	TCATCCATACTCCAGGGGCT
Axin1	CTCCAAGCAGAGGACAAAATCA	GGATGGGTTCCCCACAGAAATA
Axin1 KO	GTCTGGATACCTGCCCACTTTG	TAGCGTGTCAGCATCACTGGAC
Axin2	GCAGCTCAGCAAAAAGGGAAAT	TACATGGGGAGCACTGTCTCGT
Axin2 KO	GGCTACCTCCCCACCTTGAAT	ATAACTCGCTGTCGTTGGCG
B2M	CTTTCTGGTGCTTGTCTCACTG	AGCATTTGGATTTCAATGTGAG
β-catenin	AGTCCTTTATGAATGGGGCAA	TCTGAGCCCTAGTCATTGCATA
Birc5	GAGGCTGGCTTCATCCACTG	ATGCTCCTCTATCGGGTTGTC
c-Jun	CTTCTACGACGATGCCCTCAAC	AGTGGTGATGTGCCCATTGC
c-Myc	CTAGTGCTGCATGAGGAGACAC	GTAGTTGTGCTGGTGAGTGGAG
Caspase3	CTGATGAGGAGATGGCTTGCC	TGGATGAACCACGACCCGTC
CD44	ATCGCGGTCAATAGTAGGAGAA	AAATGCACCATTTCCTGAGACT
Cdc20	AATGACTACTACCTGAATCTTGT	GGATGTCACCAGAACCAG
Cdc25a	ACAAAGAGGAGGAAGAGTGTGCC	GGAAGACATCAGGGATAGAGACTGG
Cdca3	AAGTATTGGAGACAGAAGC	GACAGGTCCAGGTCATAA
Cdk1	GACAATCAGATTAAGAAGA	AACTATACAAGACAGGAA
Ctgf	GGGCCTCTTCTGCGATTTC	ATCCAGGCAAGTGCATTGGTA
CyclinA2	TGAATCACCACATGCTAT	TAACCTCCATTTCCCTAAG
CyclinB1	CTCTGTAGTGAATATGTG	CATCTGAACCTGTATTAG
CyclinB2	TCTTGCCTGTCTCAGAAG	CTCCATGTAGCCTGTGTAA
CyclinD1	GCGTACCCTGACACCAATCTC	CTCCTCTTCGCACTTCTGCTC
Cyr61	GATGACCTCCTCGGACTCGAT	CGTGCAGAGGGTTGAAAAGAA
EpCam	TGAAAAGGCACCCGAGTTCTCC	AACCAGGACAACAATCCCCG
Fah	TCATAACAGGTCACTGCCAGG	TGTCTTGTGACTTCCGGAGC
Fas	GCGGGTTCGTGAAACTGATAA	GCAAAATGGGCCTCCTTGATA
Foxm1	TGGCTTGGAAAGATGAGT	GCTCCAGGTGACAATTCT
Gpc3	TCGACAGCCTCTTTCCAGTCA	GGTCACGTCTTGCTCCTCG
Hmmr	CTGCGAGTAATGCTTCAC	TTCATCAATTCCAGGCTTAG
Hnf1b	AGGGAGGTGGTCGATGTCA	TCTGGACTGTCTGGTTGAACT
Hnf4a	AGAGGTTCTGTCCCAGCAGATC	CGTCTGTGATGTTGGCAATC
Ki67	AGAAGTCCAGGTCTACAG	TCGTTGCTATTGCTAAGG
Krt19	CCTCCCGAGATTACAACCACTA	AATCTTGGAGTTGTCAATGGTG
Krt7	GATGACCTCCGCAACACC	TCCAGCAGCTTGCGGTAG
Lgr5	ACATTCCCAAGGGAGCGTTC	ATGTGGTTGGCATCTAGGCG
Mastl	TGTCCTATGTCTGTAGAT	CTGGAGTAGATTAGAAGTC
Opn (Spp1)	AGCAAGAAACTCTTCCAAGCAA	GTGAGATTCGTCAGATTCATCCG
p53	CAGGGCTGAGACACAATCCTCC	GTGCCAGGGTCCAACAACTG
Prox1	ACAAAGCAAATGACTTTGAGGTTC	GGATCAACATCTTTGCCCGC
Sfrp1	TACTGGCCCGAGATGCTCAA	GAGGCTTCCGTGGTATTGGG
Sox9	AGTACCCGCATCTGCACAAC	ACGAAGGGTCTCTTCTCGCT
Tbx3	GAACCTACCTGTTCCCGGAAA	AGTGTCTCGAAAACCCTTTGC
Tiam1	CTTTCTGAGTCTGTGCATTCG	AATCGATGGTAAACCTGTTTCG
Trop2	GTGGCTGAGAGTAAATGTGGG	TTGGTGGAATACTTGTCCGCT
Wwtr1	GAAGGTGATGAATCAGCCTCTG	GTTCTGAGTCGGGTGGTTCTG
Yap	TGAGATCCCTGATGATGTACCAC	TGTTGTTGTCTGATCGTTGTGAT

2.5 Western blotting

2.5.1 Protein extraction

100-140 mg of frozen liver was added to 400 µl in pre-chilled modified RIPA buffer (Table 2.4) in screw-cap tubes containing 1.4mm ceramic beads (Lysing Matrix D tubes, MP Biomedical). Tissue samples were then homogenised using the FastPrep-24 5G Lysis System. Homogenised samples were then stored on ice for 20 minutes before being centrifuged at 13000 x g for 10 minutes at 4°C. The supernatant was transferred to a new Eppendorf tube and spun again at 13000 x g for 10 minutes at 4°C. Supernatant containing the protein was aliquoted into 50-100 µl aliquots, snap frozen in liquid nitrogen and stored at -80 °C until use.

Table 2.4 Modified RIPA Buffer

50 mM Tris pH 8.0
1% Triton X-100
0.5% Sodium Deoxycholate (Deoxycholic acid, sodium salt)
0.1% SDS (sodium dodecyl sulphate)
150 mM Sodium Chloride
Complete protease inhibitor cocktail (Roche)
Phosphatase inhibitor cocktail (Roche)

2.5.2 Protein quantification

Protein quantification was carried out using the Pierce BCA Protein Assay Kit (Thermo Scientific) according to manufacturer's instructions.

2.5.3 Protein sample preparation

Samples were removed from storage at -80 °C and defrosted on ice. 10 µg of protein was mixed with reagents detailed inTable 2.5. Protein was denatured at 70 °C for 10 minutes before loading into gel.

Table 2.5 Protein sample buffer

Reagent	Volume
Sample	x µl
NuPAGE LDS Sample Buffer (4X)	2.5 µl
Deionized Water	to 7.5 µl
Total Volume	10 µl

2.5.4 Protein separation by SDS-PAGE

Samples were loaded into wells pre-cast NuPage 4-12 % Bis-Tris Gel (Invitrogen) submerged in a Novex electrophoresis tank with NuPAGE MES SDS Running Buffer. Full-range Rainbow molecular weight marker (Amersham) was run alongside samples. Gels were then run at 120-200 V until the dye front was seen to reach the end of the gel.

2.5.5 Protein transfer

Gels were taken from the electrophoresis tank, separated from the plastic plates and assembled with the iBlot Transfer Stack, PVDF (Invitrogen). The stack was placed in the iBlot Dry Blotting System (Invitrogen) and run for 7 minutes.

2.5.6 Total protein stain

The membrane was removed from the iBlot stack and washed with TBS/T. Ponceau S stain was added to the mebrane until completely submerged and kept in the solution for 5-10 minutes with gentle rotation at RT. Ponceau S stain was removed and the membrane was washed with distilled water to remove background then imaged. To remove stain completely, the membrane was washed 4-5 x with TBS/T at RT.

2.5.7 Probing and detection of signal

To block non-specific binding, membranes were incubated in 5% w/v non-fat milk powder diluted in TBS/T with agitation for 1 hour at RT. Primary antibody was diluted and applied to membranes with agitation for 1 hour at RT or overnight at 4 °C. Membranes were then washed 3 x 10 mins in TBS/T. Secondary antibody was diluted in blocking solution and applied to membranes with agitation for 1 hour at RT. Primary and secondary antibodies and conditions are detailed in . Membranes were then

washed again for 3 x 10 mins in TBS/T. Signal was detected using SuperSignal West ECL (Thermo Fisher) and the GelDoc UV Transilluminator (Bio-Rad). Signal was quantified using imageJ and normalised to total protein or β-actin.

Table 2.6 Antibody-specific conditions for Western blotting analysis

Primary antibody	Manufacturer	Primary antibody conditions	Secondary antibody conditions
Anti-β-catenin	BD transduction (610153)	1:1000 in 5% milk in TBS/T	HRP-conjugated anti-mouse 1:2000 in 5% milk in TBS/T
Anti-Yap	Cell Signaling (#4912)	1:1000 in 5% milk in TBS/T	HRP-conjugated anti-rabbit 1:2000 in 5% milk in TBS/T
Anti β-actin	Sigma Aldrich (A2228)	1:5000 in 5% milk in TBS/T	HRP-conjugated anti-mouse 1:2000 in 5% milk in TBS/T

2.6 Immunohistochemistry

Immunohistochemistry was performed following the generic protocol described below with specific conditions/modifications to the protocol for each target described in Table 2.7.

The sections underwent the following steps: de-waxing using xylene (two immersions, each lasting 5 minutes), rehydration using sequential immersions in 100% ethanol (two immersions, each lasting 2 minutes), 95% ethanol (2 minutes), and 70% ethanol (2 minutes), and then transferred to distilled water. For antigen retrieval, slides were boiled in prewarmed citrate buffer (Sigma) for 20 minutes. Slides were then allowed to cool to room temperature and washed in distilled water. To block endogenous peroxidase activity, the slides were treated with a hydrogen peroxide solution in distilled water or Peroxidase block solution provided with the Envision* Kit (Dako), followed by 3 x 5-minute washes in distilled water. Non-specific binding of antibodies was prevented by incubating the sections in normal serum from the species in which the secondary antibody was raised in wash buffer for 30 minutes at RT. Primary antibodies (listed in Table 2.7), prepared in a blocking diluent, were applied to the sections and incubated overnight at 4°C. The sections were then washed three times

for 5 minutes in wash buffer and incubated with a secondary antibody or Horseradish peroxidase (HRP) conjugated secondary antibody polymer from the Envision+ kit (Dako). Where Envision+ kits (Dako) were not used, a signal amplification step was incorporated into the protocol using the Avidin-Biotin Complex 'Vectastain' ABC kit (Vector Labs) as described by the manufacturer. Following this incubation, the slides were washed three times for 5 minutes in wash buffer. Bound peroxidase was detected and developed by adding 3,3'-Diaminobenzidine substrate (DAB) at room temperature for 5-10 minutes or until the slides turned brown. The slides were then washed 3 x 5 minutes in distilled water. Next, the slides were counterstained with Mayers Haemalum (R.A. Lamb) for 30-60 seconds and rinsed under cold tap water until the water became clear. Subsequently, the slides were dehydrated by soaking them in increasing concentrations of ethanol (1 minute in 70% ethanol, 1 minute in 95% ethanol, 2 x 1 minute washes in 100% ethanol), followed by 2 x 5-minute washes in xylene. Finally, the slides were mounted with cover slips using DPX mounting solution (Sigma).

Table 2.7 Summary of optimised IHC protocols

Primary Antibody	Non-specific signal block	Wash Buffer	Primary antibody incubation conditions	Secondary antibody	Signal Amplification
Anti-Afp R&D (MAB1368)	Peroxidase: Envision+ Dako 20 mins Serum: 5% NRS	TBS/T	1:200 4 °C O/N	Envision+ HRP-conjugated anti-mouse for 30 mins	N/A
Anti-β-catenin BD transduction (610153)	Peroxidase: Envision+ Dako 20 mins Serum: 5% NRS	TBS/T	1:200 4 °C O/N	Envision+ HRP-conjugated anti-mouse for 30 mins	N/A
Anti-γH2AX Sigma (Upstate 07-164)	Peroxidase: 1.5% for 15 mins Serum: 5% NGS	PBS	1:2000 4 °C O/N	Biotinylated anti goat 1:200 30 mins RT	ABC Kit (Vector)
Anti-BrdU BD Bioscinces #347580	Peroxidase: Envision+ Dako 20 mins Serum: 1% BSA 1 hour	PBS	1:150 4 °C O/N	Envision+ HRP-conjugated anti-mouse for 30 mins	N/A
Anti-Cleaved Caspase 3 Cell Signaling #9661	Peroxidase: 10 mins in 3% H202 Serum: 1% NGS	TBS/T	1:20 for 2 days at 4 °C	Biotinylated anti rabbit 1:200 30 mins RT	ABC Kit (Vector)
Anti-Cps1 Santa Cruz (sc-10516)	Peroxidase: 15 mins in 3% H202 Serum: 5% NRS	TBS/T	1:200 4 °C O/N	Biotinylated anti goat 1:200 30 mins RT	ABC Kit (Vector)
Anti-GS Sigma G2781	Peroxidase: 15 mins in 3% H202 Serum: 5% NGS	TBS/T	1:5000 4 °C O/N	Envision+ HRP-conjugated anti-rabbit for 1 hour	N/A
Anti-Ki67 Vector Labs #VPK453	Peroxidase: 20 mins in 0.5% H202 Serum: 20% NGS	TBS/T	1:20 4 °C O/N	Biotinylated anti rabbit 1:200 30 mins RT	ABC Kit (Vector)
Anti-Yap Cell Signaling #4912	Peroxidase: Envision+ Dako 20 mins Serum: 5% NGS	TBS/T	1:200 4 °C O/N	Envision+ HRP-conjugated anti-rabbit for 1 hour	N/A

2.6.1 Haematoxylin and Eosin (H&E) staining

Tissue sections were de-waxed and rehydrated as described in section 2.6. Sections were then stained in Mayer's Haemalum (R. A. Lamb) for 5 mins followed by washing in running tap water for 5 mins. Sections were then stained in 1% aqueous Eosin (R. A. Lamb) for 5 mins followed by two 15 second washes in water. Sections were then dehydrated, cleared and mounted as described in section 2.6.

2.6.2 Detecting β-galactosidase activity

Mice bearing the Rosa26/LacZ reporter transgene were used to assess levels of recombination in whole mount liver and BD organoids. The liver or organoids were fixed for 1 hour in LacZ fixative solution at room temperature. Liver and organoids were then washed in LacZ washing buffer and stained overnight at 37 °C in LacZ staining solution. Liver or organoids were then washed with PBS and imaged. Solutions for LacZ staining are detailed in Table 2.8.

Table 2.8 Solutions for LacZ staining

LacZ fixative	PBS Glutaraldehyde (0.2%) EGTA (5mM) MgCl2 (2mM) NP40 (0.02%)
LacZ washing buffer	PBS MgCl2 2mM NP40 (0.02%) NaDeoxycholate (0.01%)
LacZ staining buffer	LacZ washing buffer K4Fe(CN)63H2O (5mM) K3Fe(CN)6 (5mM) - kept in the dark X-Gal solution (2 mg/ml) added directly before staining

2.7 ES cell culture

mES cells containing LoxP sites flanking exon 2 of Axin1, Axin2 and both Axin1 and Axin2 had previously been generated in the Dale lab by Anika Offergeld. To seed from frozen, cells were thawed in a water bath at 37 °C, washed in ES base medium (Table 2.9), spun at 250 x g for 5 min, aspirated and resuspended in appropriate amounts of 2i medium (Table 2.9) before being seeded on 0.1 % gelatine (Millipore) coated

Nunc™ Cell-Culture plates. Cells were maintained at 37 °C with 5 % CO2 in a humidified incubator and were fed every 1-2 days and split every 2-3 days.

To split cells, media was aspirated, cells washed with pre-warmed PBS and then disassociated with StemPro™ Accutase™ Cell Dissociation Reagent (Gibco) at 37 °C, 5% CO2 for 5-10 minutes until cells had lifted off plate. To stop the dissociation reaction, ES base medium was added (about 5 times the amount of Accutase). Cells were either split 1:4 to 1:8 or counted using a haemocytometer, the required number of cells were spun at 250 x g for 5 minutes and seeded depending on the experiment.

Table 2.9 ES cell media composition

Medium	Purpose
ES base medium	
DMEM/F12 GlutaMAX β-Mercaptoethanol (10-4M) Fetal Bovine Serum (FBS) ES qualified (10%) optional: Pen and Step (50U/ml and 50 µg/ml final)	Washing Only added when working with open plates (i.e. picking)
2i medium	
ES base medium LIF (106 U/l, ESGRO) PD0325901 (0.5 µM, Stemgent) CHIR99021 (3 µM, Stemgent)	Maintenance of ES cells
ES freezing medium	
ES base medium 50% FBS 40% DMSO 10%	Freezing ES cells
Selection medium	
2i medium Puromycin (1 µg/ml, Sigma-Aldrich, 500mg/ml) OR Genetecin™ G418 (200 µg/ml, Gibco 50 mg/ml)	Selection of antibiotic resistant cells after transfection with pCAGGS-Cre-IRESpuro or CRISPR/Cas9 constructs) Selection of antibiotic resistant cells after transfection with pAN-MerCreMer

2.7.1 Targeting constructs

Targeting constructs were designed and amplified from mouse DNA using Platinum™ Pfx DNA Polymerase (Invitrogen) by Anika Offergeld. Left and right homologous arms after exon 10 of Axin1 were cloned into pCR-XL-TOPO vector (Addgene #19688) along with a LoxP site and a Pst1 restriction site. Left and right homologous arms after exon 10 of Axin2 were cloned into pCR-BluntII-TOPO (Invitrogen K280002) with a LoxP site and a Pst1 restriction site.

2.7.2 Plasmid linearisation

For transfection, plasmids containing Axin1 or Axin2 targeting constructs were linearized by restriction digests using enzymes EcoRI-HF (NEB) and XhoI (NEB). For the digestion, 2 μg of plasmid was mixed with 1 μl EcoRI-HF, 1 μl XhoI, 2.5 μl of CutSmart® Buffer (NEB) and up to 25 μl with H2O. The mix was incubated at 37°C for at least 2 hours. This was run on a 2% agarose gel using 1:1 low melting agarose and normal agarose. For Axin1 the lower band at 2403bp or for Axin2 the band at 1835bp was cut out and a gel extraction was performed using QIAEX II Gel Extraction Kit (Qiagen, 20021) as per manufacturer's instructions.
For stable transfection of pAN-MerCreMer, the plasmid was linearized using SfiI (NEB) restriction enzyme in CutSmart® Buffer at 50°C for 1 hour.

2.7.3 Cas9 plasmid isolation and transformation of sgRNA

An Agar stab of bacteria transfected with the plasmid pSpCas9n(BB)-2A-Puro (Addgene) was grown overnight in 100 ml LB medium with 100 μg/ml ampicillin. This was followed by a maxi prep using QIAGEN Plasmid Maxi kit as per manufacturer's instructions.
Target oligos with 4nt overhangs compatible for cloning into the BBSI restriction site of the Cas9n vector and a G base at the transcription site required for the U6 promoter were synthesised by Sigma Aldrich. 1 μl of forward and 1 μl reverse sgRNA (100 μM) in 8 μl of H2O was annealed at 95°C in a thermocycler for 5 minutes and then left at RT for 1 hour to cool down, then diluted 1:200.
Cas9n vector (2 μg) was digested with 1 μl BbSI (NEB) enzyme, 2 μl 10x NEB Buffer 2.1 and H2O to final volume of 20 μl for at least 3 hours at 37°C. Digested vector (100 ng) and 2 μl of annealed oligo duplex was set up in a ligation reaction with 2 μl 10x

DNA ligase buffer and 1 μl T4 ligase up to 20 μl final volume with H2O at 4°C overnight. Each plasmid was transduced into One Shot® TOP 10 Competent cells (Invitrogen) according to manufacturer's instructions. Plasmid was isolated using Qiagen Mini Prep kit as per manufacturer's instructions and sent for sequencing at DNA Sequencing Services, University of Dundee using U6-Fwd Primer GAG GGC CTA TTT CCC ATG ATT CC

Table 2.10 Axin1 sgRNA

short name			
	2T1	A GTOP1:	Fwd: CACC**G**CATGTTATCCATTCTTGCCC Rev: AAAC**GGGCAAGAATGGATAACATG**C
	2T2	A GTOP2	Fwd: CACC**G**TAAAGGCCAGGGGCCAAACT Rev: AAAC**TAGTTTGGCCCCTGGCCTTTA**C
	2T3	A GTOP3	Fwd: CACC**G**CAGGCAAAGCCCTAAAGGCC Rev: AAAC**GGCCTTTAGGGCTTTGCCTG**C
	2B1	A GBOTTOM1	Fwd: CACC**G**AGTAGTGAAGGAGGCAAGAT Rev: AAAC**GATCTTGCCTCCTTCACTACT**C
	2B2	A GBOTTOM2	Fwd: CACC**G**CTTAACATGTTATCCATTCT Rev: AAAC**AGAATGGATAACATGTTAAG**C

Table 2.11 Axin2 sgRNA

short name			
	2T4	C TOP4:	Fwd: CACC**G**GCTTTCCCTTGCTTAAGCT Rev: AAAC**AGCTTAAGCAAGGGAAAGC**C
	2T5	C TOP5:	Fwd: CACC**G**AAGCTTGGCTCTGAGGGGTC Rev: AAAC**GACCCCTCAGAGCCAAGCTT**C
	2T6	C TOP6:	Fwd: CACC**G**AGGCACGGTAAAGTTACAC Rev: AAAC**GTGTAACTTTACCGTGCCT**C
	2B4	C Bottom 4:	Fwd: CACC**G**CCAGACATTCATGTACAAAA Rev: AAAC**TTTTGTACATGAATGTCTGG**C
	2B5	C Bottom 5:	Fwd: CACC**G**ATGTACAAAATGGGTTCCCC Rev: AAAC**GGGGAACCCATTTTGTACAT**C
	2B6	C Bottom 6:	Fwd: CACC**G**CTCAGAGCCAAGCTTAAGCA Rev: AAAC**TGCTTAAGCTTGGCTCTGAG**C

2.7.4 ES cell transfection with CRSIPR/Cas9n

Cells were plated at 0.06x106 per well on 24 well plates coated with gelatine in 500 μl 2i medium. The following day, cells were transfected with 250 ng of each sgRNA-Cas9n TOP and BOTTOM pair and 500 ng linearized targeting plasmid. In brief, 2 μl per well Lipofectamine 2000 (Invitrogen) was added to 10 μl per well OptiMEM (Gibco). 500 ng per well targeting plasmid was added to 40 μl per well OptiMEM, this mix was split, 20 μl per final well, 250 ng of the required TOP version of the sgRNA-Cas9n

plasmid was added to one tube and 250 ng of the required BOTTOM plasmid was added to the other. The TOP and BOTTOM mixes were combined in equal amounts and 40 μl for each well was added to 10 μl of Lipofectamine mix. The DNA and Lipofectamine mix was incubated for 20 minutes and 50 μl was added to each well containing cells. Cells were incubated with transfection mix for 4-6 hours and replaced with fresh 2i medium. The next day, 2-3 wells were split onto 2 wells of a 6 well plate in selection medium containing 1 μg/ml Puromycin. After 2 days, medium was changed back to normal 2i medium and left until colonies were big enough to pick, usually about 10 days with medium being changed occasionally. To pick colonies, medium was aspirated, and cells covered with 2 ml PBS. Clones were picked under a microscope using a P20 pipette set at 10 μl, they were ejected onto a 96 well v-bottomed plate containing 20 μl Accutase and incubated at 37 °C for 10 minutes. Disassociation reaction was stopped with 2i medium with pen/strep and plated out between 2 wells of a gelatine coated 96 well flat bottom plate with 100 μl 2i medium with pen/strep in each well. Clones were fed when necessary and left to grow until confluent. Once confluent, medium was removed into 8-strip PCR tubes, cells washed with PBS and 30μl of Accutase added and incubated at 37 °C for 5-10 minutes. The saved medium was used to stop the disassociation, 1/8 of cells was plated on 96 well v-bottomed plates for genotyping. The rest was returned to 8-strip PCR tubes, spun for 10-20 seconds on small tabletop centrifuge, medium was aspirated, and cells re-suspended in 200 μl freezing medium. The cells were then frozen until further use.

2.7.5 ES cell transfection with pCAGGS-Cre-IRESpuro

For transfection with pCAGGS-Cre-IRESpuro, cells were seeded at $0.06x10^6$ cells on 24 well plates in 2i medium. The following day, transfection reagents were prepared. To each well 1 μg per well of linearized plasmid with 1 μl of Lipofectamine2000 was added as per manufacturer's instructions. The cells were incubated with the DNA / Lipofectamine2000 / OptiMEM mix for 4-6 hours after which this was replaced with fresh 2i medium. The next day, 2-3 wells were split onto 2 wells of a 6 well plate in selection medium containing 1 μg/ml Puromycin. After 2 days, medium was changed back to normal 2i medium and left until colonies were big enough to pick, usually about 10 days with medium being changed occasionally. Colonies were grown for freezing and genotyping as previously described.

2.7.6 ES cell transfection with pAN-Mer-Cre-Mer and 4-OHT induction

For stable transfection, cells were transfected with Sfi1-linearized pAN-MerCreMer plasmid (Zhang et al. 1996). $0.06x10^6$ cells/well were seeded on 24 well plates in 2i medium. The following day, transfection reagents were prepared. To each well, 1 μg of linearized plasmid with 1 μl of Lipofectamine2000 was added as per manufacturer's instructions. The cells were incubated with the DNA / Lipofectamine2000 / OptiMEM mix for 4-6 hours after which this was replaced with fresh 2i medium. The next day, 2-3 wells were split onto 2 wells of a 6 well plate in selection medium containing 200 μg/ml G418. Cells were kept in selection media until clones were big enough to pick. Colonies were grown for freezing and genotyping as previously described. Clones positive for pAN-MerCreMer were induced with 0 nM 4-OHT (4-Hydroxytamoxifen, Sigma) as a control, 100 nM 4-OHT or 800 nM 4-OHT, dissolved in ethanol, for 48-96 hours.

2.7.7 ES cell viability assays

2.7.7.1 Wst-1

To determine cell viability, 10 % WST-1 reagent (Roche) was added directly to the medium of cultured cells and incubated for 1 hour. Cells were seeded at 20,000 cells / cm^2 on a 96 well, gelatine coated plate. Absorbance of wells was measured at 450 nm and 590 nm using FluoStar OPTIMA (BMG Labtech) to determine levels of formazan formed by viable cells.

2.7.7.2 CellTiter-Glo Luminescent Cell Viability Assay

CellTiterGlo (Promega) luminescent cell viability assay was performed as an endpoint assay to determine the number of viable cells. The assay relies on ATP as an indicator for metabolically active cells.
Cells were seeded at 10,000 cells / cm2 on a 96 well, gelatine coated, black clear bottom plate in 100 μl medium. For the assay, equal volume of CellTiterGlo was added to the culture medium at desired time points, incubated for 15 minutes at RT on an orbital shaker and luminescence was read using the FluoStar OPTIMA plate reader.

2.7.7.3 Simultaneous viability and toxicity assay

Real Time-Glo MT Cell Viability Assay (Promega) and CellTox Green Cytotoxicity Assay (Promega) on continuously growing ES cell cultures was used to assess the proportion of dead and live cells in each well. The viability assay depends on the reduction of a NanoLuc substrate in metabolically active cells. The cytotoxicity assay is based on the change in membrane integrity as the result of cell death. Cells were seeded at 20,000 cells / cm^2 on a 96 well, gelatine coated, black clear bottom plate in 100 µl medium containing Real Time Glo and CellTox reagents according to manufacturer's instructions. Fluorescence levels indicting dead cells and luciferase activity indicating metabolically active cells were measured after plating, at 24 hours and 48 hours.

2.8 Human hepatocyte culture

2.8.1 Collagen coating plates

For human primary hepatocyte monolayer 2D culture, plates were first coated with collagen type I from rat tail (Thermofisher) using the thin coating procedure of the manufacturer. Briefly, collagen was diluted to 50 µg/ml in 20 mM acetic acid. Plates were incubated with the collagen solution for 1 to 2 hours at RT, rinsed three times with PBS and air dried. Plates were used immediately or stored at 4 °C for up to 1 week for future use.

2.8.2 Thawing human primary hepatocytes

Cryopreserved hepatocytes were purchased from Lonza. Hepatocytes were thawed according to the manufacturer's instructions. In brief, cells were thawed at 37 °C in a water bath for 90-120 seconds. Cells were then transferred to 40-45 ml thawing media (Lonza) and carefully suspend. Cells were centrifuged at 100 x g for 8 minutes at RT and the supernatant was poured off. Cells were then gently resuspended in 3 ml of plating media (Lonza) and viability was determined using acridine orange and propidium iodide staining.

2.8.3 Determining cell concentration and viability

To determine cell viability, 18 µl of cells in suspension were mixed with 2 µl of acridine orange and propidium iodide dual stain (Thermofisher). 10 µl of mixture was then

loaded onto a LUNA cell counting slide and concentration, viability and average size of the cells was calculated by a fluorescence automated cell counter (LabTech).

2.8.4 2D plating of primary human hepatocytes

500,000 cells in 500 µl plating media were seeded per well in a collagen coated 24 well plate. Plates were placed in a 37 °C 5 % CO_2 incubator. To disperse cells evenly plates were moved in a north, south then east, west motion while in contact with the incubator shelf. This was repeated every 15 minutes for an hour, then media was aspirated and replaced with fresh plating media. Cells were then incubated for 4-6 hours to allow cells to attach, and plating media was replaced with pre-warmed maintenance media (Lonza) which was then replaced daily. For Matrigel overlay, Matrigel was diluted in maintenance media to a concentration of 0.3 mg/ml on ice then added to wells after the 4-6 hours plating media incubation and aspiration. Plates with Matrigel overlay were incubated for 2 hours before adding prewarmed maintenance media which was then replaced daily.

2.8.5 3D plating of primary human hepatocytes

Hepatocytes were resuspended in ice-cold Matrigel at a concentration of either 200, 400 or 800 cells/µl in 50 µl hydrogel drops were pipetted onto 24-well plates pre-warmed at 37°C. After seeding, plates were incubated to 2-3 minutes at 37 °C, flipped upside down and incubated for other 10-12 minutes at 37 °C to allow Matrigel to set. One of 5 media detailed in Table 2.12 was subsequently added and replaced every 2-3 days.

2.8.6 PDX tumours

Champions Oncology (USA) provided cryopreserved PDX fragments to TransCure bioServices (France). These were bilaterally implanted into one animal per PDX model. The tumours were harvested once they reached 1000 mm^3 in size, and fragments of around 300 mm^3 were immersed in Hibernate A Medium (Invitrogen) at 4 °C and shipped. Alternatively, cryopreserved PDX fragments were shipped directly to Cardiff University to try to establish PDX derived organoids from frozen.

Fresh samples of PDX were divided into four parts, one part was fixed in formalin for histological analysis, one part frozen in RNA*later*, one part snap frozen and one part used for establishing PDX derived organoids.

2.8.7 PDX digestion and seeding

PDX tumours were transferred to a 10 cm petri dish in a primary tissue culture hood and minced using a scalpel. Chopped pieces of tumour were washed in Advanced DMEM before being digested at 37 °C for 1 hour. Digestion media used: 2 mg/ml collagenase type IV, 20μg/ml DNAseI, 10 mM HEPES, 1 % FBS in Advanced DMEM/F12. The digested tissue suspension was sequentially sheared using 10 ml and 5 ml serological pipettes and then 1 ml tips. The suspension was then strained over a 100 μm filter. Any tissue retained on filter was subsequently sheared again with Advanced DMEM then passed through the filter again. FBS was added to final concentration of 2 % to the strained suspension to stop digestion and the cells were centrifuged at 300 x g for 5 minutes. Erythrocytes were lysed in 5 ml red blood cell lysis buffer for 5 min at RT before the addition of 20 ml Advanced DMEM. Cells were centrifuged at 300 x g for 5 minutes and had a repeat wash with Advanced DMEM before viability was assessed as in 2.8.3.

Table 2.12 Media compositions used for human primary hepatocytes

Media 1 (Hu Media)	Media 2 (Peng Media)	Media 3 (Peng+Hu)	Media 4 (Peng-CHIR++)	Media 5 (Peng-CHIR+6)
Advanced DMEM/F12	William's E medium	William's E medium	William's E medium	William's E medium
1% Glutamax	1% Glutamax	1% Glutamax	1% Glutamax	1% Glutamax
1% Pen/Strep	1% Pen/Strep	1% Pen/Strep	1% Pen/Strep	1% Pen/Strep
10mM HEPES	10mM HEPES	10mM HEPES	10mM HEPES	10mM HEPES
1% B27	1% Non-Essential Amino Acids	1% Non-Essential Amino Acids	1% Non-Essential Amino Acids	1% Non-Essential Amino Acids
1.25 mM n-Acetylcysteine	1% N2	1% N2	1% N2	1% N2
10 mM Nicotinamide	2% B27	2% B27	2% B27	2% B27
50 ng/ml EGF	1.25 mM n-Acetylcysteine	1.25 mM n-Acetylcysteine	1.25 mM n-Acetylcysteine	1.25 mM n-Acetylcysteine
50 ng/ml HGF	10 mM Nicotinamide	10 mM Nicotinamide	10 mM Nicotinamide	10 mM Nicotinamide
2 μM A83-01	25 ng/ml EGF	25 ng/ml EGF	25 ng/ml EGF	25 ng/ml EGF
10 μM Y27632	50 ng/ml HGF	50 ng/ml HGF	50 ng/ml HGF	50 ng/ml HGF
3 μM CHIR99021	1 μM A83-01	1 μM A83-01	1 μM A83-01	1 μM A83-01
10 nM Gastrin	10 μM Y27632	10 μM Y27632	10 μM Y27632	10 μM Y27632
100 ng/ml FGF7	3 μM CHIR99021	3 μM CHIR99021	100 ng/ml Wnt9b	100 ng/ml Wnt9b
100 ng/ml FGF10	100 ng/ml TNFα	100 ng/ml TNFα	50 ng/ml RSPO3	50 ng/ml RSPO3
20 ng/ml TGFα		10 nM Gastrin	100 ng/ml TNFα	100 ng/ml Shh
300 ng/ml RSPO1		100 ng/ml FGF7		50 ng/ml IL6
		100 ng/ml FGF10		100 ng/ml HB-EGF
		20 ng/ml TGFα		50 μM Serotonin
		300 ng/ml RSPO1		100 ng/ml TNFα

PDX cells were resuspended in ice-cold Matrigel at a concentration of 1000 cells/µl in 50 µl hydrogel drops and were pipetted onto 24-well plates. Matrigel was set using the same method described in section 2.8.5. The media added was either Hu, Peng or Hu+Peng as described in Table 2.12 or Broutier tumour isolation media or Broutier normal isolation media. After the first passage, both tumour and normal Broutier media were replaced with Broutier expansion media (Table 2.13). Media was replaced every 2-3 days.

Table 2.13 Broutier media compositions

Broutier Tumour Isolation Media	Broutier Normal Isolation Media	Broutier Expansion Media
Advanced DMEM/F12	Advanced DMEM/F12	Advanced DMEM/F12
1 % Glutamax	1 % Glutamax	1% Glutamax
1 % Pen/Strep	1 % Pen/Strep	1% Pen/Strep
10 mM HEPES	10 mM HEPES	10 mM HEPES
1 % N2	1 % N2	1 % N2
1 % B27	1 % B27	1 % B27
1.25 mM n-Acetylcysteine	1.25 mM n-Acetylcysteine	1.25 mM n-Acetylcysteine
10 mM Nicotinamide	10 mM Nicotinamide	10 mM Nicotinamide
50 ng/ml EGF	50 ng/ml EGF	50 ng/ml EGF
25 ng/ml HGF	25 ng/ml HGF	25 ng/ml HGF
5 µM A83-01	5 µM A83-01	5 µM A83-01
10 µM Y27632	10 µM Y27632	10 nM Gastrin
10 nM Gastrin	25 ng/ml Noggin	100 ng/ml FGF10
100 ng/ml FGF10	10 nM Gastrin	10 µM Forskolin
10 µM Forskolin	100 ng/ml FGF10	10 % RSPO1 conditioned media
3 nM Dexamethasone	30 % Wnt3a conditioned media	
	10 % RSPO1 conditioned media	
	10 µM Forskolin	

2.8.8 PDX organoid passage

14 days after seeding, organoids were passaged. For organoid passage, media was removed from the well and Matrigel was disrupted and collected using ice-cold PBS. Organoids were pelleted at 300 x g for 5 min, re-suspended in TrypLE (Gibco) and

incubated in a water bath at 37 °C for 5-10 min. Organoids were resuspended using a P200 every 3 min during this incubation time and organoid cell dissociation was monitored under the microscope. TrypLE digestion was interrupted by adding 10 ml of ice-cold William's E or Advanced DMEM media. Cells were pelleted at 300 x g, 5 min, and resuspended 500 cells/µl in Matrigel. Organoids were split at appropriate ratios and when required depending on growth.

2.8.9 Mouse cell depletion

Organoids were digested using TrypLE as described in 2.8.8. After the media wash, as much media as possible was aspirated away. Mouse cell depletion was then carried out using Miltenyi Biotec kit following manufacturer's instructions. In brief, 80 µl mouse depletion buffer was added per 2×10^6 cells with 20 µl Mouse Cell Depletion Cocktail. Cells were then incubated for 15 min on ice then a further 400 µl mouse depletion buffer per 2×10^6 tumour cells was added. This mix was put through the LS column in the MidiMACS separator and the flow through containing human cells was collected. Cells were centrifuged at 300 x g for 5 mins and resuspend in cold Matrigel before seeding.

2.8.10 RNA extraction from organoid cultures

Media was aspirated away from Matrigel containing organoids and the plate was placed on ice. 500 µl of Trizol was added to each well to disrupt the Matrigel and organoids, this mix was placed into an Eppendorf. A further 500 µl of Trizol was added to the well to collect any remaining material and added to the Eppendorf. Tubes were vortexed to lyse cells and the rest of the RNA extraction protocol outlined in 2.4.2 was then followed.

Table 2.14 Human primer sequences used for RT-qPCR

Gene	Forward Primer 5'-3'	Reverse Primer 5'-3'
HNF4α	CGAAGGTCAAGCTATGAGGACA	ATCTGCGATGCTGGCAATCT
SERPINA1	GATCAACGATTACGTGGAGAAGG	CCTAAACGCTTCATCATAGGCA
GLUL	CCTGCTTGTATGCTGGAGTC	GATCTCCCATGCTGATTCCT
KRT18	GGCATCCAGAACGAGAAGGAG	ATTGTCCACAGTATTTGCGAAGA
AFP	CTTTGGGCTGCTCGCTATGA	GCATGTTGATTTAACAAGCTGCT
KRT19	TGAGTGACATGCGAAGCCAAT	CTCCCGGTTCAATTCTTCAGTC

2.9 Paraffin embedding of organoids

Media was removed and organoids were fixed in Matrigel overnight with 10 % formalin at 4 °C. The next day organoids were transferred to an Eppendorf spun at 200 x g and washed twice with cold PBS. 200 μl of 4 % Low melting agarose at 60 °C was added to the organoids and re-suspended carefully to avoid creating bubbles then left on ice to set. The agarose and organoid pellet was removed and placed in 70 % ethanol before paraffin embedding by the Histology Unit staff.

2.10 Bile Duct organoid culture

2.10.1 Bile duct isolation and plating

Livers were dissected from mice of appropriate genotype and placed in extraction medium of DMEM high glucose, 10 % FBS, 50 U/ml Penicillin and 50 μg/ml Streptomycin. Livers were then transferred to a primary tissue hood and treated under sterile conditions from this point onwards. In a 10 cm petri dish liver was chopped up to small pieces using a scalpel. At this point fragments could be frozen for future use in freezing media of Advanced DMEM/F12 with 40 % FBS and 10 % DMSO or continued to be processed for bile duct isolation based on the protocol in (Huch et al. 2013). To this end, liver fragments were transferred into a 15 ml conical tube containing Advanced DMEM/F12 media and washed two times by letting the fragments to settle and replacing the media. After the second wash, media was replaced with 5 ml of digestion media (125 μg/ml collagenase type XI, 125 μg/ml dispase, 1:100 GlutaMAX, 1 % Pen/Strep, 5 % FBS in DMEM) and incubated at 37 °C in a water bath for 1 to 3 hours. Fragments were agitated in rotary motion every 5-10 min and pipetted up and down every 20-30 min. After each pipetting step, digestion media was replaced and supernatants were collected, transferred to a petri dish and screened under the microscope for the presence of bile ducts. BDs were hand-picked using a P20 pipette

and collected. Excess media was aspirated, and pooled bile ducts were then mixed with Matrigel and plated with BD Isolation Media (Table 2.15) to generate of BD organoids. After 2 days media was changed to Expansion media and changed every 2-3 days until organoids were formed and ready for passage.

Table 2.15 BD organoid media

Isolation Media	Expansion Media	Differentiation Media
Advanced DMEM/F12	Advanced DMEM/F12	Advanced DMEM/F12
1x Glutamax	1x Glutamax	1x Glutamax
1x Pen/Strep	1x Pen/Strep	1x Pen/Strep
10 mM HEPES	10 mM HEPES	10 mM HEPES
1x B27	1x B27	1x B27
1 mM n-Acetylcysteine	1 mM n-Acetylcysteine	1x N2
10 mM Nicotinamide	10 mM Nicotinamide	1 mM n-Acetylcysteine
50 ng/ml EGF	50 ng/ml EGF	50 ng/ml EGF
50 ng/ml HGF	50 ng/ml HGF	10 nM Gastrin
10 nM Gastrin	10 nM Gastrin	100 ng/ml FGF10
100 ng/ml FGF10	100 ng/ml FGF10	10 µM DAPT
300 ng/ml RSPO1	300 ng/ml RSPO1	50 nM A8301
100 ng/ml Noggin		* 3µM Dexamethasone
20 % Wnt3a Conditioned Media		*only for last 3 days

2.10.2 Passage and expansion of BD organoids

For routine maintenance, organoids were cultured in BD expansion medium (Table 2.15) and passaged at a ratio of between 1:3 to 1:6 by mechanical disruption every 5 to 7 days and cultured in 50 µl Matrigel drops. When plating for experiments such as gene expression or immunostaining, organoids were dissociated for 5 min at 37 °C with TryplE into single cells and seeded at a density of 200 cells/µl of Matrigel.

2.10.3 Cryopreservation and recovery of BD organoids

For long term storage, bile duct organoids were harvested with ice-cold PBS, pelleted by 5 min 300 x g centrifugation, and resuspended in freezing media made up of Expansion media, 40 % FBS and 10 % DMSO. BD organoids were then distributed in

2 ml cryovials and placed in a Mr. Frosty freezing container (Thermofisher) in a -80 °C freezer.

For recovery, vials were thawed in the water bath at 37 °C. Organoids were washed with pre warmed Advanced DMEM/F12 and pelleted at 250 x g for 5 min. Organoids were then resuspended in Matrigel and plated at an appropriate density and overlayed with Expansion media (Table 2.15).

2.10.4 Differentiation of BD organoids

For differentiation, organoids were passaged and allowed to recover for 2 days in EM then switched to BD organoid differentiation medium (DM) (Table 2.15) and cultured for 13 days. DM was changed every 2 days then daily when Dexamethasone was added at day 10.

2.10.5 Induction of BD organoids

For dynamic induction, 1 μM BNF diluted in DMSO and 1 μM of 4-OHT diluted in ethanol were both added to Expansion or Differentiation media 2 days after initial recovery and maintained throughout the 13 day differentiation protocol.

For stable induction organoids were passaged and allowed to recover for 2 days in Expansion media then Expansion media with 1 μM BNF diluted in DMSO and 1 μM of 4-OHT diluted in ethanol was added and changed every 2 days. After 7 days in expansion media with the inducing agents, organoids were passaged and plated at 200 cells/μl of Matrigel for the differentiation protocol.

2.10.6 Transfection of BD organoids with CAG-Cre:GFP

Organoids were grown to 80-90 % confluency and a pool of 3 wells of 24 well plate were pipetted into 15 ml falcon. Organoids were disassociated to single cell with TrypLE Express (2 ml for 5 minutes at 37 °C). To stop the reaction, 10 ml cold Advanced DMEM was added and centrifuged at 300 x g for 5 minutes. Supernatant was removed and resuspend in 450 µl expansion media plus 25 ng/ml noggin and 10 µM Y-27632 and kept on ice until transfection. Transfection reagents were prepared as follows: Tube 1 - 25 µL Opti-MEM and 1.5 µL Lipofectamine 3000 reagent, Tube 2 - 25 µL Opti-MEM, 0.5 µg DNA and 1µL P3000 reagent. Tube 2 was added to Tube 1, mixed well and incubated at RT for 15 minutes. The DNA:Lipofectamine mix was

added to the 450 µl single cell suspension and transferred to single well of 24 well plate. The plate was sealed with parafilm and centrifuged at 32 °C at 600 x g for 1 hour. The parafilm was removed and the plate was incubated in tissue culture incubator at 37 °C for 2-4 hours. The transfection mixture and cells were transferred to a 1.5 ml tube and centrifuge at 400 x g for 5 minutes at RT before being resuspend in Matrigel. Expansion medium with 25 ng/ml noggin and 10 µM Y-27632 was added and after 2-3 days cells were FACS sorted for GFP. Sorted cells were expanded until sufficient organoids were generated for experiments.

2.10.7 Whole mount staining of BD organoids

Organoids were plated in 10 µl of Matrigel in clear bottom black walled plates or an 8-well Ibidi chamber slide for differentiation. At the end of the 13-day protocol, Matrigel drops were washed twice with pre-warmed PBS then fixed for 30 mins with 4 % PFA at RT. Fixed organoids were then washed 3 x 10 mins in PBS. Plates could be stored at 4 °C with organoids covered in PBS before proceeding with immunofluorescence staining.

Organoids were washed with fresh PBS then incubated with IF blocking solution (10 % horse serum, 0.1 % BSA, 0.2 % Triton X-100, 0.05 % Tween 20 in PBS) for 3-5 hours at RT or O/N at 4 °C. Organoids were washed 3 x 10 mins PBS then primary antibody (Table 2.16) was added diluted 1:200 in IF buffer (0.1 % BSA, 0.2 % Triton X-100, 0.05 % Tween 20 in PBS) and left O/N at 4 °C. Organoids were then washed 3 x 10 mins in IF buffer and then 1 more time O/N. The next day organoids were incubated with secondary antibody (Table 2.16) diluted 1:200 in IF buffer O/N at 4 °C. Organoids were then washed 3 x 10 mins in IF buffer and then 1 more time O/N. Organoids were counterstained with 5 µg/ml Hoechst for 30 mins before a final wash of 3 x 10 mins in PBS.

Table 2.16 Antibodies used in wholemount BD organoid staining.

Primary Antibody	Secondary Antibody
Anti-β-catenin BD transduction (610153)	Goat anti-Mouse IgG (H+L) Cross-Adsorbed Secondary Antibody, Alexa Fluor 568. Catalog # A-11004
Anti-phospho-Histone H2A.X Sigma-Aldrich 05-636 (Ser139), clone JBW301	Goat anti-Mouse IgG (H+L) Cross-Adsorbed Secondary Antibody, Alexa Fluor 568. Catalog # A-11004
Anti-Ki67 Vector Labs #VPK453	Goat anti-Rabbit IgG (H+L) Highly Cross-Adsorbed Secondary Antibody, Alexa Fluor 488. Catalog # A-11008

2.10.8 CellTiter-Glo 3D luminescent BD organoid viability assay

For CellTiter-Glo 3D, BD organoid cells in 10 μl (200 cells /μl of Matrigel) were seeded in white opaque 96 well plates. Each time-point was set up on a separate plate. 3 biological and at least 3 technical repeats were plated out. All genotype groups were carried out in parallel. Media was replaced every 2 days during the differentiation protocol (daily during the last 3 days). At each time point an equal amount of RT CellTiter-Glo 3D solution to media was added to each well. Plates were covered with foil and put on an orbital shaker for 15 minutes at RT. Luminescence was read using the FluoStar OPTIMA plate reader.

2.10.9 Statistical analysis

GraphPad Prism 9.5 Software was used for all statistical analysis and graphs representation. Statistical tests used are indicated in each individual figure. Analysis of 3 or more groups used Ordinary one-way ANOVA and Tukey's multiple comparison test, with a single pooled variance. P values were adjusted to account for multiple comparisons. Comparison between 2 groups used Unpaired, 2-tailed, T-test, assuming both populations have Gaussian distribution and equal SD. Survival was calculated using Kaplan-Meier analysis with Log-rank (Mantel-Cox) test to calculate Chi square and p value

Significant differences between samples were based on a P-Value <0.05, degrees of significance are represented as *(P<0.05), **(P<0.01), ***(P<0.001), and ****(P<0.0001)

Chapter 3: Acute and long-term effects of induced Axin loss in the mouse liver

3.1 Introduction

The *in vivo* study carried out by Gui-Jie Feng (Feng et al. 2012) showed that the loss of Axin1 in the mouse liver resulted in an acute and persistent increase in proliferation and a late onset of HCC. Although a subset of Wnt target genes were shown to be activated (*Axin2, c-Myc, cyclin D1*), no increase in nuclear levels of β-catenin or changes to liver zonation were observed as seen with the loss of Apc or the constitutive activation of β-catenin. It was hypothesised that Axin2 may be acting to partially compensate for the loss of Axin1.

The tumours observed were recapitulated in a separate study by Abitbol using an alternative Axin1 deletion model (Abitbol et al. 2018). Additionally, the Abitbol study showed that these tumours show a similar phenotype as seen in cases of HCC with AXIN1 mutations which is consistent with the proliferative class of HCC as outlined by (Lee et al. 2006, Boyault et al. 2007, Hoshida et al. 2009 and Chiang et al. 2008). Furthermore, the Abitbol study identified a Yap and Notch signature common to AXIN1 mutated HCC.

In this chapter, I aimed to test the hypothesis that the lack of a clear strong Wnt/β-catenin signature in Axin1 mutant HCC was due to partial compensation via Axin2. The experimental approach employed the use of the conditional deletion of Axin1 and or Axin2 in the mouse liver. The effects of acute and long term Axin deletion on liver homeostasis will be examined.

3.2 Results – Analysis of mouse liver at Day 6 post AhCreER^T driven Axin recombination.

3.2.1 Induction of AhCreER^T drives recombination in the mouse liver.

To examine the role of Axin1 and Axin2 in the mouse liver, animals bearing the AhCreER^T transgene were crossed with those bearing *loxP* flanked alleles of Axin1 and Axin2 in which exon 2 could be deleted following Cre-mediated recombination (Figure 3.1A). The animals generated had combinations of the following alleles:

AhCreER^{T+}; Axin1$^{wt/wt}$; Axin2$^{wt/wt}$ (Control), AhCreER^{T+}; Axin1$^{fl/fl}$, AhCreER^{T+}; Axin2$^{fl/fl}$ and AhCreER^{T+}; Axin1$^{fl/fl}$; Axin2$^{fl/fl}$. Exon 2 of both Axin genes contains the ATG start codon and the RGS domain which has been shown to be important in Axin functions, including APC recruitment to the β-catenin destruction complex (Hart et al. 1998). Embryonic conditional deletion of exon 2 of Axin1 (Axin1$^{\Delta/\Delta}$) (Offergeld 2015) was shown to phenocopy the classic Axin1 null Axin$^{Tg1/Tg1}$ allele (Perry et al. 1995; Zeng et al. 1997), suggesting the Axin1$^{\Delta/\Delta}$ allele is a functional null.

Previous attempts within the lab to generate mice carrying both Axin1$^{fl/fl}$ and Axin2$^{fl/fl}$ alleles and the AhCre transgene as used by Feng (2012) to delete Axin1 were unsuccessful. Spontaneous recombination driven by AhCre has been shown to occur in cardiac muscle, kidney, liver, and intestine without administration of an Ah target gene inducer (Kemp et al. 2004) and it is probable that leaky AhCre-driven recombination may have resulted in the embryonic lethality observed. To impose tighter control on Cre activity, the AhCreER^{T} allele was used (Figure 3.1A). AhCreER^{T} is controlled at the transcriptional level (CYP1A1 promoter) as for AhCre, but the additional binding of tamoxifen is required for the Cre-ER fusion protein to become active. This additional requirement reduces the unregulated recombination seen with AhCre. However, a drawback of using AhCreER^{T} is a reduced efficiency of recombination (Kemp et al. 2004).

To confirm recombination in the liver of the mice used in this study, mice bearing AhCreER^{T} were crossed with animals bearing the ROSA26 LacZ expressing reporter transgene (Soriano 1999). The reporter construct consists of the LacZ (beta-galactosidase) transgene, containing a *loxP* flanked PGK-Neo STOP cassette (Figure 3.1A) preventing the expression of the LacZ transgene in cells that have not recombined. A regime of 4 consecutive daily intraperitoneal injections of combined 80 mg/kg body weight as a suspension in corn oil of beta-naphthoflavone (BNF) and Tamoxifen was used to induce recombination within the liver. At day 6 post induction (PI), whole mounts of liver from animals containing the ROSA26 LacZ allele and control without the reporter were subjected to X-gal staining. Induced animals bearing the AhCreER^{T} transgene and the ROSA26 LacZ reporter allele developed a blue stain suggesting the presence of significant levels of recombination at the ROSA26 locus (Figure 3.1B).

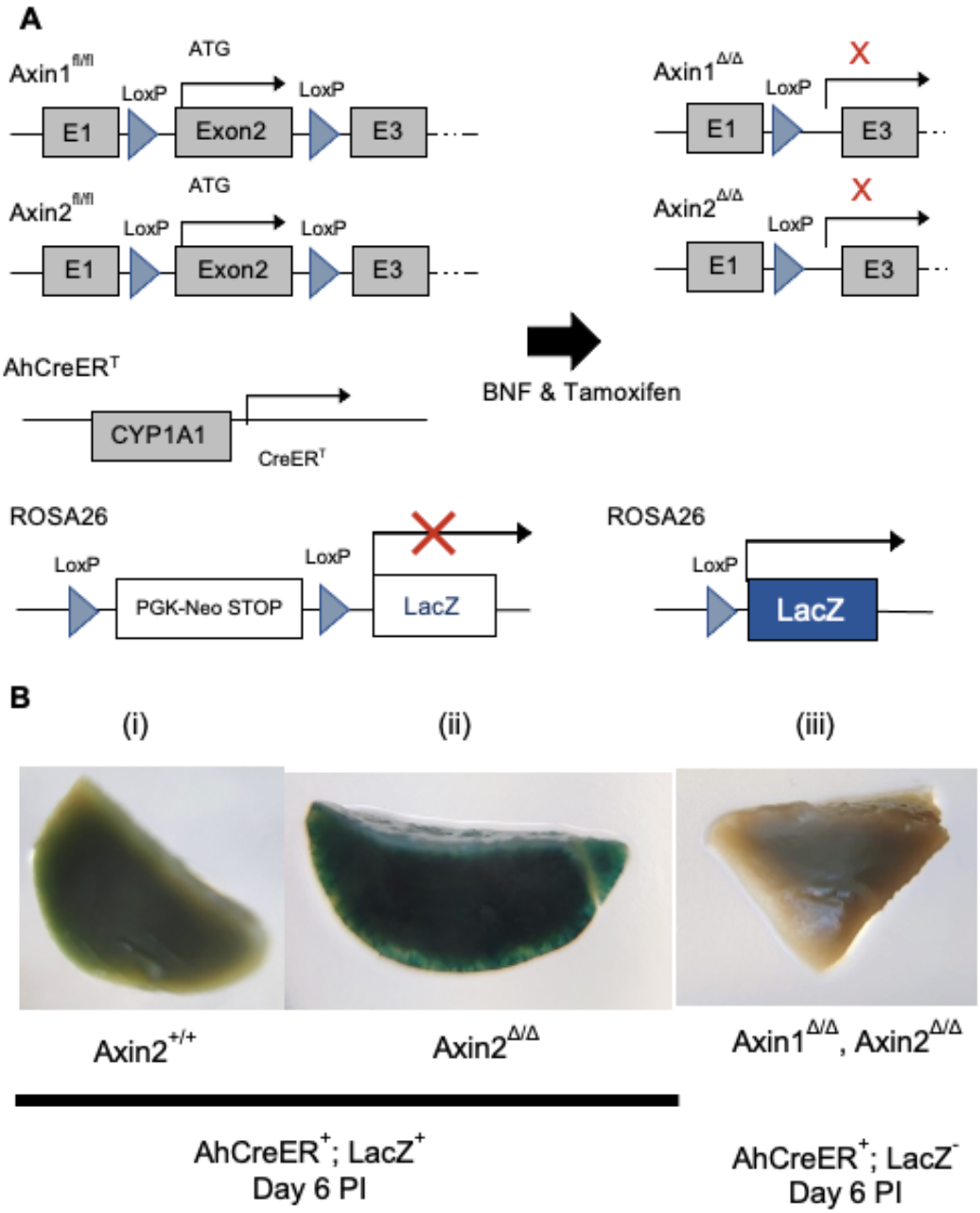

Figure 3.1 Overview of Axin alleles and evidence for inducible Cre recombination in the mouse liver

(**A**) Schematic diagram of inducible Axin1 and Axin2 deletion, AhCreER CYP1A1 promoter and LoxP sites flanking a PGK-Neo-STOP cassette inserted before the LacZ transgene on ROSA26. Following exposure to BNF and Tamoxifen, AhCreER recombinase expression will result in the excision of exon 2 of Axin1 and/or Axin2 and the PGK- Neo-STOP cassette, allowing expression of beta-galactosidase from the LacZ transgene. Cells expressing beta-galactosidase can be detected by exposure to X-Gal substrate, which results in a colourimetric change from colourless to blue. Treatment of mice with 4 consecutive daily doses of combined 80mg/kg beta-naphthoflavone and Tamoxifen resulted in a colour change, as indicated by X-Gal staining of the whole mounted liver that was taken on day 6 following the start of treatment (**B** i, ii). Absence of the LacZ transgene results in no colour change (**B** iii).

3.2.2 Genetic confirmation of AhCreER^{T} driven Axin recombination in the mouse liver

To determine whether BNF/Tamoxifen-treatment also induced deletion of exon 2 of Axin1 and Axin2, DNA was extracted from the liver 6 days post induction and was analysed by polymerase chain reaction (PCR) and agarose gel electrophoresis. Figure 3.2 A and C shows the genotyping schema for the Axin1 and Axin2 alleles respectively in the liver samples. Controls used for the rest of this chapter were age matched induced AhCreER^{T+} Axin1$^{wt/wt}$, Axin2$^{wt/wt}$ unless otherwise stated.

Primer pair A, that includes a primer within the deleted exon 2 domain of *Axin1*, amplified a band of 383 bp for wild-type (non-loxP-flanked) controls (lanes 1-3) as expected (Figure 3.2B, i). A slightly-longer floxed (but not recombined) allele of *Axin1* at 531 bp was detected following recombination, suggesting that some cells within the liver did not recombine following BNF/Tamoxifen treatment. However, the levels of the non-recombined allele appeared variable (see Figure 3.2B i; lanes 4-6), suggesting that the degree of recombination would need to be quantified. Similar variability in Axin1 deletion was observed in livers from double mutant Axin1$^{\Delta/\Delta}$, Axin2$^{\Delta/\Delta}$ animals (Figure 3.2B i; lanes 10-12). As expected, Axin2$^{\Delta/\Delta}$ samples contained wild type Axin1 alleles (Figure 3.2B i; lanes 7-9). Primer type B which was designed to amplify the locus irrespective of deletion showed the presence of the smaller, recombined Axin1 allele in Axin1$^{\Delta/\Delta}$ (Figure 3.2B ii; lanes 4-6; 402bp) and Axin1$^{\Delta/\Delta}$, Axin2$^{\Delta/\Delta}$ (Figure 3.2B ii; lanes 10-12). As expected, primer pair B produced a larger 2042 bp wild-type band from the control (lanes 1-3) and Axin2$^{\Delta/\Delta}$ (lanes 7-9) liver DNA samples that lack the floxed or recombined Axin1 alleles (Figure 3.2B ii). The efficient amplification of the shorter recombined 402bp allele but not the longer 2190 bp unrecombined allele within the same samples may be due to the increased efficiency of amplification of small PCR products.

A similar strategy was used to detect the recombination of exon 2 in Axin2. Primer pair C, that includes a primer within the deleted exon 2 domain of Axin2 amplified a band at 505 bp for wild-type (non-loxP-flanked) controls (lanes 1-3) and Axin1$^{\Delta/\Delta}$ (lanes 4-6) samples as expected (Figure 3.2D i). By contrast to Axin1 recombination, the floxed Axin2 643 bp band was not detected in Axin2$^{\Delta/\Delta}$ (lanes 7-9) and Axin1$^{\Delta/\Delta}$, Axin2$^{\Delta/\Delta}$ (lanes 10-12) samples, suggesting that there may have been a high level of recombination at the Axin2 locus. (Figure 3.2D, i). Primer type D, designed

to amplify the locus irrespective of deletion showed the presence of the smaller recombined Axin2 allele in Axin2$^{\Delta/\Delta}$ (Figure 3.2D ii; lanes 4-6; 504bp) and Axin1$^{\Delta/\Delta}$, Axin2$^{\Delta/\Delta}$ samples (Figure 3.2D ii; lanes 10-12). As expected, primer pair D produced a larger 1854 bp wild-type band from the control (lanes 1-3) and Axin1$^{\Delta/\Delta}$ (lanes 4-6) liver DNA samples that lack the floxed or recombined Axin2 alleles (Figure 3.2D ii). Taken together, the PCR results showed that the anticipated recombination events had taken place although the efficiency of recombination was hard to determine using non-quantitative PCR.

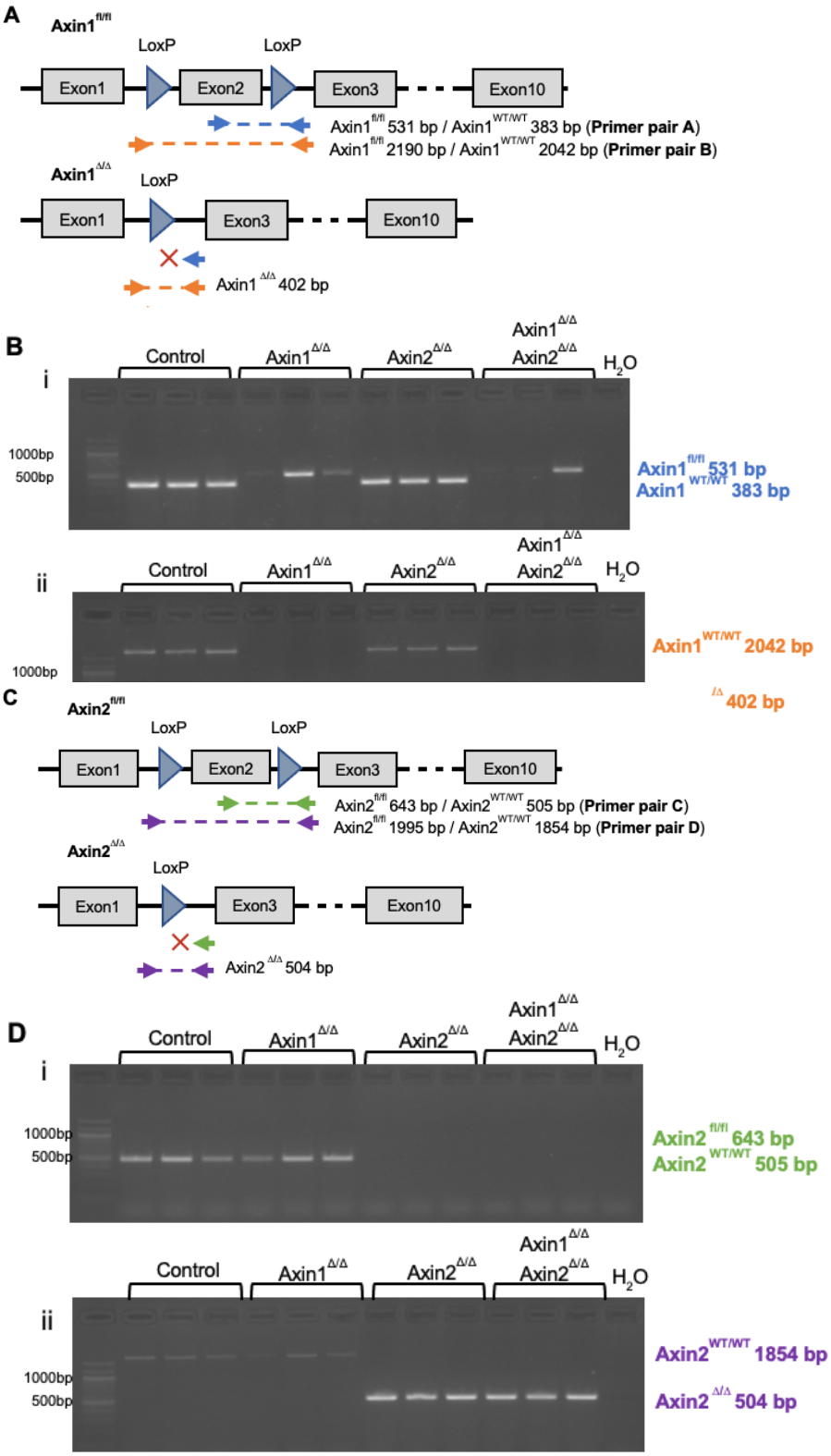

Figure 3.2 Confirmation of AhCreER^T mediated recombination

(**A, C**) Schemes of Axin1 and Axin2 alleles before and after recombination and expected PCR products using primer pairs indicated. (**B, D**) Representative gel images of PCR product from the gDNA of induced livers of genotypes indicated. Floxed Axin2 product failed to amplify after recombination suggesting complete loss of exon 2 of Axin2.

3.2.3 Quantifying levels of AhCreER^T driven Axin1 recombination.

To quantify the degree of recombination, primer pairs, A and B shown in

Figure 3.2A were used in qPCR assays with gDNA obtained from liver samples at different times after induction.

Levels of the unrecombined Axin1$^{fl/fl}$ allele were significantly reduced in all samples analysed following Cre-induction (Figure 3.3A). At day 6 post-induction, Axin1$^{fl/fl}$ levels following AhCreER^T induction were reduced by an average 66% (Figure 3.3A; compare 1st and 2nd bars). By contrast, levels of AhCre-driven recombination from samples previously generated in the lab at day 4 post BNF-induction were 90% reduced (3rd bar Figure 3.3A). However, levels of recombination between samples that had been deleted were not statistically different. Importantly, strongly reduced levels of Axin1$^{fl/fl}$ were observed in 1-year aged animals post induction using either AhCreER^T or AhCre (Figure 3.3A 3rd and 5th bars) suggesting that cells with recombined alleles are not eliminated from the liver following induction. The expected increases in levels of the recombined Axin1$^{\Delta/\Delta}$ allele were only detected following induction in all samples (Figure 3.3B).

AhCre has been shown to achieve near complete recombination in hepatocytes (Ireland et al. 2004) and several loxP flanked alleles (Méniel et al. 2015; Liko et al. 2019). In the studies shown here the DNA extracted from whole liver will contain hepatocytes in which recombination had not taken place together with cells (e.g., endothelium) in which AhCre activation would not have been induced. The 100% hepatocyte recombination observed in previous AhCre deletion studies together with the 90% gene deletion observed here suggests that the 10% of unrecombined alleles might be derived from non-hepatocyte cell types. If a similar 'recombination-resistant' fraction of total DNA were present in livers from AhCreER^T animals, this allows a crude estimate that 75-85% hepatocytes (65-75% minus 10%) likely underwent recombination following BNF/Tamoxifen treatment.

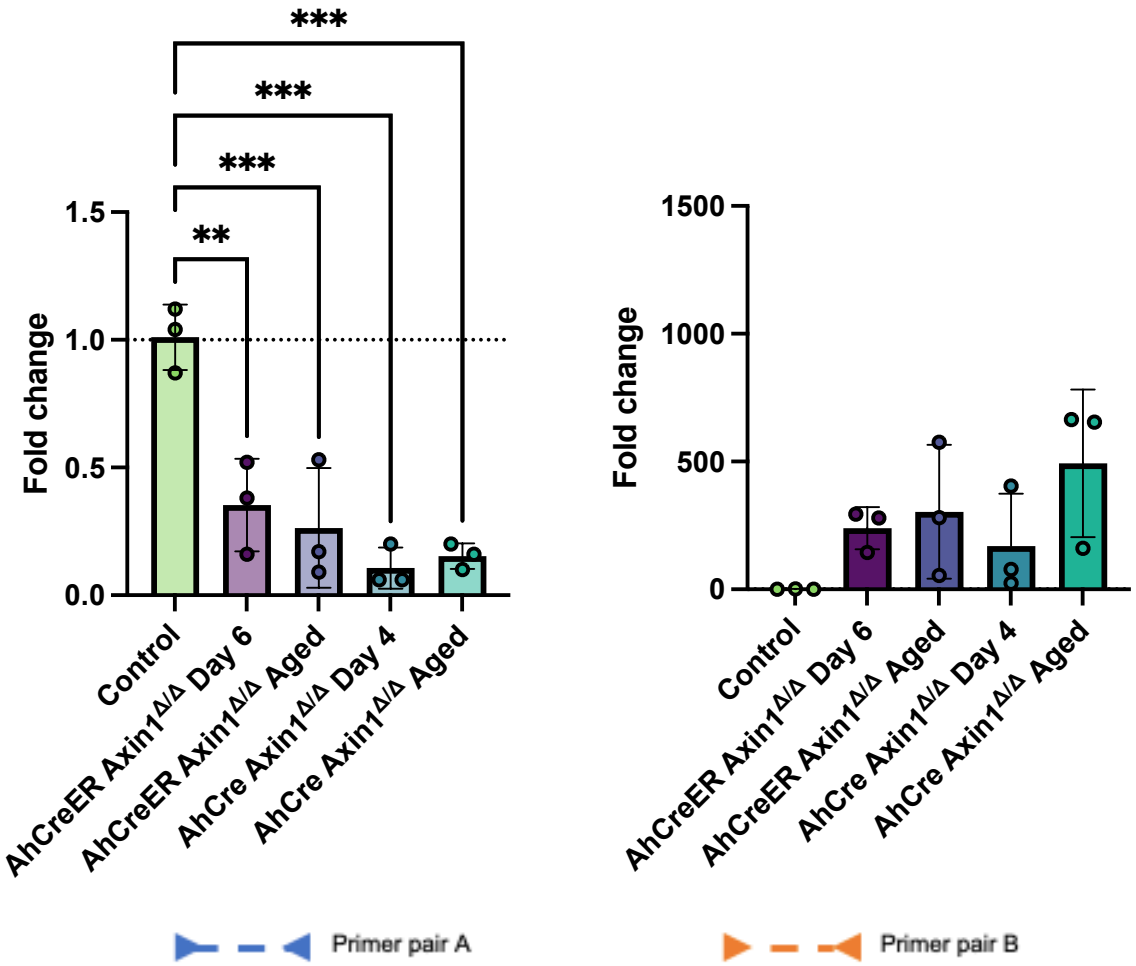

Figure 3.3 Levels of AhCreER^{T} and AhCre mediated recombination of Axin1$^{fl/fl}$ are not statistically different.
(**A**) qPCR confirmed the loss of exon 2 of Axin1 post induction in both the acute and 1-year aged mouse liver using AhCreER^{T}. Primer pair A shows an average recombination level of 66% and 75% in acute and aged livers respectively compared to control. In comparison, recombination using AhCre showed greater efficiency with an average of 90% and 86% in acute and aged mouse livers however there was no statistical significance between the use of AhCreER^{T} and AhCre. (**B**) Primer pair B show an average of 169-to-493-fold increase compared to control in induced livers of the recombined allele. Data was normalised to *ApoB* and is shown as the relative fold change to Day 6 PI AhCreER^{T+}, Axin1$^{WT/WT}$ (Control). n=3, error bars: SD. Significance was calculated using One-Way ANOVA with Tukey's multiple comparison test. **p<0.01 ***p<0.001

3.2.4 *Axin1* and *Axin2* transcript expression in the liver following AhCreER^T driven recombination 6 days post induction.

Axin1 loss would be expected to result in Wnt/β-catenin pathway activation and consequent increased expression of the Wnt target Axin2. This was seen in the liver in the study by (Feng et al. 2012) where *Axin2* expression increased an average 3-fold in AhCre, Axin1$^{\Delta/\Delta}$ cohorts at day 4 post induction. To examine the effects of CreER-deletion on *Axin1* and *Axin2* transcript levels, RNA from whole liver samples at 6 days post BNF/Tamoxifen induction of AhCreER^T Axin1$^{\Delta/\Delta}$, AhCreER^T Axin2$^{\Delta/\Delta}$, and AhCreER^T Axin1$^{\Delta/\Delta}$, Axin2$^{\Delta/\Delta}$ cohorts was used for quantitative reverse transcription PCR (RT-qPCR). Two sets of primer pairs were designed for both *Axin1* and *Axin2* (Figure 3.4A). One set includes a primer binding site within the floxed exon 2. The second pair targets regions at the C-terminus, outside the recombined region, in exons 8-9 for *Axin1* and exons 10-11 for *Axin2*, allowing assessment of changes in overall expression, regardless of recombination.

AhCreER^T driven recombination resulted in an average 75% reduction in the expression of transcripts containing exon 2 of *Axin1* in both single (Axin1$^{\Delta/\Delta}$) and double (Axin1$^{\Delta/\Delta}$, Axin2$^{\Delta/\Delta}$) mutant livers (Figure 3.4B). Exon 2-containing transcripts of *Axin2* were decreased by 12 and 10-fold respectively in Axin2$^{\Delta/\Delta}$ and Axin1$^{\Delta/\Delta}$, Axin2$^{\Delta/\Delta}$ livers (Figure 3.4C). A reduction in the levels of transcripts containing exon 2 were significant for *Axin2* but not *Axin1*, possibly associated with the lower level in gene deletion observed at the DNA level as seen in Figure 3.4A 2nd bar.

No changes in expression of the c-terminus of *Axin1* or *Axin2* were seen in Axin1$^{\Delta/\Delta}$, Axin2$^{\Delta/\Delta}$ and Axin1$^{\Delta/\Delta}$, Axin2$^{\Delta/\Delta}$ samples (Figure 3.4D, E), suggesting that the loss of exon 2 of each gene at early times following deletion does not lead to dramatic changes in overall gene transcription. This observation contrasts with (Feng et al. 2012), possibly due to the reduced levels of recombination using AhCreER^T.

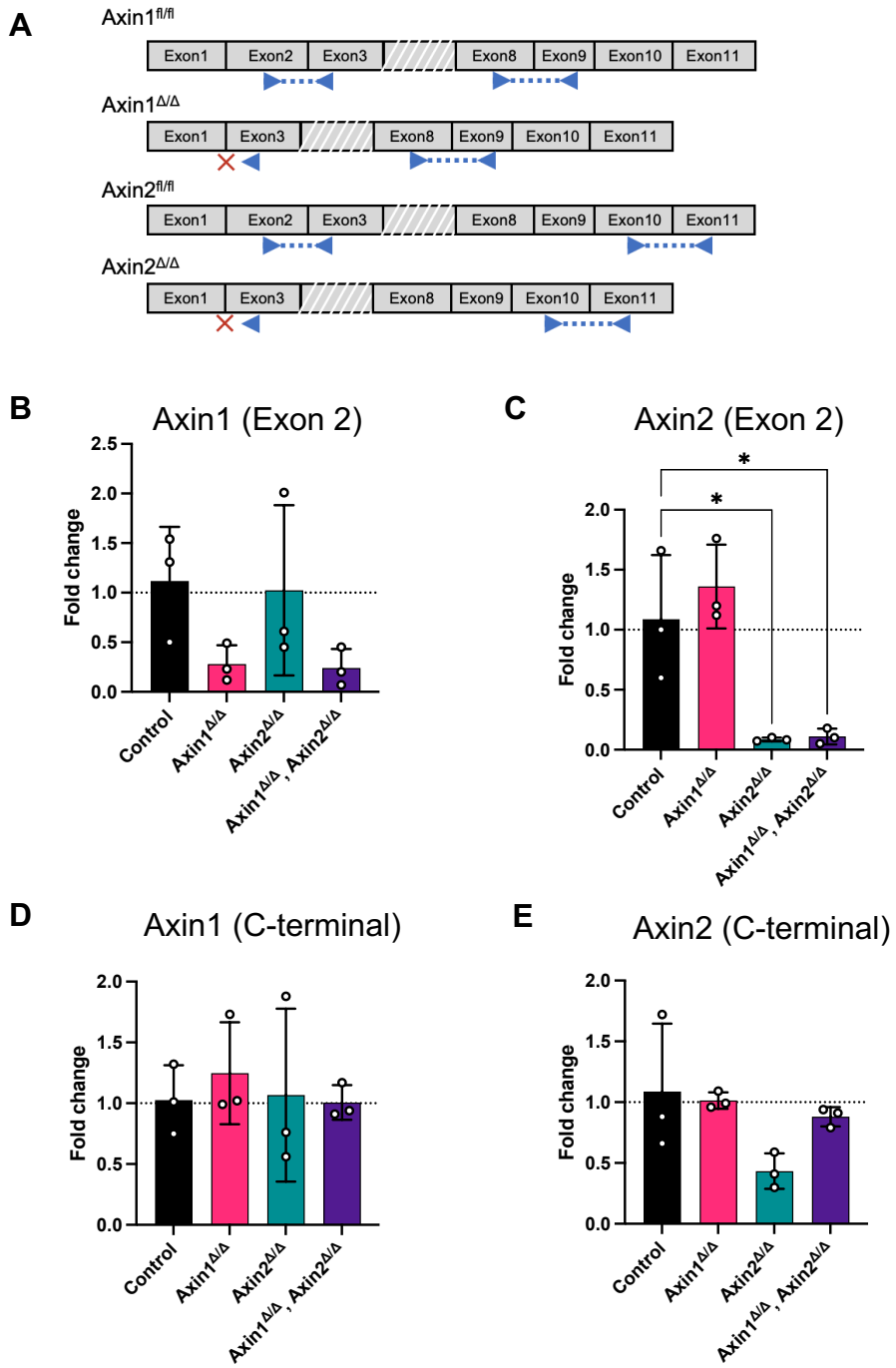

Figure 3.4 Quantification of *Axin1* and *Axin2* expression in mouse liver 6 days post AhCreER^{T} mediated recombination shows a reduction in Axin transcripts containing exon 2.

(**A**) Schema of primer binding sites. (**B**) RT-qPCR showed reduced expression of exon 2 containing transcripts of Axin1 in both the single Axin1$^{\Delta/\Delta}$ and double Axin1$^{\Delta/\Delta}$, Axin2$^{\Delta/\Delta}$ mouse liver. (**C**) Expression of exon 2 containing transcripts of Axin2 was significantly reduced in Axin2$^{\Delta/\Delta}$ and Axin1$^{\Delta/\Delta}$, Axin2$^{\Delta/\Delta}$ samples. (**D**) Expression of Axin1 exons 8-9 showed no significant difference between control and Axin mutant samples. (**E**) Expression of Axin2 exons 10-11 showed only a trend for decreased expression in Axin2$^{\Delta/\Delta}$. Data was normalised to B2M and is shown as the relative fold change to livers from BNF/Tamoxifen treated and age matched AhCreER^{+}, Axin1$^{+/+}$, Axin2$^{+/+}$ (Control). n = 3, error bars: SD. Significance was calculated using One-Way ANOVA with Tukey's multiple comparison test. *p<0.05

3.2.5 Effects of induced Axin loss in the mouse liver 6 days post induction.

Disruption of the Wnt/β-catenin pathway in the liver compromises homeostasis and has been shown to lead to the development of hepatocellular carcinoma (HCC) (Colnot et al. 2004; Feng et al. 2012). Hepatomegaly and increased proliferation are some of the immediate physiological consequences that have been observed following Axin1 loss (Feng et al. 2012). To determine whether Axin2 loss induced similar effects or cooperated with Axin1, cohorts were generated to examine the effects of their acute deletion using AhCreER^{T} in the mouse liver.

At 6 days post BNF/Tamoxifen induction, mice were culled, and their body and liver weights were measured to be used as a readout of hepatomegaly. Liver to body weight ratio of AhCreER^{T} Axin1$^{\Delta/\Delta}$ were comparable to controls suggesting no hepatomegaly (Figure 3.5A, i). This was inconsistent with the 1.2-fold increase in liver size observed in AhCre Axin1$^{\Delta/\Delta}$ cohorts as seen by Feng et al. (2012). Liver to body weight ratios from AhCreER^{T} Axin2$^{\Delta/\Delta}$ and AhCreER^{T} Axin1$^{\Delta/\Delta}$, Axin2$^{\Delta/\Delta}$ cohorts were also comparable to controls (Figure 3.5A, i). Using the same induction method as for the AhCreER^{T} Axin cohorts, AhCreER^{T}, Apc$^{\Delta/\Delta}$ mice at day 6 post induction, showed a statistically significant increase in their liver/body weight ratio as expected (Figure 3.5A, ii). This change was not as drastic when using AhCre (Reed et al. 2008), possibly due to lower levels of recombination using AhCreER^{T} and could explain why AhCreER^{T} Axin1$^{\Delta/\Delta}$ liver did not increase in size as seen by Feng et al. (2012) in AhCre Axin1$^{\Delta/\Delta}$ liver.

Microscopic examination of H&E-stained liver tissue sections (Figure 3.5B) revealed that cell size, based on the number of nuclei counted per unit area of the histological section (Figure 3.6A) and nucleus size (Figure 3.6B) increased in Axin1$^{\Delta/\Delta}$ and in Axin1$^{\Delta/\Delta}$, Axin2$^{\Delta/\Delta}$ samples. The increase in cell and nuclei size matched that previously seen in AhCre Axin1$^{\Delta/\Delta}$ animals at day 4 post BNF induction (Feng et al. 2012). No significant changes were seen in Axin2$^{\Delta/\Delta}$ alone. It was unclear why an increase in cell and nuclei size was not reflected in an increased liver to body weight ratio, but this may have been due to the greater variability of liver to body weight ratios or different levels of precision in measurement.

No differences were observed following gene deletion in the number of binucleated cells. (Figure 3.6C). Levels of mitosis were quantitatively examined based

on morphological appearance. AhCreER^{T} Axin1$^{\Delta/\Delta}$ livers showed a statistically significant increase in mitoses (Figure 3.6D), matching the phenotype of increased proliferation seen by Feng et al (2012) when using AhCre. Levels of mitosis in AhCreER^{T} Axin2$^{\Delta/\Delta}$ livers were highly variable and not statistically different to control. Mitosis in AhCreER^{T} Axin1$^{\Delta/\Delta}$, Axin2$^{\Delta/\Delta}$ livers was increased when compared to control but was lower than observed in AhCreER^{T} Axin1$^{\Delta/\Delta}$ liver alone. To confirm this proliferative phenotype, liver sections were also stained with anti-Ki67 (Figure 3.7A) and anti-BrdU (Figure 3.8A). Axin1 loss resulted in a significant increase to 15 % of total nuclei being stained with Ki67. Combined Axin1 and Axin2 loss resulted in 10 % Ki67 positively stained cells. Loss of Axin2 alone was not statistically different to control (Figure 3.7B). BrdU was administered 2 hours before mice were culled. Anti-BrdU staining revealed a similar pattern of proliferation with Axin1 loss alone resulting in the highest increase, dual Axin1 and Axin2 loss being slightly less, and Axin2 loss alone being similar to control (Figure 3.8B). Overall, the data presented here recapitulated prior observations, the loss of Axin1 resulted in immediate changes to hepatocyte cell volume and proliferation. Deletion of Axin2 alone did not lead to any significant observable changes and when combined with Axin1 deletion did not further perturb the biology attributed to Axin1 deletion alone, if anything, levels of ki67 were reduced in double mutants.

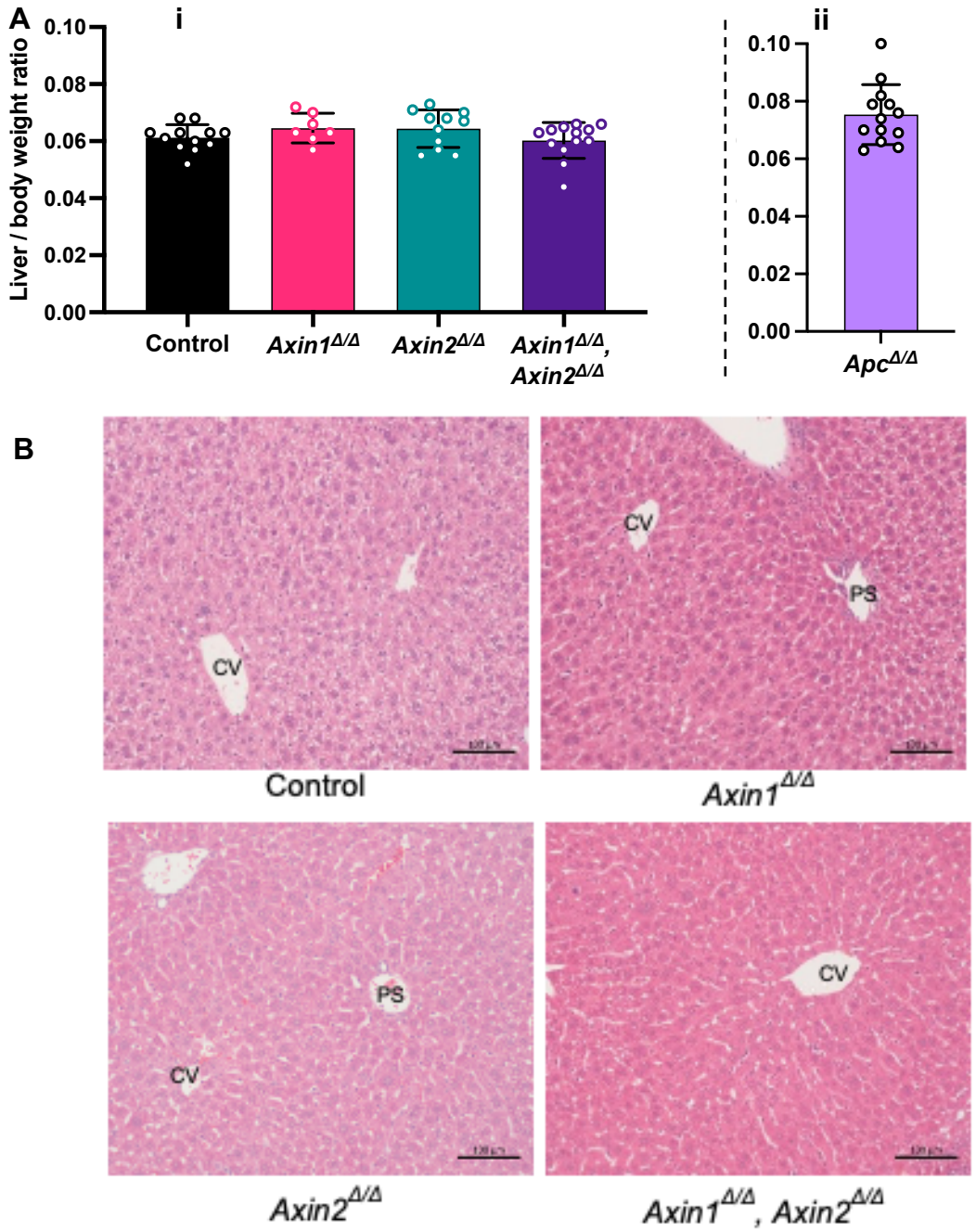

Figure 3.5 No changes in liver/body weight ratio or gross histology following Axin deletion 6 days post induction.

(**A**) (i) Liver and body weight ratio measured at sacrifice 6 days post induction showed no difference between control and Axin deleted livers. (ii) Mice induced carrying exon 14 floxed *Apc* (*Apc*^{580s}) crossed with AhCreER^{T} were used as a positive control for Wnt activation showed an increase in liver / body weight ratio as expected. Data represents mean ±s.d. from control n=12, Axin1$^{\Delta/\Delta}$ n=7, Axin2$^{\Delta/\Delta}$ n=11 and Axin1$^{\Delta/\Delta}$, Axin2$^{\Delta/\Delta}$ n=13, Apc$^{\Delta/\Delta}$ n=12 biological replicates. (**B**) H&E-stained sections of liver tissue from control and Axin mutants revealed no gross changes in histological appearance. Scale bar 100 μm CV = Central vein PS = Portal space

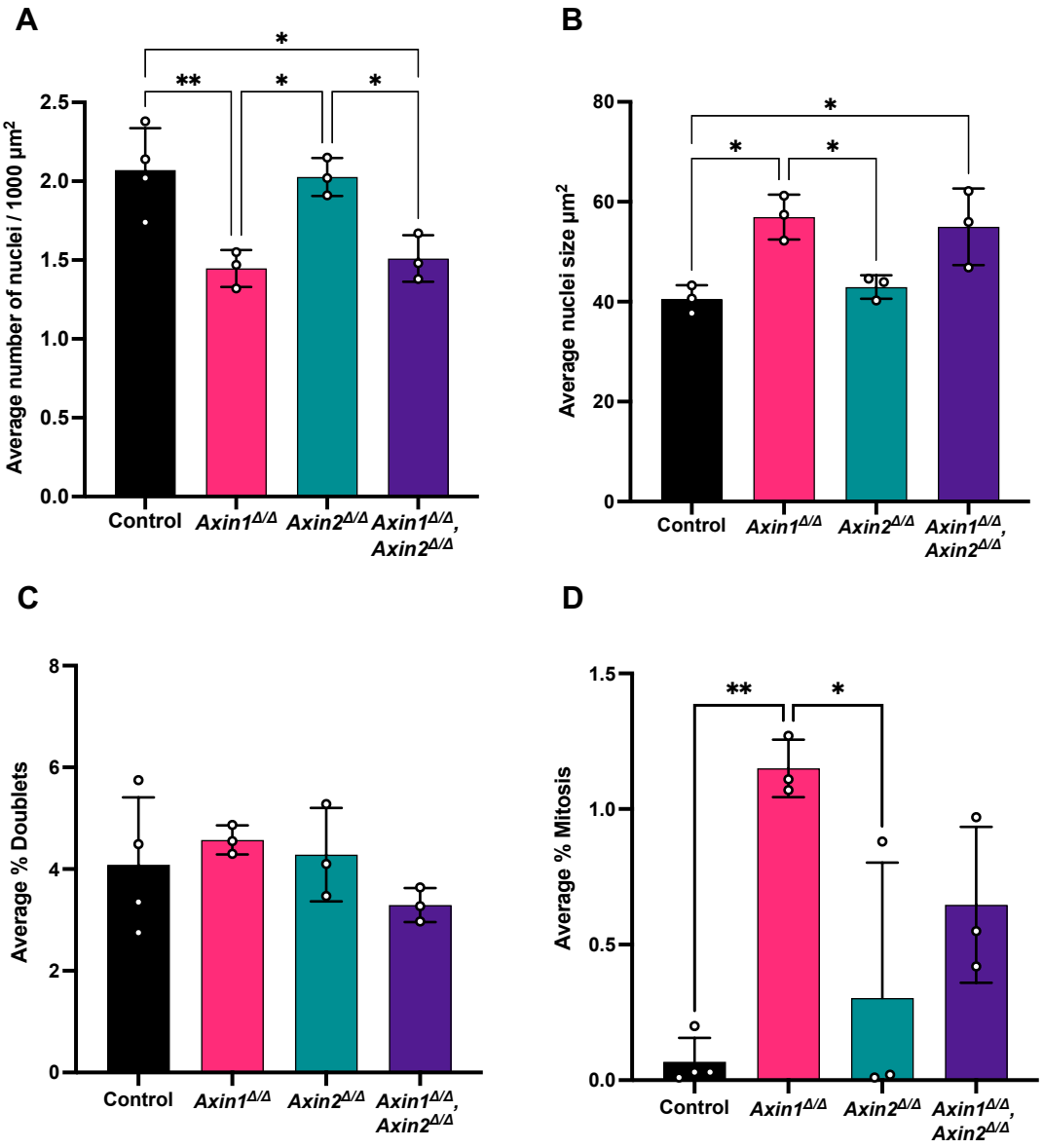

Figure 3.6 Hepatocyte cell size and nuclei size increases in AhCreER^{T} Axin1$^{\Delta/\Delta}$ and AhCreER^{T} Axin1$^{\Delta/\Delta}$, Axin2$^{\Delta/\Delta}$ mouse livers at 6 days post induction.

(**A**) The average number of nuclei counted quantified as nuclei per µm^{2}. (**B**) Average hepatocyte nucleus size. (**C**) Average percentage of bi-nucleated cells between control and Axin mutant liver as a percentage of total nuclei counted. (**D**) Average number of mitotic figures counted as a percentage of total nuclei. Data represents mean ±s.d. n = 3-4 biological replicates. Significance was calculated using Ordinary One-Way ANOVA with Tukey's multiple comparison test. *P<0.05, **P<0.01 Counts for A, C and D were carried out by Victoria Marsh Durban

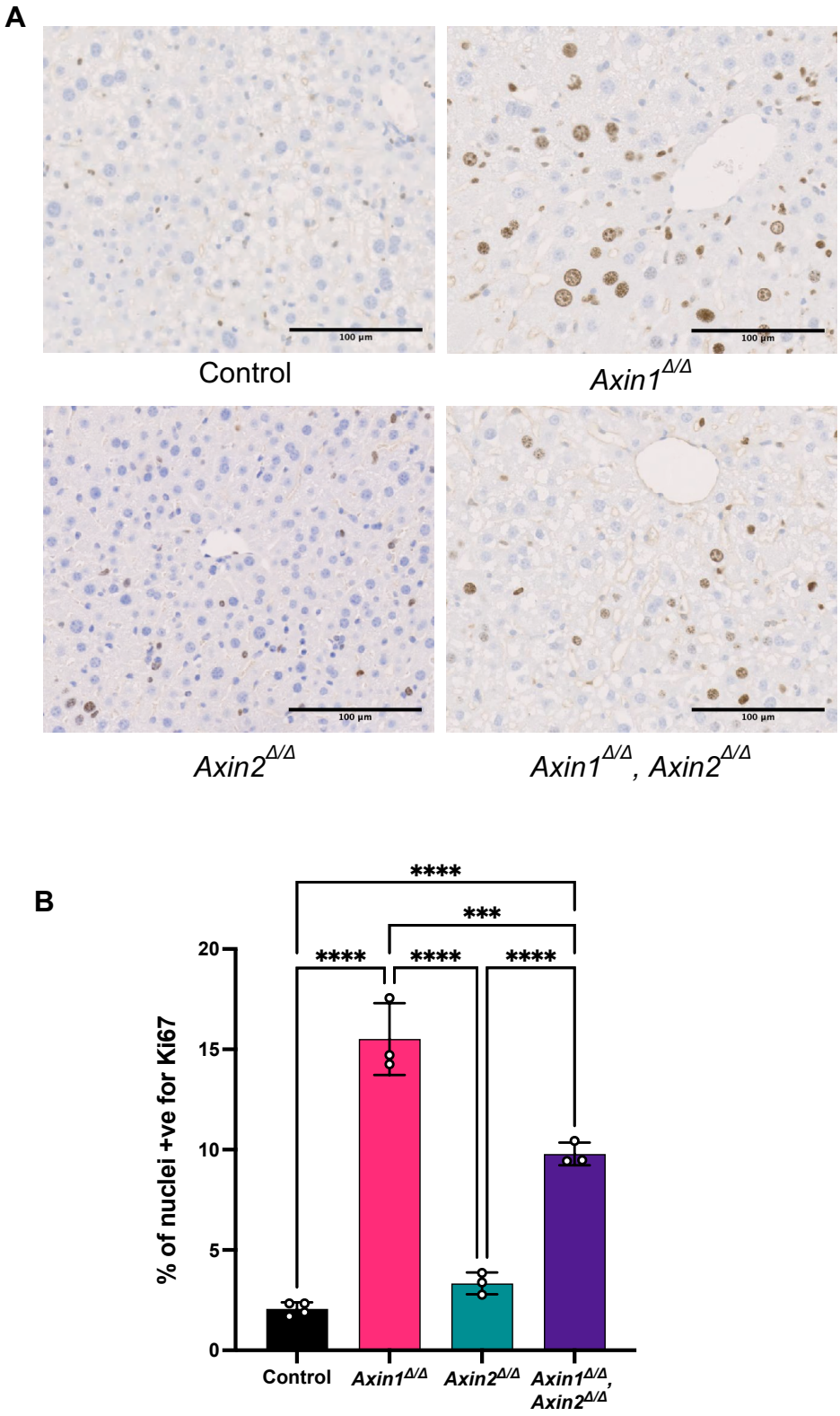

Figure 3.7 Increased proliferation in AhCreER^{T} Axin1$^{\Delta/\Delta}$ and AhCreER^{T} Axin1$^{\Delta/\Delta}$, Axin2$^{\Delta/\Delta}$ mouse livers at 6 days post induction.

(A) Representative images of Ki67 stained liver sections 6 days post induction. (**B**) Quantification of the number of Ki67 positive cells as a percentage of nuclei for each cohort. Data represents mean ±s.d. n = 3-4 biological replicates. Significance was calculated using Ordinary One-Way ANOVA with Tukey's multiple comparison test. ***p<0.001 ****p<0.0001. Scale bar 100 µm

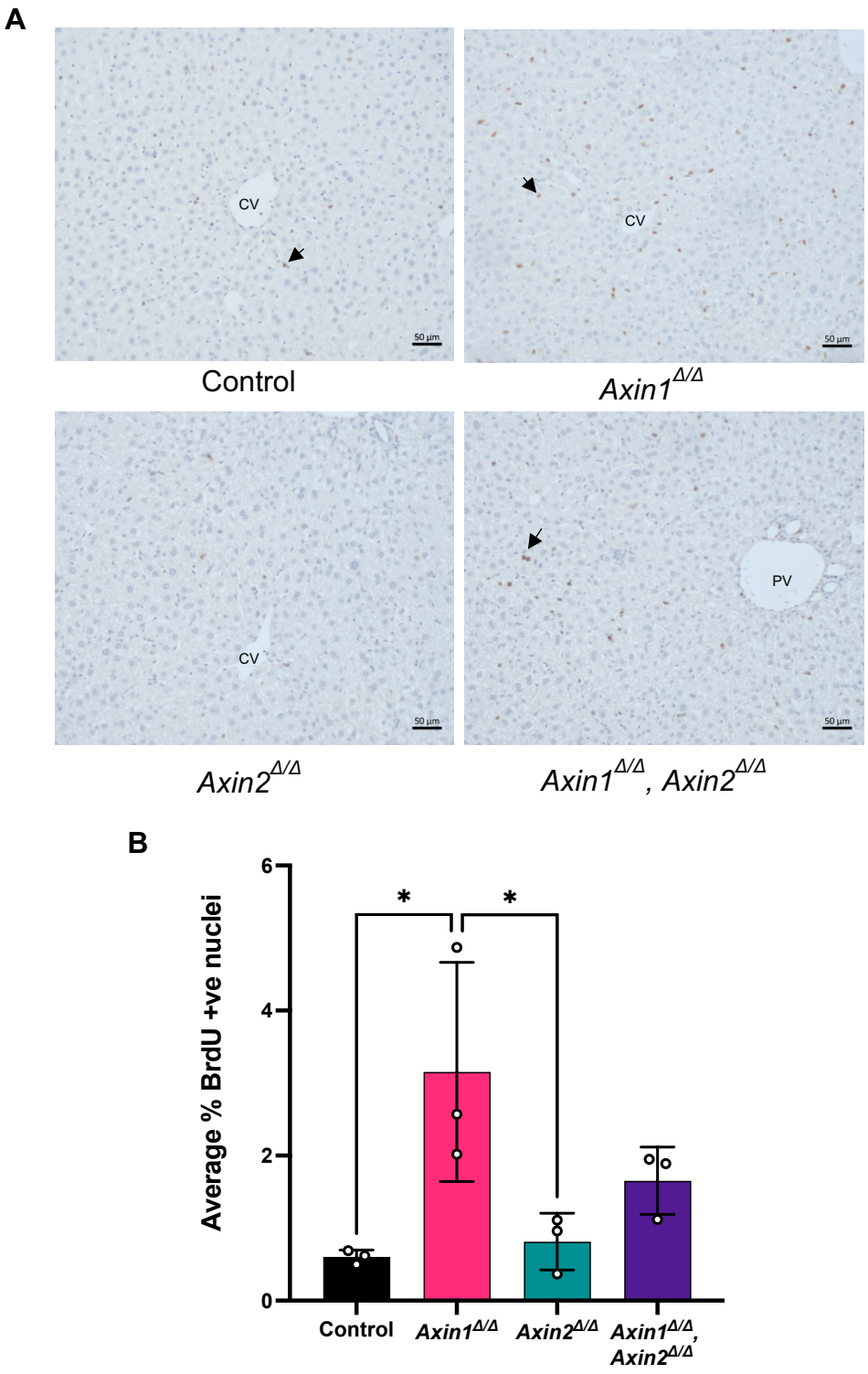

Figure 3.8 Increased BrdU incorporation in AhCreER^{T} Axin1$^{\Delta/\Delta}$ livers at 6 days post induction.

BrdU was administered 2 hours before animals were culled. (**A**) Representative images of liver sections labelled with BrdU. (**B**) Counts of BrdU labelled cells in control and Axin deleted mouse livers. Data represents mean ±s.d. n = 3 biological replicates. Significance was calculated using Ordinary One-Way ANOVA with Tukey's multiple comparison test. *p<0.05 Scale bar 50 µm CV = Central vein PS = Portal space

3.2.6 γH2AX and Caspase 3 levels following Axin loss in the mouse liver 6 days post induction.

Activation of the Wnt/β-catenin pathway in the liver through loss of Apc has been shown to not only increase proliferation but also genomic instability and an increase in markers of double strand breaks (DSBs) such as γH2AX (Méniel et al. 2015). γH2AX plays a key role in the repair of DSBs through chromatin modification to increase DNA accessibility and recruitment of DNA damage repair proteins (Mah et al. 2010). To examine whether acute loss of Axin resulted in DNA damage, anti-γH2AX staining was used as a marker for DSBs.

AhCreER^{T}, Axin1$^{\Delta/\Delta}$ and AhCreER^{T}, Axin1$^{\Delta/\Delta}$, Axin2$^{\Delta/\Delta}$ mouse livers showed an 8 to 11-fold increase in the level of γH2AX stained nuclei 6 days post induction with BNF/Tamoxifen (Figure 3.9B). Loss of Axin2 alone saw no alteration to the levels of γH2AX staining. These observations would suggest that loss of Axin1 results in DSBs but that it is not further increased with the additional loss of Axin2.

γH2AX has been associated with nuclei atypia (Hart et al. 2021) thus nuclei of the induced cohorts were also assessed for atypical appearances. For this, nuclei that were irregular in shape, had a prominent nucleolus or cytoplasmic inclusions were scored as atypical. Significant differences were seen following combined Axin1, Axin2 deletion (Figure 3.9C). Increased levels were also seen following Axin1 and Axin2 deletion alone, but this was not significant due to significant variability.

DSBs can be very deleterious to cells and activation of the DNA damage response pathway is critical for the detection and repair of the lesions. Failures in repair can lead to the cell cycle being halted by DNA damage checkpoints or induction of apoptosis. To determine whether the increase in DSBs as seen following acute Axin deletion resulted in alterations of apoptosis, liver sections were stained for cleaved caspase 3.

Quantification of the percentages of cells stained positive for caspase 3 at day 6 post induction, revealed that deletion of Axin1, Axin2 and combined Axin1 and Axin2 did not result in changes to levels of caspase 3 (Figure 3.10). This may be due to the day 6 timepoint in an AhCreER^{T} context being too early for differences in caspase 3 levels to be observed. Apc deletion using AhCre saw differences in caspase3 levels 2 days after γH2AX levels had returned to control levels at day 6 post induction (Méniel et al. 2015), suggesting differences in caspase3 may be seen at day 8 or later when using AhCreER^{T}.

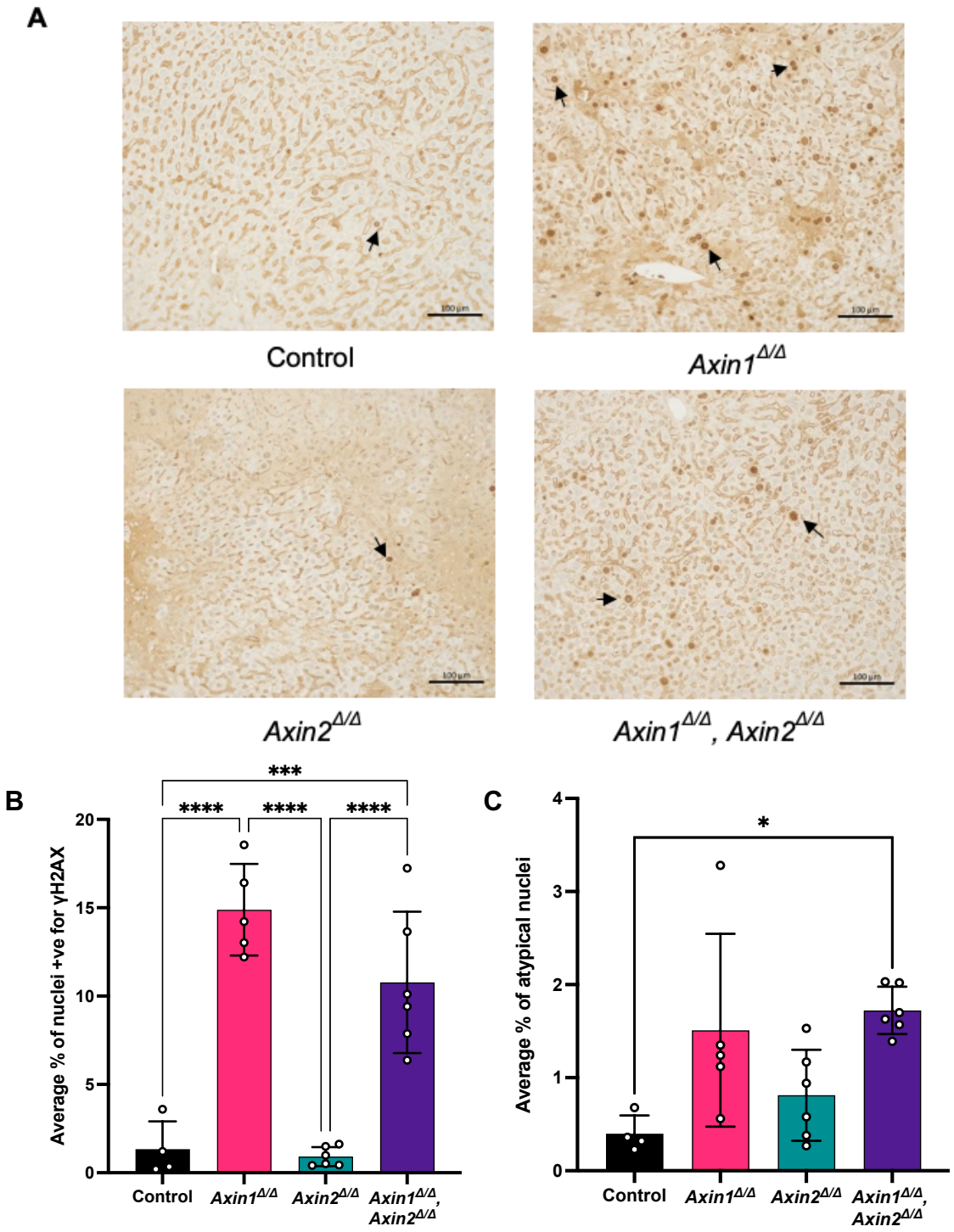

Figure 3.9 Increased staining for γH2AX and atypical nuclei in AhCreER^{T}, Axin1$^{Δ/Δ}$ and AhCreER^{T}, Axin1$^{Δ/Δ}$, Axin2$^{Δ/Δ}$ mouse livers 6 days post induction. (**A**) Representative images of liver sections labelled with anti-γH2AX. (**B**) Counts of γH2AX positive stained nuclei in control and Axin mutant liver. (**C**) Counts of atypical nuclei. Atypical Nuclei were scored as having cytoplasmic inclusions, being irregular shaped, having grooving or prominent nucleolus using Feulgen-stained sections. Data represents mean ±s.d. n = 4-6 biological replicates. Significance was calculated using Ordinary One-Way ANOVA with Tukey's multiple comparison test. *p<0.05, ***p<0.001, ****p<0.0001 Scale bar 100 μm. Counts were carried out by final year project student Chu Li under my supervision.

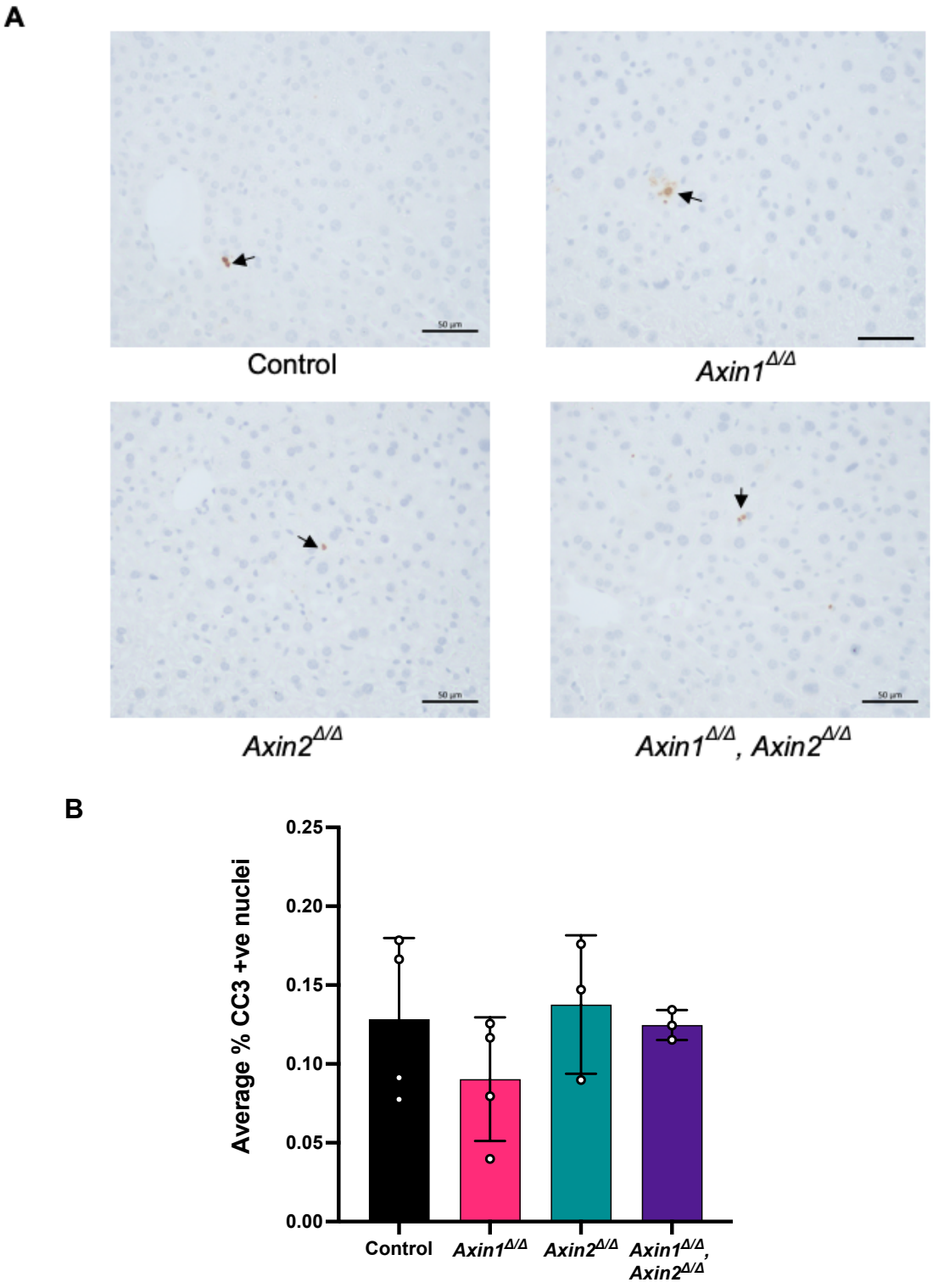

Figure 3.10 No change to Caspase3 following Axin loss in mouse livers 6 days post induction.
(**A**) Representative images of liver sections labelled with Cleaved Caspase-3 antibody that detects endogenous levels of the large fragment of activated caspase-3. (**B**) Counts of cleaved Caspase 3 positive nuclei in control and induced Axin loss in mouse liver. Data represents mean ±s.d. n = 3-4 biological replicates. Scale bar 50 μm

3.2.7 β-catenin localisation following Axin loss in the mouse liver 6 days post induction.

Activation of the canonical Wnt/β-catenin pathway through the loss of key components of the pathway such as Apc and GSK3 (Colnot et al. 2004; Dembowy et al. 2015) leads to the accumulation of β-catenin and its translocation to the nucleus, activating transcription of downstream targets. The loss of Axin1 in the study by Feng (2012) did not lead to the stabilisation of β-catenin and strong nuclear β-catenin staining as would have been expected following disruption to the destruction complex. A possible explanation for this observation was the existence of functional compensation by Axin2. If this holds true, then the dual loss of Axin1 and Axin2 would be predicted to stabilise β-catenin and induce a strong "Wnt ON" phenotype.

Following inducible deletion with BNF/Tamoxifen, liver sections from the Axin cohorts were stained for β-catenin by immunohistochemistry. As previously observed for Axin1 in AhCre samples, the loss of Axin1 in AhCreER^{T} animals did not lead to activation of β-catenin that was distinct from the weak staining around the central vein seen in control samples. Similarly, loss of Axin2 did not alter nuclear β-catenin staining. Surprisingly however, loss of both Axin alleles at day 6 post induction (AhCreER^{T}, Axin1$^{\Delta/\Delta}$, Axin2$^{\Delta/\Delta}$), did not lead to strong nuclear staining of β-catenin in the liver (Figure 3.11A). By contrast, staining of AhCreER^{T}, Apc$^{\Delta/\Delta}$ livers from mice treated with BNF/Tamoxifen did show strong nuclear β-catenin staining in a proportion of cells at day 6 post induction (Figure 3.11 see arrowheads).

Total levels of β-catenin protein in the liver were also assessed using western blot analysis following Axin loss at day 6 post induction (Figure 3.11B). When normalised to β-actin, levels of β-catenin were comparable between control samples and the cohorts with Axin loss (Figure 3.11C).

Taken together, these results suggest that the deletion of either or both Axin alleles did not result in obvious changes to β-catenin localisation or total protein levels in the liver as might have been expected.

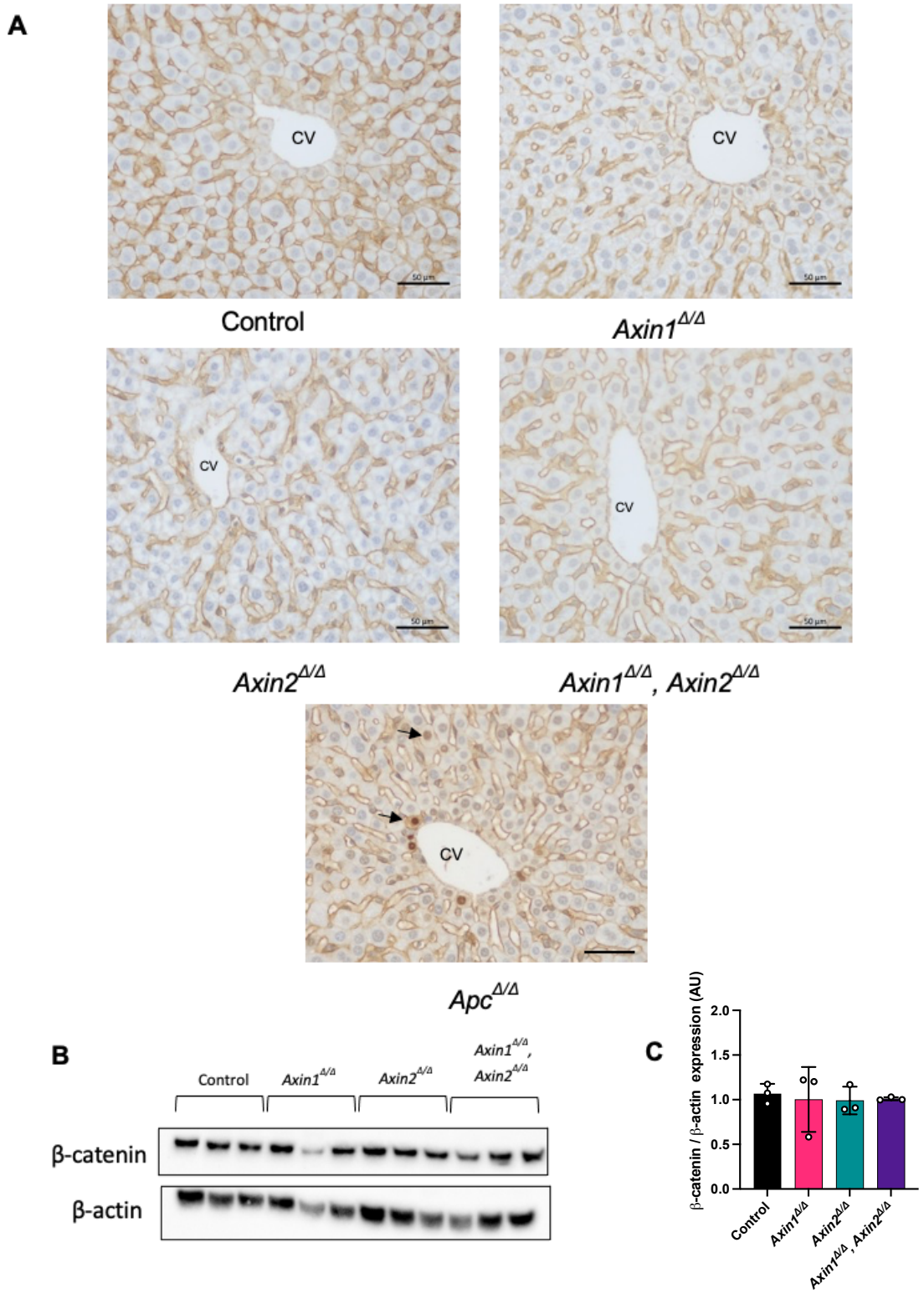

Figure 3.11 β-catenin localization and levels unchanged following Axin loss in the mouse liver 6 days post induction.

(A) Representative images of β-catenin IHC of control, Axin deleted cohorts and Apc deleted liver sections, 6 days following BNF/Tamoxifen induction. Apc deletion using AhCreER was used as a positive control to show nuclear β-catenin. CV, central vein. (**B**) Western blot of total β-catenin protein levels in Axin deleted cohorts and controls. (**C**) Quantification of β-catenin levels normalised to β-actin. n=3 Scale bar 50 μm CV = Central vein

3.2.8 GS zonation following Axin loss at day 6 post induction.

Zonation of the liver lobule along the porto-central axis is important for proper function and maintaining homeostasis in the liver (see Introduction 1.3). The Wnt/β-catenin signalling pathway has been shown to play a key role in the maintenance of liver zonation. Glutamine synthetase (GS) is a direct Wnt/β-catenin target in the liver and is involved in ammonia detoxification. GS expression is normally restricted to 2-3 hepatocyte cell layers surrounding the central vein (Burke et al. 2018). To determine whether the loss of Axin induced β-catenin dependent target gene expression, liver sections from Axin cohorts were stained for GS following inducible deletion with BNF/Tamoxifen at day 6 post induction (Figure 3.12).

As previously reported by Feng (2012), loss of Axin1 alone did not result in expansion of GS around the central vein. Axin2 loss alone also did not result in an expansion of GS staining. As previously discussed for β-catenin levels, it was anticipated that the combined loss of Axin1 and Axin2 would lead to activation of Wnt/β-catenin signalling and Wnt target genes. However, the dual loss of Axin1 and Axin2 had no discernible effect on the levels of GS staining. By contrast, deletion of Apc using the same AhCreER^T allele and BNF/Tamoxifen treatment regime did show an expansion of GS staining at day 6 (Figure 3.12).

Taking the GS staining together with the β-catenin IHC and western blot analysis, it appears that the dual loss of Axin1 and Axin2 did not result in classical activation of the Wnt/β-catenin pathway as shown here following inducible Apc deletion using AhCreER^T, or Apc deletion using AhCre (Benhamouche et al. 2006), and as has been seen with conditional β-catenin activation (Miyoshi et al. 2009).

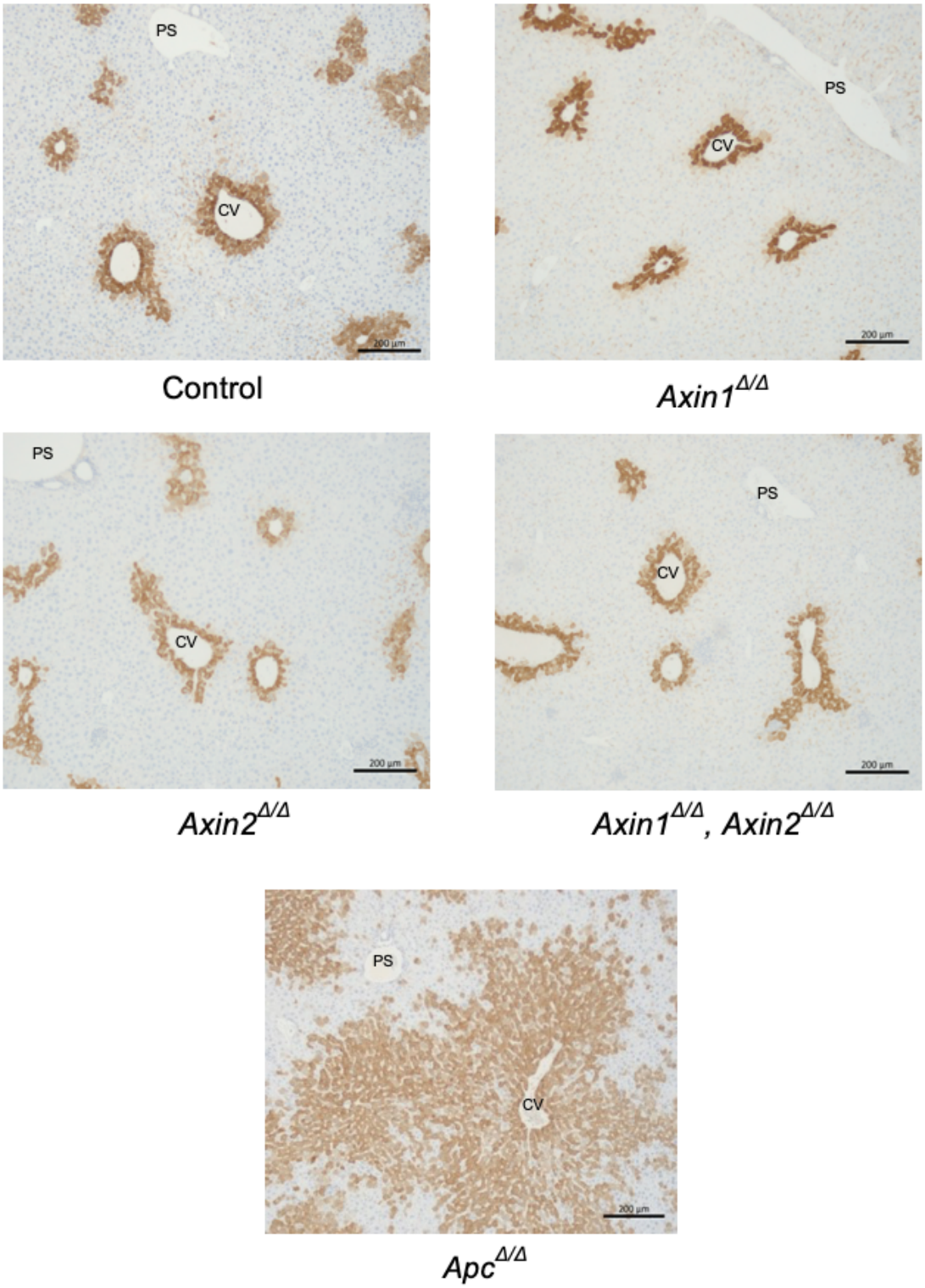

Figure 3.12 No changes to GS zonation following Axin loss in mouse livers 6 days post induction.

Representative images of GS staining in control and BNF/Tamoxifen-induced $Axin1^{\Delta/\Delta}$, $Axin2^{\Delta/\Delta}$ and $Axin1^{\Delta/\Delta}$, $Axin2^{\Delta/\Delta}$ mouse livers. Apc deletion using $AhCreER^{T}$ was used as a positive control and shows expansion of GS. CV = Central vein, PS, Portal space, Scale bar 200 µm

3.2.9 Axin, Wnt targets and cell cycle expression following Axin loss in the mouse liver 6 days post induction.

Despite the lack of expansion of GS staining after the loss of Axin1 in the study by Feng (2012), RT-qPCR did reveal that levels of select Wnt targets such as Axin2, c-Myc, c-Jun and CyclinD1 were raised 2-3-fold. However, other Wnt target genes such as Tiam1, and Cdc25a were not significantly altered. To further extend the analysis of possible Wnt targets, the same set of target genes previously used (Feng et al. 2012), were utilised to compare the loss of Axin1, Axin2 and both Axin1 and Axin2 in the AhCreER^{T} model at day 6 post BNF/Tamoxifen induction.

RNA from AhCreER^{T}, Axin1$^{\Delta/\Delta}$ livers 6 days post induction showed a reduced expression of exon 2 containing transcripts of *Axin1* as expected (Figure 3.13A). However, increases to the expression of *Axin2, c-Myc*, *c-Jun,* and *CyclinD1* and repression of *CD44*, as seen by Feng (2012) were not observed. Reduced levels and variability of recombination using AhCreER^{T} may explain why these changes in expression were not observed. As expected, AhCreER^{T}, Axin2$^{\Delta/\Delta}$ induced livers showed a reduction in expression of transcripts containing exon2 of *Axin2* but the loss of Axin2 alone led to no significant changes in the panel of Wnt target genes (Figure 3.13B). Again, as expected, AhCreER^{T}, Axin1$^{\Delta/\Delta}$, Axin2$^{\Delta/\Delta}$ induced livers had a reduction in expression of exon 2 containing transcripts of *Axin1* and *Axin2* however, this led to no significant changes in the panel of Wnt target genes (Figure 3.13C).

In the study by Feng (2012), a micro array and confirmation in an RT-qPCR assay, there was an enrichment in expression of genes associated with the G2/M phase of the cell cycle 4 days after Axin1 loss. Expression of this set of G2/M targets genes was examined in the Axin mutant livers at day 6 post induction in the AhCreER^{T} BNF/Tamoxifen model. As shown in Figure 3.13A, the expression of G2/M cell cycle genes was not obviously altered following Axin1 loss. As argued previously, the reduced levels and variability of recombination using AhCreER^{T} may explain why increases in expression of G2/M genes was not observed. No changes in the expression of the G2/M gene panel were seen in the liver of the AhCreER^{T} Axin2$^{\Delta/\Delta}$ cohort at day 6 post BNF/Tamoxifen induction (Figure 3.13B). However, in AhCreER^{T} Axin1$^{\Delta/\Delta}$, Axin2$^{\Delta/\Delta}$ livers a trend for a 2 to 4-fold increase was observed in select G2/M cell cycle gene expression including *Cyclin A2, Cyclin B1, Cyclin B2, Cdk1, Cdca3, Cdc20, Ki67* and *FoxM1*, resembling that seen by Feng (2012) with Axin1 loss alone. This data was not significant due to inter-sample variability (Figure 3.13C).

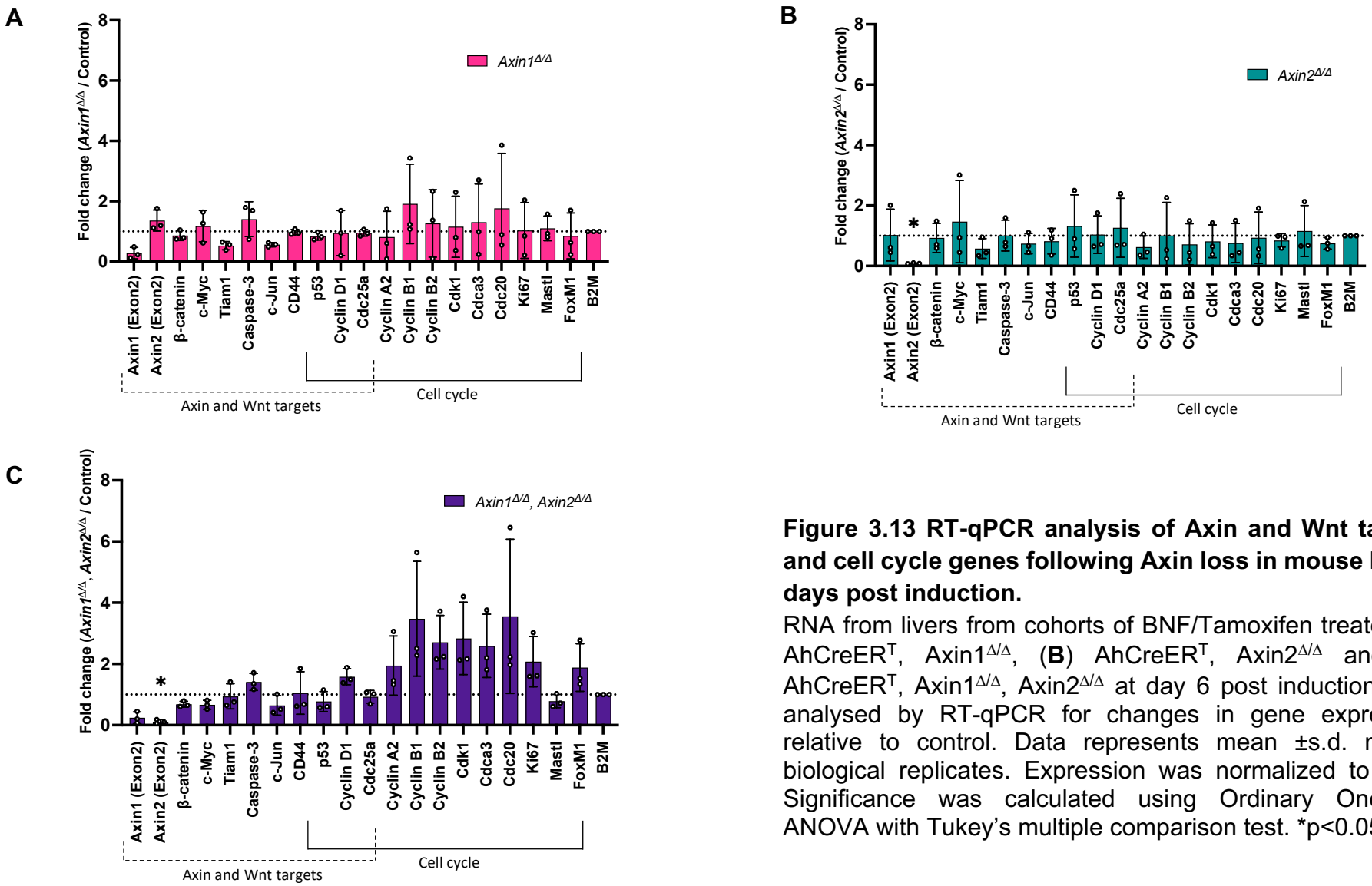

Figure 3.13 RT-qPCR analysis of Axin and Wnt targets and cell cycle genes following Axin loss in mouse liver 6 days post induction.

RNA from livers from cohorts of BNF/Tamoxifen treated (**A**) AhCreER^{T}, Axin1$^{\Delta/\Delta}$, (**B**) AhCreER^{T}, Axin2$^{\Delta/\Delta}$ and (**C**) AhCreER^{T}, Axin1$^{\Delta/\Delta}$, Axin2$^{\Delta/\Delta}$ at day 6 post induction were analysed by RT-qPCR for changes in gene expression relative to control. Data represents mean ±s.d. n = 3 biological replicates. Expression was normalized to B2M. Significance was calculated using Ordinary One-Way ANOVA with Tukey's multiple comparison test. *p<0.05

3.2.10 Effects of Axin loss in the liver on progenitor, lineage, and mature liver cell marker expression 6 days post induction.

During homeostasis, expression of the Wnt target *Lgr5* has been shown to be restricted to the central vein (Halpern et al. 2017) however, upon central vein injury using carbon tetrachloride (CCL_4), these normally quiescent stem cells give rise to new hepatocytes and ductal cells (Huch et al. 2013; Cao et al. 2017). Additionally, LGR5 expression has been shown to be elevated in human HCC and mouse liver tumours (Cao et al. 2020). To evaluate any changes to *Lgr5* and other markers of liver cell identity following Axin loss, expression of a panel of progenitor, lineage and mature liver cell markers were assessed using RNA extracted from AhCreER^T Axin1$^{\Delta/\Delta}$, AhCreER^T Axin2$^{\Delta/\Delta}$, and AhCreER^T Axin1$^{\Delta/\Delta}$, Axin2$^{\Delta/\Delta}$ livers at 6 days post BNF/Tamoxifen induction using RT-qPCR.

Expression of the hepatic progenitor marker and Wnt target *Lgr5,* was significantly increased in Axin1$^{\Delta/\Delta}$ livers. Conversely, in Axin2$^{\Delta/\Delta}$ livers, *Lgr5* expression was down 3.7-fold and significantly reduced in the Axin1$^{\Delta/\Delta}$, Axin2$^{\Delta/\Delta}$ livers but to a lesser extent than Axin2$^{\Delta/\Delta}$ alone (Figure 3.14A). No significant changes in the expression of the other progenitor markers *Epcam, Trop2*, *Spp1* and *Sox9* were observed in any of the Axin deleted cohorts.

Expression of biliary epithelial cell markers *Hnf1b*, *Krt19*, and *Krt7* were highly variable in Control livers and not significantly changed in any of the Axin deleted cohorts (Figure 3.14B). No changes in expression of hepatocyte lineage markers *Hnf4*α, *Prox1*, *Tbx3* and *Afp* were observed in any of the Axin deleted livers (Figure 3.14C). Mature hepatocyte markers *Fah*, *Albumin* and *Ass1* were not statistically different in any of the Axin deleted cohorts (Figure 3.14D).

Overall, these results would suggest that 6 days after BNF/Tamoxifen treatment, except for *Lgr5,* the loss Axin1, Axin2 or both Axins does not alter expression of progenitor, lineage, or mature liver cell marker expression.

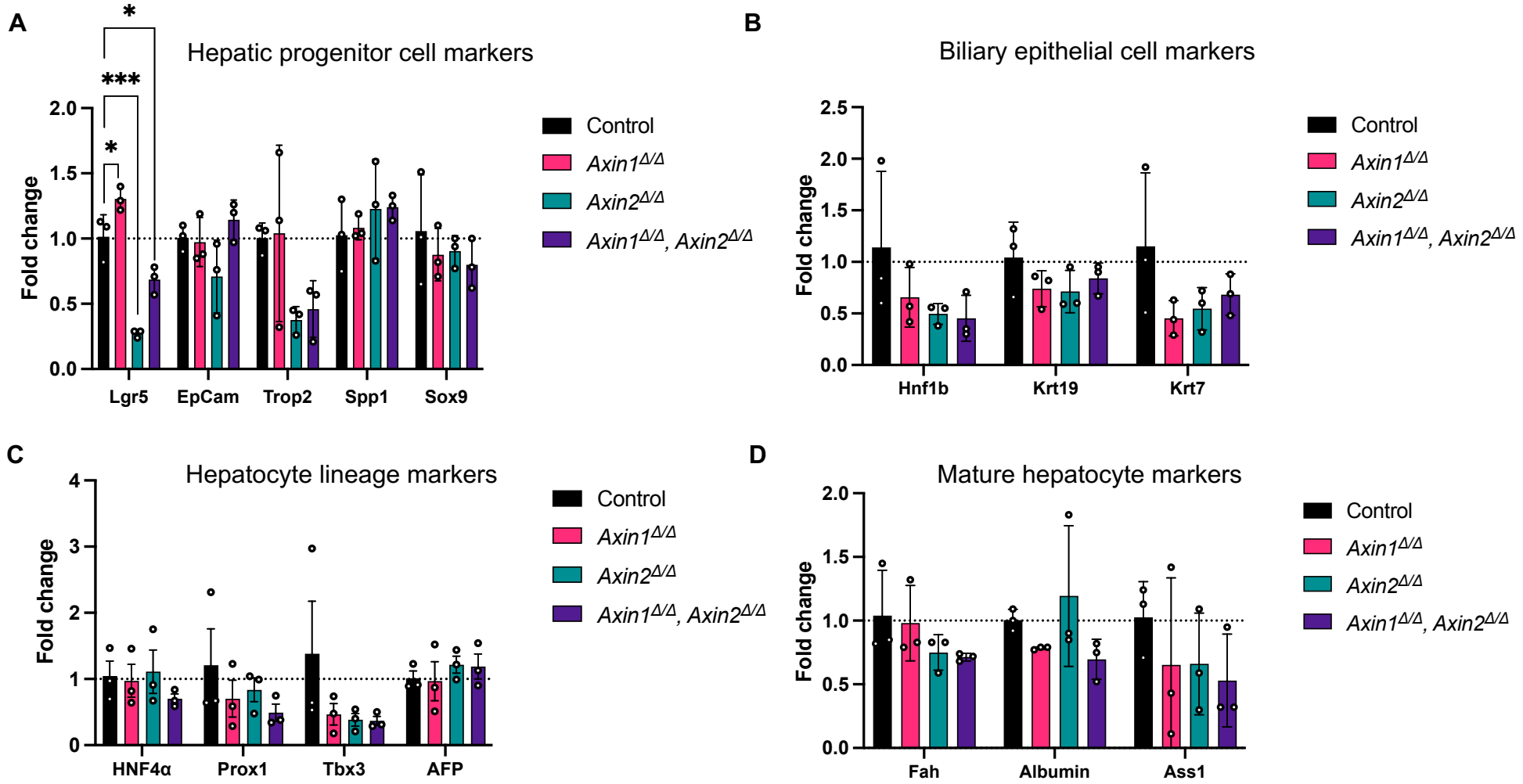

Figure 3.14 RT-qPCR of progenitor, lineage, and mature liver cell markers following Axin loss in mouse liver 6 days post induction. (**A**) Expression of hepatic progenitor cell markers. (**B**) Biliary epithelial cell markers show no significant change in expression. (**C**) Hepatocyte lineage markers show no change in expression in Axin mutant livers. (**D**) There is no significant change in mature hepatocyte marker expression. Data represents mean ±s.d. n = 3 biological replicates. Expression was normalized to B2M. Fold change calculated relative to Control samples. Significance was calculated using Ordinary One-Way ANOVA with Tukey's multiple comparison test. *p<0.05, ***p<0.001

3.2.11 Effects of Axin loss in the mouse liver 6 days post induction on Yap and downstream targets.

Having found that Axin deletion did not result in a clear strong Wnt/β-catenin pathway activation, the Hippo pathway was looked at as an alternative link to the increased proliferation. The Hippo pathway is important in the control of liver size (Camargo et al. 2007) liver regeneration (Loforese et al. 2017) and the upregulation of cell cycle gene transcription (Mizuno et al. 2012). Yap1, the downstream nuclear effector of the Hippo signalling pathway has been shown to bind to Axin1 and has been shown to be sequestered to the β-catenin destruction complex in Wnt-OFF cells (Azzolin et al. 2014). To assess the effect of Axin1, Axin2 and both Axin1 and Axin2 deletion on levels of Yap in the liver, IHC and Western blot analyses were performed on AhCreER^{T} Axin1$^{\Delta/\Delta}$, AhCreER^{T} Axin2$^{\Delta/\Delta}$, and AhCreER^{T} Axin1$^{\Delta/\Delta}$, Axin2$^{\Delta/\Delta}$ livers at 6 days post BNF/Tamoxifen induction.

Microscopic examination revealed strong staining of bile ducts and endothelial cells in control and Axin cohorts (Figure 3.15A). No significant difference in staining patterns were observed between Axin1$^{\Delta/\Delta}$, Axin2$^{\Delta/\Delta}$, and Axin1$^{\Delta/\Delta}$, Axin2$^{\Delta/\Delta}$ livers. Total proteins from whole liver were extracted from control and Axin cohorts at 6 days post induction. Yap protein levels were variable within control and Axin deleted cohorts (Figure 3.15B). Normalised to β-actin, Yap protein levels were not statistically different between control and Axin deleted cohorts apart from a possible trend for a reduced level of Yap protein in Axin2$^{\Delta/\Delta}$ livers (Figure 3.15C).

To further assess any changes in the Hippo pathway, the expression of *Yap*, the co-activator *Wwtr1* and several Yap targets were determined using RT-qPCR. cDNA was made from RNA extracted from control, AhCreER^{T} Axin1$^{\Delta/\Delta}$, AhCreER^{T} Axin2$^{\Delta/\Delta}$, and AhCreER^{T} Axin1$^{\Delta/\Delta}$, Axin2$^{\Delta/\Delta}$ livers at 6 days post BNF/Tamoxifen induction. This was then used to perform RT-qPCR with primers directed towards *Yap*, *Wwtr1*, *Cyr61*, *Ctgf*, *Gpc3*, *Birc5*, *Fas*, *Sfrp1* and *Hmmr*. The loss of either Axin1 (Figure 3.16A) or Axin2 (Figure 3.16B) alone did not result in changes to any of the targets examined. Dual loss of Axin1 and Axin2 resulted in a 2.3 to 2.7-fold increase in the expression of *Hmmr* and *Birc5* but this was not significant due to variability (Figure 3.16C).

Overall, these results would suggest that 6 days post induction, in the liver, the loss of Axin1, Axin2 or both Axin1 and Axin2 does not result in the strong alteration of Yap protein localisation or protein levels. In addition, there were no clear changes to expression of Yap downstream targets that were examined in this study.

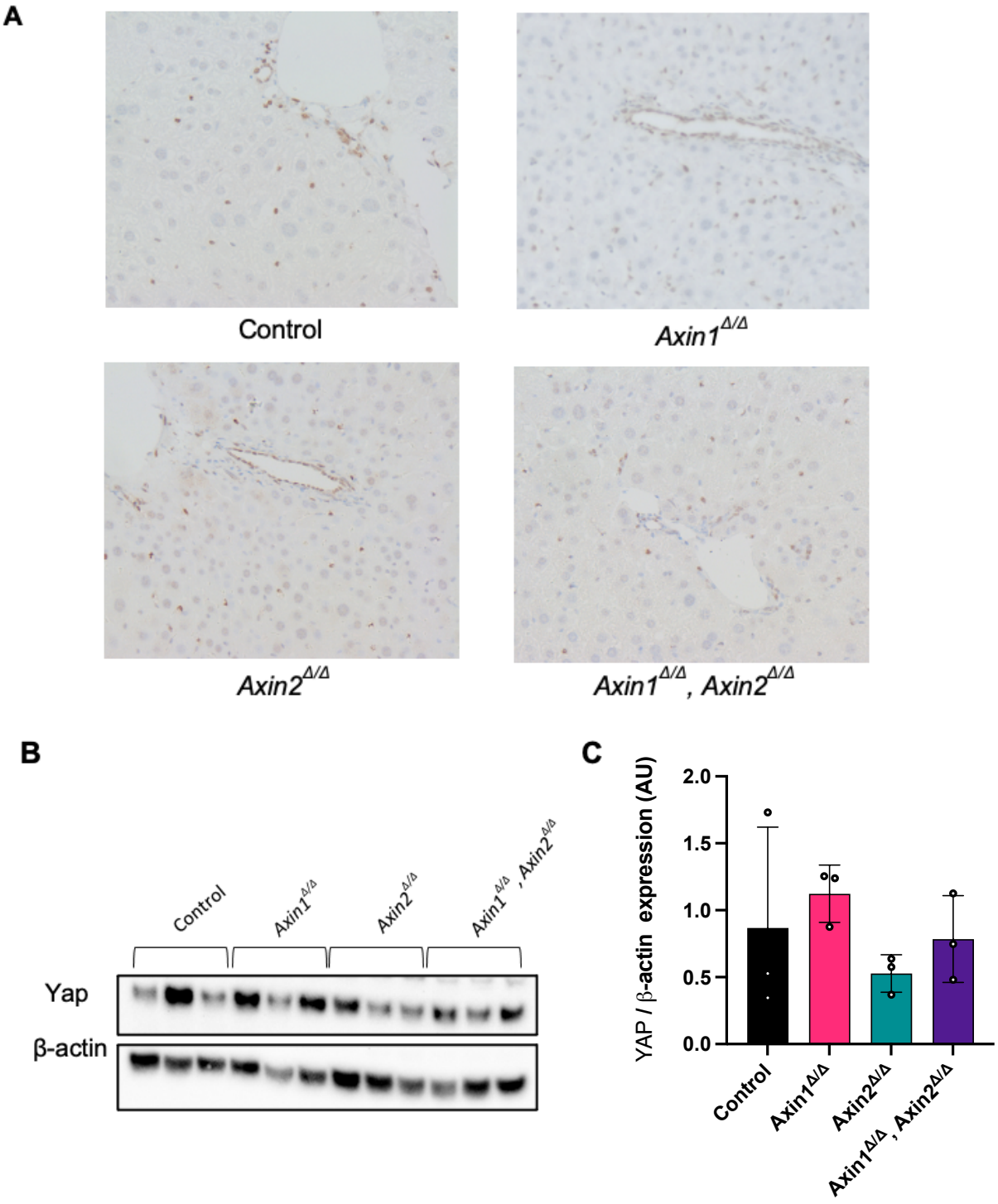

Figure 3.15 Variable total Yap protein levels following Axin loss in the mouse liver 6 days post induction.

No clear differences in Yap expression were seen between control and Axin mutants. (**A**) Representative images of Yap staining in mouse livers in Axin deleted cohorts at 6 days post BNF/Tamoxifen induction. (**B**) Western blot comparing Yap levels between control and Axin mutants. (**C**) Quantification of Yap protein normalised to β-actin. n= 3

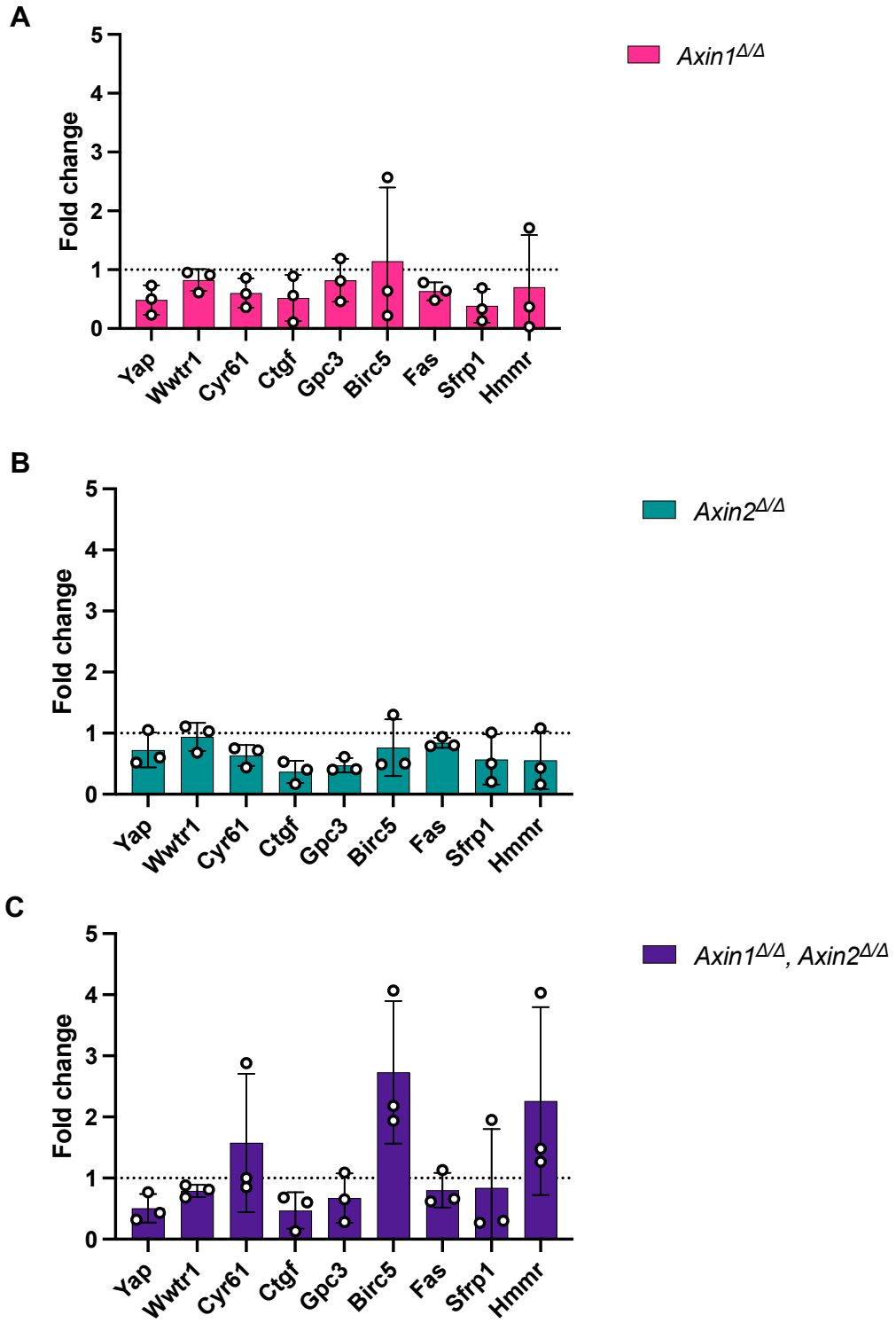

Figure 3.16 No significant changes to Yap, Wwtr1 and Yap downstream targets expression levels following Axin loss in mouse liver 6 days post induction.

No statistically significant changes were seen in (**A**) Axin1$^{\Delta/\Delta}$, (**B**) Axin2$^{\Delta/\Delta}$ or (**C**) Axin1$^{\Delta/\Delta}$, Axin2$^{\Delta/\Delta}$ livers at 6 days PI. Data represents mean ±s.d. n = 3 biological replicates. Data was normalised to B2M and is shown as the relative fold change to induced and age matched AhCreER^{+}, Axin1$^{+/+}$, Axin2$^{+/+}$ (Control). Significance was calculated using Ordinary One-Way ANOVA with Tukey's multiple comparison test.

3.3 Results – Analysis of mouse liver 1 month post AhCreER^T driven Axin recombination

To assess the short to mid-term impact of Axin deletion in the liver, cohorts were established to be taken at 1 month post induction. This was done in part to evaluate Axin deleted livers without the lingering presence of BNF/Tamoxifen. Additionally, to assess whether there were any delayed responses when using AhCreER^T compared to AhCre. Mice aged approximately 10 weeks old and bearing the transgenes AhCreER^T Axin1$^{fl/fl}$, AhCreER^T Axin2$^{fl/fl}$, or AhCreER^T Axin1$^{fl/fl}$, Axin2$^{fl/fl}$ were induced with BNF/Tamoxifen as previously described and dissected 1 month post induction. Macroscopic examination of livers at 1 month post induction revealed no gross abnormalities and liver to body weight ratios were unchanged compared to control (data not shown).

3.3.1 *Axin1* and *Axin2* transcript expression in the liver following AhCreER^T driven recombination 1 month post induction.

To determine whether the reduced expression of transcripts containing exon 2 of Axin1 and Axin2 was maintained, the same sets of primer pairs as described in section 3.2.4, were used in RT-qPCR assays using RNA extracted from whole livers of AhCreER^T Axin1$^{\Delta/\Delta}$, AhCreER^T Axin2$^{\Delta/\Delta}$, and AhCreER^T Axin1$^{\Delta/\Delta}$, Axin2$^{\Delta/\Delta}$ cohorts at 1 month post BNF/Tamoxifen induction.

AhCreER^T driven recombination resulted in an average 81% and 83% reduction in the expression of transcripts containing exon 2 of *Axin1* in Axin1$^{\Delta/\Delta}$ and double Axin1$^{\Delta/\Delta}$, Axin2$^{\Delta/\Delta}$ mutant livers respectively (Figure 3.17A). Exon 2-containing transcripts of *Axin2* were decreased by 16.7 and 13.7-fold respectively in Axin2$^{\Delta/\Delta}$ and Axin1$^{\Delta/\Delta}$, Axin2$^{\Delta/\Delta}$ livers (Figure 3.17B). These results are comparable to what was seen at day 6 post induction (Figure 3.4) suggesting recombined cells are not replaced and that the loss of transcripts containing exon 2 of *Axin1* and *Axin2* is maintained.

Using the pairs of primers that target regions at the c-terminus (see section 3.2.4), outside the recombined regions of *Axin1* and *Axin2*, expression of *Axin1* did not alter at 1 month post BNF/Tamoxifen induction in AhCreER^T Axin1$^{\Delta/\Delta}$, AhCreER^T Axin2$^{\Delta/\Delta}$, and AhCreER^T Axin1$^{\Delta/\Delta}$, Axin2$^{\Delta/\Delta}$ cohorts (Figure 3.17C), matching the results

seen at day 6 post induction. Expression of *Axin2* using primers binding at the c-terminus remained comparable to control in AhCreER^{T} Axin1$^{\Delta/\Delta}$ and AhCreER^{T} Axin2$^{\Delta/\Delta}$ samples, equivalent to the results seen at day 6 post induction. However, in contrast to day 6, overall *Axin2* expression was significantly increased 2.8-fold in the AhCreER^{T} Axin1$^{\Delta/\Delta}$, Axin2$^{\Delta/\Delta}$ livers at 1 month post induction (Figure 3.17D).

Overall, these results show that the loss of transcripts containing exon 2 of *Axin1* and *Axin2* is maintained and is slightly decreased at 1 month post induction when compared to day 6 post induction. However, unlike at day 6 post induction, expression of c-terminal transcripts of *Axin2* increased almost 3-fold in AhCreER^{T} Axin1$^{\Delta/\Delta}$, Axin2$^{\Delta/\Delta}$ livers, suggesting that at later times after gene deletion, the Wnt/β-catenin pathway may become activated.

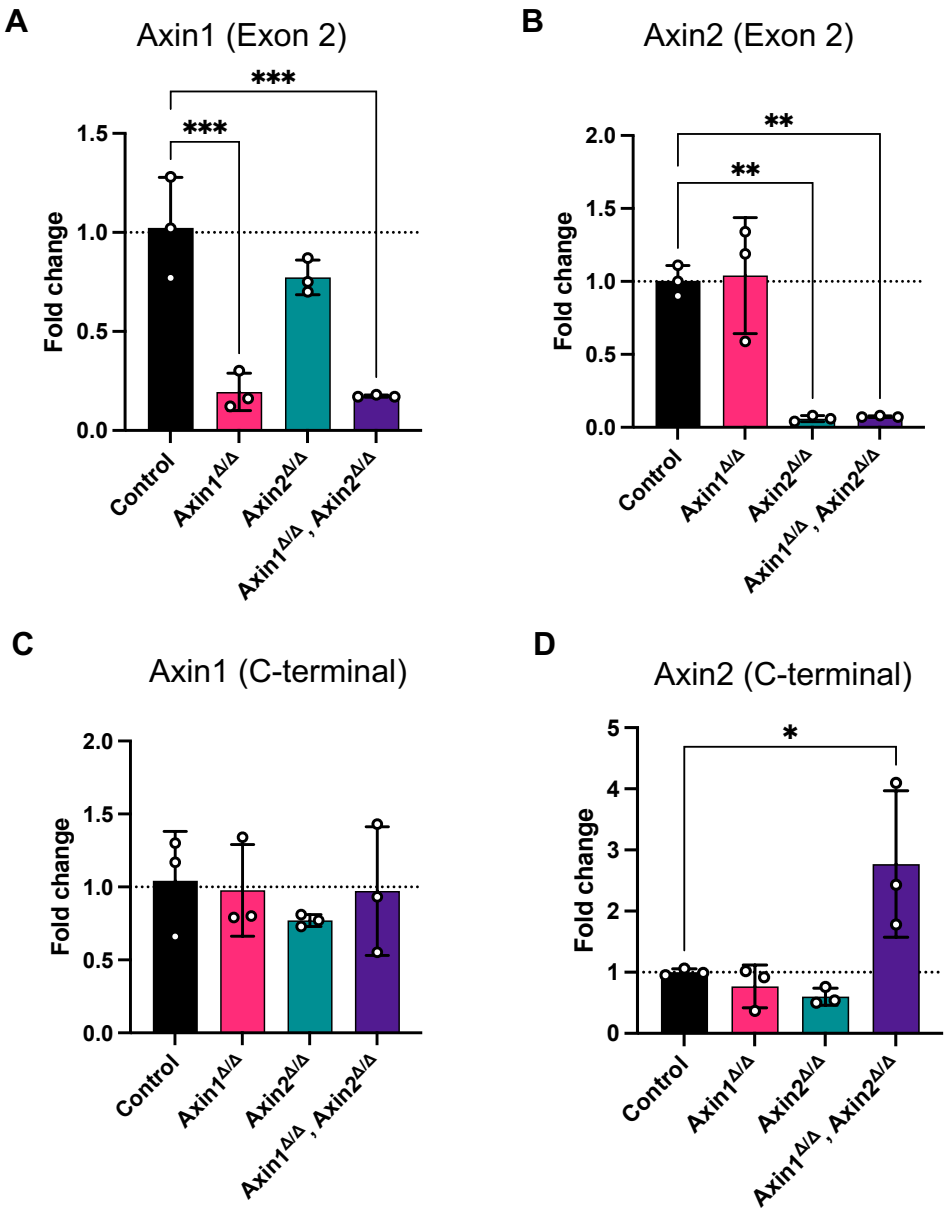

Figure 3.17 Reduced expression of *Axin1* and *Axin2* transcripts containing exon 2 at 1 month post AhCreER^{T} mediated recombination is retained in mouse livers. RT-qPCR confirmed the maintained loss of expression of exon 2 containing transcripts of Axin1 in Axin1$^{\Delta/\Delta}$ and Axin1$^{\Delta/\Delta}$, Axin2$^{\Delta/\Delta}$ livers (**A**) and exon 2 containing transcripts of Axin2 in Axin2$^{\Delta/\Delta}$ and Axin1$^{\Delta/\Delta}$, Axin2$^{\Delta/\Delta}$ livers (**B**). Expression of *Axin1* exons 8-9 (**C**) showed no significant difference in any of the mutant mice. Expression of *Axin2* exons 10-11 (**D**) showed a significant increase in Axin1$^{\Delta/\Delta}$, Axin2$^{\Delta/\Delta}$ only. Data represents mean ±s.d. n = 3 biological replicates**.** Data was normalised to B2M and is shown as the relative fold change to livers from BNF/Tamoxifen treated and age matched AhCreER^{+}, Axin1$^{+/+}$, Axin2$^{+/+}$ (Control). Significance was calculated using Ordinary One-Way ANOVA with Tukey's multiple comparison test *p<0.05 **p<0.01 ***p<0.001

3.3.2 Axin, Wnt targets and cell cycle expression following Axin deletion in the mouse liver 1 month post induction.

At 3 months post induction in the study by Feng (2012), the loss of Axin1 resulted in increased expression of Wnt targets *CD44* and *Cdc25a* which were only expressed at basal or lower levels, 4 days after Axin1 deletion. To assess possible latent Wnt target activation, the same set of Wnt target genes used at day 6 post induction and by Feng (2012) were utilised to evaluate the effects the loss of Axin1, Axin2 and both Axin1 and Axin2 in the AhCreER^{T} model at 1 month post BNF/Tamoxifen induction.

RNA isolated from AhCreER^{T}, Axin1$^{\Delta/\Delta}$, AhCreER^{T}, Axin2$^{\Delta/\Delta}$, and AhCreER^{T}, Axin1$^{\Delta/\Delta}$, Axin2$^{\Delta/\Delta}$ livers at 1 month post BNF/Tamoxifen induction revealed reduced expression of exon 2 containing transcripts of *Axin1* and *Axin2* as expected in each cohort, and as seen at day 6. However, no significant changes in expression of Axin and Wnt targets *Axin2* (in Axin1$^{\Delta/\Delta}$ cohort only), *β-catenin*, *c-Myc*, *Caspase-3*, *c-Jun*, *CD44*, *p53*, *CyclinD1* or *Cdc25a* were observed (Figure 3.18). *CyclinD1* expression was down 65% in AhCreER^{T}, Axin2$^{\Delta/\Delta}$ livers and increased an average 2.5-fold in AhCreER^{T}, Axin1$^{\Delta/\Delta}$, Axin2$^{\Delta/\Delta}$ livers, but this was not significant.

At the 3-month timepoint in the study by Feng (2012), RT-qPCR analysis of the panel of genes associated with the G2/M phase of the cell cycle revealed many were maintained at elevated levels, and some such as Cyclin B1 and Cdk1 in particular, were even higher than at day 4. Expression of the panel of G2/M cell cycle genes remained at control levels as they had been at day 6 in the livers of AhCreER^{T}, Axin1$^{\Delta/\Delta}$ (Figure 3.18A) and AhCreER^{T}, Axin2$^{\Delta/\Delta}$ (Figure 3.18B) cohorts at 1 month post BNF/Tamoxifen induction. However, in the AhCreER^{T}, Axin1$^{\Delta/\Delta}$, Axin2$^{\Delta/\Delta}$ livers, expression of *cyclins A2, B1, B2, Cdk1, Cdca3, Cdc20* and *Ki-67* were increased 2-6-fold, overall being higher than at day 6, but again, these increases were not significant due to inter sample variation (Figure 3.18C).

Overall, the loss of Axin1 in an AhCreER^{T} context does not appear to phenocopy the expression of the panel of Axin and Wnt targets, and G2/M cells cycle genes that was seen following the loss of Axin1 when using AhCre. Loss of Axin2 alone using AhCreER^{T} appears to not have any discernible effect either. However, when both Axin1 and Axin2 are deleted, the increased expression of G2/M cell cycle gene panel resembles that seen by Feng (2012) using AhCre to delete Axin1. This increase is not only maintained but produces a stronger response at later timepoints.

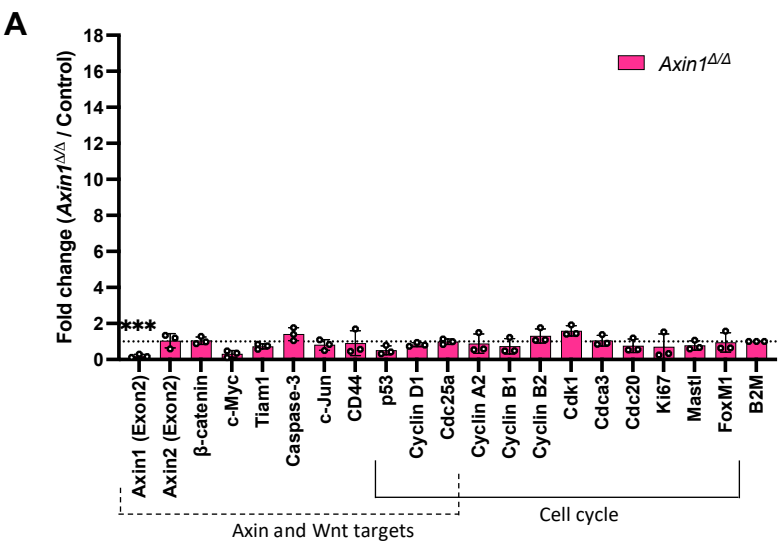

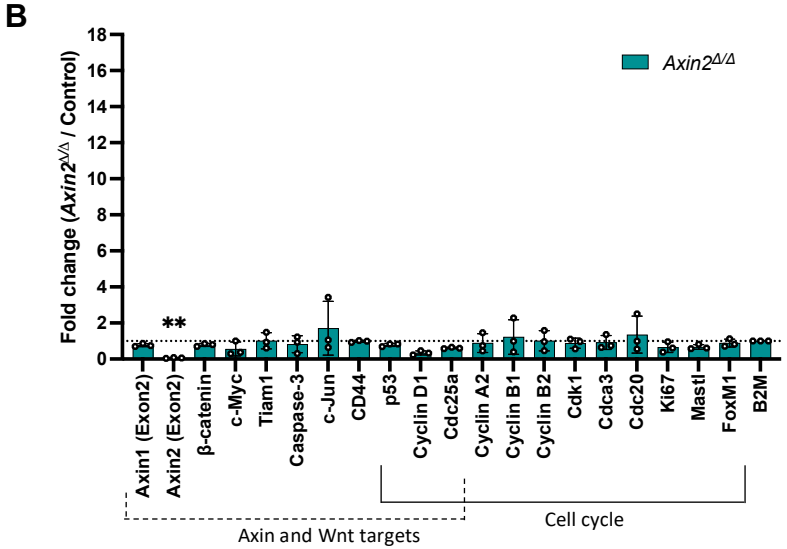

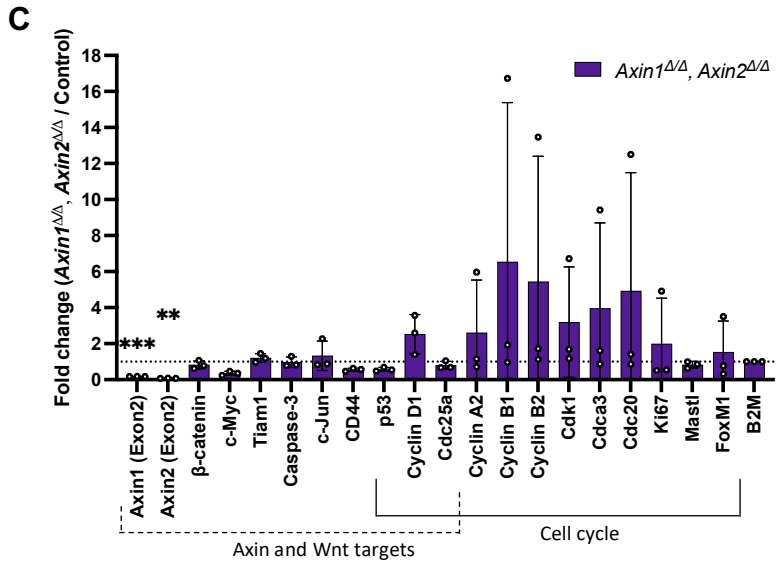

Figure 3.18 RT-qPCR analysis of Axin and Wnt targets and cell cycle gene expression in mouse liver 1 month post induction. Changes in gene expression from livers of (**A**) AhCreER^{T} Axin1$^{\Delta/\Delta}$ (**B**) AhCreER^{T}, Axin2$^{\Delta/\Delta}$ (**C**) AhCreER^{T} Axin1$^{\Delta/\Delta}$, Axin2$^{\Delta/\Delta}$ cohorts 1 month post BNF/Tamoxifen induction. Data represents mean ±s.d. n = 3 biological replicates. Expression was normalized to B2M and relative fold change calculated to age matched control (AhCreER^{T+}, Axin1$^{+/+}$, Axin2$^{+/+}$ 1 month post BNF/Tamoxifen induced). Significance was calculated using Ordinary One-Way ANOVA with Tukey's multiple comparison test. **P<0.01, ***P<0.001

3.3.3 *Lgr5* expression following Axin deletion at 1 month post induction.

Apart from the progenitor and Wnt/β-catenin target *Lgr5*, no significant changes were observed in the expression of progenitor, lineage, and mature liver cell markers at day 6 post induction. At one month post induction, overall *Axin2* expression (using primers that target outside the area of recombination) was shown to be increased in AhCreER^{T} Axin1$^{\Delta/\Delta}$, Axin2$^{\Delta/\Delta}$ livers, suggesting Wnt/β-catenin pathway activation (Figure 3.17D). To determine the effects of extended Axin deletion on *Lgr5* expression, RT-qPCR was carried out using RNA extracted from livers of AhCreER^{T} Axin1$^{\Delta/\Delta}$, AhCreER^{T} Axin2$^{\Delta/\Delta}$, and AhCreER^{T} Axin1$^{\Delta/\Delta}$, Axin2$^{\Delta/\Delta}$ cohorts at 1 month post BNF/Tamoxifen induction (Figure 3.19).

Lgr5 expression returned from slightly elevated levels at day 6, and back to control levels in AhCreER^{T} Axin1$^{\Delta/\Delta}$ livers at 1 month post induction. In the AhCreER^{T} Axin2$^{\Delta/\Delta}$ livers, *Lgr5* expression was reduced by 61%, slightly less than the 73% reduction seen at day 6. The reduction in *Lgr5* expression in AhCreER^{T} Axin1$^{\Delta/\Delta}$, Axin2$^{\Delta/\Delta}$ livers seen at day 6 was no longer observed at 1 month post induction.

This data would suggest that deletion of Axin2 results in a repression in Wnt/β-catenin signalling however, when combined with Axin1 deletion, this effect is suppressed, even though loss of Axin1 alone has no observable effect.

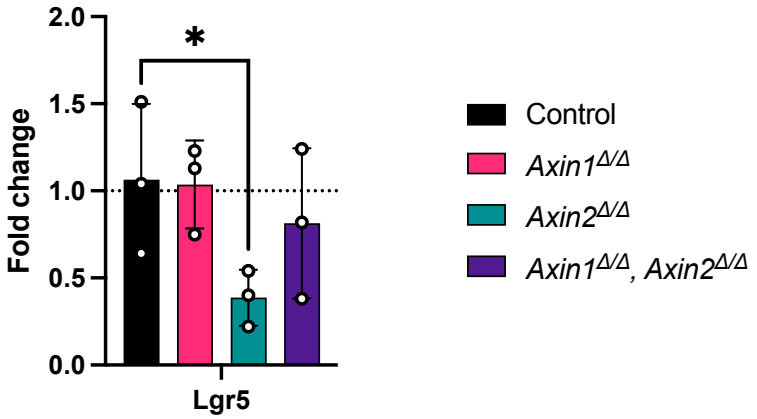

Figure 3.19 *Lgr5* expression is reduced in AhCreER^{T}, Axin2$^{\Delta/\Delta}$ livers at 1 month post induction.
RT-qPCR for *Lgr5* expression from livers of AhCreER^{T} Axin1$^{\Delta/\Delta}$, AhCreER^{T}, Axin2$^{\Delta/\Delta}$, and AhCreER^{T} Axin1$^{\Delta/\Delta}$, Axin2$^{\Delta/\Delta}$ cohorts 1 month post BNF/Tamoxifen induction. Data represents mean ±s.d. n = 3 biological replicates. Expression was normalized to B2M and relative fold change calculated to age matched control (AhCreER^{T+}, Axin1$^{+/+}$, Axin2$^{+/+}$ 1 month post BNF/Tamoxifen induced). Significance was calculated using Ordinary One-Way ANOVA with Tukey's multiple comparison test.

3.3.4 Effects of Axin loss in the mouse liver 1 month post induction on Yap and downstream targets expression.

A trend for elevated levels of *Birc5* and *Hmmr* was seen in the livers of AhCreER^{T} Axin1$^{\Delta/\Delta}$, Axin2$^{\Delta/\Delta}$ cohorts at day 6 post induction. Elevated expression of *Birc5* or *Hmmr* is associated with the G2/M phase of the cell cycle (Chandele et al. 2004; Ly et al. 2017) and a worse clinical outcome in cancer patients (Lu et al. 2021; Xu et al. 2021). To determine the effects of extended Axin deletion on expression of Yap and its downstream targets, RT-qPCR was carried out using RNA extracted from livers of AhCreER^{T} Axin1$^{\Delta/\Delta}$, AhCreER^{T} Axin2$^{\Delta/\Delta}$, and AhCreER^{T} Axin1$^{\Delta/\Delta}$, Axin2$^{\Delta/\Delta}$ cohorts at 1 month post BNF/Tamoxifen induction.

As seen at day 6 post induction (Figure 3.16), the loss of either Axin1 or Axin2 had no significant effect on the expression of *Yap*, *Wwtr1*, *Cyr61*, *Ctgf*, *Gpc3*, *Birc5*, *Fas*, *Sfrp1* and *Hmmr* at 1 month post induction (Figure 3.20A, B). The dual loss of Axin1 and Axin2 resulted in an average 4.6 and 3.2-fold increase in the expression of *Birc5* and *Hmmr* (Figure 3.20C) compared to the 2.7 and 2.3-fold increase seen at day 6 post induction. Although this increase in expression was higher, it was still not significant due to variability.

Taken together, these results suggest that there is no strong alteration to the expression of *Yap* or its downstream targets at 1 month post induction. Elevated *Birc5* expression may be explained by it having been shown to also be a Wnt/β-catenin target (Zhang et al. 2001).

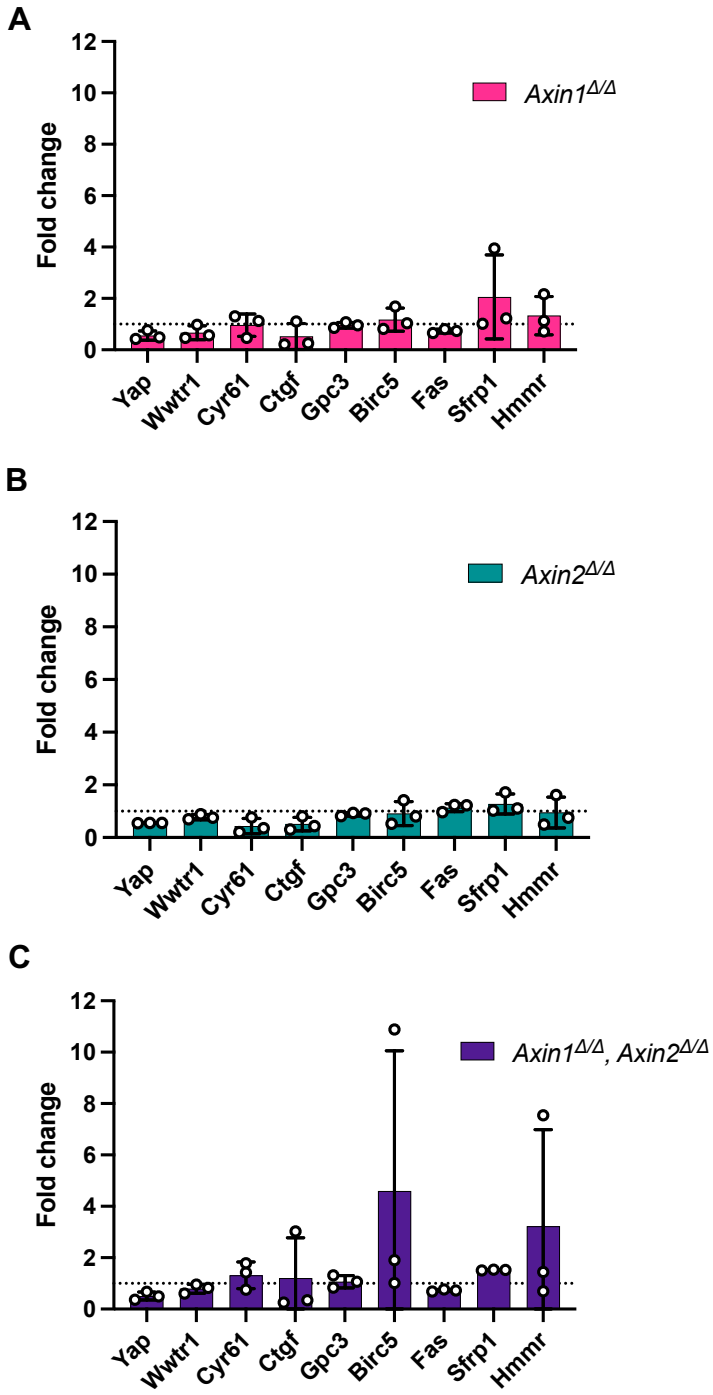

Figure 3.20 No significant changes to Yap, Wwtr1 and downstream targets expression levels in mouse liver 1 month post AhCreER^{T} mediated induction.
Changes in gene expression from livers of (**A**) AhCreER^{T} Axin1$^{\Delta/\Delta}$ (**B**) AhCreER^{T}, Axin2$^{\Delta/\Delta}$ (**C**) AhCreER^{T} Axin1$^{\Delta/\Delta}$, Axin2$^{\Delta/\Delta}$ cohorts 1 month post BNF/Tamoxifen induction. Data represents mean ±s.d. n = 3 biological replicates. Expression was normalized to B2M and relative fold change calculated to age matched control (AhCreER^{T+}, Axin1$^{+/+}$, Axin2$^{+/+}$ 1 month post BNF/Tamoxifen induced). Significance was calculated using Ordinary One-Way ANOVA with Tukey's multiple comparison test.

3.4 Results – Analysis of mouse liver at 1 year post AhCreER^T driven Axin recombination.

3.4.1 AhCreER^T Axin1$^{\Delta/\Delta}$, Axin2$^{\Delta/\Delta}$ animals show a reduced lifespan compared to controls, AhCreER^T Axin1$^{\Delta/\Delta}$ and AhCreER^T Axin2$^{\Delta/\Delta}$ mice.

To examine the effects of long term AhCreER^T Axin deletion in the liver, aging cohorts were established with the initial aim of aging the mice up to 2 years. This set up was to enable the examination of both very long-term changes and whether tumours appear. This long time-period was chosen as it exceeded the time previously shown to allow liver tumours to develop in AhCre Axin1$^{\Delta/\Delta}$ mice, which were expected to have higher levels of gene deletion. Mice of approximately 10 weeks of age, and bearing the transgenes AhCreER^T (Control), AhCreER^T Axin1$^{fl/fl}$, AhCreER^T Axin2$^{fl/fl}$, or AhCreER^T Axin1$^{fl/fl}$, Axin2$^{fl/fl}$ were induced with BNF/Tamoxifen as previously described. A summary of induced animals is provided in Figure 3.21A and a comprehensive table of information regarding each individual mouse is included in Appendix I. These mice were then aged and regularly monitored for signs of ill health. If animals were found to be sick, they were killed and dissected. By 1 year post induction, 7 of the AhCreER^T Axin1$^{\Delta/\Delta}$, Axin2$^{\Delta/\Delta}$ animals had to be culled. Four of these animals were dissected due to having distended abdomens and following dissection, they were found to have liver tumours. These tumours appeared as large masses with minimal liver appearing as what could be considered “normal” (Figure 3.21C). For all mice with liver tumours, any normal liver was dissected away separately for downstream analysis. Based on the high tumour burden, the view was taken that it was likely that no AhCreER^T Axin1$^{\Delta/\Delta}$, Axin2$^{\Delta/\Delta}$ animals would survive until the original 2-year goal. A decision was therefore taken to sacrifice 5 animals from each cohort at 1 year post induction to allow for a meaningful comparison of aged non-tumour liver tissue from the different cohorts before the mice became ill. The last AhCreER^T Axin1$^{\Delta/\Delta}$, Axin2$^{\Delta/\Delta}$ mouse had to be culled at day 542 due to sickness. Any remaining mice were culled 100 days after this or earlier if found sick.

The numbers of animals that were aged until they had to be culled due to ill health allowed a Kaplan-Meier survival analysis to be performed (Figure 3.21B). AhCreER^T Axin1$^{\Delta/\Delta}$, Axin2$^{\Delta/\Delta}$ mice had a median survival time of 401 days after

induction which was significantly different ($p<0.0001$, $\chi^2= 29.75$, DF=3) from that of control, AhCreER^T Axin1$^{\Delta/\Delta}$ or AhCreER^T Axin2$^{\Delta/\Delta}$ animals. Notches above the lines indicate the mice that were culled at 1 year post induction or at the final timepoint of 1 ¾ years and were censored for the Kaplan-Meier survival analysis.

Upon dissection, the 5 randomly selected AhCreER^T Axin1$^{\Delta/\Delta}$ and AhCreER^T Axin2$^{\Delta/\Delta}$ animals at one year post induction showed no macroscopic signs of liver tumours or any other notable malignancies. However, of the 5 randomly selected AhCreER^T Axin1$^{\Delta/\Delta}$, Axin2$^{\Delta/\Delta}$ animals, 2 had visible liver tumours. Tumours were identified as solid overgrown masses measuring approximately 8-13 mm in diameter. Non-tumour and tumour regions of the liver were separated based on morphology during dissection for downstream analysis.

From the mice left to age, the remaining 3 AhCreER^T Axin1$^{\Delta/\Delta}$ animals were culled at the 1 ¾ year endpoint and at dissection, no liver tumours were observed. Four aged AhCreER^T Axin2$^{\Delta/\Delta}$ animals after the one-year timepoint between 455- and 594-days post induction had to be culled due to non-liver related reasons. This included overgrown teeth, a sore eye, a lump on the neck and seizures however, no liver tumours were observed. Upon dissection, none of the AhCreER^T Axin2$^{\Delta/\Delta}$ animals aged to the 1 ¾ year post induction timepoint had signs of liver tumours however one animal had an enlarged spleen and one male had enlarged seminal vesicles. In total, 11 out of the 20 AhCreER^T Axin1$^{\Delta/\Delta}$, Axin2$^{\Delta/\Delta}$ mice had visible liver tumours. 10 out of the 11 mice presenting with tumours that were large masses, 1 to 2 per mouse, measuring 10-20 mm in diameter, with one of these tumours being cystic and filled with fluid. The other mouse identified as having liver tumours had small white tumours 2-5 mm in size throughout the liver. One mouse had a pale liver upon dissection (not classed as tumour) and the others appeared to have normal livers. Of note, 4 of the aged AhCreER^T Axin1$^{\Delta/\Delta}$, Axin2$^{\Delta/\Delta}$ females had mammary lumps and 2 males had possible colon polyps but these were not investigated further. Details of malignancies for each mouse are summarised in Appendix I.

Liver/body weight ratios were measured at sacrifice for all animals in the ageing cohorts except those found dead. Aged AhCreER^T Axin1$^{\Delta/\Delta}$, Axin2$^{\Delta/\Delta}$ mice showed close to an average 3 times higher liver/body weight ratio compared to control and single Axin deleted animals. The liver weight was highly variability due to the inclusion of the mass of the tumours (Figure 3.21D).

In summary, the majority of AhCreER^{T} Axin1$^{\Delta/\Delta}$, Axin2$^{\Delta/\Delta}$ mice had to be culled early and many of them due to the presence of liver tumours. A number of AhCreER^{T} Axin2 $^{\Delta/\Delta}$ animals had to be culled sick, however this was not due to any obvious liver complications. In contrast to the study by Feng (2012), none of the 5 AhCreER^{T} Axin1$^{\Delta/\Delta}$ mice dissected at 1 year post induction or the 3 mice at 1 ¾ years post induction showed any obvious signs of liver tumours. This may be due to lower levels of liver recombination using the CreER driver, or potentially through variation in the health status of the animal unit since the time of the previous published studies (Feng et al. 2012). Of note, 45 % of males but only 10 % of females from the whole cohort had liver tumours at dissection. Post hoc analysis using Fisher's exact test revealed this to have a p value of 0.0648. Though this was not significant is does support the observation that rates of liver cancer are 2 to 4 times higher in men than women (Bosch et al. 2004).

A

Genotype	Total number in cohort	Number of death/events	Number of censored subjects	Median Survival	% of all animals in cohort with liver tumour
Control	9	1	5 at 1 year and 3 at 1 3/4 years	Undefined	0.00%
$Axin1^{\Delta/\Delta}$	8	0	5 at 1 year and 3 at 1 3/4 years	Undefined	0.00%
$Axin2^{\Delta/\Delta}$	25	8	5 at 1 year and 12 at 1 3/4 years	Undefined	0.00%
$Axin1^{\Delta/\Delta}$, $Axin2^{\Delta/\Delta}$	20	15	5 at 1 year	401	55.00%

B

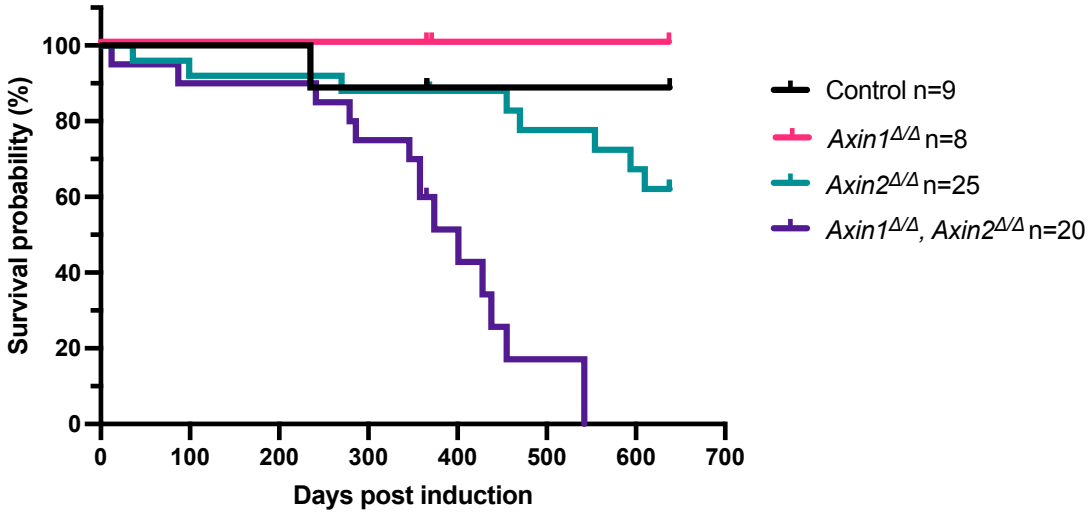

C

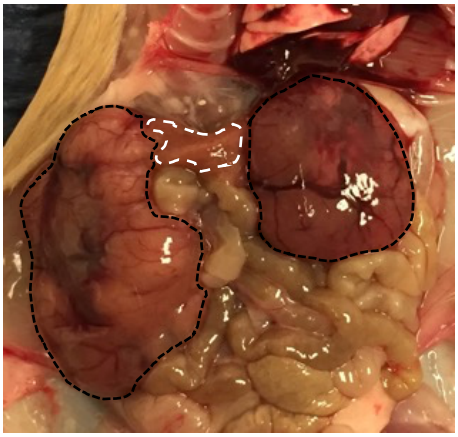

D

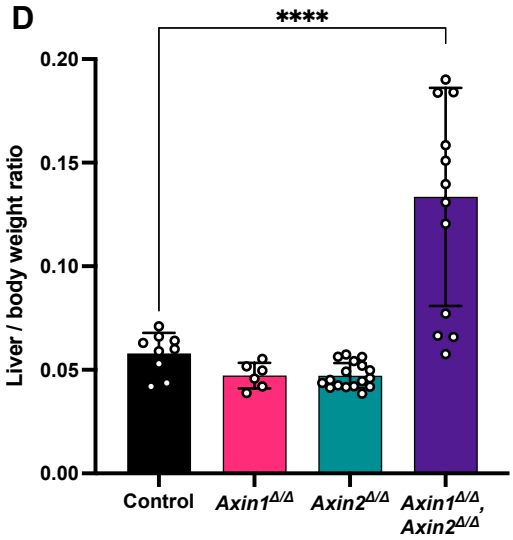

Figure 3.21 Aged AhCreER^{T} Axin1$^{\Delta/\Delta}$, Axin2$^{\Delta/\Delta}$ mice develop HCC.
(A) Summary table of Axin deleted animals used in ageing study. **(B)** Cohorts of control (AhCreER^{T+}, Axin1$^{+/+}$, Axin2$^{+/+}$), AhCreER^{T} Axin1$^{\Delta/\Delta}$, AhCreER^{T} Axin2$^{\Delta/\Delta}$, and AhCreER^{T} Axin1$^{\Delta/\Delta}$, Axin2$^{\Delta/\Delta}$ mice were aged whilst being monitored for signs of ill health. Animals were culled when moribund or by 640 days and Kaplan-Meier survival was performed. Animals culled at the 1-year timepoint and at 640 days are censored and are shown as notches on survival curve. Double Axin1 and Axin2 deleted animals were observed to have a much-reduced survival probability, with a median survival time of 401 days, compared to control or single Axin deleted animals. Reduction in survival probability in AhCreER^{T} Axin1$^{\Delta/\Delta}$, Axin2$^{\Delta/\Delta}$ mice was found to be extremely significant ($p<0.0001$, $\chi^2=29.75$, DF=3). **(C)** Image of liver tumour from AhCreER^{T} Axin1$^{\Delta/\Delta}$, Axin2$^{\Delta/\Delta}$ mouse culled and dissected due to distended abdomen. Black outline indicates liver tumour. White outline indicates non-tumour. **(D)** Liver/body weight ratio (including all tumour mass if applicable) of all BNF/Tamoxifen induced and aged cohorts at sacrifice that were dissected, including those culled at 1-year timepoint. Those found dead before dissection are not included.

3.4.2 Analysing the long-term effects of induced Axin deletion in the mouse liver.

The next section will focus on the examination of Axin deletion in the liver from the cohorts of mice that were killed at the 1-year timepoint to first consider "normal" tissue biology. As already mentioned, 2 of the AhCreER^{T} Axin1$^{\Delta/\Delta}$, Axin2$^{\Delta/\Delta}$ that were killed for this cohort already had visible liver tumours. Care was taken at dissection to separate normal and tumour at the macro level for downstream analysis however, this does not exclude the possibility that the tissue considered normal may contain areas that are in the early stages of tumourigenesis or sites that are neoplastic at the micro level.

3.4.3 Effects of induced Axin deletion in the mouse liver at 1 year post induction.

Examination of H&E liver sections from control, AhCreER^{T} Axin1$^{\Delta/\Delta}$, and AhCreER^{T} Axin2$^{\Delta/\Delta}$, showed no obvious gross abnormalities from animals taken at 1-year post induction (Figure 3.22A). H&E sections from AhCreER^{T} Axin1$^{\Delta/\Delta}$, Axin2$^{\Delta/\Delta}$ showed some disorganisation to the liver parenchyma and notably larger cells and nuclei in some sections (Figure 3.22A). Cell size, based on the number of nuclei counted per unit area of the histological section, followed a trend for an increase in AhCreER^{T} Axin1$^{\Delta/\Delta}$ and in AhCreER^{T} Axin1$^{\Delta/\Delta}$, Axin2$^{\Delta/\Delta}$ samples (Figure 3.22B) as previously seen at day 6 (Figure 3.6A). Significantly increased nucleus size persisted in AhCreER^{T} Axin1$^{\Delta/\Delta}$ and in AhCreER^{T} Axin1$^{\Delta/\Delta}$, Axin2$^{\Delta/\Delta}$ samples (Figure 3.22C). No significant changes in cell or nuclei size were seen in AhCreER^{T} Axin2$^{\Delta/\Delta}$ alone.

In summary, AhCreER^{T} Axin1$^{\Delta/\Delta}$ and AhCreER^{T} Axin1$^{\Delta/\Delta}$, Axin2$^{\Delta/\Delta}$ animals show a trend for an increase in liver cell size and a significant increase in the size of hepatocyte nuclei at 1 year post induction. Despite this, only mice with the combined deletion of Axin1 and Axin2 in the liver showed a susceptibility for tumourigenesis in this study.

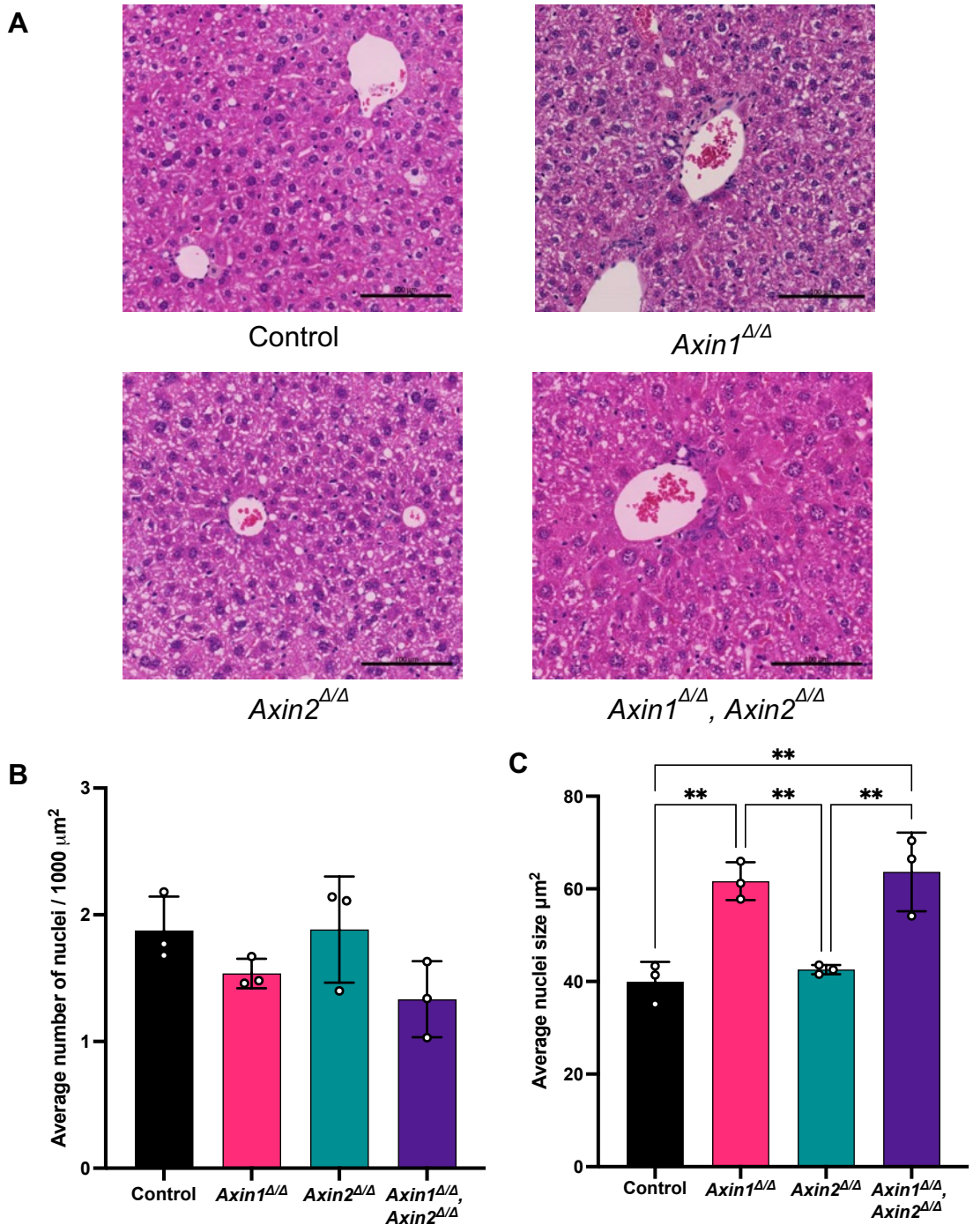

Figure 3.22 H&E liver sections and cell and nuclei size of non-tumour Axin deleted cohorts at 1 year post induction.

Representative images of H&E-stained liver sections from control, AhCreER^{T} Axin1$^{\Delta/\Delta}$, AhCreER^{T} Axin2$^{\Delta/\Delta}$ and AhCreER^{T} Axin1$^{\Delta/\Delta}$, Axin2$^{\Delta/\Delta}$ liver identified as non-tumour at dissection, 1 year post BNF/Tamoxifen induction. (**B**) Quantification of nuclei size based on the average number of nuclei counted per μm^2. Data represents mean ±s.d. from 20 fields of view from 3 biological replicates. **(C)** Quantification of the average size of hepatocyte nuclei. Data represents mean ±s.d. from 10 fields of view from 3 biological replicates. Scale bar 100 μm. CV = Central vein PS = Portal space. Significance was calculated using Ordinary One-Way ANOVA with Tukey's multiple comparison test. **p<0.01

3.4.4 *Axin1* and *Axin2* transcript expression in non-tumour livers following AhCreER^T driven Axin recombination at 1 year post induction.

It was predicted that the additional deletion of Axin2 with Axin1 would result in a stronger Wnt/β-catenin pathway activation. AhCreER^T mediated deletion of Axin1 or Axin2 alone or in combination, did not result in the expected increase in expression of non-deleted exons (C-terminal) of *Axin2* at day 6 post BNF/Tamoxifen induction (Figure 3.4E lanes 2-4). Expression of non-deleted exons of *Axin2* did increase 2.8-fold in AhCreER^T Axin1$^{\Delta/\Delta}$, Axin2$^{\Delta/\Delta}$ livers at 1 month post induction (Figure 3.17D), suggesting some latent Wnt/β-catenin pathway activation and fitting with the hypothesis that combined Axin1 and Axin2 deletion would result in a strong Wnt/β-catenin pathway activation. To confirm expression of transcripts without the recombined regions was maintained and whether there are long term changes to overall *Axin1* and *Axin2* expression, RNA from whole liver samples of AhCreER^T Axin1$^{\Delta/\Delta}$, AhCreER^T Axin2$^{\Delta/\Delta}$, and AhCreER^T Axin1$^{\Delta/\Delta}$, Axin2$^{\Delta/\Delta}$ cohorts at 1 year post BNF/Tamoxifen induction were assessed by RT-qPCR using the same primer pairs as used previously (Figure 3.4A).

As expected from the qPCR data of *Axin1* recombination at 1 year post induction (Figure 3.3A lane 3), expression of transcripts containing exon 2 of *Axin1* in AhCreER^T Axin1$^{\Delta/\Delta}$ and in AhCreER^T Axin1$^{\Delta/\Delta}$, Axin2$^{\Delta/\Delta}$ livers was reduced by an average 63% and 74% respectively (Figure 3.23A). Exon 2-containing transcripts of *Axin2* were decreased by 7.2 and 13.8-fold in AhCreER^T Axin2$^{\Delta/\Delta}$ and AhCreER^T Axin1$^{\Delta/\Delta}$, Axin2$^{\Delta/\Delta}$ livers (Figure 3.23B). This suggests good levels of recombination of both *Axin1* and *Axin2* persists in the liver and that recombined cells are not replaced.

In contrast to day 6- and 1-month post induction, expression of *Axin2* was increased 2-fold in AhCreER^T Axin1$^{\Delta/\Delta}$ livers at 1 year post induction (Figure 3.23B, D). Expression of non-deleted exons of *Axin2* (using primers outside the recombined region at the C-terminal) increased 4-fold in AhCreER^T Axin1$^{\Delta/\Delta}$, Axin2$^{\Delta/\Delta}$ liver samples (Figure 3.23D) compared to only 2.8-fold at 1 month. This may suggest that levels of Wnt pathway activation increase over time in double Axin deleted livers. No changes in non-deleted exons of *Axin2* expression were seen following Axin2 deletion alone (Figure 3.23D). *Axin1* expression is not known to be modulated by alterations in other genes, interestingly however, expression of *Axin1* transcripts increased 2.8-fold in

AhCreER^{T} Axin2$^{\Delta/\Delta}$ livers at 1 year post induction (Figure 3.23A). However, this increase was not significant when using primers binding at the c-terminal of *Axin1* (Figure 3.23C). Elevated expression of non-deleted exons of *Axin1* was also observed in AhCreER^{T} Axin1$^{\Delta/\Delta}$, Axin2$^{\Delta/\Delta}$ liver samples (Figure 3.23C). These observations may suggest that the loss of Axin2 may increase the expression of *Axin1* through some unknown compensatory mechanism.

In summary, from the qPCR (Figure 3.3A lane 3) and RT-qPCR data, recombination of *Axin1* persists and it is reasonable to assume from the RT-qPCR data that recombination of *Axin2* does so also. This suggests recombined cells are not replaced in single or double Axin mutants. Increases in *Axin2* expression suggests some Wnt/β-catenin pathway activation in AhCreER^{T}, Axin1$^{\Delta/\Delta}$ livers at a later timepoint. This contrasts with what was seen in the study by Feng (2012), who saw elevated expression of *Axin2* at the early timepoint but return to control levels at 1 year post induction. Some data suggests AhCreER^{T}, Axin2$^{\Delta/\Delta}$ livers at 1 year post induction result in increases to *Axin1* expression. Expression of transcripts of both *Axin1* and *Axin2* using primers outside the recombined exon 2 increases in AhCreER^{T}, Axin1$^{\Delta/\Delta}$, Axin2$^{\Delta/\Delta}$ non-tumour liver at 1 year post induction.

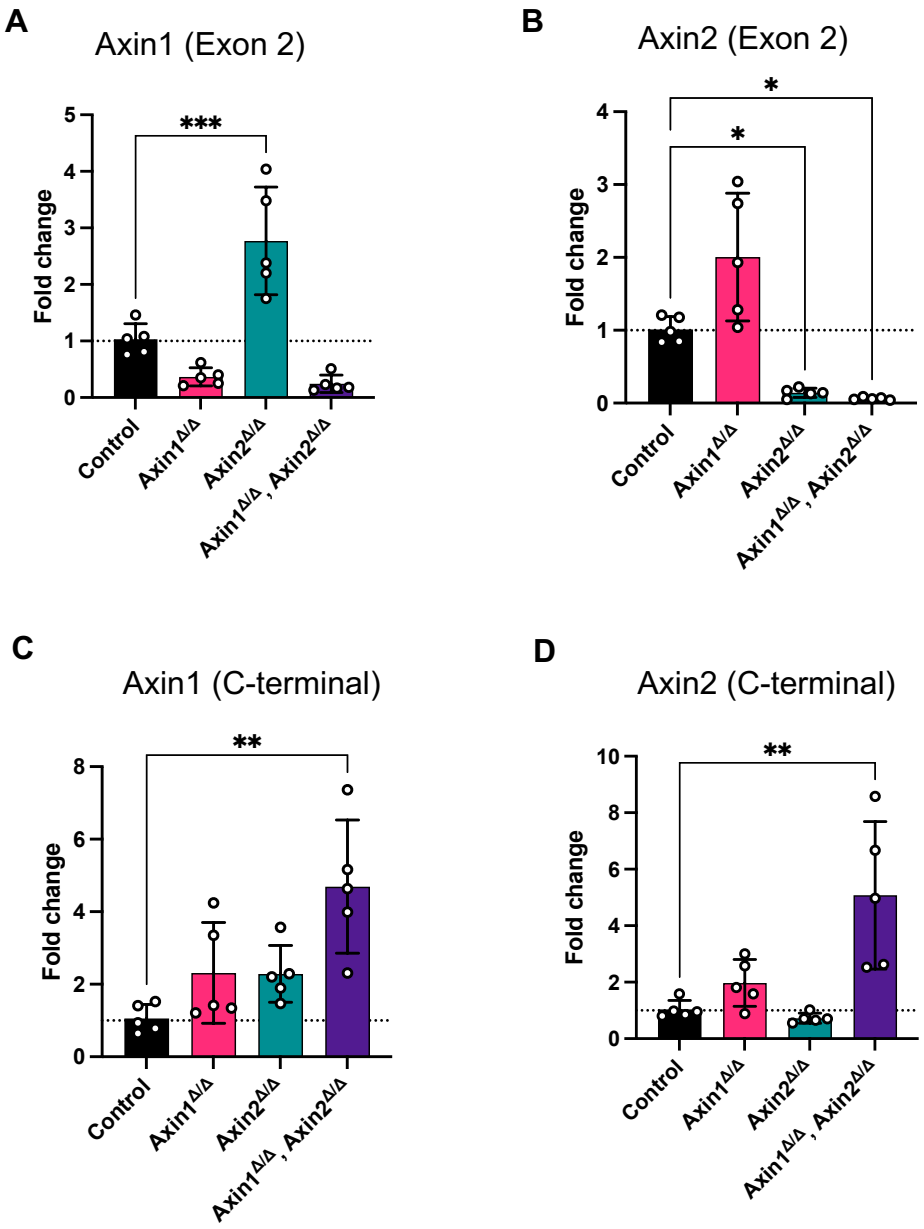

Figure 3.23 Reduced expression of *Axin1* and *Axin2* transcripts containing exon 2 in mouse liver at 1 year post AhCreER^{T} mediated recombination is retained.
(**A**) Expression of Axin1 transcripts containing exon 2 from mouse liver post AhCreER mediated recombination in 1 year post induction cohorts. (**B**) Expression of Axin2 transcripts containing exon 2 from mouse liver post AhCreER mediated recombination in 1 year post induction cohorts. (**C**) Overall expression of Axin1 using primers outside recombined region in mouse liver post AhCreER mediated recombination in 1 year post induction cohorts. (**D**) Overall expression of Axin2 using primers outside recombined region in mouse liver post AhCreER mediated recombination in 1 year post induction cohorts. Data represents mean ±s.d. n = 5 biological replicates**.** Data was normalised to B2M and is shown as the relative fold change to induced and age matched AhCreER^{+}, Axin1$^{+/+}$, Axin2$^{+/+}$ (Control). Significance was calculated using Ordinary One-Way ANOVA with Tukey's multiple comparison test. *p<0.05 , **p<0.01, ***p<0.001

3.4.5 Staining for zonation markers GS and CPS1 in Axin deleted cohorts at 1 year post induction.

As discussed previously, GS is a β-catenin target and expression is tightly regulated in the liver. Expanded expression of GS has been seen with disruption to the β-catenin destruction complex with APC loss or conditional β-catenin activation (Benhamouche et al. 2006, Miyoshi et al. 2009). No changes in GS staining were observed in the study by Feng (2012) with the loss of Axin1 alone. It was hypothesized that Axin2 may be acting in a compensatory way and that the loss of both Axin1 and Axin2 would increase levels of β-catenin and induce expanded GS expression. Surprisingly, this was not seen at day 6 post induction in AhCreER^{T} Axin1$^{\Delta/\Delta}$, Axin2$^{\Delta/\Delta}$. To assess the long-term impact of Axin deletion, immunohistochemistry for GS was carried out on liver tissue sections from AhCreER^{T} Axin1$^{\Delta/\Delta}$, AhCreER^{T} Axin2$^{\Delta/\Delta}$, and AhCreER^{T} Axin1$^{\Delta/\Delta}$, Axin2$^{\Delta/\Delta}$ cohorts at 1 year post BNF/Tamoxifen induction. Sections were also stained for CPS1 which is normally expressed periportally but is excluded from the layers with GS staining (see Introduction section 1.3).

GS expression remained restricted to 2-3 cells surrounding the central vein in Axin1 deleted livers and as seen in control livers (Figure 3.24). CPS1 staining also showed the expected normal staining from the portal space and up to the 2-3 cells layer where GS expression would be. Surprisingly, GS expression was reduced in the aged Axin2 deleted livers. The expression of GS appeared thinner, accompanied by the observation of gaps in GS staining surrounding the central vein (Figure 3.24). Conversely, CPS1 staining appeared to encroach closer to the central vein and occasionally showed expression at the central vein.

Double Axin1 and Axin2 deleted livers showed a variety of phenotypes in their GS and CPS1 expression patterns (Figure 3.24). As seen in the Axin2 livers, GS expression could be reduced or absent in some double Axin1 and Axin2 deleted livers with CPS1 staining strongly around the central vein instead. In other cases, GS expression would show gaps in expression around the central vein but also have patches of GS staining that was not associated with the central vein. In these cases, CPS1 showed patchy staining but the inverse of GS staining. Additional staining patterns are shown in Appendix II.

The aberrant patterns of GS and CPS1 staining was unexpected. The decrease in GS staining in the Axin2 deleted livers might suggest that β-catenin levels were

lower than that observed in the control liver. Four of the aging AhCreER^{T} Axin1$^{\Delta/\Delta}$, Axin2$^{\Delta/\Delta}$ animals were culled before the one-year timepoint due to liver tumours and two of the mice dissected at the one-year time-point had obvious liver tumours. Aberrant GS expression has been reported in up to 70% of early HCC (Nguyen et al. 2016) therefore it is probable that the varying staining patterns are signs of different stages of early development of HCC.

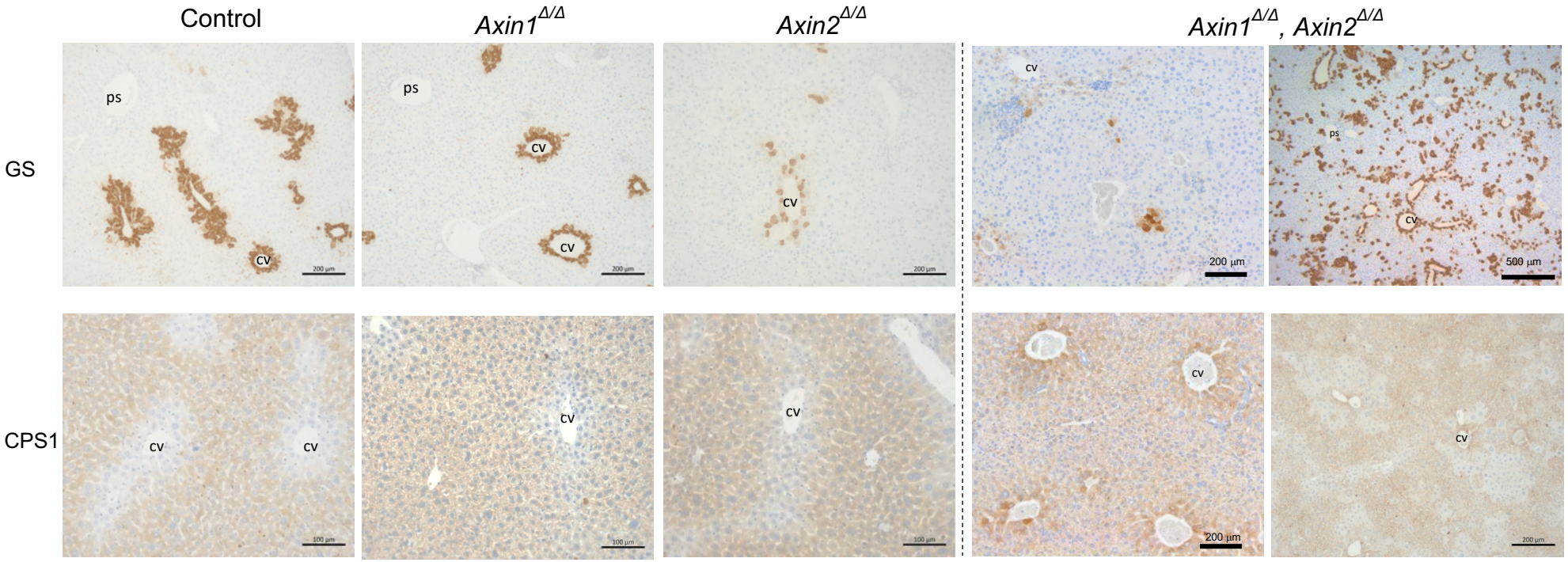

Figure 3.24 Liver zonation markers GS and CPS1 IHC show variability in Axin deleted cohorts at 1 year post induction.
Representative images of GS and CPS1 staining in AhCreER^{T} Axin1$^{\Delta/\Delta}$, AhCreER^{T} Axin2$^{\Delta/\Delta}$, and some of the variety of staining in AhCreER^{T} Axin1$^{\Delta/\Delta}$, Axin2$^{\Delta/\Delta}$ liver identified as non-tumour at dissection at 1 year post BNF/Tamoxifen induction. CV = central vein, PS = portal space

3.4.6 β-catenin localisation and total levels following Axin loss in the mouse liver 1 year post BNF/Tamoxifen induction.

Combined deletion of Axin1 and Axin2 at day 6 post induction did not result in nuclear mis-localisation of β-catenin (Figure 3.11). This challenged the hypothesis that the lack of a strong Wnt-ON phenotype following Axin1 deletion described in the study by Feng (2012) was due to the compensation by Axin2. To assess the long-term impact of AhCreER^{T} mediated Axin deletion on β-catenin localisation, liver sections from AhCreER^{T} Axin1$^{\Delta/\Delta}$, AhCreER^{T} Axin2$^{\Delta/\Delta}$, and AhCreER^{T} Axin1$^{\Delta/\Delta}$, Axin2$^{\Delta/\Delta}$ cohorts at 1 year post BNF/Tamoxifen induction were stained for β-catenin.

β-catenin staining of AhCreER^{T} Axin1$^{\Delta/\Delta}$ liver sections did not appear to have aberrant localisation of β-catenin, phenocopying the results seen in the study by Feng (2012) (Figure 3.25A). No nuclear β-catenin staining was seen in AhCreER^{T} Axin2$^{\Delta/\Delta}$ liver sections at 1 year post BNF/Tamoxifen induction though membrane staining appeared reduced however, this was not quantified. AhCreER^{T} Axin1$^{\Delta/\Delta}$, Axin2$^{\Delta/\Delta}$ liver sections identified as non-tumour at dissection in the 1-year post induction cohort had very occasional nuclear β-catenin staining and cell membrane staining appeared to stain more intensely than control in some sections (Figure 3.25A).

To further assess levels of β-catenin in the Axin deleted cohorts at 1 year post induction, total protein was extracted from liver whole cell extracts and quantified in a western blot assay (Figure 3.25B). Levels of total β-catenin were variable in the Axin1 deleted cohort and not significantly different to the control samples. β-catenin levels in Axin2 deleted samples were lower than control however, this was not significant. Double Axin1 and Axin2 deleted cohorts showed highly variable levels of total β-catenin and were also not significantly different to controls (Figure 3.25C).

In summary these results show that the loss of Axin1 alone does not result in aberrant translocation or stabilisation of β-catenin. The data suggests Axin2 deletion at late times may result in reduced levels of β-catenin. The double Axin1, Axin2 deleted cohort had occasional nuclear β-catenin staining, suggesting some mis-localised stabilisation which occurs at later time-points. Total levels of β-catenin protein were highly variable from the samples examined, possibly due to early neoplasia as noted from the GS staining.

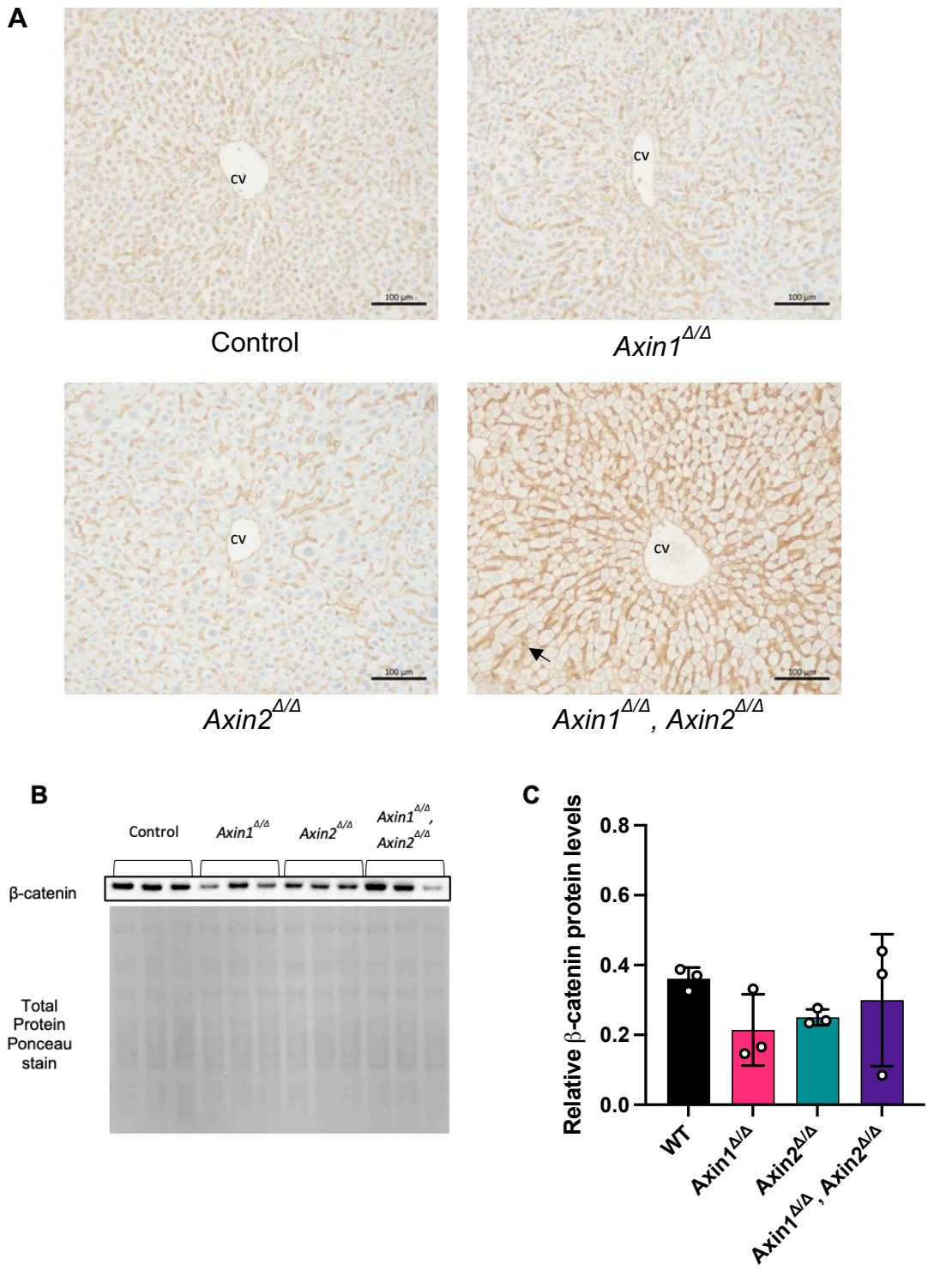

Figure 3.25 Variable β-catenin staining and total protein levels in Axin deleted cohorts at 1 year post induction.
(**A**) Representative images of β-catenin-stained liver sections of control and Axin deleted liver 1 year post BNF/Tamoxifen induction. CV = Central vein Scale bar 100 µm (**B**) Total β-catenin western blot from whole liver of Axin deleted cohorts at 1 year post induction. (**C**) Quantification of total β-catenin protein normalised to total protein using Ponceau stain. n = 3

3.4.7 Axin, Wnt targets and cell cycle expression following Axin loss in the mouse liver 1 year post induction.

Wnt targets examined at day 6 and at 1 month post induction were not significantly changed in any of the Axin deleted cohorts. To examine whether this altered following long-term deletion in the liver, the same set of Wnt target genes examined previously were used in RT-qPCR assays using RNA from livers of AhCreER^{T} Axin1$^{\Delta/\Delta}$, AhCreER^{T} Axin2$^{\Delta/\Delta}$, and AhCreER^{T} Axin1$^{\Delta/\Delta}$, Axin2$^{\Delta/\Delta}$ cohorts at 1 year post BNF/Tamoxifen induction.

RT-qPCR revealed reduced expression of exon 2 containing transcripts of *Axin1* and *Axin2* as expected in each cohort, as seen at day 6 and at 1 month. AhCreER^{T}, Axin1$^{\Delta/\Delta}$ livers had a significant 2-fold increase in the expression of *Axin2* and a trend for an increase in the expression of *c-Myc*. No changes in expression of *β-catenin*, *Tiam1*, *Caspase-3*, *c-Jun*, *CD44*, *p53*, *CyclinD1* and *Cdc25a* were observed as was seen at earlier timepoints (Figure 3.26A). AhCreER^{T}, Axin2$^{\Delta/\Delta}$ livers showed a significant increase in the expression of *Axin1* however, similarly to early timepoints, there were no changes to the other genes examined (Figure 3.26B). In contrast to early timepoints, AhCreER^{T}, Axin1$^{\Delta/\Delta}$, Axin2$^{\Delta/\Delta}$ livers showed a significant 6.2-fold increase in *c-Myc* and 2 to 4-fold increases in *c-Jun, CD44*, and *Cdc25a* expression (Figure 3.26C).

Expression of the panel of G2/M cell cycle genes (as used previously) remained at control levels as they had been at day 6 and 1-month post induction in the livers of AhCreER^{T}, Axin1$^{\Delta/\Delta}$ and AhCreER^{T}, Axin2$^{\Delta/\Delta}$ cohorts at 1 year post induction (Figure 3.26A, B). By contrast, AhCreER^{T}, Axin1$^{\Delta/\Delta}$, Axin2$^{\Delta/\Delta}$ livers had shown increased expression of *cyclins A2, B1, B2, Cdk1, Cdca3, Cdc20* and *Ki-67* though this was non-significant due to the degree of variability at early timepoints. At 1 year post induction the intra sample variability was still present however, 3 to 12-fold increases in the expression *cyclins A2, B1, B2, Cdk1, Cdca3, Cdc20, Ki67* and *FoxM1* were now significant.

In summary, apart from a 2-fold increase in *Axin2* expression and a 2.8-fold increase in *Axin1* expression overall, the loss of Axin1 or Axin2 appears to have little effect on the expression of Axin and Wnt targets and no effect on the panel of G2/M cell cycle genes at 1 year post induction. Deletion of both Axin1 and Axin2 at 1 year post induction shows significant increases in the expression of *c-Myc*, *c-Jun* and *CD44* which was not seen at day 6 or 1-month post induction. Average expression of genes associated with the G2/M of the cell cycle were found to be increased compared to earlier timepoints and were now significant, despite the variability.

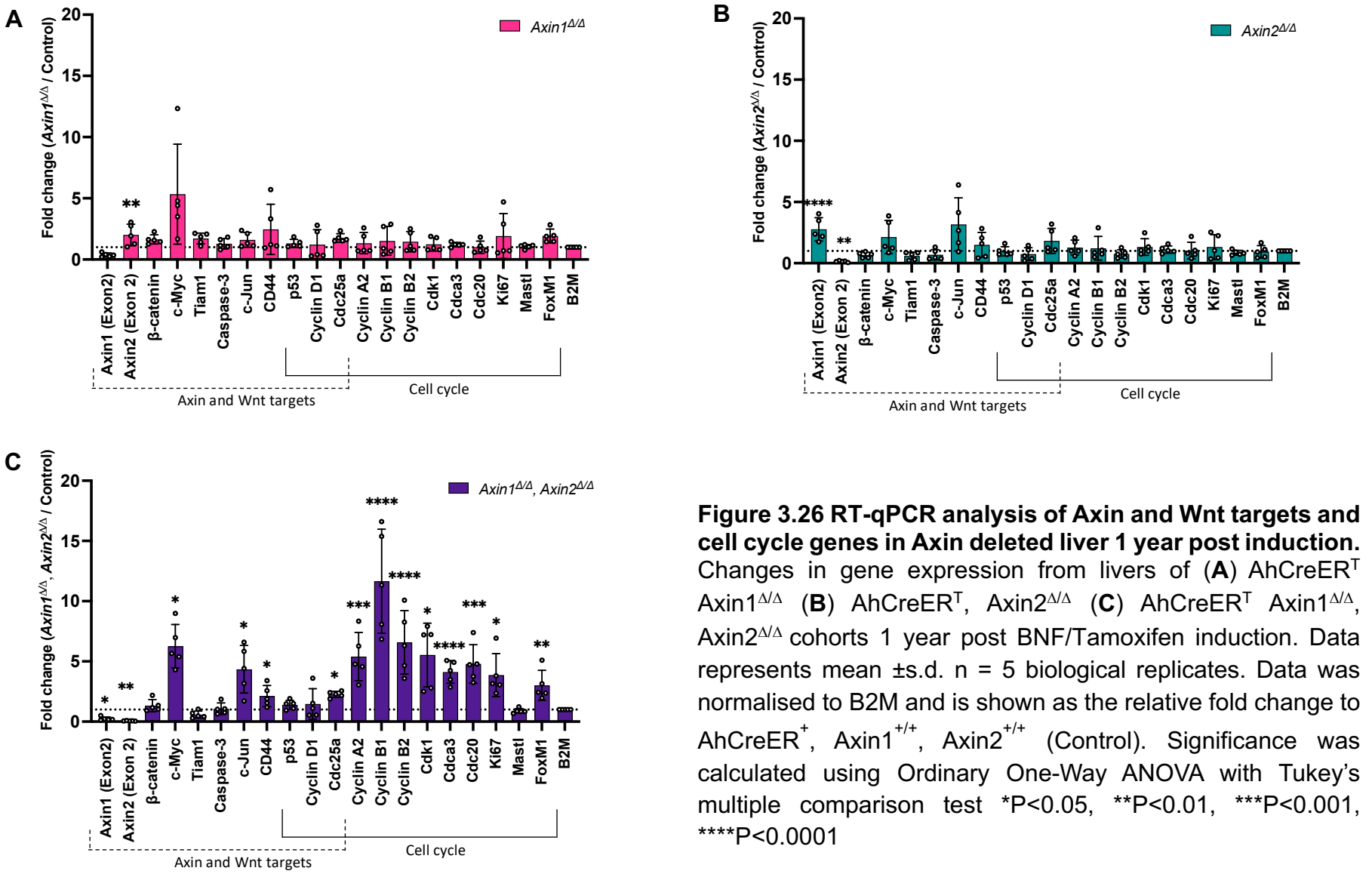

Figure 3.26 RT-qPCR analysis of Axin and Wnt targets and cell cycle genes in Axin deleted liver 1 year post induction. Changes in gene expression from livers of (**A**) AhCreER^{T} Axin1$^{\Delta/\Delta}$ (**B**) AhCreER^{T}, Axin2$^{\Delta/\Delta}$ (**C**) AhCreER^{T} Axin1$^{\Delta/\Delta}$, Axin2$^{\Delta/\Delta}$ cohorts 1 year post BNF/Tamoxifen induction. Data represents mean ±s.d. n = 5 biological replicates. Data was normalised to B2M and is shown as the relative fold change to AhCreER^{+}, Axin1$^{+/+}$, Axin2$^{+/+}$ (Control). Significance was calculated using Ordinary One-Way ANOVA with Tukey's multiple comparison test *P<0.05, **P<0.01, ***P<0.001, ****P<0.0001

3.4.8 Proliferation in Axin deleted livers 1 year post induction.

In the study by Feng (2012), the increase in proliferation seen in Axin1 deficient liver at day 4 post induction returned to control levels in non tumour areas of liver at 1 year post induction. To assess whether increased levels of proliferation persist in the livers of AhCreER^{T} Axin1$^{\Delta/\Delta}$, Axin2$^{\Delta/\Delta}$ cohorts at 1 year post induction, tissue sections were stained for Ki67 (Figure 3.27A) and BrdU (Figure 3.28A).

No differences in levels of Ki67 staining were seen in the liver sections from AhCreER^{T} Axin1$^{\Delta/\Delta}$ and AhCreER^{T} Axin2$^{\Delta/\Delta}$ cohorts at 1 year post BNF/Tamoxifen induction. This matched previous observations in AhCre Axin1$^{\Delta/\Delta}$ animals and suggested that Axin2 loss alone did not lead to the long-term activation of proliferation in the liver. However, Ki67 staining was significantly increased in the livers of AhCreER^{T} Axin1$^{\Delta/\Delta}$, Axin2$^{\Delta/\Delta}$ cohort, though this was highly variable (Figure 3.27B). This variability could be due to some areas of the liver that were scored as non-tumour did in fact contain poorly defined areas of neoplastic development. No significant differences in proliferation were observed as assessed by BrdU incorporation which was administered 2 hours before the animals were culled. This may be because different regions of the livers were imaged and analysed to those for Ki67 staining. No differences were seen in the percentages of BrdU staining in liver sections from AhCreER^{T} Axin1$^{\Delta/\Delta}$ or AhCreER^{T} Axin2$^{\Delta/\Delta}$ cohorts (Figure 3.28B).

These results suggest that the increase in proliferation seen at day 6 post induction in AhCreER^{T} Axin1$^{\Delta/\Delta}$ livers, does not persist to 1 year post BNF/Tamoxifen induction. However, the loss of both Axin1 and Axin2 using AhCreER^{T} results in livers presenting with a proliferative phenotype.

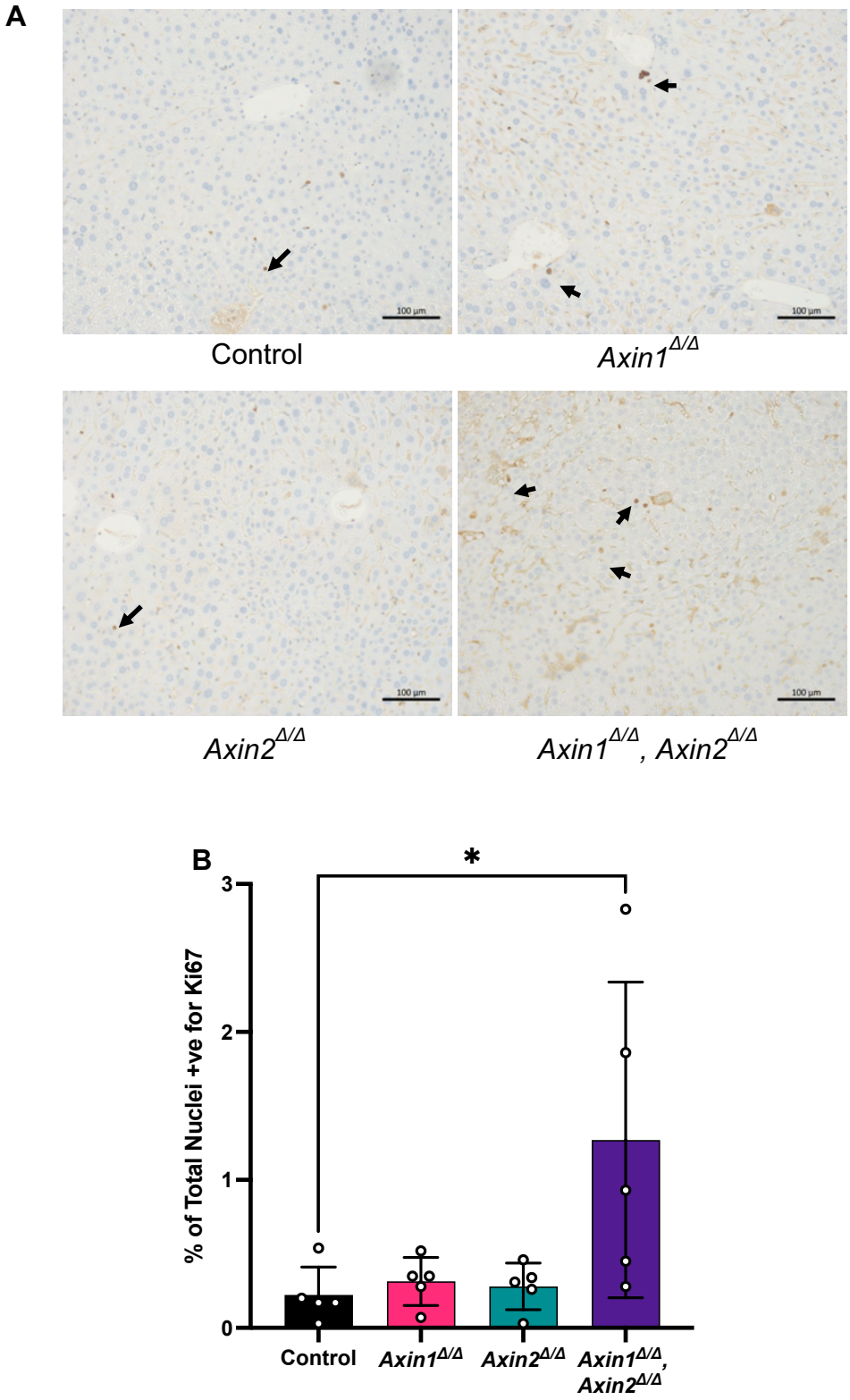

Figure 3.27 Ki67 staining increased in AhCreER^{T} Axin1$^{\Delta/\Delta}$, Axin2$^{\Delta/\Delta}$ livers from Axin deleted cohorts at 1 year post induction.
(**A**) Representative images of anti Ki67 stained liver tissue sections. (**B**) Counts of Ki67 positive cells in liver tissue sections as a percentage of total. Data represents mean ±s.d. from 5 biological replicates. Significance was calculated using Ordinary One-Way ANOVA with Tukey's multiple comparison test. *p<0.05 Scale bar 100 μm

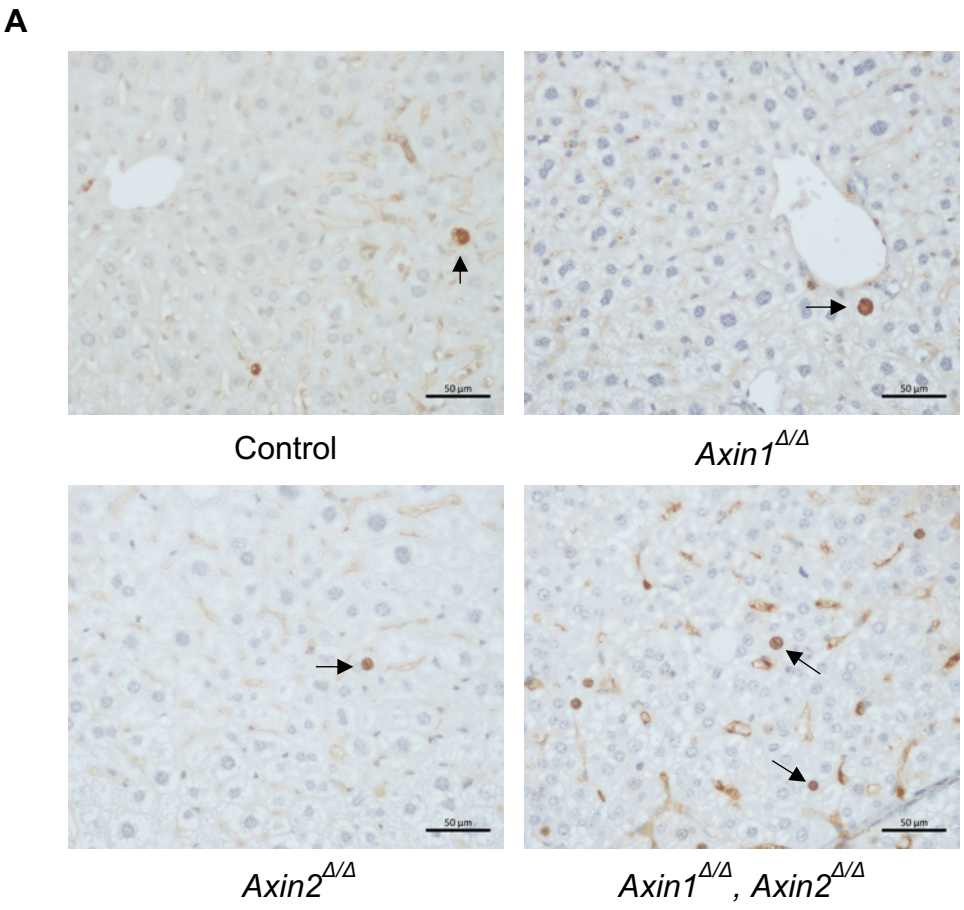

Figure 3.28 BrdU staining in livers from Axin deleted cohorts is not statistically different at 1 year post induction.

BrdU was administered 2 hours before dissection (**A**) Representative images of anti BrdU stained liver tissue sections. (**B**) Counts of BrdU positive cells in liver tissue sections as a percentage of total nuclei. Data represents mean ±s.d. from 3-5 biological replicates. Significance was calculated using Ordinary One-Way ANOVA with Tukey's multiple comparison test. Scale bar 50 μm

3.4.9 γH2AX staining and atypical nuclei in Axin deleted liver 1 year post induction.

Acute AhCreER^{T} mediated loss of Axin1 at day 6 post induction resulted in increased expression of γH2AX in the liver (Figure 3.9). Additional loss of Axin2 did not further perturb this phenotype and Axin2 loss alone showed similar staining to controls. Despite high levels of γH2AX following Axin1 loss alone, only the dual loss of both Axin1 and Axin2 resulted in tumour formation. To assess the long-term impact of Axin loss on γH2AX expression and nuclear atypia, sections of liver from control, AhCreER^{T} Axin1$^{\Delta/\Delta}$, AhCreER^{T} Axin2$^{\Delta/\Delta}$, and AhCreER^{T} Axin1$^{\Delta/\Delta}$, Axin2$^{\Delta/\Delta}$ mice at 1 year post BNF/Tamoxifen induction were stained and scored for γH2AX and assessed for atypical nuclei. Nuclei classed as atypical included those that were irregular shaped, had cytoplasmic inclusions, grooving or prominent nucleolus.

γH2AX staining in AhCreER^{T} Axin1$^{\Delta/\Delta}$ and AhCreER^{T} Axin2$^{\Delta/\Delta}$ were at similar levels to control liver at 1 year post BNF/Tamoxifen induction (Figure 3.29A, B). Liver from AhCreER^{T} Axin1$^{\Delta/\Delta}$, Axin2$^{\Delta/\Delta}$ mice had an increase in the average percentage of nuclei stained for γH2AX (Figure 3.29B) however this was not significant due to variability. Scored for atypical nuclei, loss of either Axin1 or Axin2 alone resulted in no change compared to control, however, loss of both Axin1 and Axin2 saw a significant increase in the number of nuclei noted as atypical (Figure 3.29C).

These results suggest that the loss of Axin1 alone and the increase in γH2AX seen at day 6 does not persist to 1 year post induction. However, when combined with the loss of Axin2 (which has no effect on γH2AX levels alone) mice have greater levels of γH2AX and atypical nuclei at 1 year post induction and show a propensity to develop liver tumours.

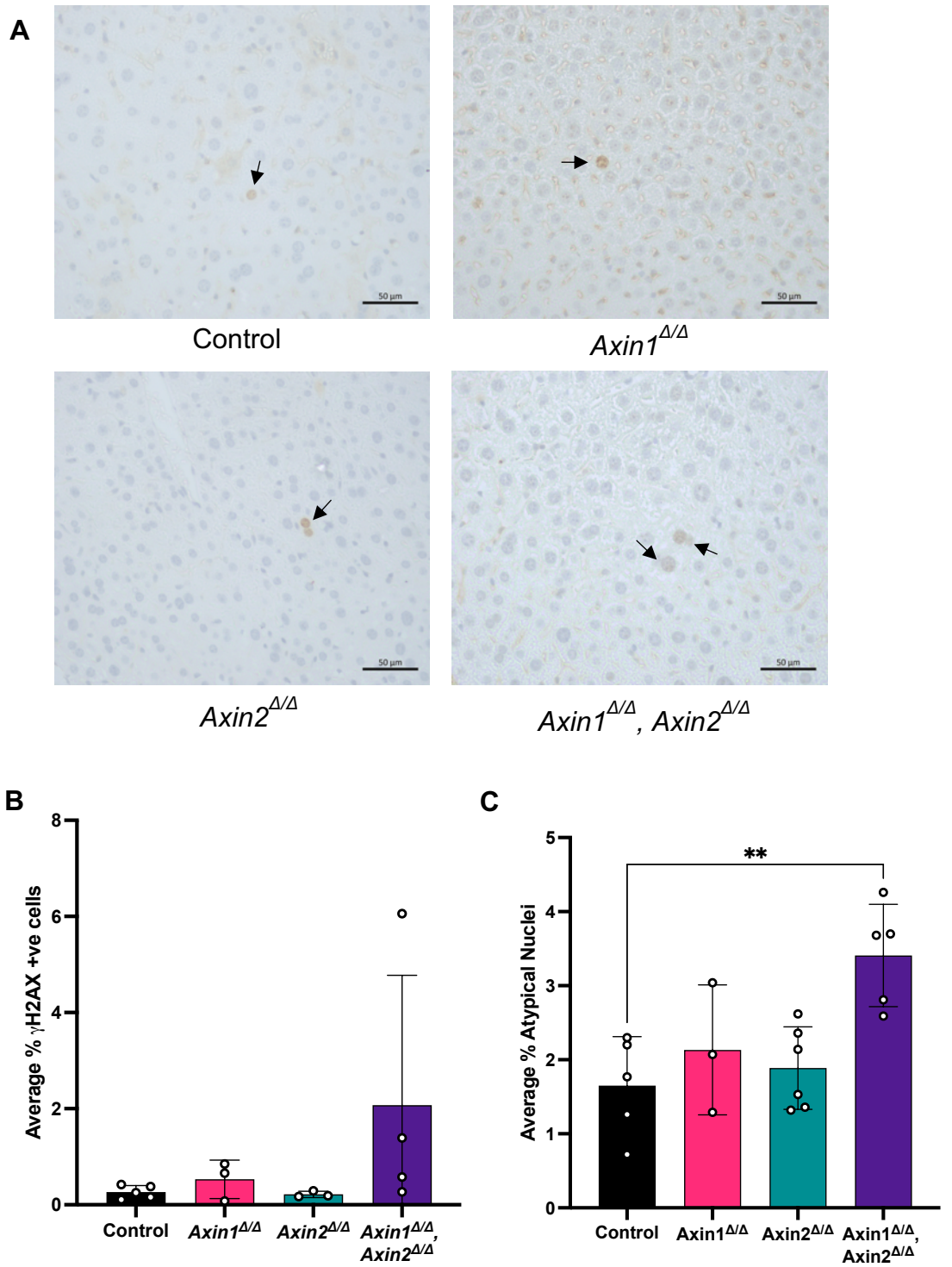

Figure 3.29 Increased levels of γH2AX and atypical nuclei in AhCreER^{T}, Axin1$^{Δ/Δ}$, Axin2$^{Δ/Δ}$ mouse livers at 1 year post induction.
Atypical nuclei = Irregular shaped, cytoplasmic inclusions, grooving or prominent nucleolus. (**A**) Representative images of γH2AX stained aged liver sections. Scale bar 50 μm (**B**) Average percentage of γH2AX stained cells in control and aged Axin deleted cohorts. (**C**) Average percentage of nuclei scored as atypical in aged control and Axin deleted liver sections. Data represents mean ±s.d. n = 3-5 biological replicates. Significance was calculated using Ordinary One-Way ANOVA with Tukey's multiple comparison test **p<0.01. Counts were performed by FYP student Chu Li under my supervision.

3.4.10 AFP staining in Axin deleted mouse liver at 1 year post induction.

AFP expression has long been established as a marker of HCC (Sato et al. 1998). High levels of AFP are associated with the proliferative class of HCC, a high tumour grade with poor cell differentiation and a worse clinical outcome (Villanueva 2019). In the study by Feng (2012), most AhCre Axin1 deleted liver with or without tumour stained positive for AFP at 1 year post induction. To examine the effects of AhCreER^{T} mediated Axin deletion on AFP levels in the liver, sections from samples of AhCreER^{T} Axin1$^{\Delta/\Delta}$, AhCreER^{T} Axin2$^{\Delta/\Delta}$, and AhCreER^{T} Axin1$^{\Delta/\Delta}$, Axin2$^{\Delta/\Delta}$ cohorts at 1 year post BNF/Tamoxifen induction were stained for AFP.

In contrast to the study by Feng (2012) using AhCre, AhCreER^{T} mediated deletion of Axin1 at 1 year post induction did not result in positive AFP staining in the liver (Figure 3.30). Loss of Axin2 alone at 1 year post induction also did not result in positive staining for AFP (Figure 3.30). Liver tissue identified as non-tumour at dissection from AhCreER^{T} Axin1$^{\Delta/\Delta}$, Axin2$^{\Delta/\Delta}$ mice at 1 year post induction showed some mild cytoplasmic staining with patches of more intense cytoplasmic staining for AFP (Figure 3.30).

Taken together, these results suggest that AhCreER^{T} mediated deletion of Axin1 or Axin2 alone does not result in tumourigenesis at 1 year post induction. However, AhCreER^{T} Axin1$^{\Delta/\Delta}$, Axin2$^{\Delta/\Delta}$ livers identified as non-tumour during dissection at 1 year post induction overall, display higher levels of proliferation, γH2AX expression, nuclei atypia and AFP staining in some areas of the liver, suggesting early signs of neoplasia.

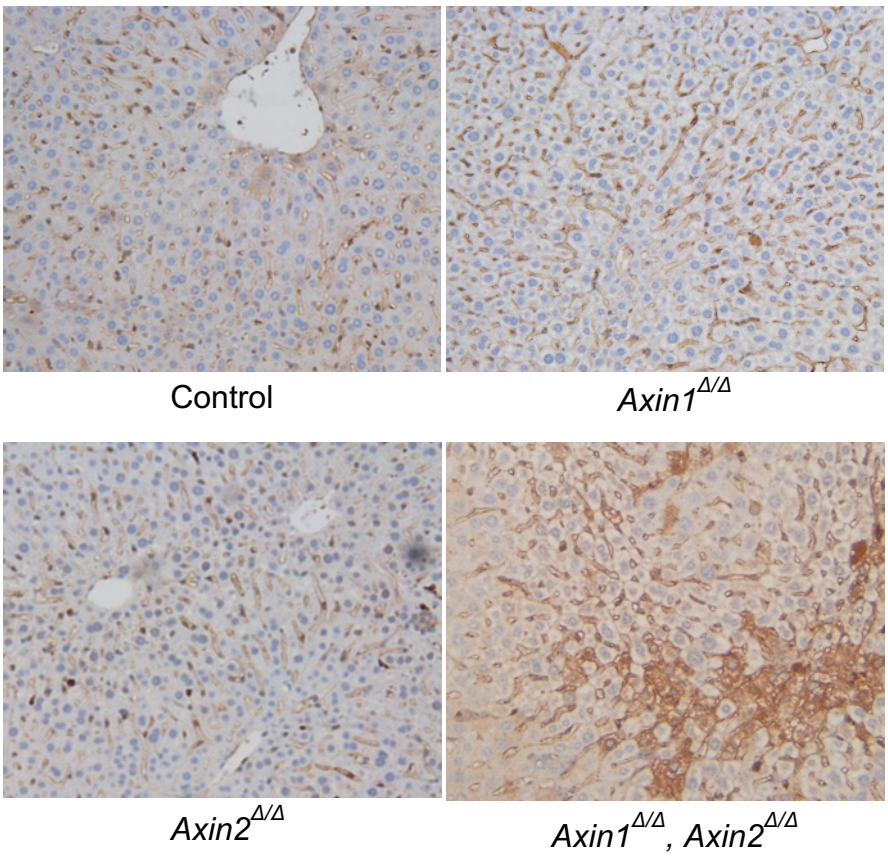

Figure 3.30 Evident AFP immunohistochemical staining in AhCreER^{T}, Axin1$^{\Delta/\Delta}$, Axin2$^{\Delta/\Delta}$ mouse livers at 1 year post induction.
Representative images of liver sections stained for AFP from control, AhCreER^{T} Axin1$^{\Delta/\Delta}$, AhCreER^{T} Axin2$^{\Delta/\Delta}$, and AhCreER^{T} Axin1$^{\Delta/\Delta}$, Axin2$^{\Delta/\Delta}$ cohorts at 1 year post BNF/Tamoxifen induction. Scale bar 100 μm

3.4.11 Progenitor, lineage, and mature liver cell markers in Axin deleted mouse liver 1 year post induction.

At day 6 post induction, *Lgr5* expression was slightly increased in AhCreER^{T} Axin1$^{\Delta/\Delta}$ livers but reduced 3.7-fold and 1.5-fold in AhCreER^{T} Axin2$^{\Delta/\Delta}$, and AhCreER^{T} Axin1$^{\Delta/\Delta}$, Axin2$^{\Delta/\Delta}$ livers respectively. No significant differences were seen in any of the other hepatic progenitor, lineage, or mature liver cell markers. Reduced expression of *Lgr5* persisted in AhCreER^{T} Axin2$^{\Delta/\Delta}$ livers at 1 month post induction. To examine the long-term impact of Axin deletion in the liver, the same set of progenitor, lineage and mature liver cell markers as examined previously at day 6 were used in RT-qPCR assays using RNA from livers of AhCreER^{T} Axin1$^{\Delta/\Delta}$, AhCreER^{T} Axin2$^{\Delta/\Delta}$, and AhCreER^{T} Axin1$^{\Delta/\Delta}$, Axin2$^{\Delta/\Delta}$ cohorts at 1 year post BNF/Tamoxifen induction.

The increase in *Lgr5* expression observed in the AhCreER^{T} Axin1$^{\Delta/\Delta}$ livers was found to be variable. *Lgr5* expression was again found to be decreased in AhCreER^{T} Axin2$^{\Delta/\Delta}$ livers as at earlier time-points, though this was not significant when compared to control. In contrast to day 6 and 1-month post induction, AhCreER^{T} Axin1$^{\Delta/\Delta}$, Axin2$^{\Delta/\Delta}$ livers showed just over 2-fold increase in the expression of *Lgr5*. *Epcam* and *OPN* expression were also found to be elevated in double Axin1 and Axin2 deleted livers, though due to inter sample variation, this was not significant. No significant changes were seen in the expression of the other hepatic progenitor markers Trop2 and Sox9 in the other cohorts (Figure 3.31A). The biliary epithelial cell marker *Krt19* was significantly increased in the AhCreER^{T} Axin1$^{\Delta/\Delta}$, Axin2$^{\Delta/\Delta}$ cohort only. No changes were seen in *Hnf1b* or *Krt7* expression in any of the cohorts (Figure 3.31B). The hepatocyte lineage marker *Tbx3* showed a 5.4-fold decrease in expression in the AhCreER^{T} Axin2$^{\Delta/\Delta}$ livers, though this was not significant compared to control livers. No changes to *Tbx3* expression were observed in Axin1 or double Axin1, Axin2 deleted livers. As expected from the AFP immunohistochemistry, *AFP* expression was found to be elevated in AhCreER^{T} Axin1$^{\Delta/\Delta}$, Axin2$^{\Delta/\Delta}$ livers only. No significant changes in *HNF4*α or *Prox1* were seen in any of the cohorts (Figure 3.31C). The mature hepatocyte marker *Fah* showed only a modest increase in expression in AhCreER^{T} Axin1$^{\Delta/\Delta}$, Axin2$^{\Delta/\Delta}$ livers. No significant changes were seen in *Albumin* or *Ass1* expression in any of the cohorts (Figure 3.31D).

These results suggest that deletion of Axin1 has little effect on any of the liver cell markers. Of interest, the decrease in the expression of *Lgr5* and *Tbx3* in Axin2 deleted livers, both of which are also Wnt targets, suggests some repression of the Wnt/β-catenin pathway and backs up the data of decreased GS staining. Axin1 and Axin2 livers have been shown to have highly variable histology and zonation expression, so it was not surprising that expression of certain some zonated, stem and Wnt target genes would also be variable between samples since subsets of the genes fall into multiple classes. For example, Lgr5 is a stem cell marker, a Wnt target and is zonated. The increases in expression of *Lgr5*, *EpCam* and *OPN* would suggest some cells are becoming more progenitor like. Counterintuitively, the mature hepatocyte marker *Fah* was also elevated, though this was only a 1.5-fold increase. There was however a suggestion of a reduction in expression of *Albumin* a marker of mature hepatocytes.

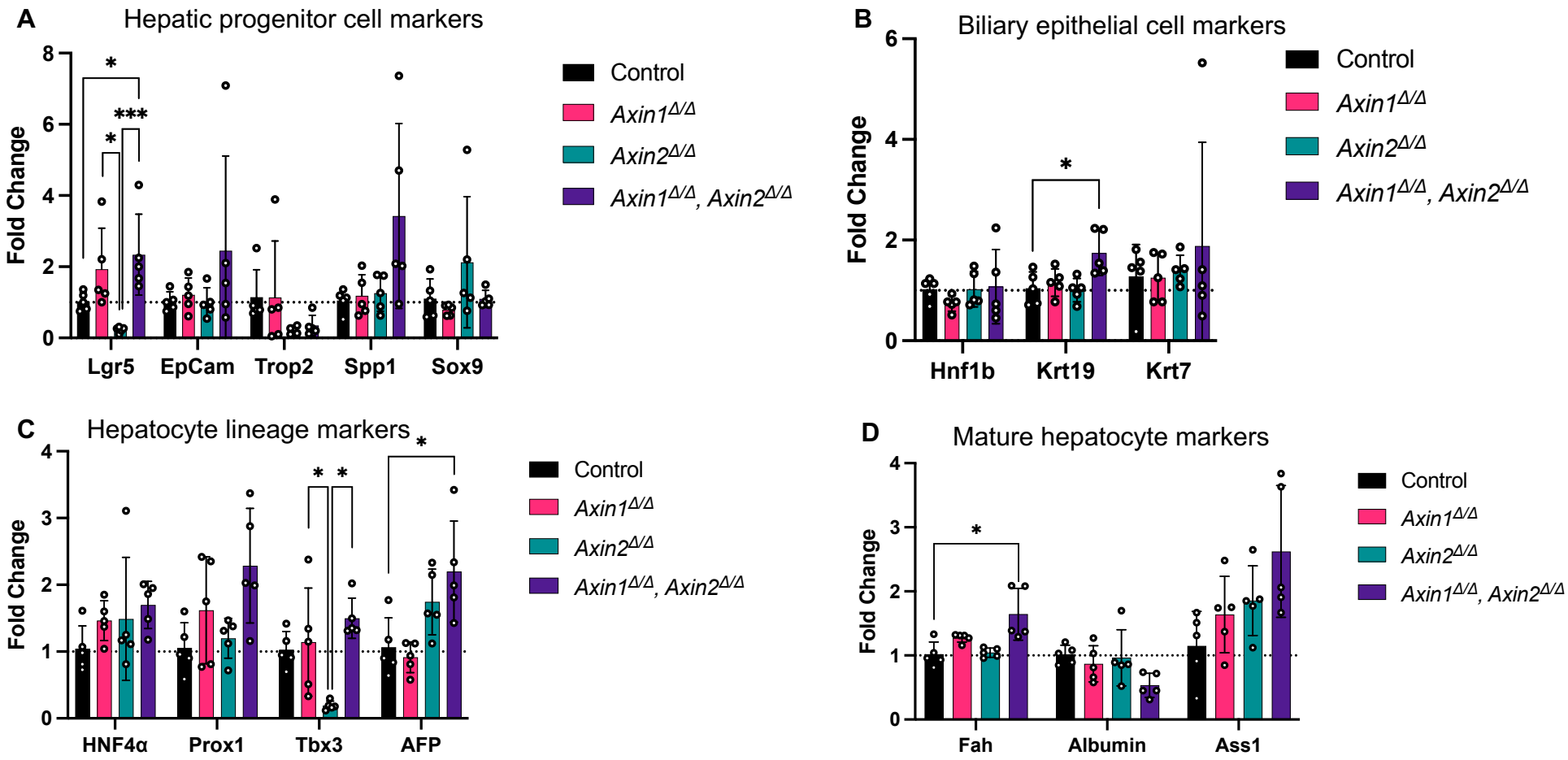

Figure 3.31 RT-qPCR of progenitor, lineage, and mature liver cell markers in Axin deleted mouse liver 1 year post induction. (**A**) Expression of hepatic progenitor cell markers. (**B**) Expression of biliary epithelial cell markers. (**C**) Expression of hepatocyte lineage markers. (**D**) Expression of mature hepatocyte markers. Data represents mean ±s.d. n = 5 biological replicates. Expression was normalized to B2M. Fold change calculated relative to Control samples. Significance was calculated using Ordinary One-Way ANOVA with Tukey's multiple comparison test. *p<0.05, ***p<0.001

3.4.12 Yap IHC, protein levels and RT-qPCR in the liver of Axin deleted cohorts at 1 year post induction.

Transcriptional co-activators Yap/Taz have been found to play a role in the development of HCC (Zhang and Zhou 2019) and Yap has been shown to co-operate with β-catenin to drive oncogenesis in basal breast cancer (Quinn et al. 2021). As discussed previously, Yap protein has been shown to bind to Axin1 and to be sequestered to the β-catenin destruction complex in Wnt-OFF cells (Azzolin et al. 2014). It may therefore be reasonable to assume that the tumourigenesis seen in the Axin1, Axin2 deleted livers may in part be driven by Hippo pathway deregulation due to the loss of Axin1. Yap protein levels were comparable to control in Axin deleted livers at day 6 post induction. However, expression of *Birc5* and *Hmmr* that has previously been shown to have increased expression in an Axin1 deleted HCC model (Abitbol et al. 2018), showed trends for an increase in expression at day 6 and even more so at 1 month post induction. To examine the long-term impact of Axin deletion in the liver on Yap protein and some of its downstream targets, IHC staining, western blot analysis and RT-qPCR assays were carried out using liver sections, whole liver cell protein extracts and RNA from livers of AhCreER^{T} Axin1$^{\Delta/\Delta}$, AhCreER^{T} Axin2$^{\Delta/\Delta}$, and AhCreER^{T} Axin1$^{\Delta/\Delta}$, Axin2$^{\Delta/\Delta}$ cohorts at 1 year post BNF/Tamoxifen induction.

At day 6 post induction, IHC staining for Yap revealed strong staining of bile ducts and endothelial cells in both control and Axin deleted cohorts with no apparent differences between the cohorts. At 1 year post induction, bile duct and endothelial Yap staining remained strong but comparable to control. Occasional nuclear Yap staining was observed in AhCreER^{T} Axin1$^{\Delta/\Delta}$ and AhCreER^{T} Axin2$^{\Delta/\Delta}$ livers but was more evident in AhCreER^{T} Axin1$^{\Delta/\Delta}$, Axin2$^{\Delta/\Delta}$ livers (Figure 3.32A). Total Yap protein levels were slightly variable at day 6 post induction. At 1 year post induction, total Yap protein levels were even more variable, particularly in the double Axin1, Axin2 deleted liver (Figure 3.32B, C). This could be down to some areas of the double Axin deleted liver being neoplastic.

No changes were observed in the expression of *Yap* or its downstream targets in Axin1 or Axin2 deleted livers at day 6- or 1-month post induction. *Birc5* and *Hmmr* expression showed trends for increases at both early timepoints in double Axin1, Axin2 deleted livers but was not significant. At 1 year post induction AhCreER^{T} Axin1$^{\Delta/\Delta}$ and AhCreER^{T} Axin2$^{\Delta/\Delta}$ livers both showed an increase in the expression of *Ctgf* only

(Figure 3.33A, B). *Birc5* and *Hmmr* expression were now significantly increased in AhCreER^{T} Axin1$^{\Delta/\Delta}$, Axin2$^{\Delta/\Delta}$ livers (correlating with increased expression in Axin1 deleted HCC (Abitbol et al. 2018)) as was the expression of *Ctgf* and *Gpc3*, and a trend for an increase in the expression of *Cyr61* (Figure 3.33C). No changes were observed in the expression of *Fas* and *Sfrp1*.

Overall, these results suggest that Yap protein localization and total levels are not significantly altered in AhCreER^{T} Axin1$^{\Delta/\Delta}$ or AhCreER^{T} Axin2$^{\Delta/\Delta}$livers. Ctgf protein levels have been shown to increase with age in rat liver (Kim et al. 2004) and is associated with fibrosis (Lipson et al. 2012) thus the increased expression of *Ctgf* observed in single Axin deleted livers may be due to low levels of fibrosis compared to controls. As seen with GS expression, loss of both Axin1 and Axin2 has resulted in high variability of total Yap protein levels. The increase in the expression of a number of Yap targets suggests activation of the Hippo pathway, though this is variable between samples. Whether this is a direct or indirect result of loss of both Axins remains unclear.

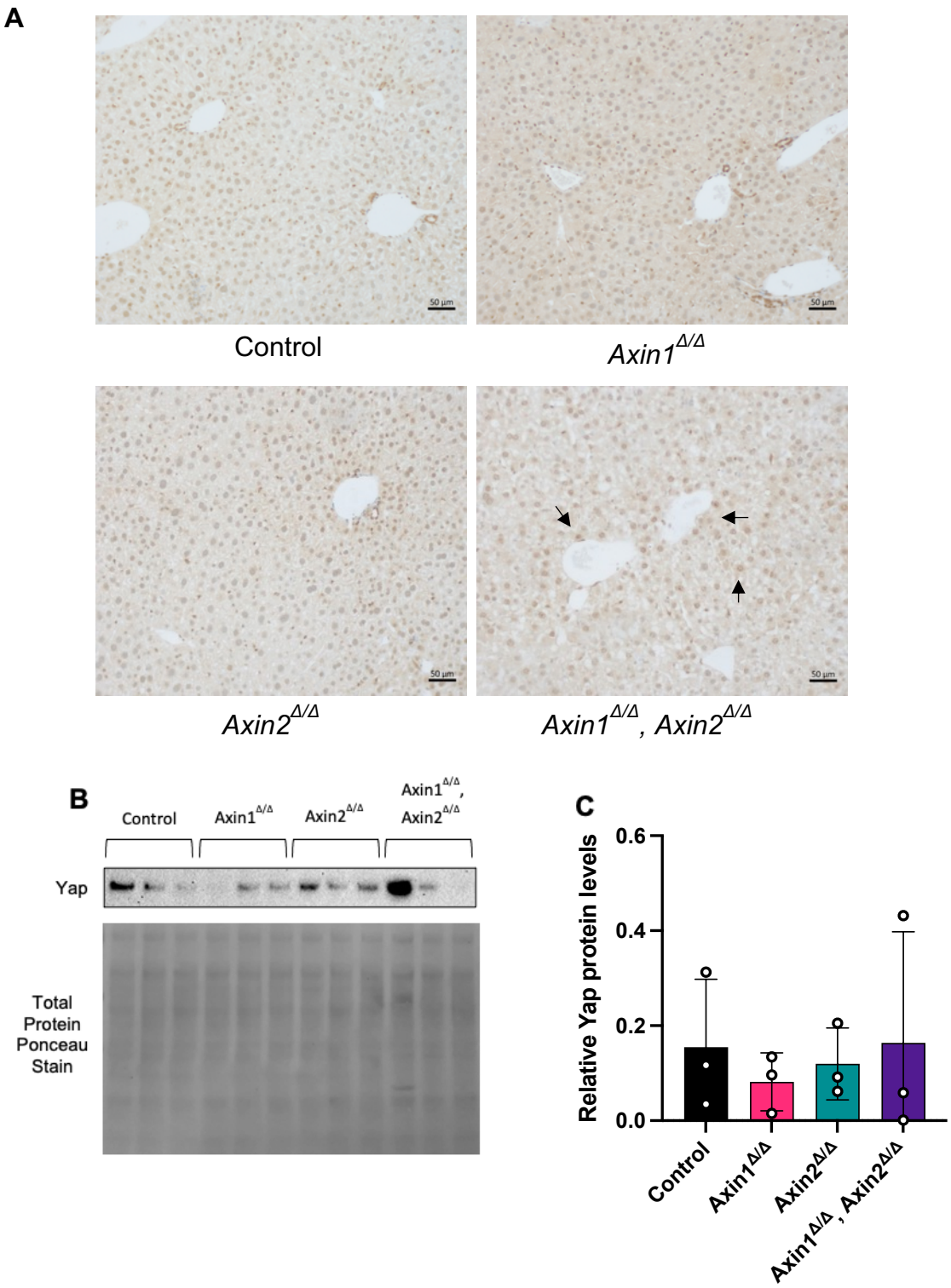

Figure 3.32 Yap IHC staining and protein levels in Axin deleted livers 1 year post induction found to be variable.

(A) Representative images of Yap staining in livers from control, AhCreER^{T} Axin1$^{\Delta/\Delta}$, AhCreER^{T} Axin2$^{\Delta/\Delta}$, and AhCreER^{T} Axin1$^{\Delta/\Delta}$, Axin2$^{\Delta/\Delta}$ cohorts at 1 year post BNF/Tamoxifen induction. Scale bar 50 μm. **(B)** Yap western blot from whole liver of Axin deleted cohorts at 1 year post induction. (**C**) Quantification of Yap protein normalised to total protein using Ponceau stain. n = 3

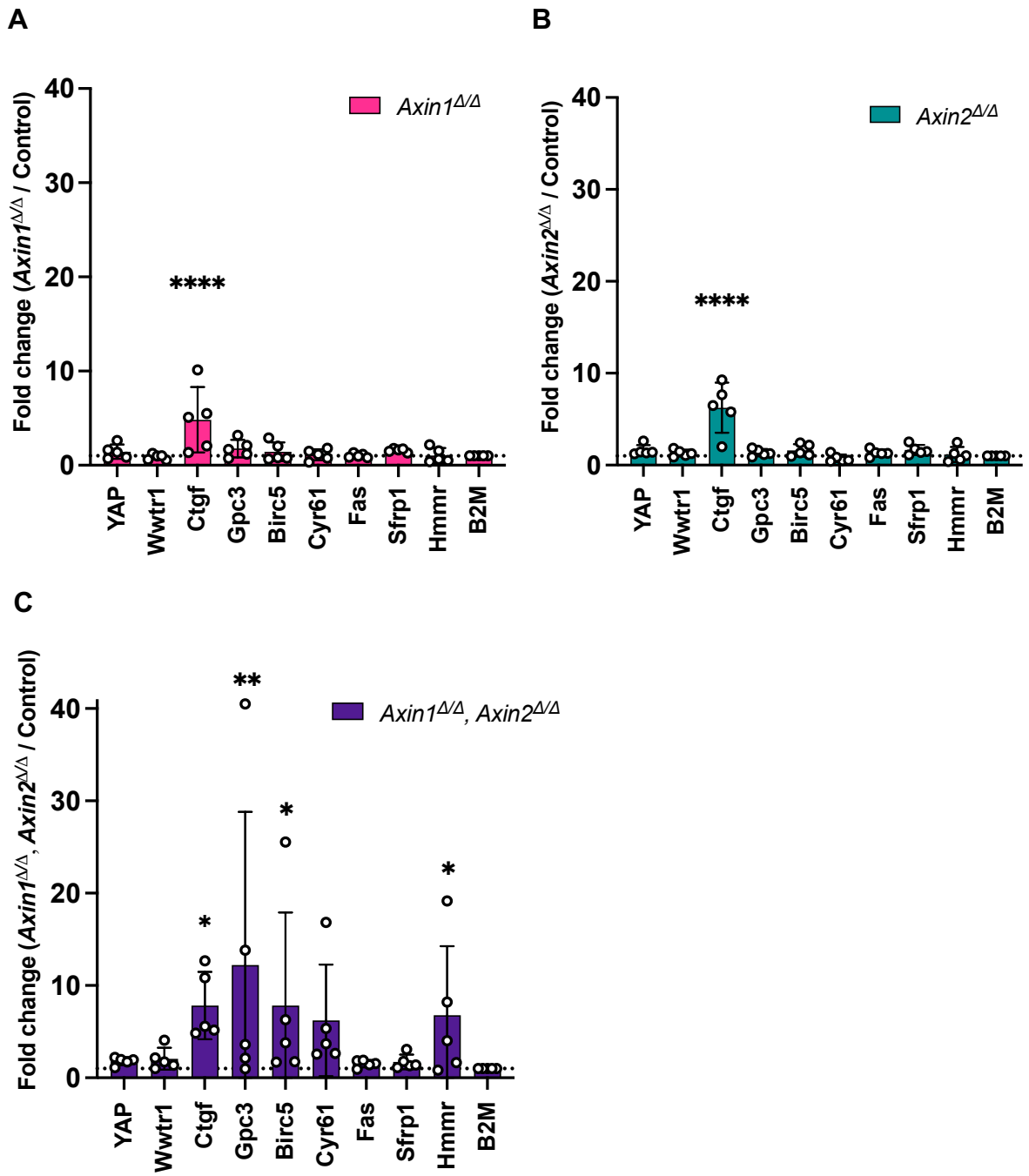

Figure 3.33 Yap, Wwtr1 and Yap downstream targets expression levels in Axin deleted mouse livers at 1 year post induction.

Changes in gene expression from livers of (**A**) AhCreER^{T} Axin1$^{\Delta/\Delta}$ (**B**) AhCreER^{T}, Axin2$^{\Delta/\Delta}$ (**C**) AhCreER^{T} Axin1$^{\Delta/\Delta}$, Axin2$^{\Delta/\Delta}$ cohorts 1 year post BNF/Tamoxifen induction. Data represents mean ±s.d. n = 5 biological replicates. Data was normalised to B2M and is shown as the relative fold change to AhCreER^{+}, Axin1$^{+/+}$, Axin2$^{+/+}$ (Control). Significance was calculated using One-Way ANOVA and Tukey's multiple comparison test *P<0.05, **P<0.01, ****P<0.0001

3.5 Analysis of AhCreER^{T} Axin1$^{\Delta/\Delta}$, Axin2$^{\Delta/\Delta}$ tumours.

The next section will focus on the examination of AhCreER^{T} Axin1$^{\Delta/\Delta}$, Axin2$^{\Delta/\Delta}$ liver tumours. Where used, controls in this section are AhCreER^{T} Axin1$^{wt/wt}$, Axin2$^{wt/wt}$ liver taken at 1 year post induction as used in the previous section to illustrate normal liver.

3.5.1 AhCreER^{T} Axin1$^{\Delta/\Delta}$, Axin2$^{\Delta/\Delta}$ liver tumours show varied histology and are AFP positive.

Examination of H&E liver tissue sections identified as tumour at dissection from aged AhCreER^{T} Axin1$^{\Delta/\Delta}$, Axin2$^{\Delta/\Delta}$ mice revealed varying histopathology. Tumours were observed to be moderate to well differentiated tumour cells with a trabecular pattern and some signs of intracytoplasmic accumulation of lipids (Figure 3.34). Tumours were also seen with solid growth pattern with tumour cells resembling non-neoplastic hepatocytes. As would be expected, tumours stained very strongly for AFP however there were areas with less intense staining (Figure 3.34).

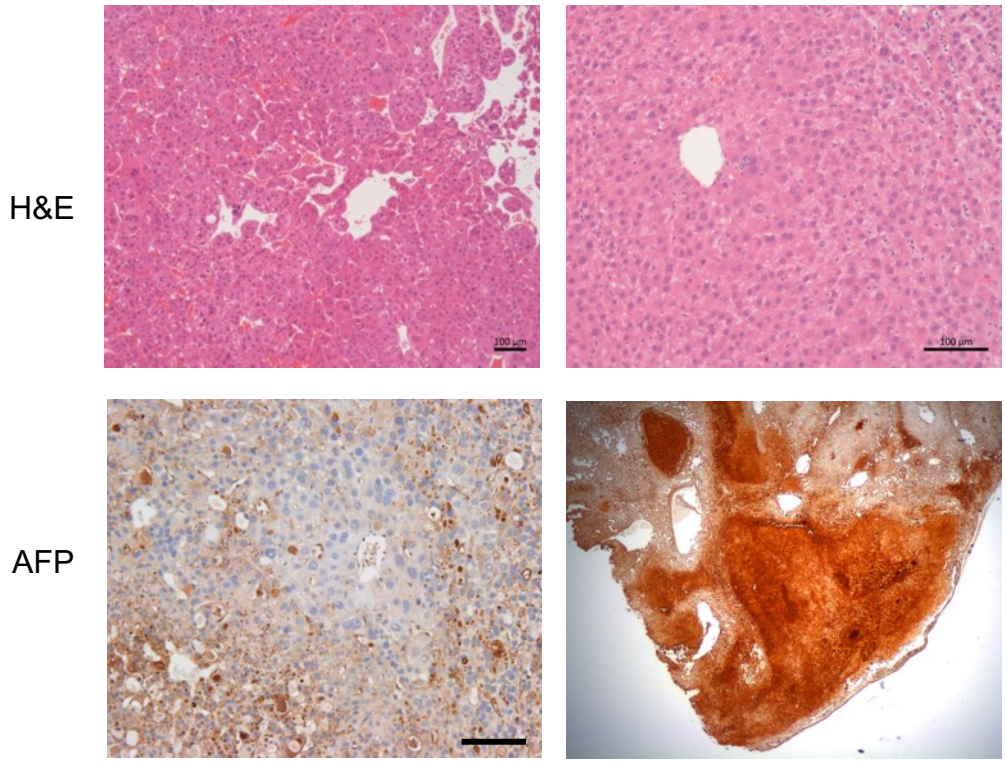

Figure 3.34 H&E and AFP staining in AhCreER^{T} Axin1$^{\Delta/\Delta}$, Axin2$^{\Delta/\Delta}$ liver tumours. Representative images of H&E-stained from AhCreER^{T} Axin1$^{\Delta/\Delta}$, Axin2$^{\Delta/\Delta}$ liver tumour sections. Left image showing a trabecular pattern and right image is of solid growth pattern with cells resembling non-neoplastic hepatocytes. AFP staining was present in most tumours though some areas did not stain as strongly. Scale bar shown 100 μm.

3.5.2 GS and CPS1 staining in AhCreER^{T} Axin1$^{\Delta/\Delta}$, Axin2$^{\Delta/\Delta}$ liver tumours.

In the study by Feng (2012), tumours in livers from Axin1 deleted mice presented with increased GS staining with irregular distribution. Wnt pathway activation via mutant β-catenin is strongly correlated with increases in GS expression (Austinat et al. 2008) and diffuse GS expression has been reported in up to 70% of early HCC (Nguyen et al. 2016). GS and CPS1 expression has already been shown to vary in non-tumour Axin1 and Axin2 deleted samples at 1 year post induction, possibly signifying varying stages of early HCC development. Sections were therefore stained to assess GS and CPS1 expression in AhCreER^{T} Axin1$^{\Delta/\Delta}$, Axin2$^{\Delta/\Delta}$ liver tumours.

GS staining varied between AhCreER^{T} Axin1$^{\Delta/\Delta}$, Axin2$^{\Delta/\Delta}$ liver tumours. Staining was observed to be nodular in some tumour sections with surrounding areas showing irregular distribution of GS, though still predominately associated with the central vein (Figure 3.35). CPS1 staining in these areas was patchy and irregular as seen in some sections in the non-tumour sections. Tumours also presented with diffuse GS staining throughout the section corresponding with an absence of CPS1 staining.

In summary, AhCreER^{T} Axin1$^{\Delta/\Delta}$, Axin2$^{\Delta/\Delta}$ liver tumours show a variety of staining patterns for the zonation markers GS and CPS1, similar to what was seen in normal AhCreER^{T} Axin1$^{\Delta/\Delta}$, Axin2$^{\Delta/\Delta}$ liver at 1 year post induction.

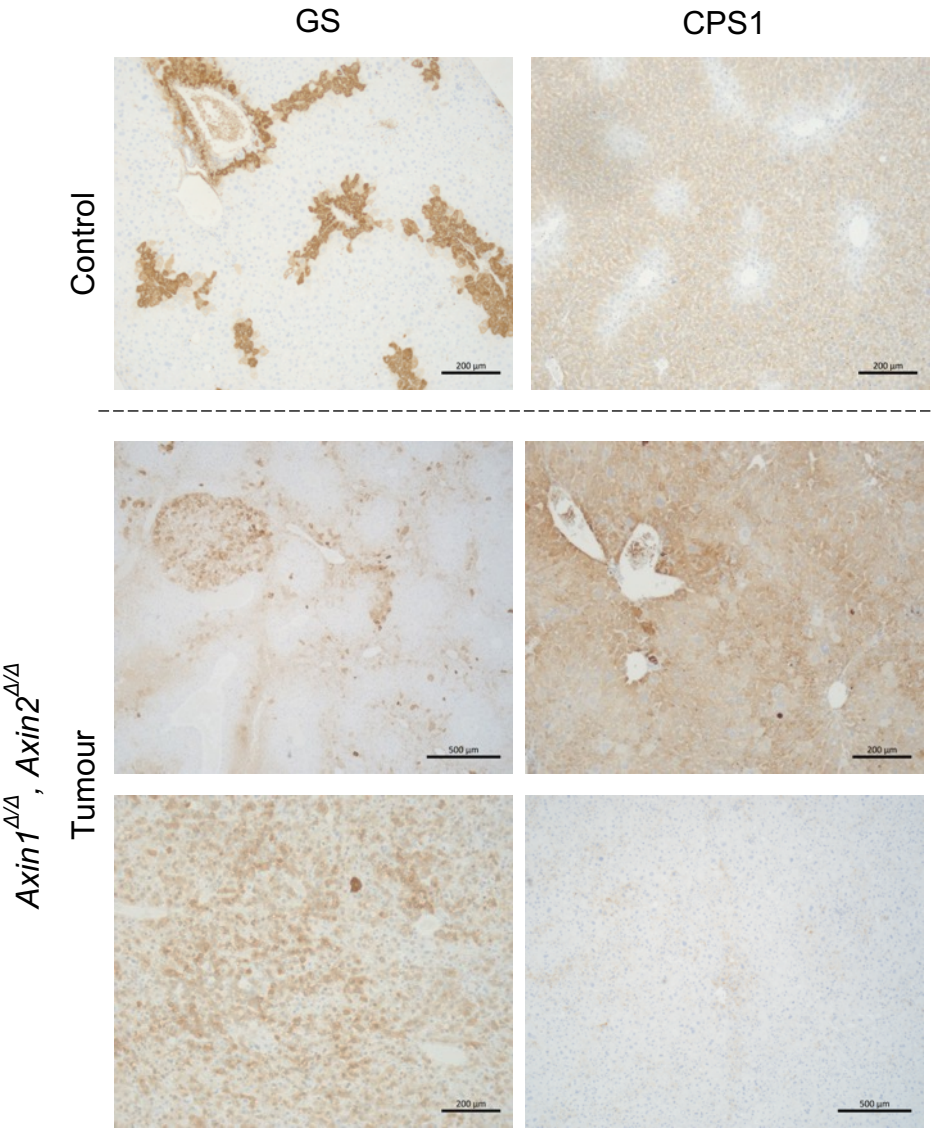

Figure 3.35 Mis-localised GS and CPS1 staining in AhCreER^{T} Axin1$^{\Delta/\Delta}$, Axin2$^{\Delta/\Delta}$ tumours.

Representative images of GS and CPS1 staining in AhCreER^{T} Axin1$^{\Delta/\Delta}$, Axin2$^{\Delta/\Delta}$ tumours. Control samples are from induced AhCreER^{T} samples dissected 1 year post induction to show normal, expected staining patterns of GS and CPS1.

3.5.3 Axin expression in AhCreER^{T} Axin1$^{\Delta/\Delta}$, Axin2$^{\Delta/\Delta}$ liver tumours

AhCreER^{T} Axin1$^{\Delta/\Delta}$, Axin2$^{\Delta/\Delta}$ liver classed as normal at dissection 1 year post induction showed significant decrease in the expression of Axin1 and Axin2 transcripts containing exon 2. Conversely, expression of transcripts from non-deleted exons using primers targeting the C-terminal of *Axin1* and *Axin2* was found to be increased. To assess Axin expression in the AhCreER^{T} Axin1$^{\Delta/\Delta}$, Axin2$^{\Delta/\Delta}$ liver tumours, RT-qPCR using RNA from the tumours was carried out.

AhCreER^{T}, Axin1$^{\Delta/\Delta}$, Axin2$^{\Delta/\Delta}$ liver tumours showed a 7.5-fold and a 44-fold decrease in the expression of transcripts containing exon 2 of *Axin1* and *Axin2* respectively (Figure 3.36A, B) suggesting that the deleted Axin alleles were retained within the tumour cells. There was only a 3.9-fold and 13.8-fold decrease in normal Axin1, Axin2 deleted liver at 1 year post induction. Using primers that bind outside the recombined region, expression of non-deleted exons of *Axin1* and *Axin2* increased 2.9-fold and 2.5-fold respectively (Figure 3.36C, D). This was slightly less than what was observed in the normal AhCreER^{T} Axin1$^{\Delta/\Delta}$, Axin2$^{\Delta/\Delta}$ liver at 1 year, which showed increases of 3.6- and 4-fold in the expression non-deleted exons of *Axin1* and *Axin2*. The significant reduction in the expression of exon 2 containing transcripts of *Axin1* and *Axin2* in the tumours suggests that tumours arise from Axin deficient cells. This does not result in greater transcript of non-deleted exons of *Axin1* and *Axin2* as seen in non-tumour double Axin deleted liver at 1 year post induction.

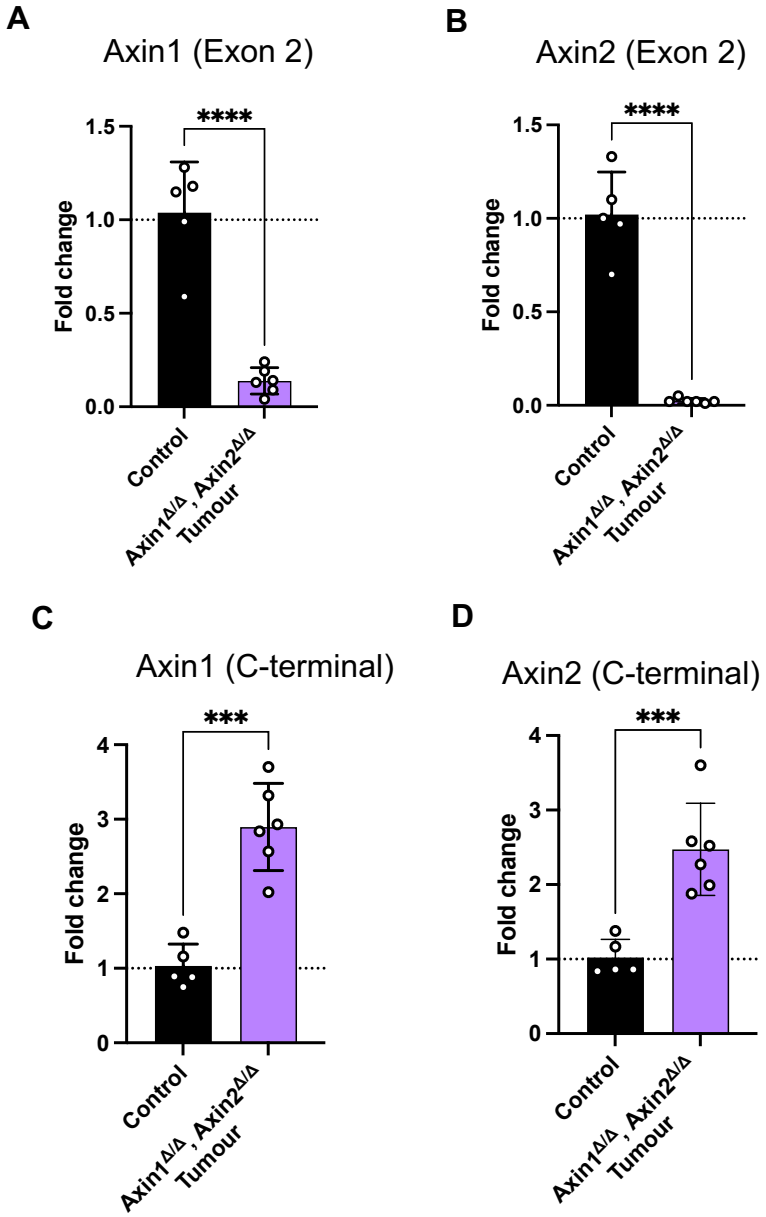

Figure 3.36 Axin expression in AhCreER^{T} Axin1$^{\Delta/\Delta}$, Axin2$^{\Delta/\Delta}$ liver tumours.
Axin expression in AhCreER Axin1 $^{\Delta/\Delta}$, Axin2 $^{\Delta/\Delta}$ liver tumour samples. (**A**) Expression of *Axin1* transcripts containing exon 2. (**B**) Expression of *Axin2* transcripts containing exon 2. (**C**) Overall expression of Axin1 using primers outside recombined region. (**D**) Overall expression of Axin2 using primers outside recombined. Data represents mean ±s.d. n = 5-6 biological replicates. Data was normalised to B2M and is shown as the relative fold change to induced AhCreER^{+}, Axin1$^{+/+}$, Axin2$^{+/+}$ (Control) dissected 1 year post induction. Significance was calculated using unpaired t-test ***p<0.001, ****p<0.0001

3.5.4 β-catenin localisation and total levels in AhCreER^{T} Axin1$^{\Delta/\Delta}$, Axin2$^{\Delta/\Delta}$ liver tumours.

In the study by Feng (2012), Axin1 deleted tumours only occasionally had positive nuclear β-catenin staining in a few cells. These results were supported in the study by (Abitbol et al. 2018), where the majority of Axin1 deficient HCC tumours were found to have an absence of activation of the Wnt/β-catenin pathway. It may be expected that the additional loss of Axin2 may lead to a pronounced activation of the Wnt/β-catenin pathway. To assess β-catenin localisation and total protein levels, sections of AhCreER^{T} Axin1$^{\Delta/\Delta}$, Axin2$^{\Delta/\Delta}$ liver tumours were stained for β-catenin and protein whole cell extracts were used in western blot analysis.

AhCreER^{T} Axin1$^{\Delta/\Delta}$, Axin2$^{\Delta/\Delta}$ liver tumours varied in their staining for β-catenin. Approximately half of the tumour sections examined had strong nuclear β-catenin in most cells and the other half were restricted to membrane and some cytoplasmic staining (Figure 3.37A). Total β-catenin protein levels were variable in control and tumour samples (Figure 3.37B). No difference was observed in total β-catenin levels when normalised to total protein (Figure 3.37C)

As tumours that arose from Axin1 and Axin2 deleted livers varied in their staining for nuclear β-catenin it made it unclear whether it was the loss of both Axins that results in nuclear β-catenin staining or whether some tumours acquire further mutations that result in the nuclear staining that was observed.

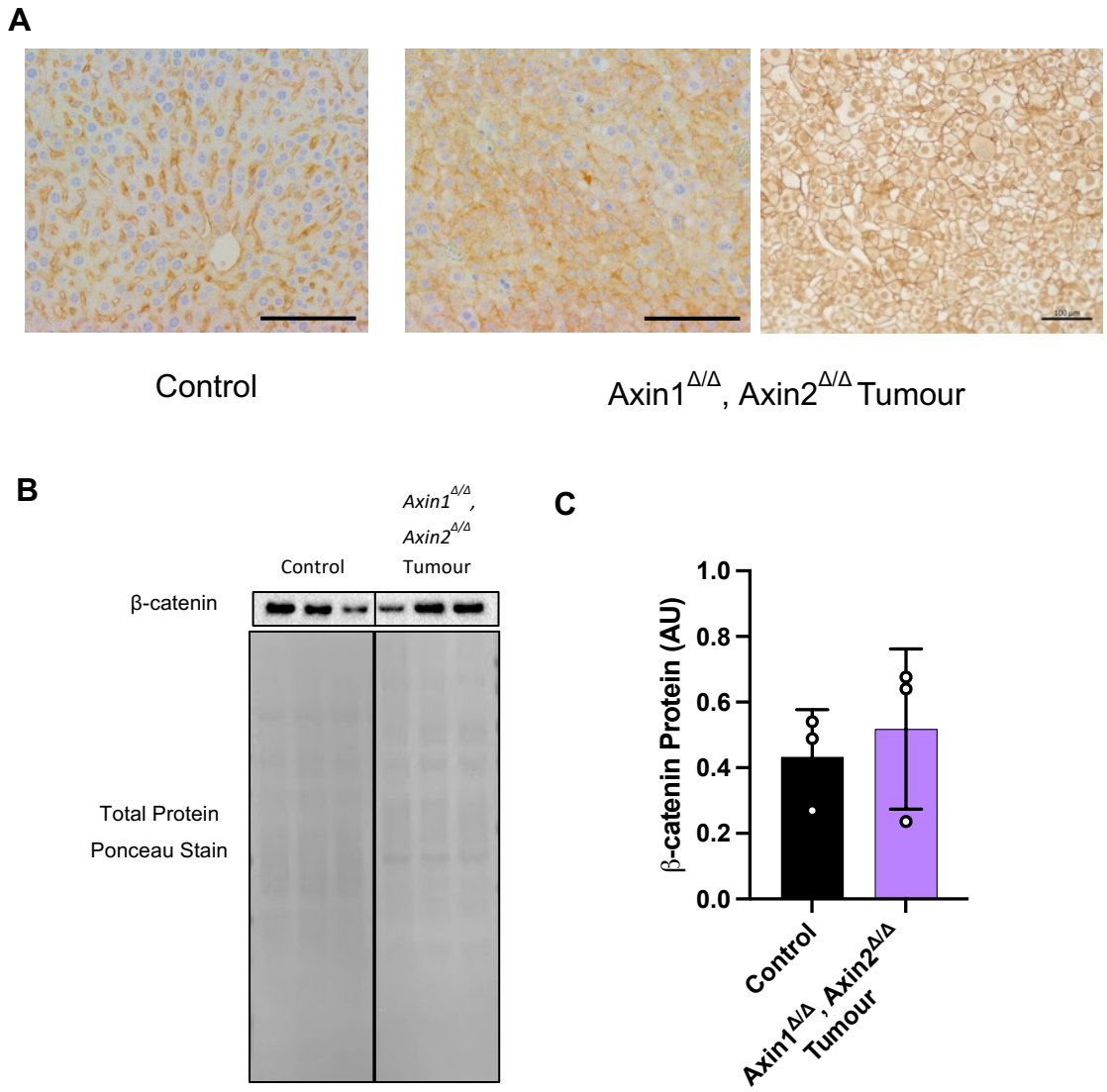

Figure 3.37 Mis-localised β-catenin in AhCreER^{T} Axin1$^{Δ/Δ}$, Axin2$^{Δ/Δ}$ liver tumours. **(A)** Representative images of β-catenin staining in control livers (AhCreER^{T}, Axin1$^{+/+}$, Axin2$^{+/+}$ at 1 year post induction) and AhCreER^{T} Axin1$^{Δ/Δ}$, Axin2$^{Δ/Δ}$ liver tumours showing membrane, cytoplasmic and nuclear staining. Scale bar 100 μm **(B)** Total β-catenin western blot from whole cell extracts from liver tumours. **(C)** Quantification of total β-catenin normalised to total protein from Ponceau stain. n = 3

3.5.5 Proliferation in AhCreER^{T}, Axin1$^{\Delta/\Delta}$, Axin2$^{\Delta/\Delta}$ tumours.

Axin1 deleted livers developed highly proliferative tumours without a clear Wnt/β-catenin pathway activation in the study by Feng (2012). In the study by (Abitbol et al. 2018), it was also found that the majority of Axin1 deficient human HCCs developed in the absence of β-catenin pathway activation and were associated with the proliferative class of HCC's. To assess the levels of proliferation in AhCreER^{T} Axin1$^{\Delta/\Delta}$, Axin2 $^{\Delta/\Delta}$ liver tumours, sections were stained for Ki67 and BrdU (Figure 3.38A, B). BrdU was administered 2 hours before dissection.

AhCreER^{T} Axin1$^{\Delta/\Delta}$, Axin2 $^{\Delta/\Delta}$ tumours had a significant increase in Ki67 (Figure 3.38C) and BrdU (Figure 3.38D) staining compared to control livers. Levels of staining for both were found to be highly variable across sections of the same tumour and between tumours from different mice.

Unsurprisingly, the tumours were found to be more proliferative than control liver. However, what was interesting to note was that the tumours had very heterogenous levels of proliferation as marked by Ki67 and BrdU. This may suggest that various regions within the tumours harbour distinct genetic alterations that drive variable rates of proliferation.

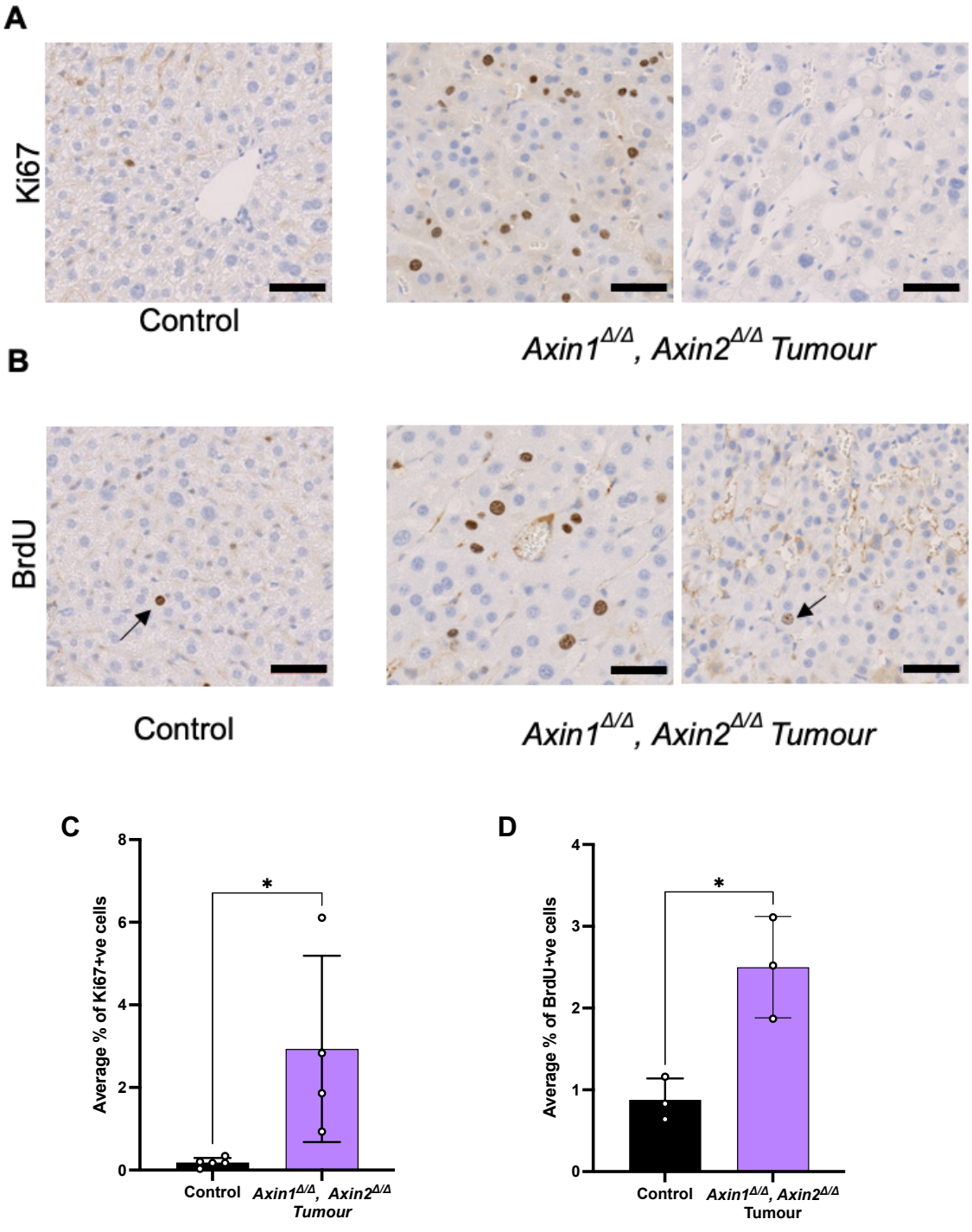

Figure 3.38 Increased proliferation in AhCreER^{T}, Axin1$^{\Delta/\Delta}$, Axin2$^{\Delta/\Delta}$ tumours
(A, B) Representative images of Ki67 and BrdU staining in liver from control (AhCreER^{T}, Axin1$^{+/+}$, Axin2$^{+/+}$) at 1 year post induction and AhCreER^{T} Axin1$^{\Delta/\Delta}$, Axin2$^{\Delta/\Delta}$ tumours showing varying levels of staining. **(C, D)** Quantification of Ki67 and BrdU staining in liver from control and AhCreER^{T} Axin1$^{\Delta/\Delta}$, Axin2$^{\Delta/\Delta}$ tumours. Scale bar 50 μm. Data represents mean ±s.d. from 3-5 biological replicates. Significance was calculated using unpaired t-test *p<0.05

3.5.6 Axin and Wnt targets and G2/M cell cycle gene expression in AhCreER^{T} Axin1$^{\Delta/\Delta}$, Axin2$^{\Delta/\Delta}$ liver tumours

Tumours showed nuclear β-catenin and increased proliferation as marked by Ki67 and BrdU. This may suggest increases in expression to Wnt targets and cell cycle genes. RT-qPCR was carried out using RNA from AhCreER^{T} Axin1$^{\Delta/\Delta}$, Axin2$^{\Delta/\Delta}$ liver tumours to assess changes in expression to the panel of Axin and Wnt targets and cell cycle genes associated with G2/M used previously.

Expression of *c-Myc*, *c-Jun* and *CD44* was increased as was seen in the normal AhCreER^{T} Axin1$^{\Delta/\Delta}$, Axin2$^{\Delta/\Delta}$ liver, but to a greater extent. Interestingly *Tiam1*, which has previously been found to be overexpressed in HCC patients with poor prognosis (Huang et al. 2013), was found to have significantly decreased expression. The expression of the cell cycle genes *p53*, *Cdc25a*, *Cyclins A2*, *B1* and *B2, Cdk1*, *Cdca3*, *Cdc20*, *Ki67* and *FoxM1* were found to be significantly increased as would be expected and to a much higher degree than was found in normal double Axin1, Axin2 deleted liver at 1 year post induction. *CyclinD1* showed a trend towards an increase but was variable between samples. Interestingly, *Mastl* expression was found to be significantly decreased. MASTL is essential for mitotic progression and overexpression of *MASTL* has been observed in HCC and shown to promote proliferation (Cao et al. 2019).

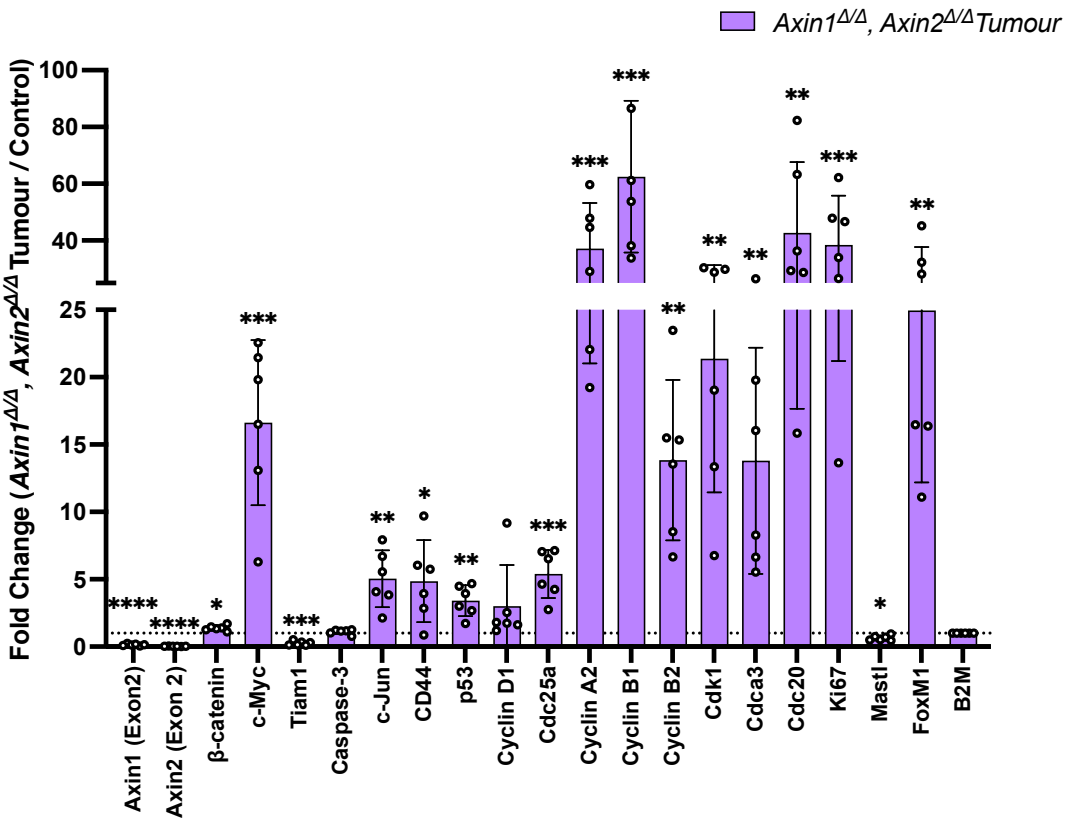

Figure 3.39 RT-qPCR analysis of Axin and Wnt targets and cell cycle genes in AhCreER^{T} Axin1$^{\Delta/\Delta}$, Axin2$^{\Delta/\Delta}$ liver tumours.

Data represents mean ±s.d. n = 6 biological replicates. Data was normalised to B2M and is shown as the relative fold change to induced AhCreER^{+}, Axin1$^{+/+}$, Axin2$^{+/+}$ (Control n=5) dissected 1 year post induction. Significance was calculated using unpaired t-test ***p<0.001, ****p<0.0001

3.5.7 Progenitor, lineage, and mature liver cell markers in AhCreER^{T} Axin1$^{\Delta/\Delta}$, Axin2$^{\Delta/\Delta}$ liver tumours.

H&E staining revealed that the tumours that arose could be divided into two growth patterns, that of a trabecular pattern with pleomorphic hepatocytes, and solid growth pattern with hepatocytes appearing very similar to normal hepatocytes. Using the panel of progenitor, lineage and mature liver cell markers as used previously, RT-qPCR was carried out using RNA from AhCreER^{T} Axin1$^{\Delta/\Delta}$, Axin2$^{\Delta/\Delta}$ liver tumours to assess changes to cell identity.

The hepatic progenitor markers *Lgr5*, *Trop2*, *OPN* and *Sox9* showed trends for an increase in expression however, due to variability between samples, this was not significant. No changes were seen in *EpCam* expression (Figure 3.40A). The biliary epithelial cell marker *Hnf1b* was significantly increased however no changes were seen in the expression of *Krt19* and *Krt7* (Figure 3.40B). Hepatocyte lineage markers *Hnf4*α and *Tbx3* were found to be significantly increased and *Prox1* showed a trend for a moderate increase. As may be expected from AFP staining, *AFP* expression was found to be an average 110-fold increased (Figure 3.40C). In contrast to non-tumour Axin1, Axin2 deleted liver at 1 year post induction, *Fah* expression was found to be significantly decreased. Reduced expression of *Albumin* was significant in tumour. No changes were seen in the expression of *Ass1* (Figure 3.40D)

Overall, these results suggest that AhCreER^{T} Axin1$^{\Delta/\Delta}$, Axin2$^{\Delta/\Delta}$ liver tumours have more of a progenitor cell phenotype and lose expression of mature hepatocyte markers.

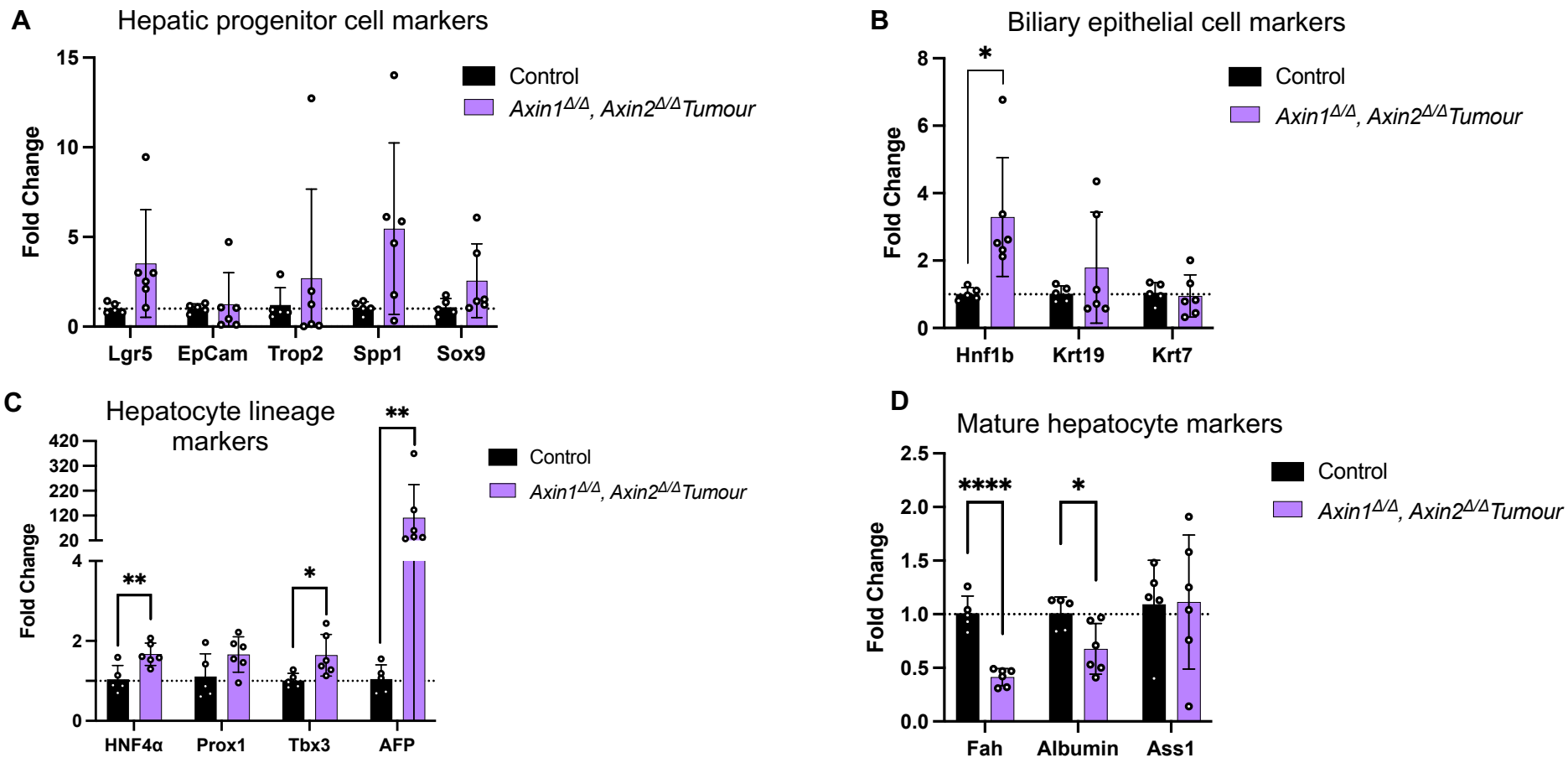

Figure 3.40 RT-qPCR of progenitor, lineage, and mature liver cell markers in AhCreER^{T} Axin1$^{\Delta/\Delta}$, Axin2$^{\Delta/\Delta}$ tumours.
RT-qPCR of AhCreER^{T} Axin1$^{\Delta/\Delta}$, Axin2$^{\Delta/\Delta}$ tumours (**A**) Expression of hepatic progenitor cell markers. (**B**) Expression of biliary epithelial cell markers. (**C**) Expression of hepatocyte lineage markers. (**D**) Expression of mature hepatocyte markers. Data represents mean ±s.d. n = 6 biological replicates. Data was normalised to B2M and is shown as the relative fold change to induced AhCreER^{+}, Axin1$^{+/+}$, Axin2$^{+/+}$ (Control n = 5) dissected 1 year post induction. Significance was calculated using unpaired t-test *p<0.05 **p<0.01, ****p<0.0001

3.5.8 Yap IHC, total protein levels and downstream target expression in AhCreER^{T} Axin1$^{\Delta/\Delta}$, Axin2$^{\Delta/\Delta}$ liver tumours.

In a recent study (Liang et al. 2022) it was found that loss of function mutations to Axin1 requires Yap and Taz during tumour progression. Deletion of Yap and Taz was found to suppress tumours formed in c-Met/sgAxin1 liver tumours. Positive nuclear staining of Yap and upregulation of Yap downstream targets in the livers of Axin1, Axin2 deleted livers at 1 year post induction gives a hint of the involvement of Yap in the tumourigenesis observed in AhCreER^{T} Axin1$^{\Delta/\Delta}$, Axin2$^{\Delta/\Delta}$ livers. To investigate whether Yap protein is stabilised and whether downstream Yap targets are upregulated, IHC, western blot and RT-qPCR was carried on using sections, whole cell protein extracts and RNA from AhCreER^{T} Axin1$^{\Delta/\Delta}$, Axin2$^{\Delta/\Delta}$ liver tumours.

Nuclear staining was observed in both the solid and trabecular growth patterned tumours (Figure 3.41A). Total Yap protein levels were found to be 7-fold higher in AhCreER^{T} Axin1$^{\Delta/\Delta}$, Axin2$^{\Delta/\Delta}$ liver tumours (Figure 3.41B, C). Expression of Yap downstream targets *Gpc3*, *Birc5* and *Hmmr* were found to be significantly increased and to a greater extent than non-tumour liver of Axin1, Axin2 deleted liver at 1 year post induction. Trends of an increase for *Ctgf* and *Cyr61* were also observed but were not significant due to variation between samples. No changes were seen in the expression of *Fas* and *Sfrp1*.

Overall, this data suggests that loss of Axin1 and Axin2 results in latent upregulation of Yap and its downstream targets which contributes to tumourigenesis. Acute loss of Axin1 or both Axin1 and Axin2 does not appear to increase Yap protein expression, so it is unclear whether later events result in the upregulation of Yap. Strikingly, the deletion of Axin1 and Axin2 did not result in the stabilisation of β-catenin or the clear expansion of GS expression as seen with the deletion of Apc.

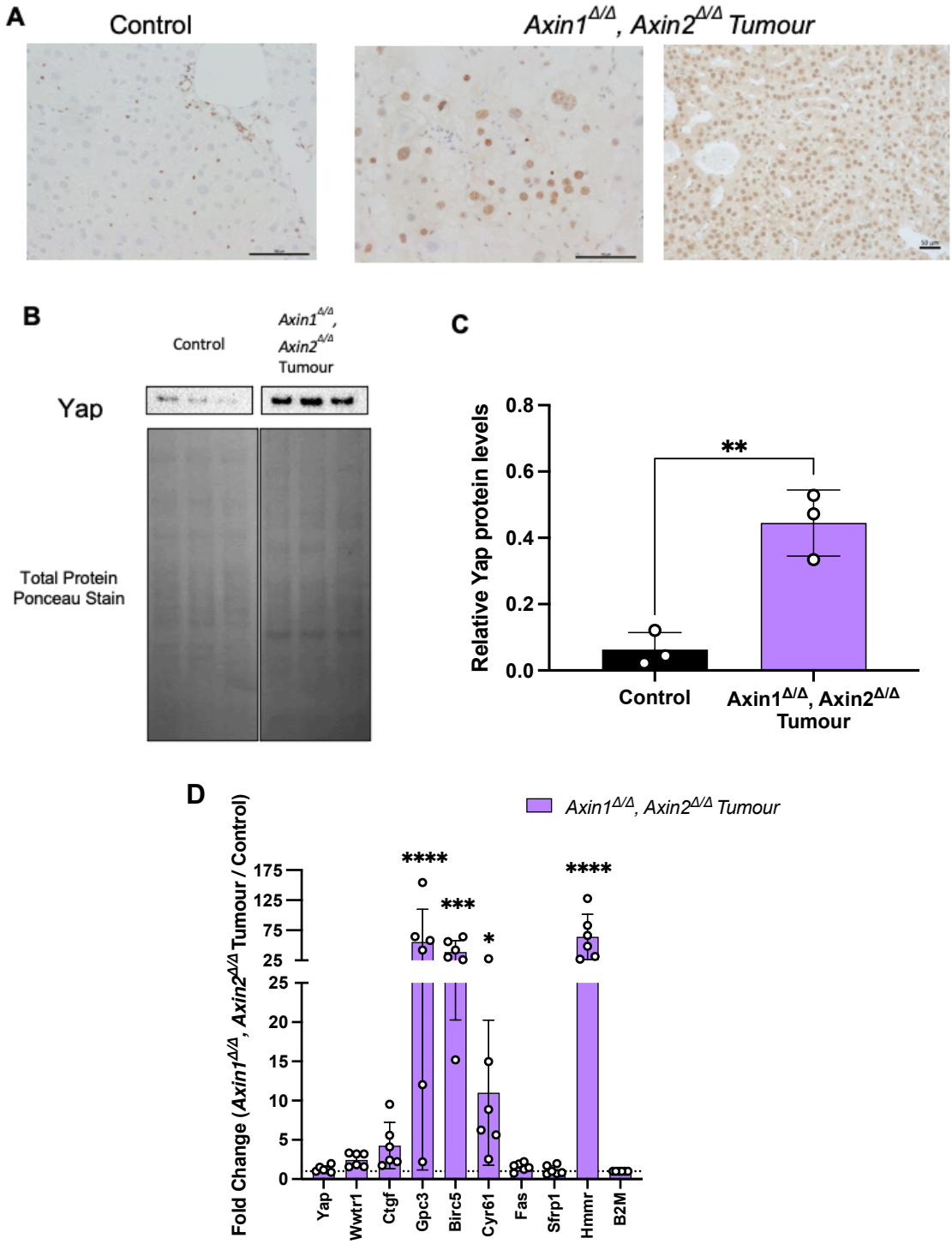

Figure 3.41 Increased Yap levels in AhCreER^{T} Axin1$^{\Delta/\Delta}$, Axin2$^{\Delta/\Delta}$ liver tumours. **(A)** Representative images of Yap IHC staining in liver tissue from AhCreER^{T} mice 1 year post induction (control) and AhCreER^{T} Axin1$^{\Delta/\Delta}$, Axin2$^{\Delta/\Delta}$ liver tumours with solid and trabecular growth pattern. **(B)** Western blot of total Yap protein in control and tumour liver. **(C)** Quantifiation of total Yap protein relative to total protein from Ponceau stain. n=3 **(D)** RT-qPCR of Yap, Wwtr1 and downstream Yap targets. Data represents mean ±s.d. n = 6 biological replicates. Data was normalised to B2M and is shown as the relative fold change to induced AhCreER^{+}, Axin1$^{+/+}$, Axin2$^{+/+}$ (Control n = 5) dissected 1 year post induction. Significance was calculated using unpaired t-test ***p<0.001, ****p<0.0001

Chapter 4: Utilising CRISPR/Cas9 targeting to generate conditional definitive Axin nulls in ES cells.

4.1 Introduction

Despite the liver tumourigenesis observed in the Axin1 and Axin2 deleted cohort, acute loss of both Axins did not produce the strong Wnt ON phenotype expected. One of the concerns previously mentioned was that one or both Axin alleles were not definitive nulls and that remaining β-catenin turnover activity might have been sufficient to explain the lack of a strong Wnt-ON signature.

Immunoblotting and immunoprecipitation with antibodies against different regions of the Axin1 protein provided strong evidence for the loss of Axin1 protein using conditional deletion of exon 2 in the study by (Feng et al. 2012). Additionally, embryonic deletion of exon 2 resulted in embryonic lethality (Offergeld 2015 PhD Thesis), phenocopying the results of the established $Axin1^{Tg1}$-null allele (Zeng et al. 1997) and as seen with an alternative $Axin1^{\Delta RGS}$, exon 2 floxed allele (Chia et al. 2009).

The commercially available Axin2 deleted mouse line the $Axin2^{lacZ/lacZ}$ (Conductin LacZ) has the LacZ gene inserted into exon 2, replacing most of the exon (Lustig et al. 2002a). It is presumed null, but there is little evidence that confirms or disproves this. The Axin2 allele used for this study also relied on the removal exon 2 that contains the ATG start codon. This was done using a similar strategy as for the $Axin1^{fl/fl}$ allele (Feng et al. 2012) by inserting loxP sights flanking exon 2 (Figure 4.1A). Unfortunately, there are no good anti-mouse Axin2 antibodies, that bind to sequences outside exon 2. However, the use of the embryonically active CMV-Cre to delete the floxed Axin2 allele studied here, generated embryos that were found to be greatly reduced in size and died at E 9.5 (Offergeld 2015 PhD Thesis). This contrasts with the $Axin2^{lacZ/lacZ}$ mouse which has been shown to be viable and fertile and shows only minor defects in embryonic skull formation (Yu et al. 2005). The different phenotypes of the Axin2 alleles may be used to suggest that at least one of the alleles was not a true null. The more severe embryonic phenotype of the $Axin2^{\Delta/\Delta}$ allele as discussed in Chapter 6 could be used to suggest that the $Axin2^{\Delta/\Delta}$ allele was the full null.

However, transcription of regions of both Axins lacking exon 2 was detected by RT-qPCR and sequence analysis using the online tool ATGpr (Salamov et al. 1998)

identified alternative potential initiation codons. As long as coding regions of Axin remain, it would not be possible to confirm the complete loss of Axin proteins without doubt. To this end, we aimed to generate a series of ES cells that had alleles that would remove the whole coding region of Axin1, Axin2 or both Axin1 and Axin2.

Mouse embryonic stem (mES) cells bearing homozygous exon 2 floxed alleles of Axin1 and or Axin2 (Figure 4.1A) that were previously generated in the Dale lab, were used to introduce a 3rd LoxP site via CRISPR/Cas9 and homology directed repair at the end of the coding regions of both Axin genes (Figure 4.1B). The rational to use ES cells with exon 2 floxed alleles of Axin1 and or Axin2 was that this would reduce the workload as only 1 additional loxp site would need to be introduced. Cre recombination should leave only exon 1 of Axin1 and or Axin2, removing any protein coding regions for the protein (Figure 4.1C). The aim was to generate mES cell lines carrying conditional definitive null combinations of different Axin alleles. Once generated, they would be tested in ES cell functional assays in direct comparison to the work carried out in the thesis of Anika Offergeld. Additionally, following mouse generation, by comparison in the liver presented in this thesis.

Homology directed repair (HDR) templates were designed and amplified from mouse DNA by Anika Offergeld. Left and right homologous arms of Axin1 after the final coding exon (Figure 4.1B) were cloned into the pCR-XL-TOPO vector along with a LoxP site and a Pst1 restriction site (Figure 4.2A). Left and right homologous arms of Axin2 after the last coding exon (Figure 4.1B) were cloned into pCR-BluntII-TOPO, again with a LoxP site and a Pst1 restriction site (Figure 4.2A). The vector pSpCas9n(BB)-2A-Puro was chosen to clone sgRNA sequences for Axin1 and Axin2 for co-expression of the sgRNA and nickase. Genome editing is achieved by double nicking via appropriately spaced guide RNAs and repair via HDR using the templates (Figure 4.2C). The vector has a Cas9 D10A nickase mutant and requires paired TOP and BOTTOM guide RNAs for targeting opposite strands of the target site which is meant to reduce off target activity (Ran et al. 2013).

To ensure several independent clones would be available for subsequent analyses, multiple parental ES cell clones were prepared by Anika Offergeld to help exclude clone-dependent differences that might not be related to the intended loxP flanked alleles. The clone lines used for targeting for the insertion of the 3rd LoxP site were previously used in the work carried out by Anika Offergeld in her thesis and were homozygous exon 2 flanked by LoxP sites for Axin1, Axin2 or both Axin1 and Axin2

(Axin1$^{Ex2fl/fl}$, Axin2$^{Ex2fl/fl}$ and Axin1$^{Ex2fl/fl}$ Axin2$^{Ex2fl/fl}$). All used clones had previously been genotyped by Anika Offergeld and confirmed to have homozygous LoxP sites flanking exon 2 for the Axin series of ES cells.

For insertion of the 3rd LoxP site, ES cell clones were transfected with appropriate paired TOP and BOTTOM guide RNAs cloned into the Cas9 D10A vector and linearised targeting plasmid (HDR template). As an example, Axin1$^{Ex2fl/fl}$ ES cells were transfected with an Axin1 TOP sgRNA, an Axin1 BOTTOM sgRNA and the Axin1 linearised targeting plasmid containing the LoxP site. ES cells were subsequently selected in media containing puromycin. Any clones that grew would indicate successful transfection as the Cas9 D10A vector contains a puromycin resistance sequence. Individual clones were picked, and replica plated in two separate plates, one plate for growing and freezing for future use and one plate for genotyping to confirm successful transfection.

The strategy used was successful in generating full Axin2 deletion in ES cells. Unfortunately, it was only successful in generating a full null of one allele of Axin1 and only heterozygous null alleles of both Axin1 and Axin2 in double mutants. This chapter will examine the targeting approach used and discuss some of the methodology used to address potential technical explanations for the results seen.

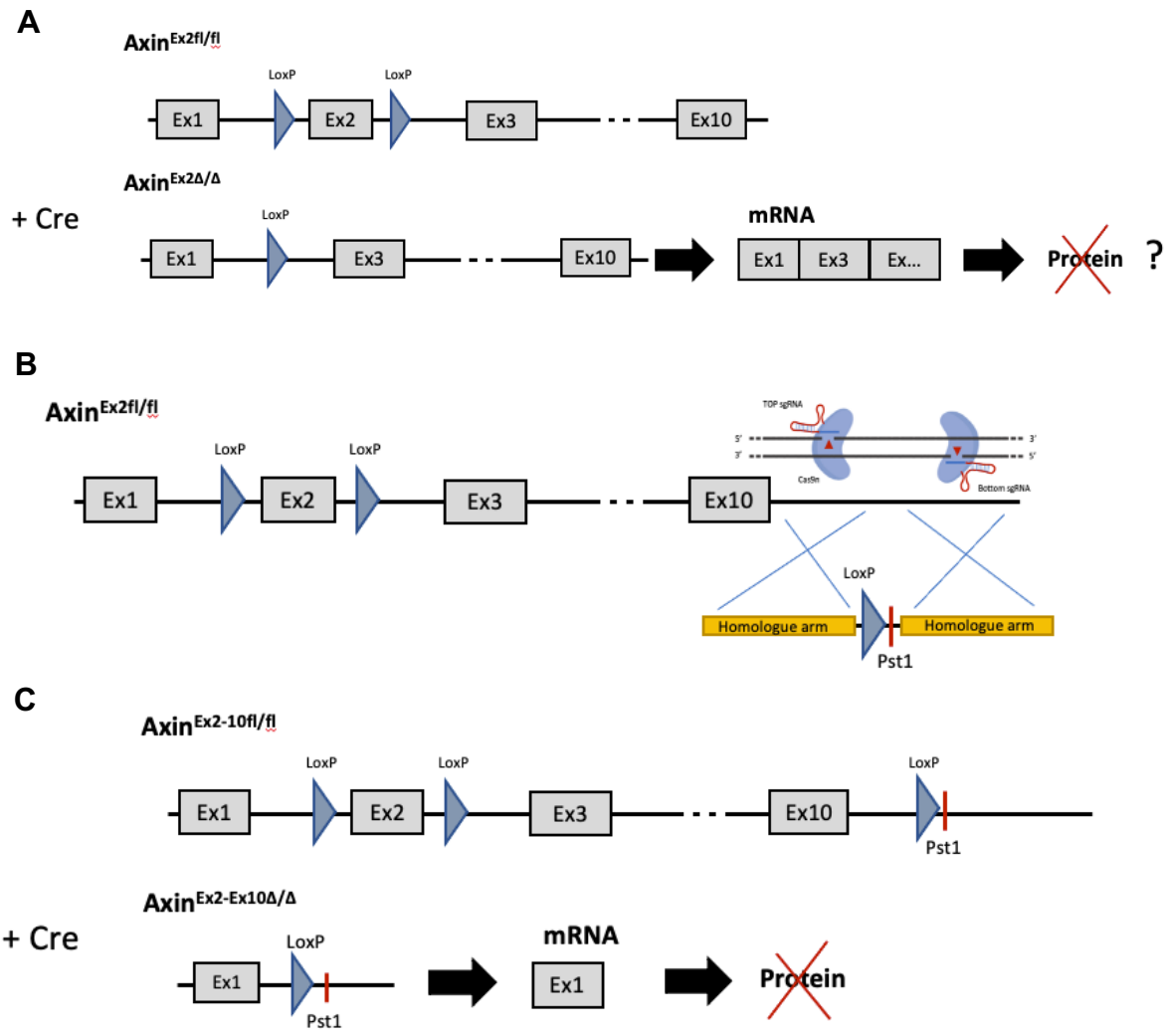

Figure 4.1 Schematic of current and intended Axin alleles.
(A) Axin1 and Axin2 both contain homozygous loxP sites flanking exon 2 that contains the ATG start codon for both genes. However, it has not been possible to definitively prove complete loss of protein **(B)** Using CRISPR Cas9n and a template containing a LoxP site, the goal was to add a LoxP site at the end of both Axin1 and Axin2 coding regions. **(C)** Addition of Cre recombinase to the 3 floxed Axin alleles should result in the removal of all the coding regions of Axin1 and Axin2 thus generating a definitive null.

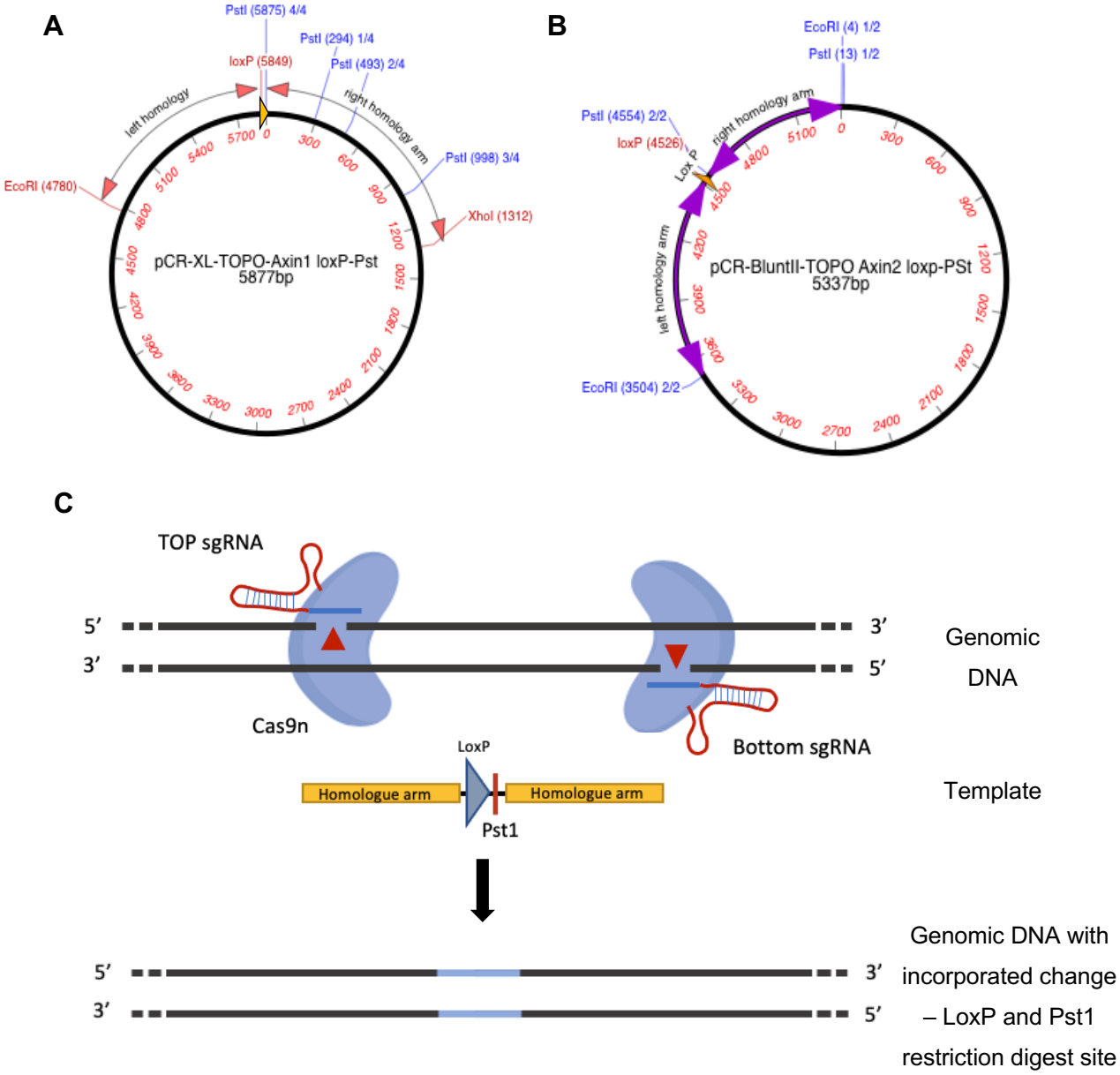

Figure 4.2 HDR templates and Cas9n targeting.
(A) A region of Axin1 was cloned into pCR-XL-TOPO together with a loxP-PST1 site. For transfection, restriction digest using EcoRI and XhoI were used to linearise and cut out the required template. **(B)** A region of Axin2 was cloned into pCR-BluntII-TOPO together with a loxP-PST1 site. For transfection, restriction digest using EcoRI was used to linearise and cut out the required template. **(C)** Graphical representation illustrating DNA double strand breaks using a pair of Cas9 D10A nickases. A pair of sgRNA-Cas9n complexes are used to nick both strands simultaneously. (Adapted from Ran 2013). Linearised Axin template is used for HDR. Genomic DNA now should have the 3rd LoxP site integrated after the final coding exon of Axin.

4.1.1 Screening for the insertion of 3rd LoxP site and recombination in ES cells.

Replica plating of individual ES clones that had been transfected allowed for the confirmation of the presence of the 3rd LoxP site of both alleles before subsequent Cre recombination.

Primer types C were used to identify successful integration of the 3rd LoxP site and could be further confirmed with Pst1 digest for both Axin1 and Axin2 alleles (Figure 4.3B ii, v). Pst1 digest was particularly important for Axin1 3rd LoxP integration as the WT and Axin1$^{Ex2\text{-}10fl}$ PCR product was the same size. Pst1 digest of Axin1 PCR product that no longer had the 509bp band were considered to be homozygous for integration of the 3rd LoxP site. As a secondary screen, clones identified as most likely to have the 3rd LoxP site homozygously integrated were then co transfected with pCAGGS-Cre-IRESpuro, a plasmid containing puromycin resistance and Cre recombinase under the control of the chicken-beta-actin promoter to induce recombination. Individual clones were picked after selection in media containing puromycin and were grown for genotyping and banking. Clones were genotyped using primer types B to check for recombination of exon 2 (Figure 4.3B iii, vi), and primer type D to check for recombination of exon 2 to 10 (Figure 4.3B iv, vii). Successful homozygous recombination of exon 2 to exon 10 for both alleles using primer type D would result in a band for Axin$^{Ex2\text{-}10\Delta}$ only. The presence of a band for Axin$^{Ex2\Delta}$ using primer type B would suggest that integration of the 3rd LoxP site only occurred on one allele, or that full recombination only occurred on one allele.

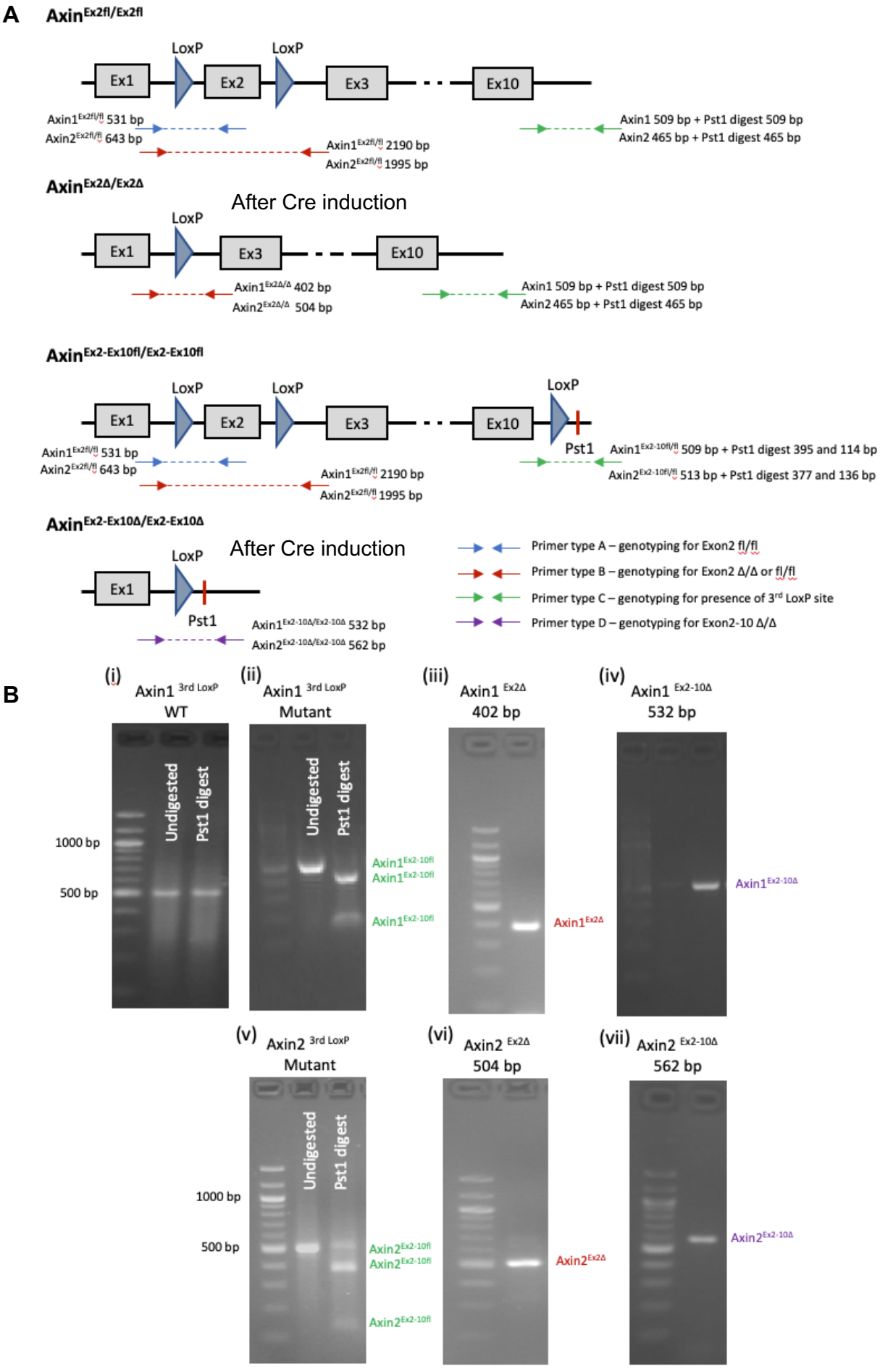
A
Axin Ex2fl/Ex2fl
LoxP
LoxP
Ex1
Ex2
Ex3
Ex10
Axin1 Ex2fl/fl 531 bp
Axin2 Ex2fl/fl 643 bp
Axin1 Ex2fl/fl 2190 bp
Axin2 Ex2fl/fl 1995 bp
Axin1 509 bp + Pst1 digest 509 bp
Axin2 465 bp + Pst1 digest 465 bp
Axin Ex2Δ/Ex2Δ
After Cre induction
LoxP
Ex1
Ex3
Ex10
Axin1 Ex2Δ/Δ 402 bp
Axin2 Ex2Δ/Δ 504 bp
Axin1 509 bp + Pst1 digest 509 bp
Axin2 465 bp + Pst1 digest 465 bp
Axin Ex2-Ex10fl/Ex2-Ex10fl
LoxP
LoxP
LoxP
Ex1
Ex2
Ex3
Ex10
Pst1
Axin1 Ex2fl/fl 531 bp
Axin2 Ex2fl/fl 643 bp
Axin1 Ex2fl/fl 2190 bp
Axin2 Ex2fl/fl 1995 bp
Axin1 Ex2-10fl/fl 509 bp + Pst1 digest 395 and 114 bp
Axin2 Ex2-10fl/fl 513 bp + Pst1 digest 377 and 136 bp
Axin Ex2-Ex10Δ/Ex2-Ex10Δ
After Cre induction
LoxP
Ex1
Pst1
Axin1 Ex2-10Δ/Ex2-10Δ 532 bp
Axin2 Ex2-10Δ/Ex2-10Δ 562 bp
Primer type A – genotyping for Exon2 fl/fl
Primer type B – genotyping for Exon2 Δ/Δ or fl/fl
Primer type C – genotyping for presence of 3rd LoxP site
Primer type D – genotyping for Exon2-10 Δ/Δ
B
(i) Axin1 3rd LoxP WT
(ii) Axin1 3rd LoxP Mutant
(iii) Axin1 Ex2Δ 402 bp
(iv) Axin1 Ex2-10Δ 532 bp
Undigested
Pst1 digest
1000 bp
500 bp
Axin1 Ex2-10fl
Axin1 Ex2-10fl
Axin1 Ex2-10fl
Axin1 Ex2Δ
Axin1 Ex2-10Δ
(v) Axin2 3rd LoxP Mutant
(vi) Axin2 Ex2Δ 504 bp
(vii) Axin2 Ex2-10Δ 562 bp
Undigested
Pst1 digest
1000 bp
500 bp
Axin2 Ex2-10fl
Axin2 Ex2-10fl
Axin2 Ex2-10fl
Axin2 Ex2Δ
Axin2 Ex2-10Δ

Figure 4.3 Genotyping ES cell clones
(A) Shematic for the approximate position of primer sets used to identify Axin1 and Axin2 clones with or without a 3rd LoxP site and resulting alleles post Cre recombination. **(B)** Subset of representative genotyping results for the presence of 3rd LoxP site, $Ex^{2\Delta}$ and $Ex^{2\text{-}10\Delta}$ in Axin1 and Axin2 mutant mES cells. After transfection using the appropriate template and sgRNA, PCR was carried out to test for successful integration of the 3rd LoxP site. Successful Axin1 3rd LoxP integration could not be distinguished from WT as both PCR products were the same size 509 bp, therefore a Pst1 digest was used to confirm successful transfection as only the mutant allele should have the Pst1 restriction site producing bands of 395 bp and 114 bp. The first track **(i)** (Axin1 3rd LoxP WT) shows an unsuccessful transfection of the 3rd LoxP site. The second track **(ii)** (Axin1 3rd LoxP Mutant) shows the successful transfection of the 3rd LoxP site as the PCR product of 509 bp was able to be digested by Pst1 to 395 and 114 bp. Successful transfection of 3rd LoxP site of Axin2 should produce a PCR product with the size of 513 bp as shown in track **(v)** Axin2 3rd LoxP Mutant (WT for $Axin2^{Ex2\text{-}10fl}$ of 465 bp was not seen indicating the transfection was homozygous) which can be further confirmed with Pst1 digest producing bands of 377 bp and 136 bp. Clones identified as having a 3rd LoxP site through genotyping with Pst1 digest were selected for Cre mediated deletion to confirm that both alleles of Axin1 and or Axin2 were transfected. The rationale was that if the 3rd LoxP site was on both alleles, that after successful Cre deletion there would be a band for $Axin^{2\text{-}10\Delta}$ **(iv)** 532 bp for Axin1, **(vii)** 562 bp for Axin2 and no band for $Axin^{2\Delta}$ **(iii)** 402 bp for Axin1, **(vi)** 504 bp for Axin2. If a band came up for both $Axin^{2\Delta}$ and $Axin^{2\text{-}10\Delta}$ in one clone, then it would indicate that the 3rd LoxP site was only transfected heterozygously.

4.1.2 Full knockout alleles achieved in ES cells with CRISPR Cas9n and CAGGS Cre induction.

Initial screening for the integration of the 3rd LoxP were carried out by Anika Offergeld. Efficiency for the Integration of the 3rd LoxP site for the series of Axin mutant ES cells was in the region of 90-100% (data not shown). I took over with the CAGGS Cre induction and subsequent genotyping of full knockout alleles. All clones used for CAGGS Cre recombination were identified as having homozygous integration of the 3rd LoxP site for Axin1, Axin2 or both Axin1 and Axin2.

Post CAGGS Cre transfection of clones identified as $Axin1^{Ex2\text{-}10fl/Ex2\text{-}10fl}$, the expectation was to see $Axin1^{Ex2\text{-}10\Delta/Ex2\text{-}10\Delta}$. Genotyping of the initial 96 Axin1 mutant ES clones picked showed deletion of exon 2 only (Table 4.1).

Full deletion of Axin2 was more successful than for Axin1. Out of the total of 140 clones picked after transfection with CAGGS Cre, 133 showed full $Axin2^{Ex2\text{-}10\Delta}$. However, 58 of these clones also showed recombination of $Axin2^{Ex2\Delta}$ (Table 4.2). The other 7 clones only showed recombination of $Axin2^{Ex2\Delta}$. In total, 75 clones were identified as having full homozygous $Axin2^{Ex2\text{-}10\Delta/Ex2\text{-}10\Delta}$ recombination. The results would however suggest that full recombination may not be 100% efficient. Whether this was because the alleles were correctly targeted but did not recombine, or whether the 3rd LoxP site integration was only heterozygous was not determined. Genotyping for the 3rd LoxP site using Primer type C would help to resolve this question. To further confirm full deletion of Axin2, PCR product from several clones identified as $Axin2^{Ex2\text{-}10\Delta/Ex2\text{-}10\Delta}$ was sent for sequencing. Unfortunately, sequencing failed to show the sequence expected after recombination of exons 2 to 10. This may be down to technical error such as gel purification of the PCR product not being optimal and in future could be repeated using a plasmid for a better read of the sequence.

Axin1 and Axin2 clones showed a similar pattern of recombination using CAGGS Cre as would have been expected based on a combination of the success rates for the single Axin1 and Axin2 alleles alone. 96 out of 96 clones from 2 parental lines (A34-39-49 and A34-39) showed loss of exon 2 of Axin1, however none showed Axin1 full exon 2 to 10 recombination. 68 out 96 of these clones showed loss of exons 2 to 10 of Axin2, however all 96 clones also showed loss of exon 2 of Axin2 which would suggest two thirds were heterozygous for full deletion of Axin2 (Table 4.3). Parental clone line 9F2 1-2-1 generated 28 clones that were previously identified as

Table 4.1 Axin1 mutant ES cell recombination summary

Parental Clone	**1wt 8-18**	48 clones picked
Genotyping	$Axin1^{Ex2\Delta}$	48/48
Results	$Axin1^{Ex2\text{-}10\Delta}$	0/48
Parental Clone	**1wt 8-37**	16 clones picked
Genotyping	$Axin1^{Ex2\Delta}$	not checked
Results	$Axin1^{Ex2\text{-}10\Delta}$	0/16
Parental Clone	**1wt 4-47-8**	16 clones picked
Genotyping	$Axin1^{Ex2\Delta}$	not checked
Results	$Axin1^{Ex2\text{-}10\Delta}$	0/16
Parental Clone	**1wt 5-38**	16 clones picked
Genotyping	$Axin1^{Ex2\Delta}$	16/16
Results	$Axin1^{Ex2\text{-}10\Delta}$	0/16

Table 4.2 Axin2 mutant ES cell recombination summary

Parental Clone	**2wt 12**	48 clones picked
Genotyping	$Axin2^{Ex2\Delta}$	17/48
Results	$Axin2^{Ex2\text{-}10\Delta}$	47/48
Parental Clone	**2wt 15-44-2**	16 clones picked
Genotyping	$Axin2^{Ex2\Delta}$	0/16
Results	$Axin2^{Ex2\text{-}10\Delta}$	16/16
Parental Clone	**2wt 41-84**	16 clones picked
Genotyping	$Axin2^{Ex2\Delta}$	0/16
Results	$Axin2^{Ex2\text{-}10\Delta}$	16/16
Parental Clone	**2wt 44-68**	16 clones picked
Genotyping	$Axin2^{Ex2\Delta}$	16/16
Results	$Axin2^{Ex2\text{-}10\Delta}$	16/16
Parental Clone	**2wt 24**	44 clones picked
Genotyping	$Axin2^{Ex2\Delta}$	32/44
Results	$Axin2^{Ex2\text{-}10\Delta}$	38/44

Table 4.3 Double Axin1 and Axin2 mutant ES cell recombination summary

Parental Clone	**A34-39-49**	48 clones picked
Genotyping Results	$Axin1^{Ex2\Delta}$	48/48
	$Axin1^{Ex2\text{-}10\Delta}$	0/48
	$Axin2^{Ex2\Delta}$	48/48
	$Axin2^{Ex2\text{-}10\Delta}$	26/48

Parental Clone	**A34-39**	48 clones picked
Genotyping Results	$Axin1^{Ex2\Delta}$	48/48
	$Axin1^{Ex2\text{-}10\Delta}$	0/48
	$Axin2^{Ex2\Delta}$	48/48
	$Axin2^{Ex2\text{-}10\Delta}$	35/48

Parental Clone	**9F2 1-2-1; *6,7,8,9***	16 clones picked
Genotyping Results	$Axin1^{Ex2\Delta}$	16/16
	$Axin1^{Ex2\text{-}10\Delta}$	16/16
	$Axin2^{Ex2\Delta}$	16/16
	$Axin2^{Ex2\text{-}10\Delta}$	16/16

having homozygous integration of the 3rd LoxP site for both Axin1 and Axin2. The 28 clones were re-genotyped, and this was re-confirmed. Clones 6, 7, 8, and 9 from this line were selected for Cre induction. A total of 16 clones were picked and genotyped after transient CAGGS Cre transfection and puromycin selection. All 16 clones were heterozygous for exon 2 and exons 2 to 10 deletion for both Axin1 and Axin2 ie. $Axin1^{Ex2\Delta/Ex2\text{-}10\Delta}/Axin2^{Ex2\Delta/Ex2\text{-}10\Delta}$.

The limited success in the full deletion of Axin1 led to further investigations in Axin1 floxed only ES cells. This was done in order to initially remove the complexity of looking at both Axin1 and Axin2.

48 clones from the targeted parental clone line Ax1 CRISPR (not previously induced with CAGGS Cre) were re-genotyped to confirm insertion of the 3rd LoxP site. 4 of these clones were induced. Of the subsequent 86 clones picked, PCR showed no recombination and retention of LoxP sites flanking exon 2 and presence of the 3rd LoxP site. This would suggest a possible failure of recombination in these clones or that only clones that failed to recombine had survived.

Determining the homozygous insertion of the 3rd LoxP site for Axin1 relied on interpretation of PCR product after Pst1 digest, PCR product from a selection of Ax1

CRISPR clones were sent for sequencing. The premise was that if the PCR product contained both a WT (no 3rd LoxP site) and mutant allele, there would be an overlap of trace data covering the LoxP site as they are both WT and mutant PCR products are the same size. The sequence trace results showed no overlap and only a trace for the mutant sequence containing the 3rd LoxP insertion. This, with the initial PCR results provided strong evidence that the 3rd LoxP site was inserted on both alleles in Axin1. However, CAGGS Cre induction and genotyping of the subsequent 51 clones revealed no Axin1 exon 2 to exon 10 deletion and only 2 clones were identified as having lost exon 2. This was surprising as the parental clones were $Axin1^{Ex2fl/fl}$ and after targeting and confirming with PCR and sequencing were suggested to be $Axin1^{Ex2\text{-}10fl/fl}$. It was hypothesised that only cells that failed to recombine or cells only losing exon 2 ($Axin1^{Ex2\Delta}$) had survived and that the complete loss of Axin1 might be lethal.

4.1.3 Investigation of full Axin1 deletion viability, alternate floxing, and on target insertion of the 3rd LoxP site.

To test the theory that the full loss of Axin1 might be lethal to the ES cells, uninduced Axin1 clones bearing homozygous 3rd LoxP sites as supported by PCR and sequencing data were stably transfected with an inducible Cre, pAN-MerCreMer. pAN-MerCreMer is an expression vector with Cre recombinase, hygromycin resistance and a mutated hormone-binding domain of the murine oestrogen receptor that can be activated by 4-hydroxy-tamoxifen (4-OHT) but not by endogenously expressed oestrogen. Clones successfully transfected with pAN-MerCreMer were identified by PCR for Cre. Cre negative and Cre positive clones were then used for multiple viability assays. The hypothesis was that ES cells with homozygous 3rd LoxP sites and positive for pAN-MerCreMer and exposed to 4-OHT would die and this could be quantified in viability assays.

No differences in total number of live cells or percentage of viability were seen between the Cre negative or the Cre positive treatment and control groups (Figure 4.4A, B). This would suggest that if full loss of Axin1 is occurring then this does not affect viability as determined by this readout. PCR results from the pools of Cre positive clones with 800nM 4-OHT showed recombination of Axin1 exon 2 but no full recombination. WST-1 (Figure 4.4C) and a simultaneous RealTimeGlo viability and toxicity assay (Figure 4.4D, E) were unable to find differences between Cre negative

and Cre positive clones. As these assays tested a pool of induced cells, it remained unclear if the cells with full recombination were viable and only cells that recombined exon 2 of Axin1, or did not recombine, were the ones that survived. Axin1 exon 2 deleted ES cells may have had increased viability and therefore masked the loss of fully recombined cells. Attempts were made to pick individual clones after MerCreMer induction, however, only exon 2 was shown to be recombined and none of the 32 clones picked showed full Axin1 exon 2 to 10 recombination. It was concluded that full recombination was either not occurring or that it was occurring with low efficiency and that full recombination may be leading to rapid cell loss before clones could be established.

Two sets of primers were designed to assess whether recombination was occurring between the 2nd and 3rd LoxP sites (Figure 4.5A). Unfortunately, PCR products for $Axin1^{Ex3\text{-}10\Delta}$ using either set of primers could not be detected. Due to the lack of a positive control, it was impossible to ascertain whether there was no recombination between the 2nd and 3rd LoxP site or that the PCR did not work.

Primers used to identify the Axin1 3rd LoxP site targeted sequences within the homologue arms used as part of the targeting construct template. It is therefore possible the detection of the 3rd LoxP site was occurring away from Axin1 due to the template being incorrectly integrated. Primers were designed that would reach outside the right homologue arm to ensure that the site being amplified was the Axin1 allele. Due to a number of Pst1 restriction sites within the PCR product making correct identification difficult, a second PCR was performed on the long PCR product. This now shorter PCR product could be digested with Pst1 to confirm whether the LoxP site was inserted in the correct position (Figure 4.5B). 8 clones that were initially identified as having a 3rd LoxP site in Axin1 were used for the nested PCR. None of the 8 clones tested were found to have the LoxP insertion at the correct site of Axin1 as determined by this method. These results are likely to be clone dependent as recombined $Axin1^{Ex2\text{-}10}$ PCR product was detected using primers that bind outside the targeting template in recombined 9F2 1-2-1 clones.

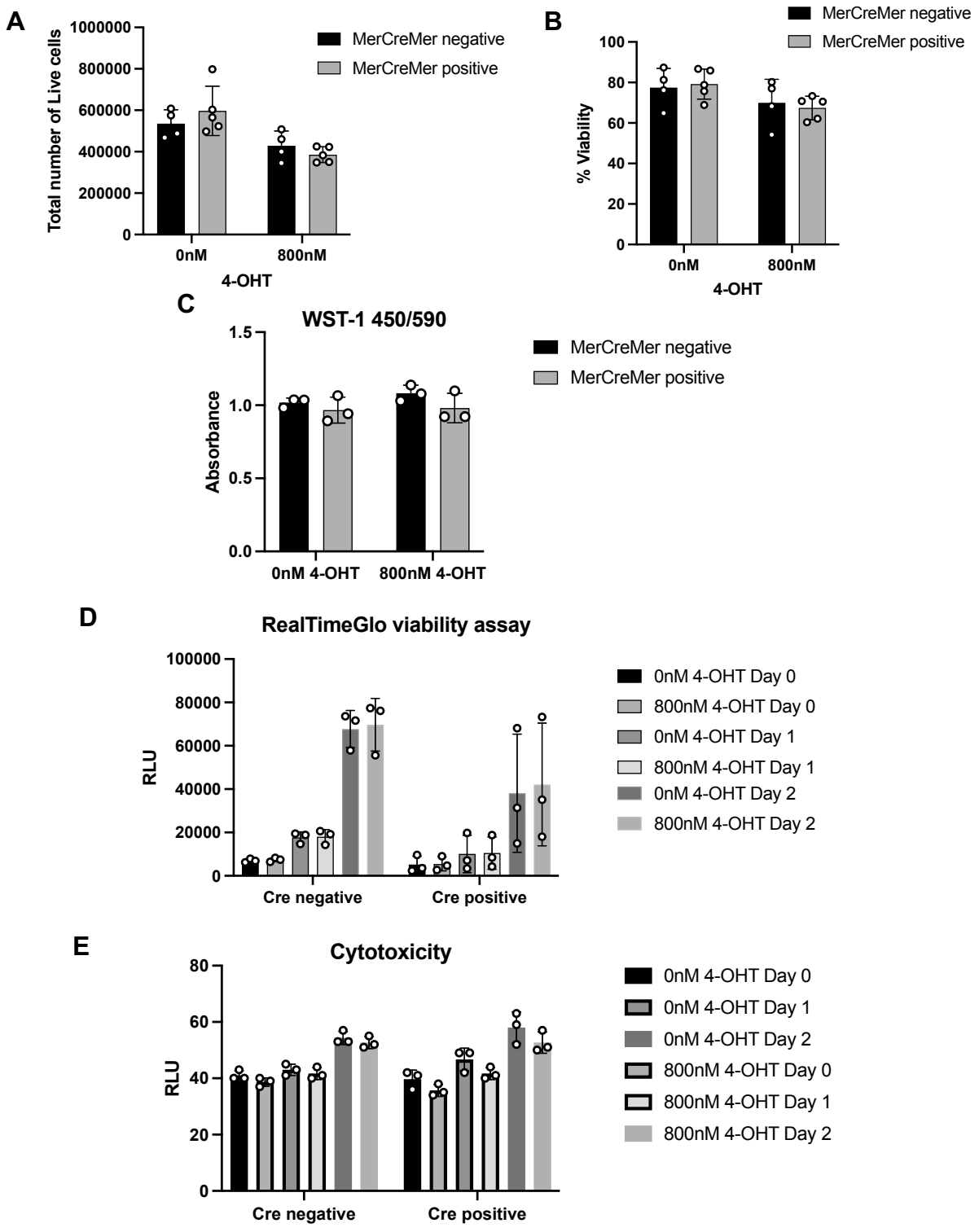

Figure 4.4 No change in Axin1 deleted ES cell viability using Mer-Cre-Mer induction
(A) 5 clones positive for Cre and 4 negative for Cre were dissociated and 60,000 cells/ well per ES cell clone were plated and treated for 48 hours with 0nM or 800nM of 4-OHT. Total cell counts 48 hours after treatment. **(B)** Percentage of viable cells after 48 hours treatment. Cell counts and viability were carried out using Acridine Orange/Propidium Iodide stain and automatically counted using Luna™ *fl* Dual Fluorescence Cell Counter with PhotonSlide™ Ultra-low Fluorescence Counting Slides. **(C)** 48 hours after induction with 0nM 4-OHT (control) or 800nM 4-OHT, Wst-1 reagent was added, and absorption was measured at 450 and 590 nm. n = 3 in triplicate **(D, E)** RealTimeGlo viability and cytotoxicity assay measuring live and dead cells at plating, 24 hours and at 48 hours. n = 3 in triplicate

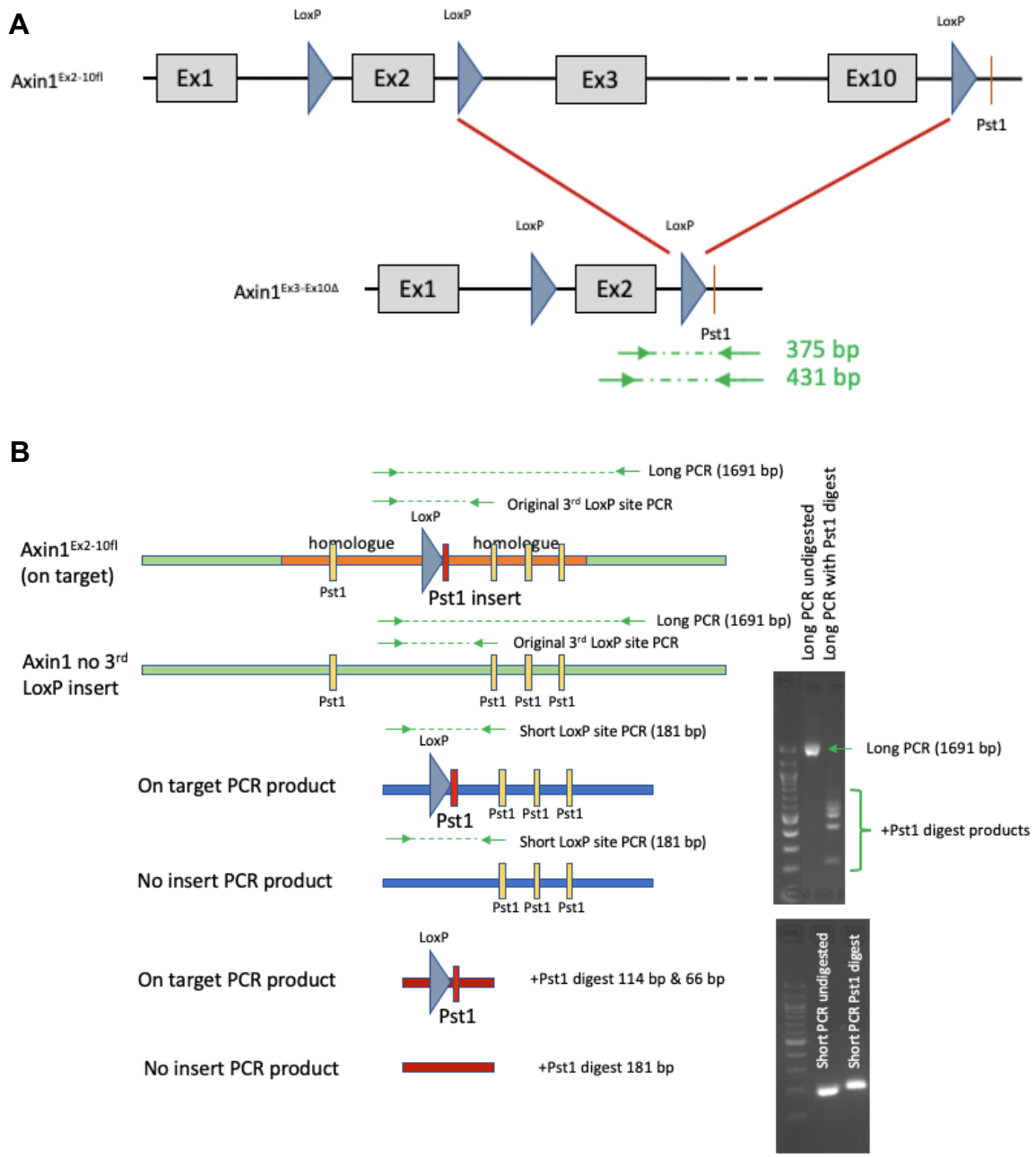

Figure 4.5 Alternate floxing and nested PCR

(A) Two sets of primers were designed to check recombination between the 2nd and 3rd LoxP site that would delete exons 3 to 10. A positive result was not able to be generated. **(B)** PCR primers were designed that would amplify a product that was outside of the right homologue arm – long PCR (1691 bp). Due to multiple Pst1 restriction sites being in the long PCR and digested PCR products being of similar size, a second PCR was performed that amplified only the area that should contain the LoxP site with the inserted Pst1 site. A Pst1 digest of this short PCR product (181 bp) would digest to 114 bp and 66 bp only if the LoxP site was on the Axin1 allele. No digest of the short PCR was seen from the 8 clones tested.

4.1.4 Discussion

From the results it appeared that insertion of the 3rd LoxP site to both alleles of Axin2 was successful and that full Axin2 nulls could be generated after transient CAGGS-Cre induction, pending sequencing confirmation. Comparing future functional assay results between $Axin2^{Ex2\text{-}10\Delta}$ and results obtained by Anika Offergeld using $Axin2^{Ex2\Delta}$ and $Axin2^{LacZ}$ ES cells will help determine if either of the latter alleles are also null. By contrast, generation of full Axin1 nulls was not successful. This may have been due to off target integration of the LoxP site or that full loss of Axin1 is not viable. Assays to assess whether complete loss of Axin1 was lethal were inconclusive in the clones tested using an alternative induction method. For double Axin1 and Axin2 deletion the alleles that could be generated were $Axin1^{Ex2\Delta/Ex2\text{-}10\Delta}$, $Axin2^{Ex2\Delta/Ex2\text{-}10\Delta}$ (heterozygous deletion of exon 2 and exons 2-10 for both Axin1 and Axin2). The success in getting at least one Axin1 allele fully deleted shows that the approach can work but may need refinement.

Genome engineering using CRISPR/Cas9 has been hailed as a revolution for creating genetically modified organisms and cell lines. However, reports of 50% or more of off target activity are a major concern (Zhang et al. 2015). To limit off target effects, this study used an approach that nicks the genome with pairs of guide RNAs combined with a Cas9 nickase mutant that reduces off target activity by 50-1000 fold (Ran et al. 2013). However, even with this method, off target activity was seen.

Efficiency of CRISPR/Cas9 and HDR using a template is cell type dependent. In the study by (Zhang et al. 2017) HEK293 HDR mCherry insertion had an efficiency of around 25% whereas, iPSCs CTNNB1 locus editing showed an efficiency of only around 12%. HDR gene manipulation also varies depending on target gene and among laboratories (Oji et al. 2016) therefore, the failure of generating a full Axin1 knockout could be down to technical competence. This was mitigated as much as possible through repeated attempts and using varying constructs of the pairs of guide RNAs.

The region of Axin1 that was targeted is relatively highly conserved and is close to another gene Pdia2, going in the opposite direction, any disruption to this area could have been lethal to the cells. There could also have been some sort of selection going on against the double alleles being generated. An updated version of the Cas9n vector used in this study is now available, as the previous version was found to have a mutation in the puromycin resistance selectable marker. Options are available to obtain

a custom-made targeting construct containing the LoxP site rather than generating these in house. Picking a new site for the insertion of the 3rd LoxP site in Axin1, away from the conserved area and Pdia2 may generate greater success. Using ES cells already flanking exon 2 with LoxP sites should not have affected the generation of full nulls and was meant to save time by only having to insert one LoxP site. Future attempts may be better off using unmodified ES cells.

Despite multiple attempts at obtaining ES cell clones with definitive deletion of all Axin1 and Axin2 alleles, the approaches taken were ultimately unsuccessful and a decision was taken to analyse liver organoids as they would be a useful tool and give relevance to the study of liver biology.

Chapter 5: Utilising organoids to study Axin function

5.1 Introduction

Organoids have made it possible to partially recapitulate the complexity and function of mammalian tissues *in vitro* by producing structures in culture that resemble an adult organ. Deletion of Axin *in vivo* has provided details of the long-term impact of disruption to the Wnt/β-catenin pathway but important changes to underlying tumour development may happen very rapidly after gene deletion followed by cellular adaptation. Use of *in vivo* gene deletion is not particularly practical to ascertain this early biology. Conversely, *in vitro* gene deletion provides the advantage of being able to directly follow various parameters, including morphology and proliferation over a time course as these changes occur. Furthermore, organoids offer rapid and controlled experiments, that avoids the complexity of systemic effects and the ethical concerns associated with *in vivo* experiments.

Various *in vitro* liver systems exist such as 2D monolayers, hydrogel sandwich cultures, 3D spheroids, induced pluripotent stem cell (iPSCs) derived hepatocytes and liver organoids. Each has their own advantages and imitations that has already been discussed (see Introduction section 1.6.2). Primary human hepatocytes are traditionally seen as the "gold standard" for hepatic *in* vitro culture in pharmacological and toxicological research as they reflect the metabolism and functionality of the *in vivo* liver. However, acquisition and the long-term culture, maintenance and expansion of definitive hepatocyte cultures that retain functionality has proven to be challenging. Developments in liver organoids have shown promise in being able to recapitulate *in vivo* liver characteristics, however there is currently no consensus on culture conditions.

In the following section, 2 distinct culture systems, and variations thereof, will be compared: primary hepatocyte (PH) organoid conditions and bile duct derived (BD) organoid conditions ((Huch et al. 2013; Hu et al. 2018; Peng et al. 2018) Figure 5.1). Several tissue sources were examined with the goal of identifying systems in which Axin dysregulation could be examined. Both normal and tumour tissues were analysed with the initial goal of identifying conditions that would support the long-term expansion and robust maintenance of liver organoids that could subsequently be used to study Axin function. Tissue sources that have been studied in the following studies include normal human primary hepatocytes, HCC tumours from PDX-bearing mice and liver

tumours from the Axin mutant mice described in Chapter 3. As will be shown, success was limited using PH conditions. However, the more robust BD organoid system allowed Axin loss to be studied in the context of the partial differentiation of BD stem cells towards hepatocyte and biliary fates.

A

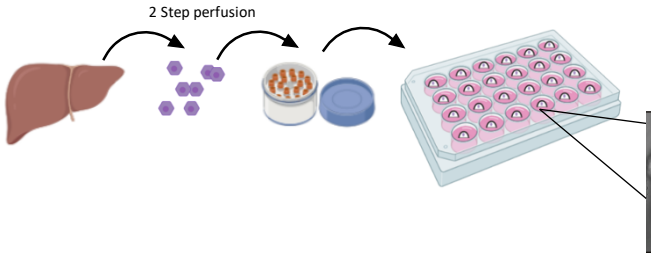

Low plating efficiency

Limited expansion time

B

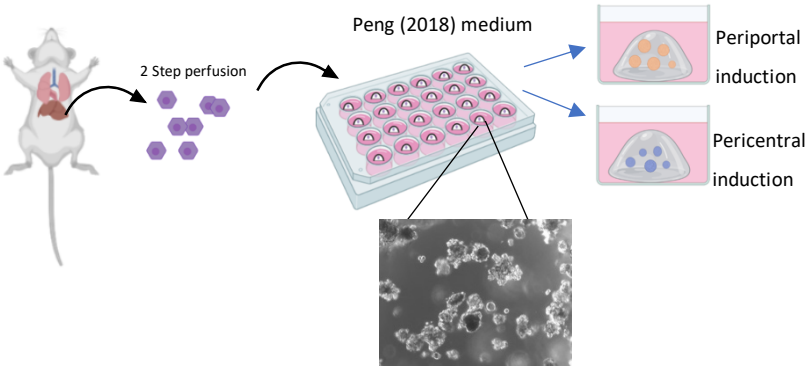

C

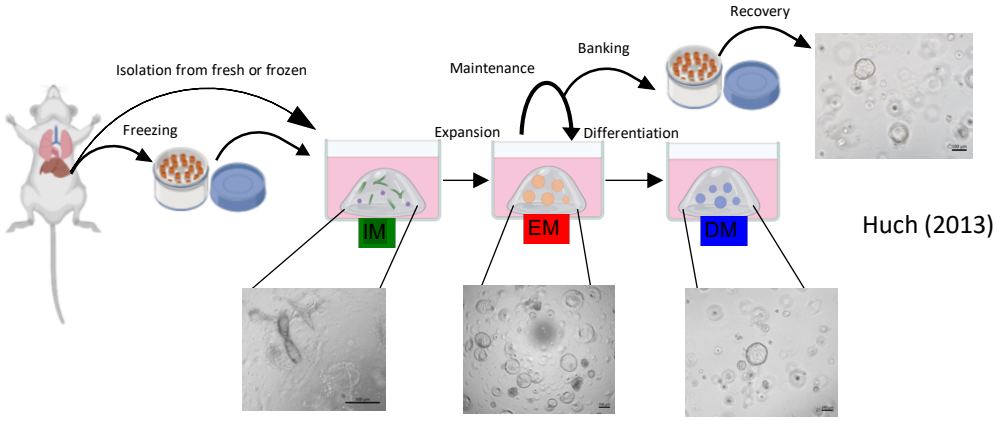

Huch (2013)

D

PH organoid media		BD organoid media		
Hu Media	**Peng Media**	**Isolation Media**	**Expansion Media**	**Differentiation Media**
RSPO1 CHIR	**CHIR TNFa**	**RSPO1 Wnt3a**	**RSPO1**	**DAPT A8301 Dexamethasone**

Figure 5.1 Overview of PH and BD liver organoid system culture conditions.
(A) Human and mouse mature hepatocytes were able to generate hepatocyte derived organoids in the study by Hu (2018). Drawbacks were low plating efficiency and a limited expansion time of 2-3 months. **(B)** Peng et al (2018) were able to use mature mouse hepatocytes obtained using a 2-step perfusion protocol to establish definitive hepatocyte organoids with the addition of TNFα in the media conditions. Eider Valle-Encinas was successful in establishing these organoids in the Dale lab. Unfortunately, using the published recovery protocol or with modifications, these organoids could not be recovered in the Dale lab which limited their practicality. **(C)** Bile-duct organoids using the protocols of Huch (2013) were able to be established from freshly digested liver or from frozen liver fragments. Established organoids are robust enough for genetic manipulation and are easily expanded, banked, and recovered. **(D)** Table outlining key differences between published PH organoid media and components used in BD organoid media. CHIR (99021) is a GSK3 inhibitor, DAPT – Notch signalling inhibitor, A8301 – TGF-β inhibitor.

5.2 Human hepatocyte culture

5.2.1 Assessing various media conditions to establish hepatic organoids from normal human hepatocytes.

In the study by (Hu et al. 2018), organoids established from human hepatocytes had a limited expansion time of between 2 and 2.5 months. Published concurrently, in the study by (Peng et al. 2018), it was shown that TNFα enabled the establishment of the long-term (greater than 6 months) culture of organoid cultures from mouse hepatocytes. To assess whether the combination of factors used by Hu and Peng in the presence of TNFα would allow the growth and expansion of human hepatocyte organoids derived from primary human hepatocytes, cultures were set up using frozen normal human hepatocytes sourced from Lonza with varying media conditions (Figure 5.2A, B). In addition to the Hu and Peng media and their combination, additional refinement of Peng media was also assessed. Namely, to mitigate off-target effects of the GSK3 inhibitor, replacement of CHIR99021 with Wnt9b and Rspo3. Combination of Wnt9b and Rspo3 has been shown to synergize to potently activate the Wnt/β-catenin pathway in mouse hepatocyte organoid cultures in the work by Eider Valle Encinas (2020 PhD Thesis). To identify additional mitogens that might better support primary human liver organoid expansion, a small number of mitogens that are found to be induced following partial hepatectomy (see Introduction section 1.4.1), were screened based on the idea that optimal hepatocyte organoid growth conditions need to recapitulate aspects of hepatocyte proliferation following partial hepatectomy.

Hepatocytes were thawed as per the Lonza protocol using their proprietary reagents and assessed for viability using Acridine Orange/Propidium Iodide stain and the Luna-FL cell counter before seeding in Matrigel. Viability was found to be 77.8% close to the 80% viability expected from the cell lot details. To ensure hepatocytes appeared as expected using Lonza protocols and reagents, cells were also seeded on collagen coated plates with or without a Matrigel overlay. Hepatocytes attached to plates and were comparable to Lonza data at 24 and 72 hours presenting as a confluent monolayer with a cobblestone morphology and distinct nuclei (Appendix IV).

Hepatocytes were seeded at 3 different concentrations of 200, 400 and 800 cells per μl of Matrigel in 50 μl domes. Once set, 500 μl of the varying media was added and replaced every 2 to 3 days (Figure 5.2A). Media 1 was based on the Human-Hep medium used in the study by Hu (2018) with the 15 % RSPO1 conditioned medium

(home-made) being replaced with 300 ng/ml of recombinant Human R-Spondin-1 allowing for a defined medium without the presence of any FBS. Media 2 was based on the Expansion medium used in the study by Peng (2018). This would allow direct comparison of two published PH organoid media conditions using the same source of cells. Media 3 was a combination of the Hu and Peng medium, in particular the key components; Rspo1, CHIR and TNFα. Media 4 was based on the Peng medium (Media 2) but replaced CHIR99021 with recombinant Wnt9b and RSPO3 and Media 5 additionally contained Shh, IL6, HB-EGF and Serotonin (Figure 5.2B) in order to assess if the published conditions could be refined.

At the time of seeding, hepatocytes seeded in Matrigel were mostly single cell with some clumps of 2-5 cells. Formation of organoids was initially only visually assessed for up to 20 days. Unfortunately, no clear growth or expansion was observed in any of the seeding densities or culture mediums used (Figure 5.2C). By day 20, the Matrigel integrity had deteriorated, and it was decided to passage the cells and seed in fresh Matrigel. A fraction of these cells was also seeded for a CellTiter-Glo 3D assay to assess cell viability by measuring ATP levels. By day 2 after the passage, cystic structures resembling bile duct organoids began to appear in Media 1. By day 7 after the passage large numbers of cystic structures were obvious in Media 1 with a few also present in Media 4 (Figure 5.3A). Counts of cystic structures showed an average of almost 60 per well in Media 1 and 2.25 in Media 4. No cystic structures were present in Media conditions 2, 3, and 5 (Figure 5.3B). CellTiter-Glo 3D correlated with the number of cystic structures counted (Figure 5.3C). No ATP levels were detected in the cultures using Media 2, 3, and 5 suggesting that the cells in these were dead.

Transdifferentiation of mature rat hepatocytes to biliary epithelial cells in culture in the presence of EGF and HGF has been reported previously (Limaye et al. 2008) however it is not possible to exclude the possibility of biliary cell contamination in the Lonza supplied hepatocytes that were used. To rule out possible contamination, staining with hepatocyte and biliary markers and sorting could be carried out before seeding. Despite reported success of establishing PH organoids from Lonza hepatocytes in the study by (Hu et al. 2018), growth of hepatic organoids appeared to be unsuccessful under conditions tested here. This may be down to variation in lots of hepatocytes used or the replacement of RSPO1 conditioned media with recombinant RSPO1.

A

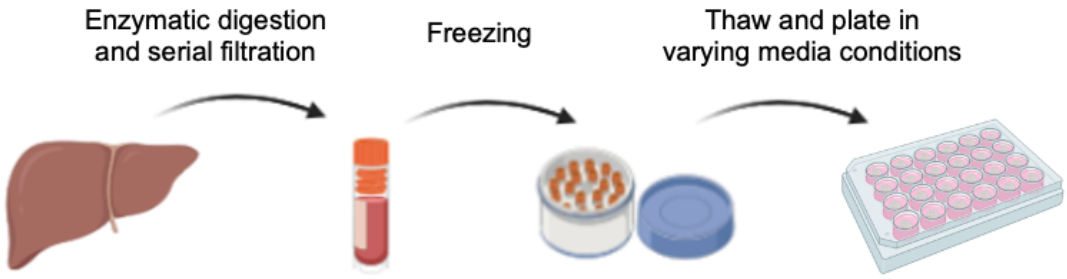

B

Media 1 (Hu)	Media 2 (Peng)	Media 3 (Peng+Hu)	Media 4 (Peng-CHIR++)	Media 5 (Peng-CHIR +6)
RSPO1 CHIR	CHIR TNFa	RSPO1 CHIR TNFa	TNFa Wnt9b RSPO3	TNFa Wnt9b RSPO3 Shh, IL6, HB-EGF, Serotonin

C

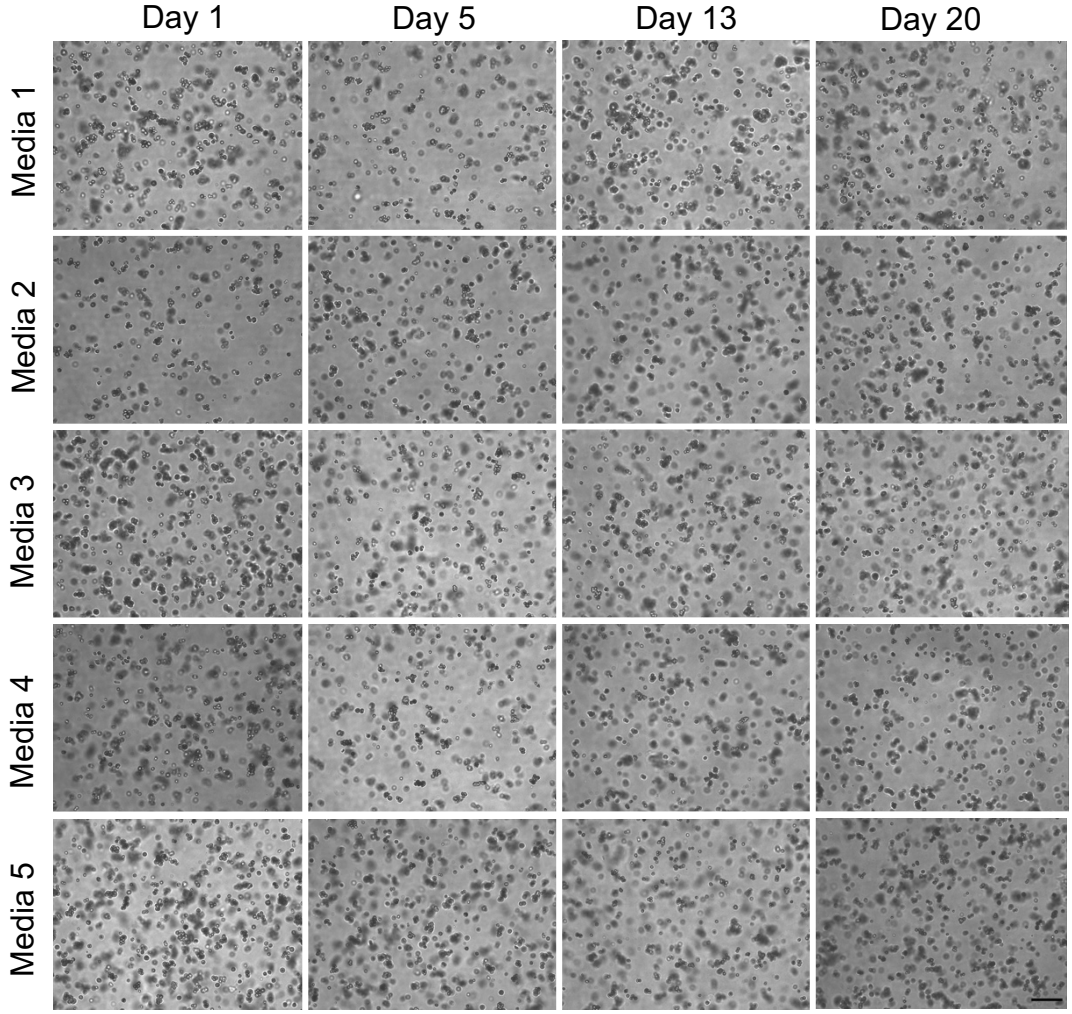

Figure 5.2 Human normal hepatocyte culture did not form hepatic organoids.
(A) Schematic of frozen hepatocytes sourced from Lonza and seeding in Matrigel **(B)** Table outlining the key different components of media contents to be tested. Full details of components and concentrations provided in Chapter 2 **(C)** Representative images of hepatocytes seeded at 400 cells/μl in Matrigel from day 1 to day 20 in the 5 varying media conditions. Scale bar 200 μm

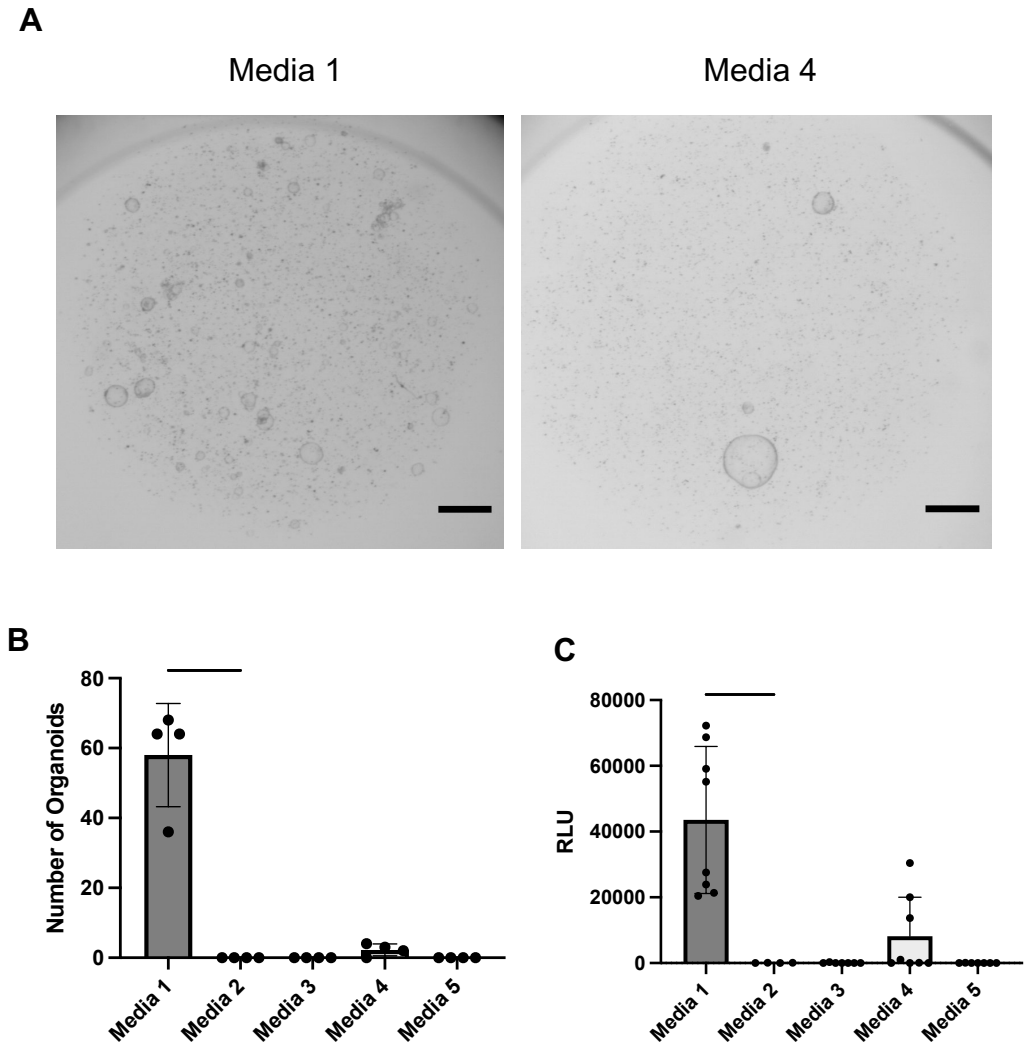

Figure 5.3 Select media conditions allow cystic organoid formation from normal human hepatocytes.
(A) Representative images of organoids formed after the first passage at day 7 in media conditions 1 and 4. Scale bar 1000 μm. **(B)** Counts of organoids after first passage at day 14 in media conditions 1 to 5 from an average of 4 wells **(C)** CellTitre-Glo 3D assay results measuring relative ATP levels per well at day 7 after first passage (Relative Luminescence Units, n=8 technical replicates)

5.3 HCC patient derived xenograft culture.

5.3.1 Establishing PDX derived tumour organoids.

In the study by (Broutier et al. 2017) tumour organoid cultures were able to be established from three of the most common primary liver cancers, hepatocellular carcinoma (HCC), cholangiocarcinoma (CC) and combined HCC/CC (CHC) tumours using components that were similar to those described for BD organoid culture, Wnt3a and Rspo1. Of note, (Broutier et al. 2017) were only able to establish organoid cultures from poorly to moderately well differentiated tumours and not from well differentiated tumours, suggesting culture conditions could be improved. In the studies described below, protocols based on those published in (Broutier et al. 2017) were used to determine whether human liver tumour derived cancer organoids could be established from PDX material using BD conditions. Additionally, PH organoid culture conditions would be used to directly compare efficiency of growth and the preservation of the original histological character and gene expression of the original PDX material between BD and PH and between PH culture conditions. Access to primary HCC material was available through collaboration with Champions Oncology and HCC PDX material was used to establish PDX derived tumour organoids (Figure 5.4A). The conditions tested here should allow future studies to be implemented with PDX tumours that have Axin1 mutations and from tumours that developed from Axin mutant mice.

A total of 4 separate HCC PDX lines with varying mutations and differentiation status, implanted at 3 timepoints, allowing for multiple attempts to establish cultures were planned to be used for establishing PDX derived cancer organoids. Unfortunately, only 1 sample (lot info supplied in Appendix) was able to be shipped fresh due to the timing of the implantations that were scheduled, success rate of implantations and the logistical and cost-based difficulties of international shipping presented by lockdowns during the first year of the covid-19 pandemic. Attempts were made using frozen material however this was met with limited success and not enough material could be generated for analysis (data not shown).

Upon delivery, PDX material was divided, and part was fixed for immunohistochemical staining, part snap frozen for DNA/RNA extraction and part used for establishing organoids. Dissociation of PDX tumour was carried out following the

protocol in the study by (Broutier et al. 2017), full details in Chapter 2. PDX tumour was dissociated to single cell with some clumps of 2-5 cells remaining. The viability of cells was found to be approximately 50% before seeding (data not shown), possibly due to the delay experienced in shipment. Cells were initially seeded at high density of approximately 1000 cells/fragments per μl of Matrigel. After setting, Hu, Peng, Peng-CHIR++, Broutier tumour and Broutier normal mediums (Figure 5.4B) were used to overlay the Matrigel and replaced every 2-3 days. As in the study by (Broutier et al. 2017), two isolation mediums were used to establish 'tumouroid' cultures, one termed normal, containing Rspo1 and Wnt3a conditioned media, and a tumour isolation medium without Wnt pathway activating factors but supplemented with Dexamethasone, that was used to reduce expansion of non-tumoural contaminating tissue that appeared as cystic BD organoids. After the first passage, cultures from both tumour and normal isolation mediums were transferred to Broutier expansion medium. Organoids grown in Hu, Peng and Peng-CHIR++ media were maintained in their respective media conditions throughout in this study. Growth was monitored visually, for the initial 14 days (Figure 5.5). During this time, access to the lab was restricted and limited to the expansion and banking of novel lines.

Most notably, cells grown in Hu medium showed the greatest increase in growth as seen by size and density increase from day 1 to day 14. Cells grown in Broutier tumour media showed the second highest increase, and cells grown in Broutier normal media showed the third highest levels of growth as judged by size and density. Organoid formation occurred in Peng and Peng-CHIR++ media but was limited and not visible from images obtained using the Gel Count. As the starting material for these organoids was PDX derived and not patient biopsies that may contain normal cells, cyst like hollow structures indicative of healthy liver derived BD organoids (Broutier et al. 2017) were not present in any of the medium conditions. Interestingly, despite the addition of Wnt/β-catenin pathway activating ligands Rspo1 and Wnt3a in the Broutier Normal media (that would be expected to drive proliferation), reduced levels of growth were seen when compared to Broutier Tumour media. This may possibly be due to too much Wnt pathway activation as hypothesised by the just-right Wnt levels in (Albuquerque et al. 2002) as the PDX line used also has a CTNNB1 p.S33F gain of function mutation.

A

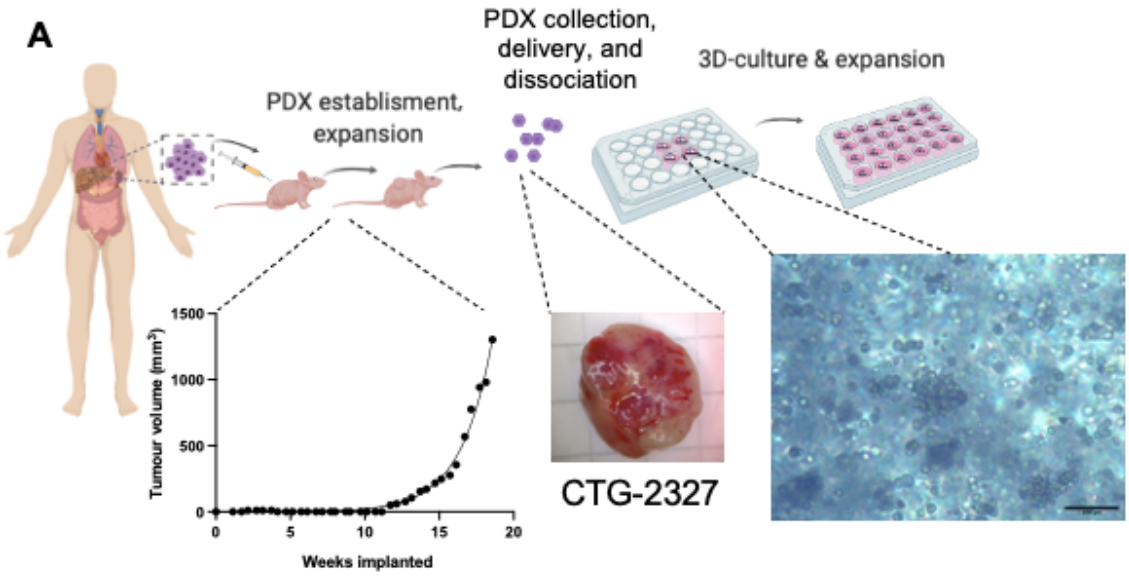

B

Hu Media	Peng Media	Peng -CHIR++ Media	Broutier Tumour Isolation Media	Broutier Normal Isolation Media	Broutier Expansion Media
RSPO1 CHIR	CHIR TNFa	TNFα Wnt9b RSPO3	No Wnt pathway activation	RSPO1 Wnt3a	RSPO1

Figure 5.4 Establishing PDX derived organoids using various culture conditions. **(A)** Schematic showing the establishment of PDX derived organoids from patient sample and seeding of PDX material in culture. The graph shows the timescale and the actual growth rate of the implanted PDX line that was able to be delivered fresh. Image of PDX tumour that was delivered. Part was fixed for immunohistochemistry, part frozen for DNA and RNA extraction and part used for establishing organoid cultures. Image of dissociated PDX seeded in Matrigel at initial seeding. Scale bar 100 μm. **(B)** Table displaying the key components of the media conditions used. Hu, Peng and Peng-CHIR++ are PH conditions. Broutier tumour and normal are based BD conditions. After first passage, organoids in Broutier tumour and normal isolation media were switched to Broutier expansion media.

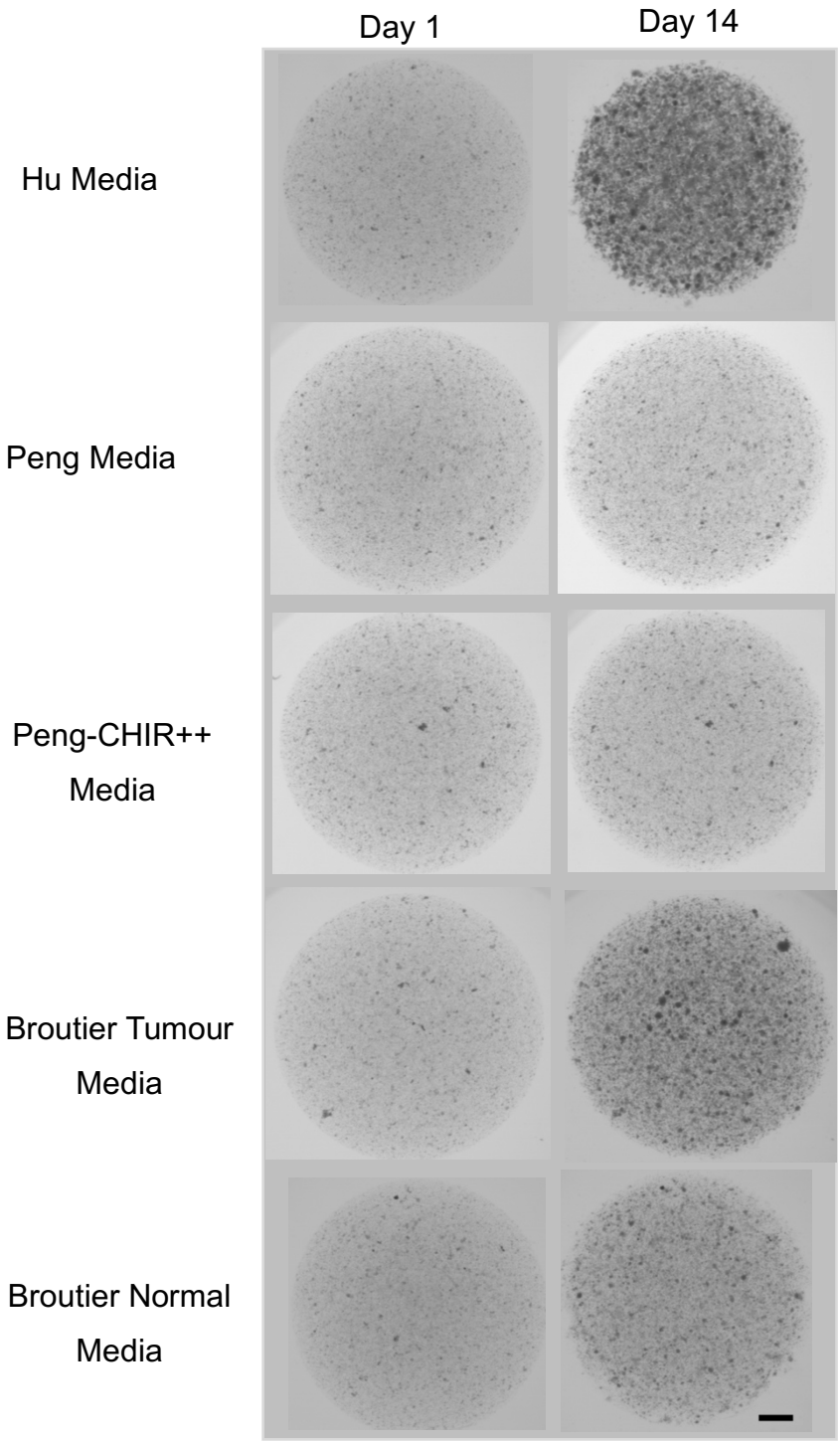

Figure 5.5 PDX organoid expansion from initial seeding in various culture mediums.
Representative images of whole wells from freshly isolated PDX material at day 1 and day 14. Scale bar 1000 μm

5.3.2 Maintenance and expansion of PDX derived organoids.

After the first passage, cultures in Broutier Normal and Broutier Tumour media were transferred to Broutier Expansion media for subsequent maintenance and expansion. Organoids from all culture conditions were dissociated to single cell with TrypLE and seeded at 500 cells per μl of Matrigel. Media was refreshed every 2 to 3 days and passaged when confluent or when Matrigel integrity had deteriorated.

Organoids grown in Hu media were continuously split at a ratio of between 1:3-1:4 every 7-10 days and continued to be passaged for a total of 14 passages totaling 4 months in culture before being stopped due to reasons explained in section 5.3.3. Early passage organoids appeared to have a solid morphology with a tightly packed bunch of grapes appearance (Figure 5.6A). As previous attempts in the Dale lab to grow PDX derived organoids resulted in mouse fibroblasts outcompeting growth of tumour material, a mouse cell depletion cell was carried out at passage 3 and later at passage 8. This did not appear to affect the growth rate of the organoids (Figure 5.7).

Organoids grown in both Peng and Peng-CHIR++ were both condensed at a ratio of 1:0.5 at the first passage. At early passage organoids in both Peng media had a similar appearance to those grown in Hu Media (Figure 5.6A). After the first passage, Peng-CHIR++ organoids were passaged at a ratio of 1:1 or less. As organoids in the media could not be expanded and began to decrease in number, it was decided to fix and embed, and carry out RNA extraction on the remaining organoids (Figure 5.6B). Organoids could be expanded in the Peng media at a ratio of 1:1.5. When sufficiently expanded, at passage 5, organoids were put through mouse cell depletion. Unfortunately, recovery of cells was insufficient to carry on with the culture (Figure 5.6B). It was unclear whether this was due to technical error or severe contamination of mouse cells in the culture.

At first passage, organoids originally grown in Broutier tumour and normal media were split at a ratio of around 1:1.8. At early passage, organoids from the two different Broutier isolation media had a solid 3D morphology, though were more spherical when compared to those grown in Hu or the Peng medias (Figure 5.6A). In Broutier expansion media, subsequent passages required condensing splits of the remaining organoids at a ratio of 1:0.5. As the organoids could not be expanded, at passage 4, remaining organoids were either fixed and embedded or used for RNA extraction.

Organoids grown in Hu media had the most robust growth and appeared to be unaffected by mouse cell depletion. Future attempts with PDX material and the Peng media may have better success if mouse cell depletion is carried out before initial seeding. Details of the PDX line used described the tumour as poorly differentiated and thus should have grown according to (Broutier et al. 2017). This study used recombinant Rspo1 rather than Rspo1 condition media and may account for the difference seen. Future attempts could use a titration of Rspo1 to establish the right levels required.

A

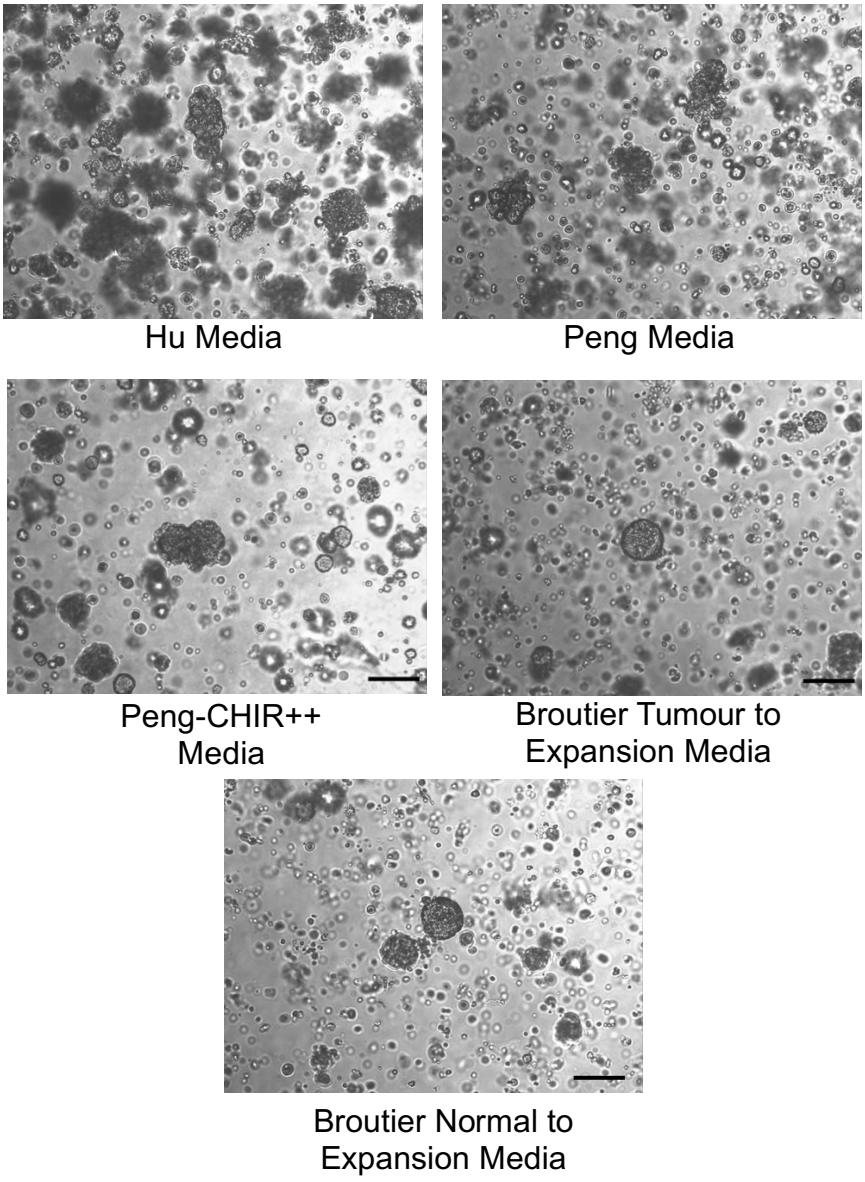

B

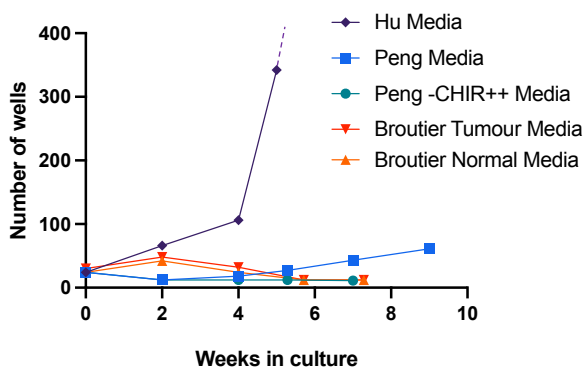

Figure 5.6 PDX derived organoid line showed varied expansion rates in various culture conditions.

(A) Representative images of PDX organoids at early passage in various media conditions (P.3 to 4). Scale bar 200 µm **(B)** Extrapolation of the expansion of PDX from ratio of the number of wells passaged and frozen. Each point marks a passage. Organoids in Hu Media continued to be expanded.

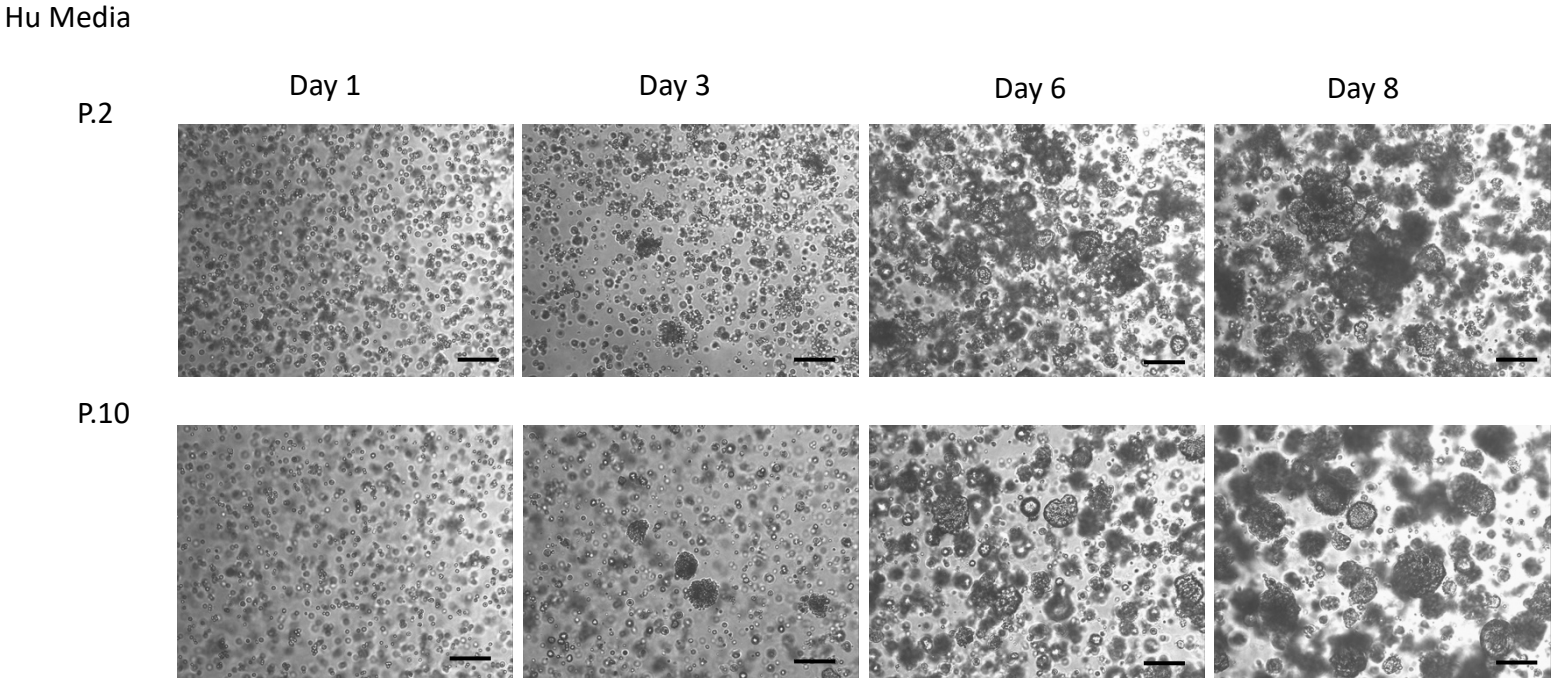

Figure 5.7 Expansion of PDX derived organoids in Hu media at early and later passage was comparable.
Representative images of organoids grown in Hu media at passage 2 before mouse cell depletion and at passage 10 after mouse cell depletion was carried out showed comparable expansion rates. Scale bar 200 μm

5.3.3 Organoids in Hu medium lose histological and gene expression features of original PDX over time.

For PDX derived organoids to serve as a useful *in vitro* model they need to faithfully retain and recapitulate the pathophysiology of the original tumour. Organoids from early and later passages were fixed and embedded in paraffin and stained for H&E, and RT-qPCR assays were carried out to compare structure and gene expression to the original PDX material. Unfortunately, due to failures in expansion and limited material from some culture conditions, comparisons could not be made between all mediums used.

Organoids grown in Hu Media retained the compacted morphology seen in the PDX at both passage 4 and passage 10 (Figure 5.8A). However, organoids at passage 10 appeared to have a less complex structure compared to organoids at passage 4. Expression of the hepatic marker HNF4α was elevated at passage 1 compared to the PDX. However, at passage 10 expression of HNF4α was near zero. Expression of hepatocyte markers SERPINA1 and GLUL were reduced by one third at passage 1 compared to PDX, and near nonexistent at passage 10. KRT18 expression initially increased at passage 1 but returned to the levels seen in the PDX at passage 10. AFP expression was reduced in comparison to PDX at passage 1 and found to be almost absent at passage 10. Expression of the biliary marker initially decreased at passage 1 but at passage 10, levels were higher than found in the PDX (Figure 5.8B).

These results suggest that organoids derived from PDX material quickly begin to lose expression of hepatic cell markers and that by passage 10, expression of some of these markers is lost. By contrast, expression of the biliary marker KRT19 increased, suggesting the organoids transition towards a biliary cell like state when cultured in Hu media. This may not be the case for all PDX lines and will need to be confirmed with subsequent trials with the same line.

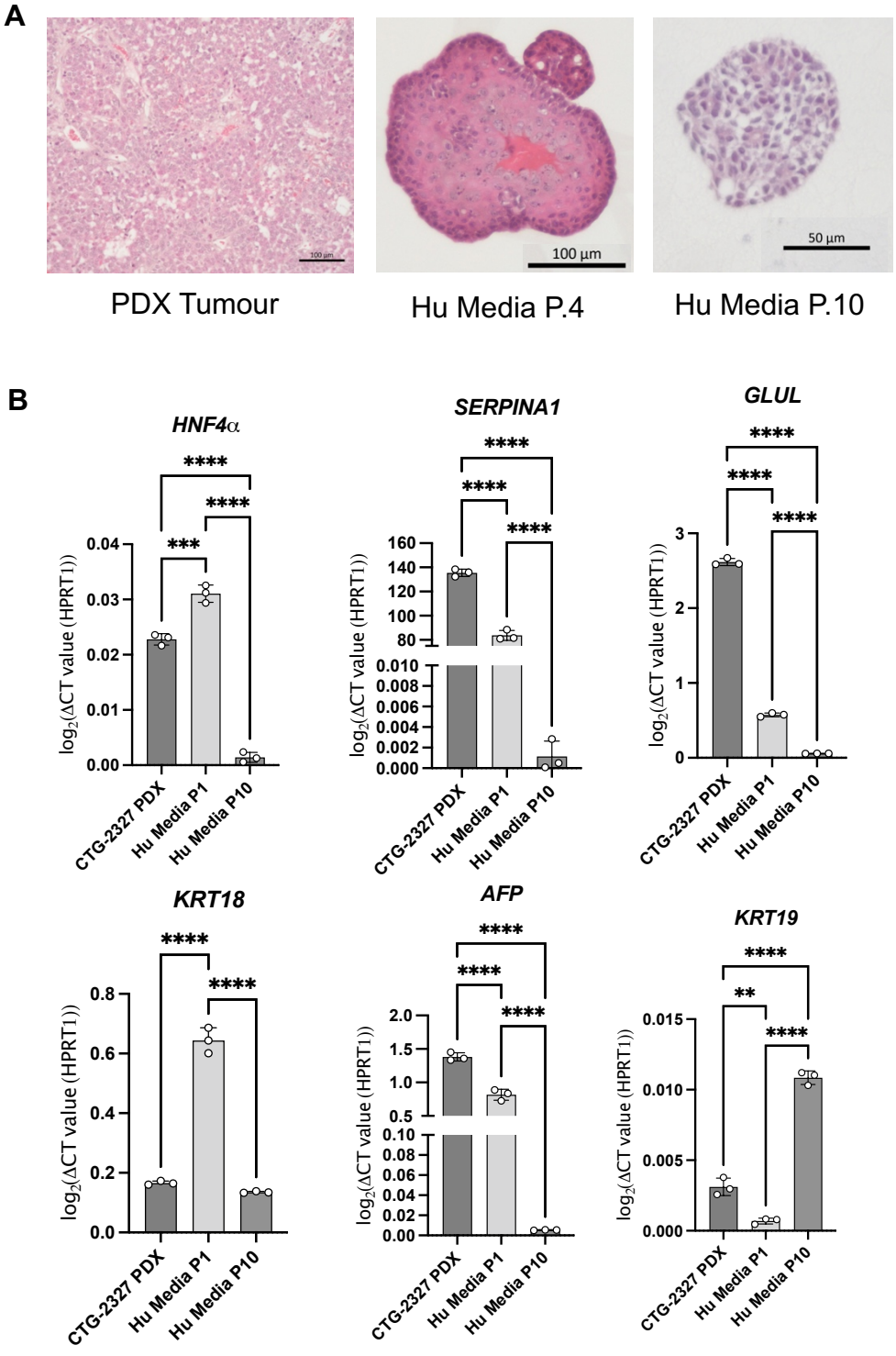

Figure 5.8 Characterisation of PDX derived organoids grown in Hu Media.
(A) Images of H&E stained sections of original PDX material used for establishing organoid cultures, and early and late organoids grown in Hu media fixed at day 10 of passage 4 and passage 10. **(B)** RT-qPCR of liver cell markers. n = 3 technical replicates. Significance was calculated using Ordinary One-Way ANOVA with Tukey's multiple comparison test **P<0.01 ***P<0.001 ****P<0.0001.

5.4 Mouse liver organoid culture

5.4.1 Using frozen liver tumour fragments to establish hepatic tumour organoids.

PH organoids established using two-step perfusion of fresh mouse liver and media conditions outlined in (Peng et al. 2018) had previously been prepared and frozen by Eider Valle-Encinas (Figure 5.1A). Unfortunately, recovery of these organoids from the frozen lines into PH culture conditions was unsuccessful (data not shown). Though recovery of mouse PH organoids proved to be unsuccessful it was hypothesized that tumour cells might have a growth and survival advantage and that it might nonetheless have been possible to establish organoids from frozen liver fragments. Using PH organoid media outlined in section 5.2.1 and Figure 5.2B, and frozen fragments of an AhCreER^{T}, Axin1$^{\Delta/\Delta}$, Axin2$^{\Delta/\Delta}$ liver tumour, cultures were set up to ascertain whether tumour organoids could be established.

Dissociated fragments of mouse liver tumour embedded in Matrigel had no perceptible growth after 17 days in culture in any media tested (Figure 5.9A, B). After the first passage, cystic single-layered organoids indicative of bile-duct derived organoids began to appear (Figure 5.9C). Cultures were continued for a few more weeks but only cystic organoids were found to grow.

In summary, the culture conditions for definitive PH organoid culture of normal or tumour hepatocyte-derived cells is still in its early stages and culture conditions will likely require further refinement. The *in vivo* biology that has been characterised in Chapter 3 suggests that the immediate effects of Axin deletion in the liver were likely to be in hepatocytes. Generation of PH organoids from the various floxed Axin lines would have been the better system to examine the immediate early phenotype of Axin loss since they better recapitulate hepatocyte biology. However, because the conditions for reproducible expansion, maintenance and recovery could not be achieved for the studies that are required to investigate Axin loss *in vitro*, establishment of PH organoids wasn't possible at this time.

By contrast, bile duct derived organoids are easily established from fresh mouse liver and from frozen liver fragments (Figure 5.1C) using the protocols published in (Huch et al. 2013). Expansion, banking, and recovery of these organoids was achieved without difficulty and thus provides a more robust model with which to work. Upon differentiation, biliary derived organoids do express hepatocyte markers and

development of HCC may include cells that are partially differentiated meaning that BD organoids and HCC initiating cells may share phenotypic characteristics making them a great model for the study of development of HCC. Using biliary derived organoids from mice that carry floxed Axin alleles will thus provide a great tool and relevant insight into the signal transduction events that occur following Axin deletion and the role Axin plays in differentiation in a liver model context.

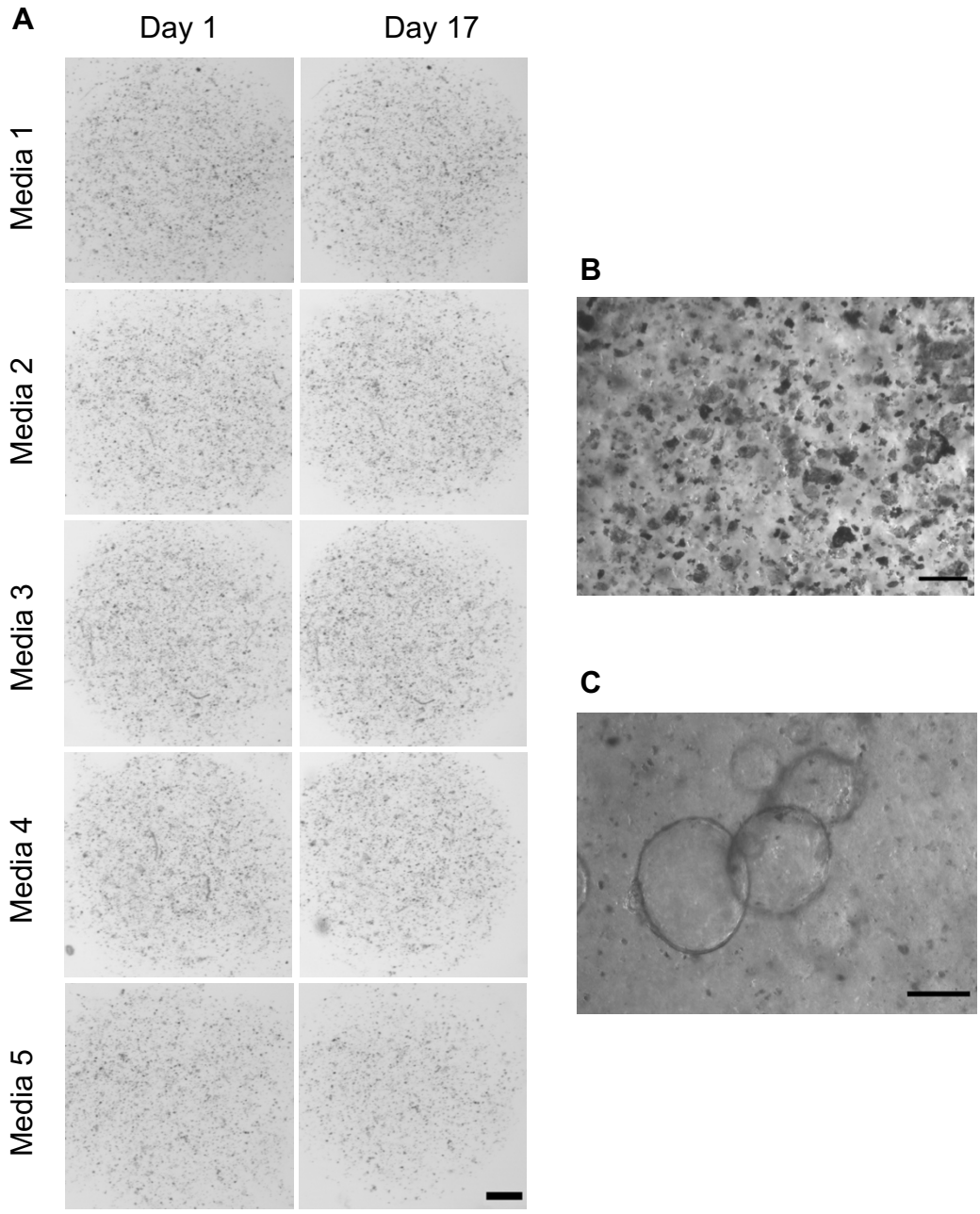

Figure 5.9 Frozen liver fragments failed to give rise to hepatic organoids.
(A) Whole well images of seeded liver fragments show no growth after 17 days in culture using 5 different media conditions. Scale bar 1000 µm. **(B)** Representative image of seeded liver fragments. Scale bar 200 µm. **(C)** Bile duct organoids were seen clearly after the first passage in Media 2 at day 7. Scale bar 200 µm

5.5 BD organoid system.

Mouse BD organoids were first established in the Clever's laboratory by Meritxel Huch in 2013 (Huch et al. 2013) using Lgr5+ cells derived from the liver's biliary epithelium using an Rspo1 containing medium. The organoids formed were cystic and hollow in shape and could be differentiated towards a hepatocyte like fate by switching from expansion media to a differentiation media. Differentiation media removed the Wnt signalling potentiator Rspo1 and inhibited TGFβ and Notch signalling. In expansion media, *Lgr5* expression was maintained at similar levels to intrahepatic bile-ducts after injury. In differentiation conditions expression of the Wnt transcriptional target *Lgr5* was lost and gene expression of *Tbx3*, essential for liver maturation, and hepatic markers such as Albumin and Fah increased (Huch et al. 2013) (Figure 5.10A).

To confirm the system worked as expected, control BD organoids were differentiated using the conditions based on the protocol published by Huch et al. (Figure 5.10B). Organoids were grown in Expansion media (EM) alongside those in Differentiation media (DM). RT-qPCR using a panel of liver progenitor, lineage and mature hepatocyte markers that included markers used by Huch et al., was carried out to confirm expected changes in expression of organoids in DM.

As in the study by Huch et al., *Lgr5* expression was lost in differentiation conditions (Figure 5.11A). Expression of hepatic progenitor marker *Spp1* was also reduced by half. *Spp1* or *Osteopontin* (OPN) is also a Notch target, so this was to be expected. However, other hepatic progenitor markers; *EpCam, Trop2* and *Sox9* were not significantly altered. Biliary epithelial cell markers *Hnf1b, Krt19* and *Krt7* were found to be increased to varying degrees between samples (Figure 5.11B). Though somewhat surprising, this has previously been observed by Valle-Encinas (2020 PhD Thesis). As expected, *Tbx3* was found to be elevated though this was variable between samples and not significant. Further hepatocyte lineage markers *Hnf4α*, *Prox1*, and *Afp* showed a trend for an increase, but again, responses were variable between samples (Figure 5.11C). As expected from the study by Huch et al., expression of the mature hepatocyte markers *Fah* and *Albumin* were found to be increased (Figure 5.11D). *Ass1* expression was also elevated but extremely variable.

These results suggest that the bile-duct organoids that have been grown in differentiation conditions replicate observations seen in the study by (Huch et al. 2013), such as the loss of *Lgr5* expression and the increase in the expression of mature

hepatocyte markers *Albumin* and *Fah*. Notably however, responses in gene expression after differentiation were variable between samples and expression of biliary epithelial cell markers increased.

The following section will focus on the establishment and utilization of bile duct derived organoids using these expansion and differentiation conditions in the context of Axin loss.

A

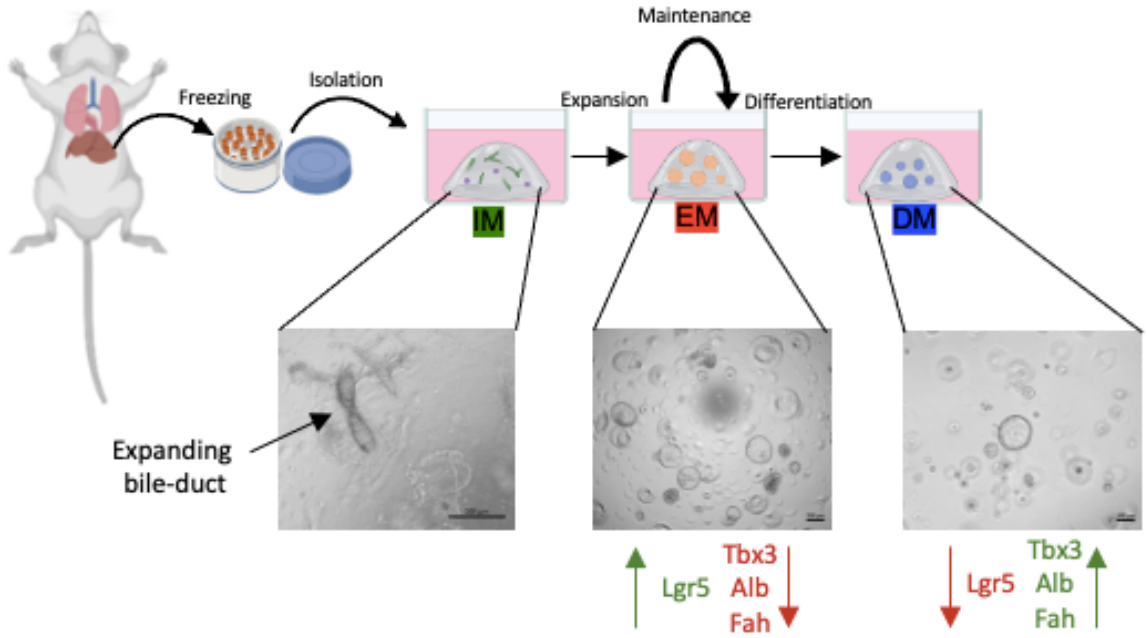

B

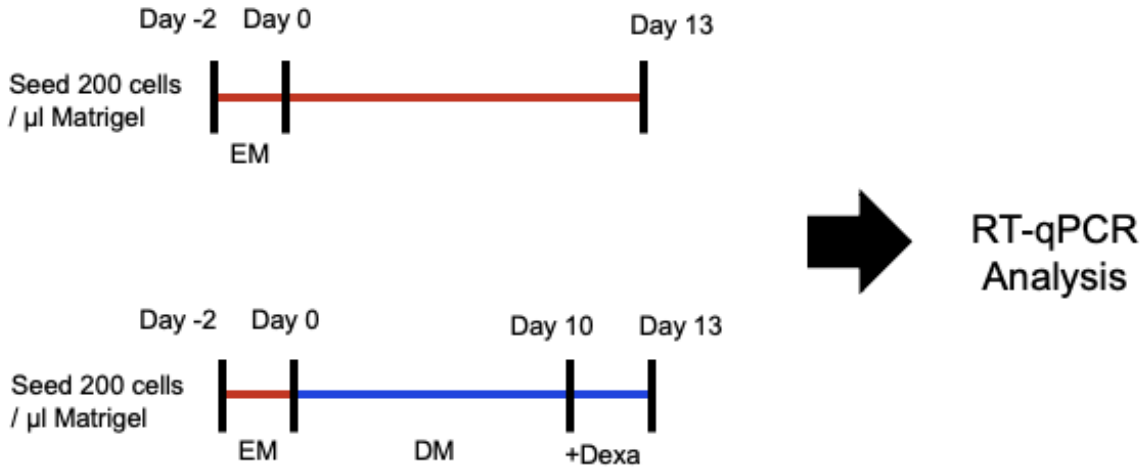

Figure 5.10 BD organoid system.
(A) For these studies, BD organoids were established from frozen liver fragments. Fragments were digested and bile ducts were seeded in isolation media. After 24 hours bile ducts could be seen to balloon out and grow into organoids. According to Huch et al, in expansion conditions organoids maintained Lgr5 expression and bile duct markers Sox9 and Krt19. In differentiation conditions, Lgr5 expression would be lost, biliary marker expression would be reduced, and mature hepatocyte expression would increase. (B) Schematic of the timeline of differentiation used in these studies. For experiments, organoids maintained in expansion media would be disassociated to single cells and seeded at a density of 200 cells per µl of Matrigel. Cells were allowed two days to recover in expansion media. At day 0 cells continued to be maintained in expansion media or switched to differentiation media for 13 days. At day 10, Dexamethasone was added to differentiation media. Analysis of organoids was carried out at Day 13.

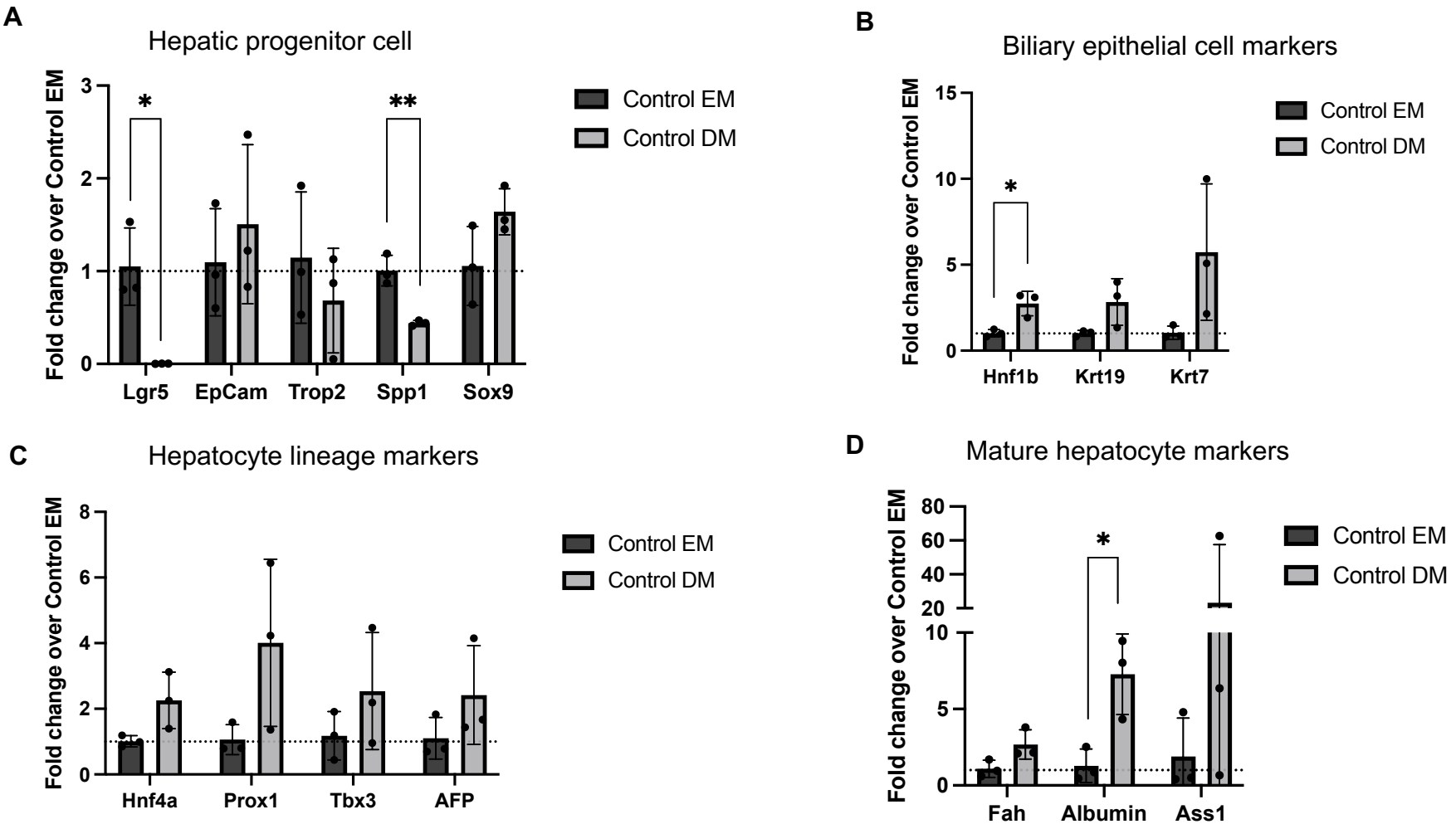

Figure 5.11 RT-qPCR analysis of differentiation in control bile-duct organoids.
(**A**) Expression of hepatic progenitor cell markers. (**B**) Expression of biliary epithelial cell markers. (**C**) Expression of hepatocyte lineage markers. (**D**) Expression of mature hepatocyte markers. Data represents mean ±s.d. n = 3 biological replicates. Expression was normalized to B2M. Fold change calculated relative to Control samples grown in EM. Significance was calculated using unpaired t-test *p<0.05, **p<0.01

5.5.1 AhCreER^T mediated recombination in bile duct organoids.

Recombination in bile duct organoids has previously been shown to be possible using AhCre with the introduction of beta-naphthoflavone (BNF) into culture medium in the work by (Offergeld 2015 PhD thesis). To ensure that recombination and deletion of Axin could occur in a AhCreER^T context, bile duct organoids were established from the livers of mice carrying both the AhCreER^T and the ROSA26 Flox STOP LacZ alleles, described previously in Figure 3.1. Induction was assessed in BD organoids that were grown in EM and DM. To visualize gene deletion in the organoids, they were subsequently stained with X-gal to identify gene deletion at the LacZ allele. (Figure 5.12).

Organoids dissociated to single cell were seeded at 200 cells per ul of Matrigel and allowed 2 days to recover in expansion media. At day 0, 1μM BNF and 1μM 4-OHT were added to both expansion and differentiation media to induce recombination within the organoids. Media was changed every 2-3 days and BNF and 4-OHT was maintained throughout. At day 13 post induction (PI) (Figure 5.12A), X-gal-stained organoids bearing the AhCreER^T transgene and the ROSA26 LacZ reporter allele developed a blue stain suggesting the presence of significant levels of recombination at the ROSA26 locus. Control organoids were not seen to develop a blue stain, suggesting no spontaneous recombination (Figure 5.12B).

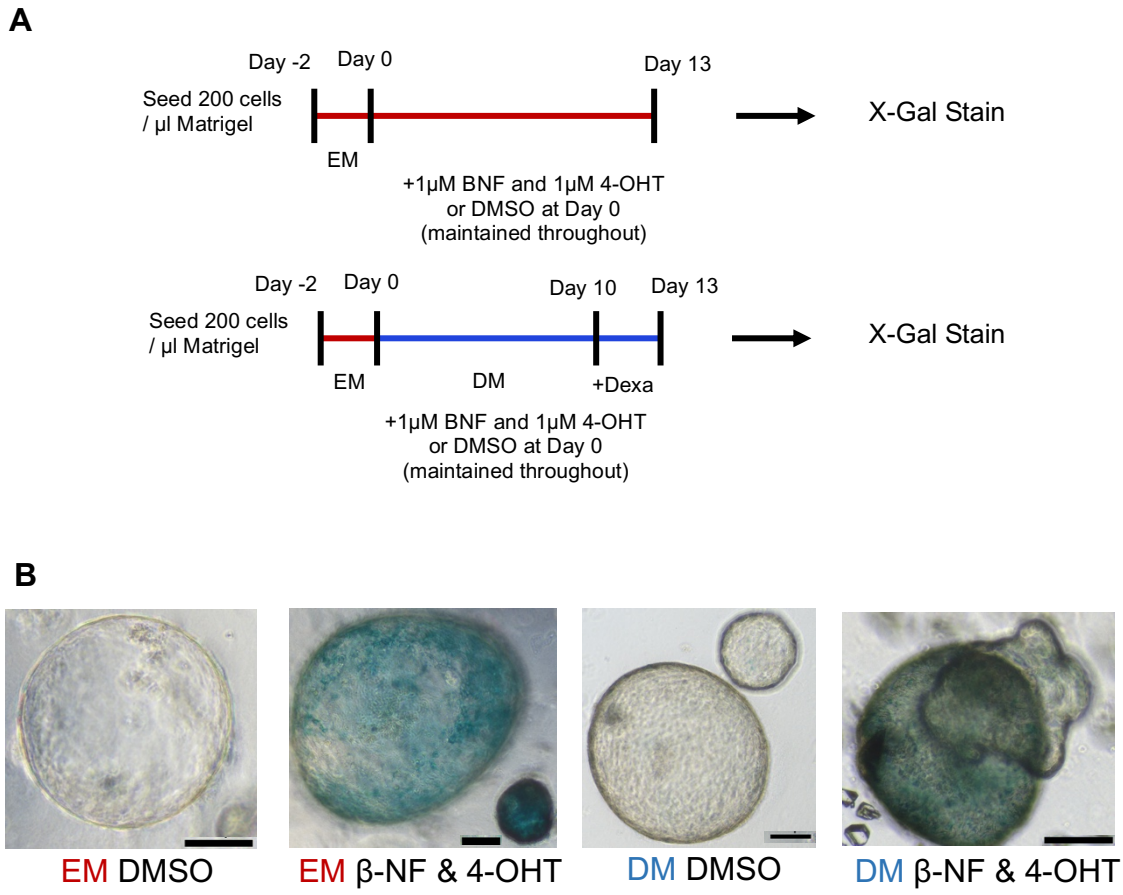

Figure 5.12 AhCreER^{T} mediated recombination in bile duct organoids.
(A) Scheme depicting the induction and differentiation protocol. 1µM β-NF and 1µM 4-OHT was maintained in the culture media throughout starting at day 0. DMSO was used as control. **(B)** Representative images of organoids induced in expansion media (EM) or differentiation media (DM) with X-gal staining performed at day 13 showing blue staining in cultures with β-NF and 4-OHT (and not in control DMSO cultures) indicating recombination of the ROSA26 Flox STOP LacZ allele. Scale bar 100 µm.

5.5.2 Dynamic and stable bile duct organoid induction strategies.

Having successfully shown that AhCreER^{T}, ROSA-LacZ bile duct organoids undergo recombination in culture in expansion media (EM) and differentiation media (DM), organoids were established from the livers of mice bearing the following alleles: AhCreER^{T+}; Axin1$^{wt/wt}$; Axin2$^{wt/wt}$ (Control), AhCreER^{T+}; Axin1$^{fl/fl}$, AhCreER^{T+}; Axin2$^{fl/fl}$ and AhCreER^{T+}; Axin1$^{fl/fl}$; Axin2$^{fl/fl}$ as used for the *in vivo* studies in Chapter 3. Three separate mice were used to establish organoids for each genotype.

To study the immediate effects of Axin loss using AhCreER^{T} requires the inducing agent BNF however, BNF has been shown to alter cell biology in BD organoids (Offergeld 2015 PhD Thesis). Even though this BNF dependent biology would be controlled with the use of control organoids, the effects might mask the underlying Axin deleted dependent biology. By contrast the effects of deletion followed by onward culture in the absence of an inducer might allow the induced cells to adapt to their environment and might obscure immediate responses that are key to understanding the direct effects of Axin loss. Therefore, it was decided to use two different protocols to induce recombination and analyse the loss of Axin in bile-duct organoids (Figure 5.13). The two protocols involved were Dynamic Induction and longer-term Stable Induction of gene deletion with BNF and 4-OHT. It was anticipated that phenotypes that were observed under these conditions would most likely be driven by the underlying genetic changes than by culture-induced artefacts.

Dynamic induction maintained the inducing agents BNF and 4-OHT in the culture medium from day 0 for 13 days with subsequent analysis to be carried out on the organoids at the end of the time course (Figure 5.13A). To produce Stably-Induced cells, BNF and 4-OHT induction was initially used to induce the organoids in expansion media for 7 days. These induced organoids were then passaged for expansion and differentiation protocol without the presence of BNF or 4-OHT thus mitigating the effects of BNF (Figure 5.13B). The stable induction protocol was believed to more likely show that any differences seen are the result of the underlying biology driven by loss of Axin and not the exposure to BNF or adaptation in culture as Axin deleted organoids are grown from single cell with no BNF in the culture medium.

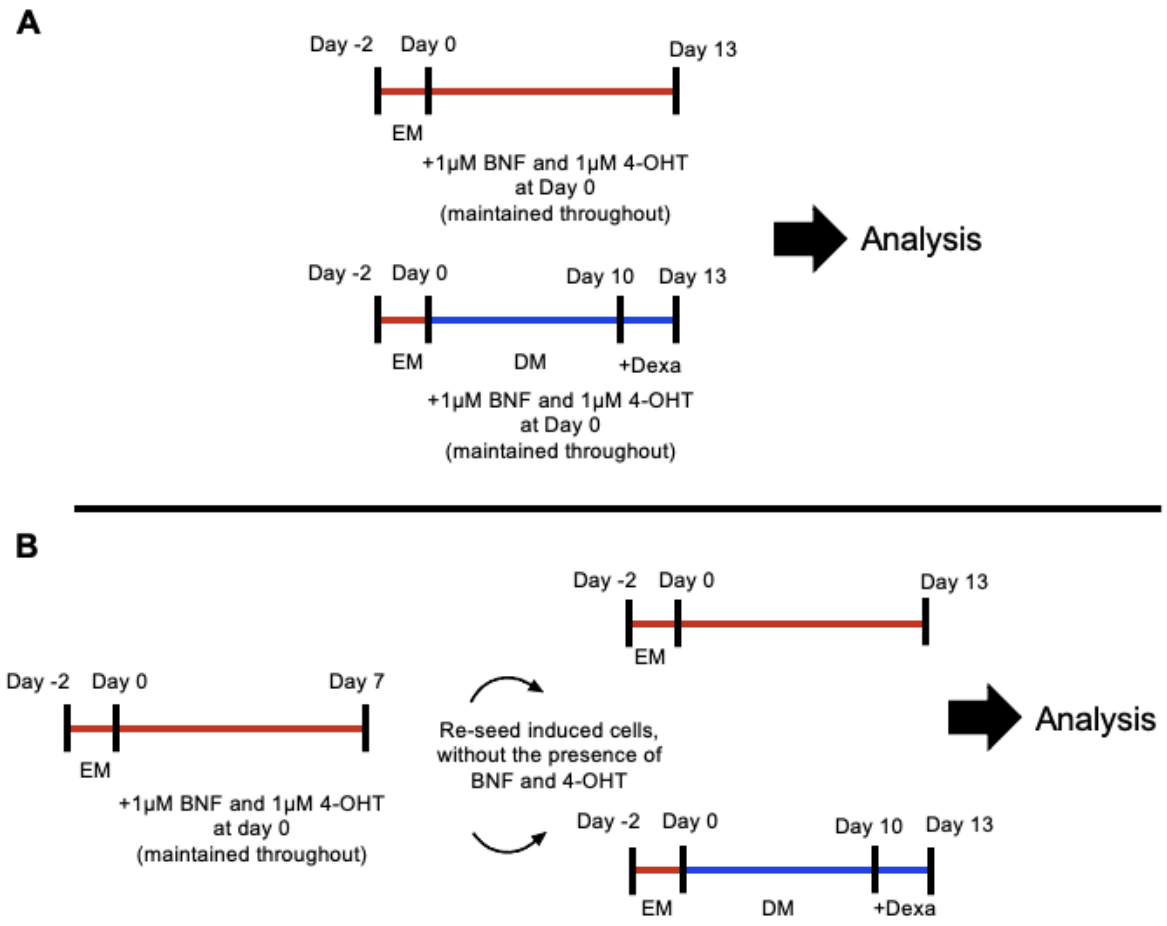

Figure 5.13 Bile duct organoids induction strategies.
(A) Schematic for dynamic induction strategy. Inducing agents BNF and 4-OHT are maintained in culture starting at day 0 to induce Cre recombination. Analysis is carried out at day 13 at the end of the differentiation protocol. **(B)** Schematic for stable compound induction strategy. Inducting agents BNF and 4-OHT are maintained in culture from day 0 for 7 days in EM media. Organoids are dissociated and seeded for differentiation protocol without the presence of BNF or 4-OHT.

5.5.3 Quantification of AhCreER^{T} mediated recombination of Axin1 in dynamic and stably induced bile-duct organoids.

One concern of the stable induction method was whether any cells that did not undergo recombination during the 7-day induction period, could repopulate once the inducing agents are no longer present. Using gDNA from dynamic and stably induced organoids grown in EM at the end of each respective time-course, qPCR was carried out to quantify levels of recombination of Axin1 with the same primer pairs as used previously (Figure 5.14A).

Levels of the unrecombined Axin1$^{fl/fl}$ allele were reduced by 97% and 93% in AhCreER^{T} Axin1$^{\Delta/\Delta}$ and AhCreER^{T} Axin1$^{\Delta/\Delta}$, Axin2$^{\Delta/\Delta}$ samples grown in EM using the dynamic and stable induction protocols respectively (Figure 5.14B, D). The expected increases in levels of the shorter recombined Axin1$^{\Delta/\Delta}$ allele using primer pair B were only detected following induction of AhCreER^{T} Axin1$^{fl/fl}$ and AhCreER^{T} Axin1$^{fl/fl}$, Axin2$^{fl/fl}$ samples (Figure 5.14D, E) and were comparable between dynamic and stable induction protocols.

These results suggest that levels or recombination at the time of analysis are comparable between dynamic and stable induction strategies thus any differences in biology observed would not be due to variations in levels of recombination.

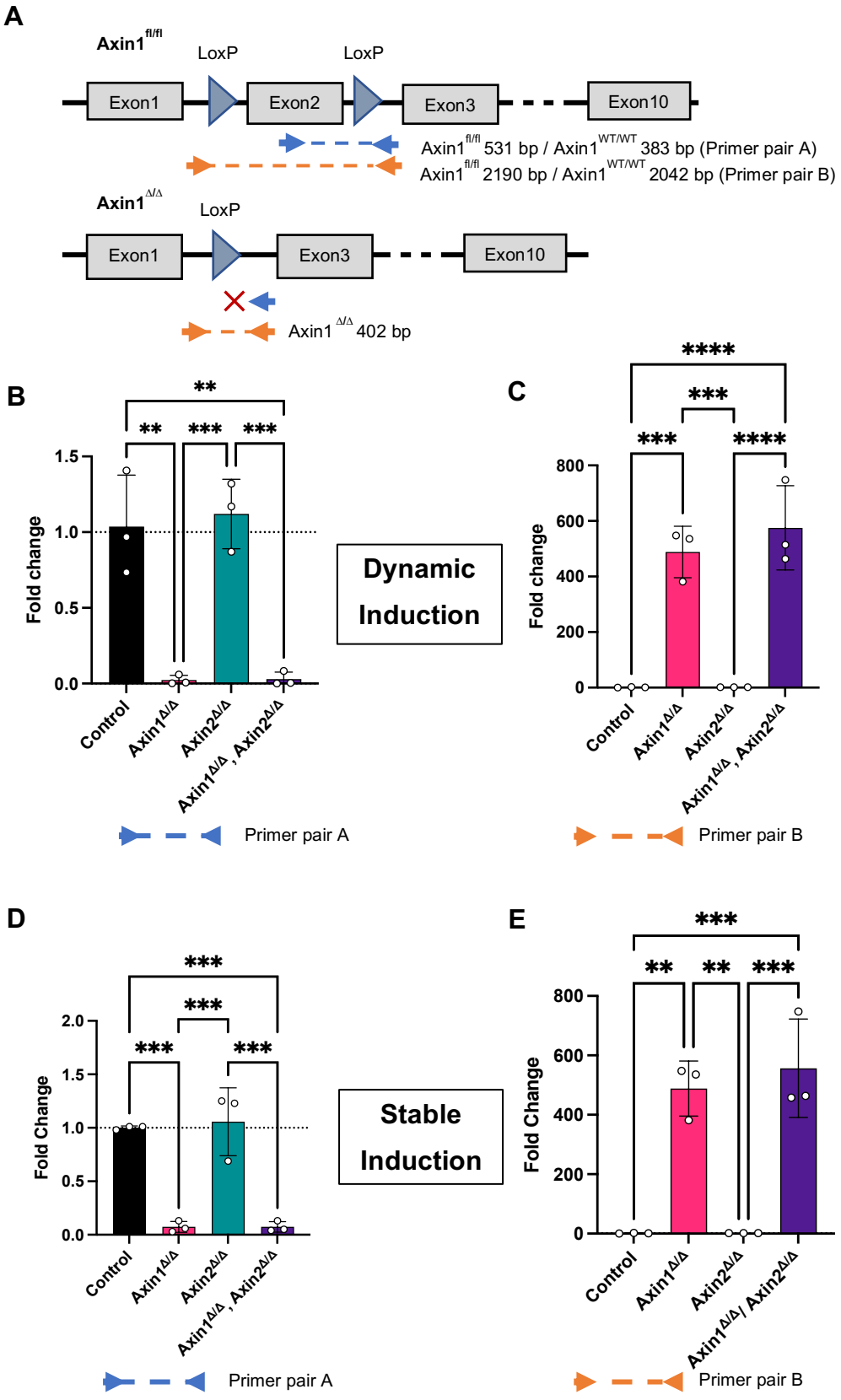
A
Axin1fl/fl
LoxP
LoxP
Exon1
Exon2
Exon3
Exon10
Axin1fl/fl 531 bp / Axin1WT/WT 383 bp (Primer pair A)
Axin1fl/fl 2190 bp / Axin1WT/WT 2042 bp (Primer pair B)
Axin1Δ/Δ
LoxP
Exon1
Exon3
Exon10
Axin1Δ/Δ 402 bp
B
Fold change
Control
Axin1Δ/Δ
Axin2Δ/Δ
Axin1Δ/Δ, Axin2Δ/Δ
Primer pair A
Dynamic Induction
C
Fold change
Primer pair B
D
Fold Change
Primer pair A
Stable Induction
E
Fold Change
Axin1Δ/Δ/ Axin2Δ/Δ
Primer pair B

Figure 5.14 AhCreER^T mediated recombination of Axin1 in Dynamic and Stably induced bile-duct organoids was comparable.
(A) Schematic of primer pair binding sites. **(B, D)** qPCR results using primer pair A showed comparable recombination levels of 97% and 93% of Axin1 in Axin1 and Axin1, Axin2 deleted bile-duct organoids using Dynamic and Stable induction strategies. **(C, E)** qPCR results using primer pair B showed between 450 and 580-fold increase of the recombined allele in Axin1 and Axin1, Axin2 deleted bile-duct organoids for both induction strategies. Data was normalised to *ApoB* and is shown as the relative fold change to Control organoids. n=3, error bars: SD. Significance was calculated using One-Way ANOVA with Tukey's multiple comparison test. **p<0.01 ***p<0.001 ****p<0.0001

5.5.4 Growth and viability in Axin deleted bile duct organoids.

Acute deletion of Axin1 and to a lesser extent the deletion of Axin1 and Axin2 resulted in increased proliferation in the mouse liver as scored by Ki67 staining in hepatocytes. BD organoids in EM represent injured bile duct cells however, in DM these cells represent an intermediate on the transdifferentiation route to hepatocytes. It is therefore expected that changes after the loss of Axin would most likely be notable in differentiated BD organoids as they would better recapitulate mutant hepatocyte behaviour. Bile duct organoids were dynamically and stably induced with BNF and 4-OHT to delete Axin to assess and compare induction strategies and their effects on growth and viability in the context of Axin deletion. Viability was measured using CellTiter-Glo 3D to quantify ATP levels. Deletion of Axin1 and Axin1 and Axin2 in bile duct organoids was expected to result in increased viability, particularly in DM conditions.

Dynamic induction to delete Axin1, Axin2 and both Axin1 and Axin2 had no discernible effect on BD organoid viability grown in EM and DM as measured by CellTiter-Glo 3D (Figure 5.15A). AhCreER^{T} Axin1$^{\Delta/\Delta}$, Axin2$^{\Delta/\Delta}$ BD organoids grown in EM showed a slight fluctuation at day 7 in viability, but this was possibly due to technical error. Size of organoids appeared comparable between cohorts grown in EM and DM, but this was not quantified (Figure 5.15B).

Stable induction to delete Axin1 and both Axin1 and Axin2 in BD organoids grown in EM or DM did not result in changes to viability as measured by CellTiter-Glo 3D. A trend for decreased viability was observed in Axin2 deleted organoids (Figure 5.16A). This was more pronounced in DM conditions but was not significant at any timepoint. Select Axin1 deleted BD organoids were found to be larger by day 2 in EM (Figure 5.16B). At Day 13, stable deletion of Axin2 resulted in stunted growth of organoids in EM and to a greater extent in DM (Figure 5.16A) however, this was not quantified.

Axin deletion using dynamic induction did not show changes in viability in EM or DM conditions as expected. Stable induction showed similar levels of viability of Axin deleted BD organoids when grown in EM. However, stable induction showed reduced viability of Axin2 deleted BD organoids which correlated with their noted reduced size. Reduced expression of Lgr5 was observed in Axin2 deleted livers thus stable induction may be better at recapitulating the *in vivo* scenario. The expected

increase in the viability in Axin1 and both Axin1 and Axin2 deleted BD organoids was not observed in either induction method. This may be due to fewer but bigger organoids, a hint of this is seen in Axin1 deleted organoids using stable induction. It was felt that to get the best readouts, further analysis of Axin deletion would be carried out using Stable induction as this may better represent the *in vivo* model and mitigate the effects of BNF allowing for a clearer examination of the effects of Axin deletion.

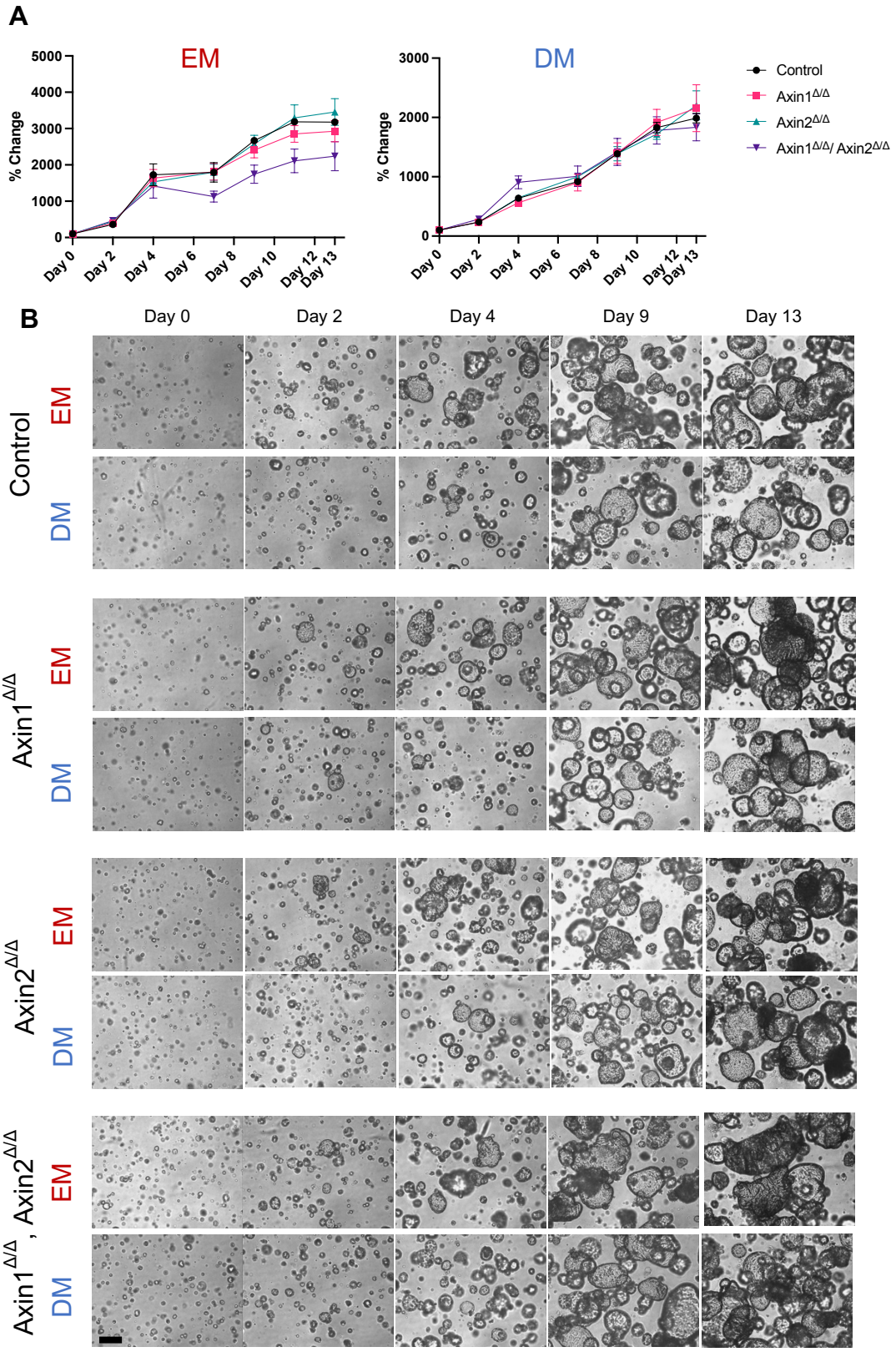

Figure 5.15 Bile-duct growth and viability using dynamic induction to delete Axin. **(A)** CellTiter-Glo viability analysis of control and Axin mutant organoids induced in culture (Stable induction) in expansion and differentiation media n = 3 done in triplicate **(B)** Representative images of control and Axin deleted organoids induced in culture in expansion and differentiation media. Scale bar 100 μm

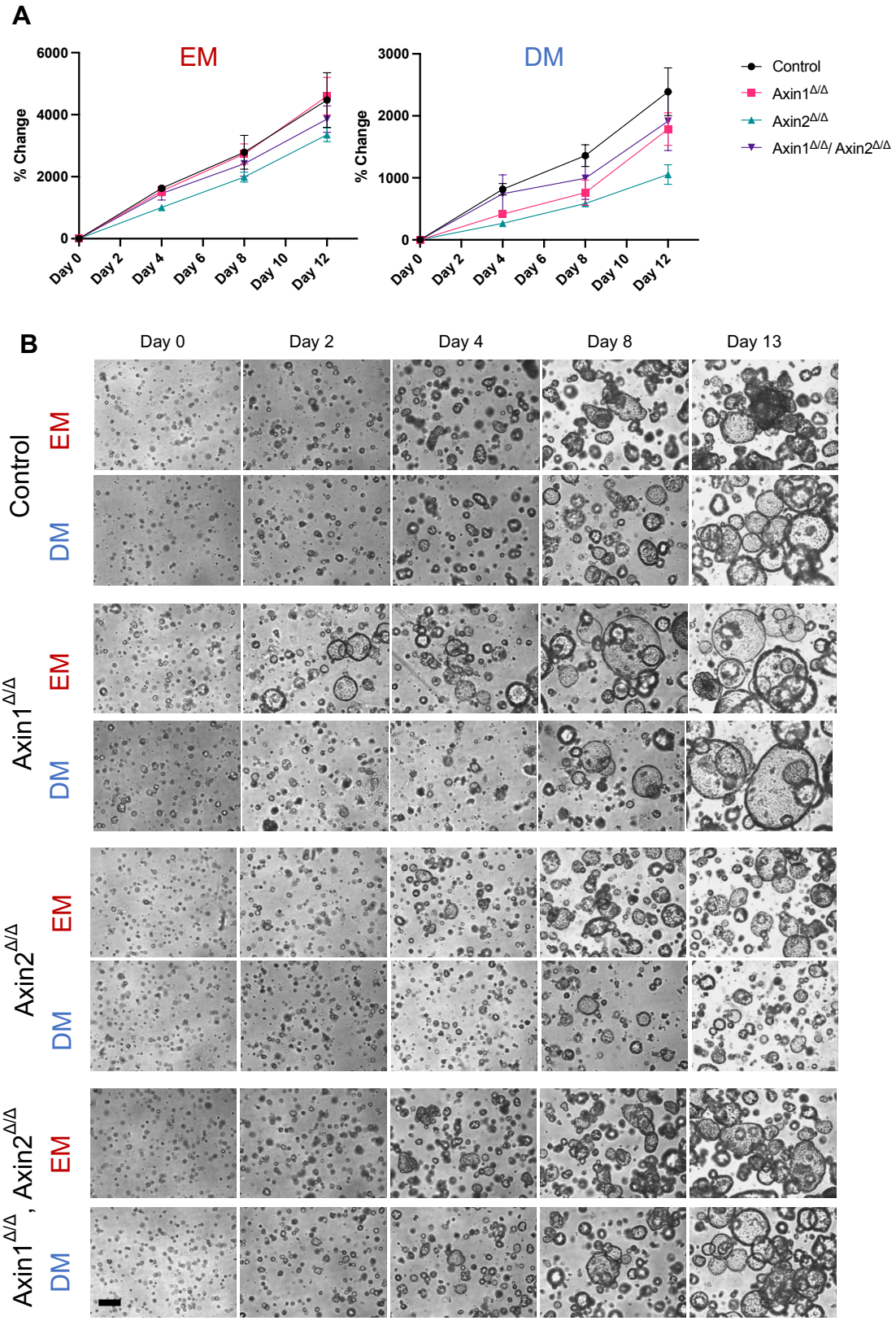

Figure 5.16 Bile-duct growth and viability using stable induction of Axin deletion. **(A)** CellTiter-Glo 3D readout of stably induced organoids grown in EM and DM. n = 3 each with 4 technical replicates. **(B)** Representative images of stably induced organoids grown in EM and DM at varying time-points. Scale bar 100 μm

5.5.5 Changes in hepatic lineage and mature marker expression following differentiation of Axin deleted bile-duct organoids.

Axin loss would be predicted to result in the increase in expression of stem cell markers. In BD organoids following differentiation this in turn may result in reduced expression of mature hepatocyte expression. Using the same panel of liver progenitor, lineage, and mature cell markers as used previously, RT-qPCR was carried out using RNA from Axin deleted organoids grown in EM and DM following stable induction.

In EM, *Lgr5* expression had a trend for an increase in AhCreER^{T} Axin1 and AhCreER^{T} Axin1$^{\Delta/\Delta}$, Axin2$^{\Delta/\Delta}$ organoids and was found to be 3-fold lower in AhCreER^{T} Axin2$^{\Delta/\Delta}$ organoids though this was not significant. Reduced levels of Lgr5 mRNA was consistent with results from AhCreER^{T} Axin2$^{\Delta/\Delta}$ livers at day 6, 1 month, and 1 year post induction. *Trop2* expression was found to be highly variable between samples in AhCreER^{T} Axin1 and AhCreER^{T} Axin1$^{\Delta/\Delta}$, Axin2$^{\Delta/\Delta}$ organoids. No changes were seen in the expression of *EpCam*, *Spp1* or *Sox9* in any of the cohorts (Figure 5.17A). *Hnf1b* and *Krt7* were significantly increased in AhCreER^{T} Axin1$^{\Delta/\Delta}$, Axin2$^{\Delta/\Delta}$ and AhCreER^{T} Axin1$^{\Delta/\Delta}$ respectively (Figure 5.17B). Hepatic lineage markers were not significantly altered though *Tbx3* a downstream Wnt/β-catenin, showed a trend for an increase in Axin1 deleted cohorts (Figure 5.17C). No significant changes to the expression of mature hepatocyte markers *Fah*, *Albumin* and *Ass1* were seen in Axin deleted cohorts grown in EM (Figure 5.17D).

AhCreER^{T} Axin1$^{\Delta/\Delta}$ organoids grown in DM had a 6.7-fold increase in *Lgr5* expression compared to Control organoids (Figure 5.18A). Loss of Axin2 alone did not have a significant effect on *Lgr5* expression however, combined deletion of Axin1 and Axin2 resulted in a significant 47-fold increase, suggesting loss of both Axins results in a stronger Wnt pathway activation in bile-duct organoids grown in DM. The increase in Lgr5 expression was significantly higher in double Axin deleted organoids than Axin1 alone which may relate to the increased tumourigenesis observed *in vivo*. *Trop2* expression was found to be increased by an average 29-fold in AhCreER^{T} Axin1$^{\Delta/\Delta}$, Axin2$^{\Delta/\Delta}$ organoids however, this was not significant due to high variability between samples. No changes were seen in the other hepatic progenitor markers (Figure 5.18A). Expression of biliary epithelial cell markers *Hnf1b*, *Krt19* and *Krt7* were unaffected by Axin deletion (Figure 5.18B). The hepatic progenitor marker and Wnt

target Tbx3, was found to have 4-fold higher expression in AhCreER^{T} Axin1$^{\Delta/\Delta}$ and AhCreER^{T} Axin1$^{\Delta/\Delta}$, Axin2$^{\Delta/\Delta}$ organoids though this was not significant due to variability between samples. AhCreER^{T} Axin2$^{\Delta/\Delta}$ organoids had a 2-fold increase in *Hnf4*α expression and elevated *AFP* expression (Figure 5.18C). No significant changes were seen in mature hepatocyte marker expression though there was a trend for a decrease in *Albumin* expression in AhCreER^{T} Axin1$^{\Delta/\Delta}$ and AhCreER^{T} Axin1$^{\Delta/\Delta}$, Axin2$^{\Delta/\Delta}$ organoids (Figure 5.18D).

These results suggest that the loss of Axin1 and combined deletion of Axin1 and Axin2 results in elevated expression of the stem cell marker Lgr5, which has previously been linked with liver injury (Huch et al. 2013). Additionally, the elevated expression of Tbx3, also a Wnt/β-catenin target suggests activation of Wnt/β-catenin pathway. This, coupled with reduced expression of Albumin, suggests that Axin1 and combined Axin1, Axin2 deleted bile duct organoids are more stem like. Increased Lgr5 expression was also found in Axin1 deleted liver at day 6 post induction and in double Axin1, Axin2 deleted livers at 1 year post induction.

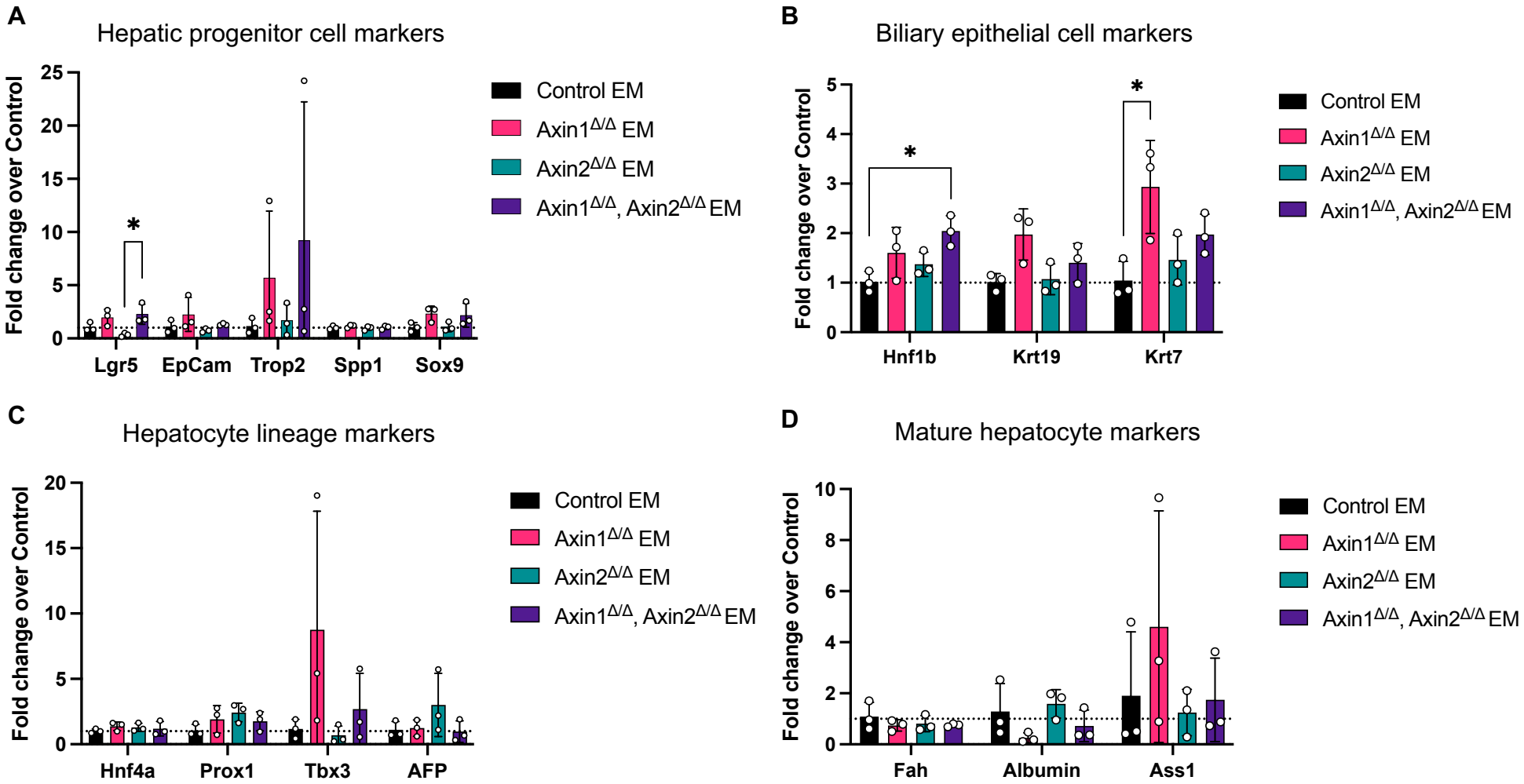

Figure 5.17 RT-qPCR analysis of liver progenitor, lineage, and mature cell markers in expansion conditions in Axin deleted organoids. **(A)** Expression of hepatic progenitor cell markers. (**B**) Expression of biliary epithelial cell markers. (**C**) Expression of hepatocyte lineage markers. (**D**) Expression of mature hepatocyte markers. Data represents mean ±s.d. n = 3 biological replicates. Expression was normalized to B2M. Fold change calculated relative to Control samples grown in EM. Significance was calculated using One-Way ANOVA with Tukey's multiple comparison test. *p<0.05

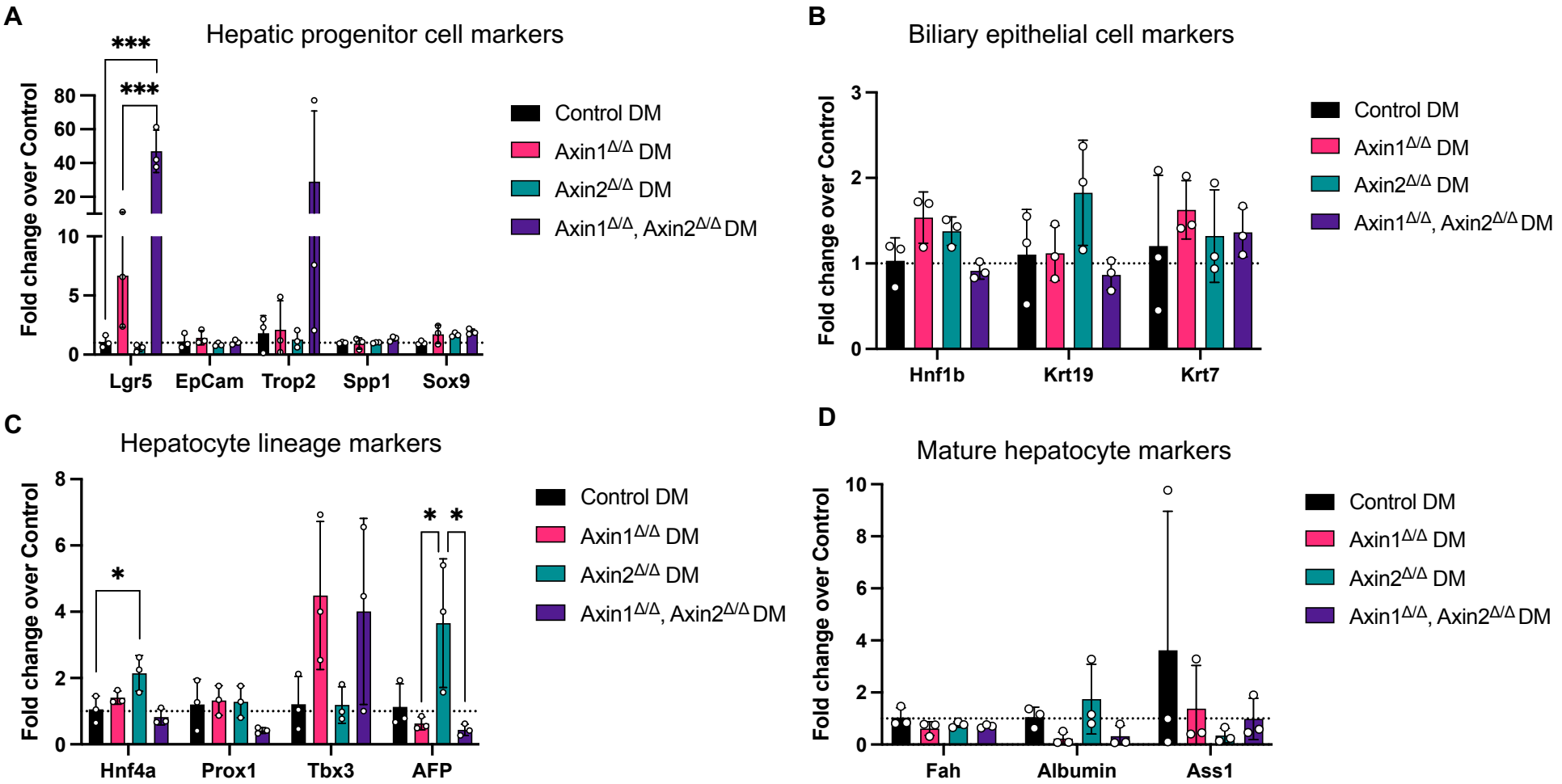

Figure 5.18 RT-qPCR analysis of liver progenitor, lineage, and mature cell markers in differentiation conditions in Axin deleted organoids. (**A**) Expression of hepatic progenitor cell markers. (**B**) Expression of biliary epithelial cell markers. (**C**) Expression of hepatocyte lineage markers. (**D**) Expression of mature hepatocyte markers. Data represents mean ±s.d. n = 3 biological replicates. Expression was normalized to B2M. Fold change calculated relative to Control samples grown in DM. Significance was calculated using One-Way ANOVA with Tukey's multiple comparison test. *p<0.05 ***p<0.001

5.5.6 Axin, Wnt targets and cell cycle expression in control and Axin deleted mouse bile duct organoids following Stable induction.

Axin deletion in the liver resulted in increased transcription of genes associated with the G2/M transition of the cell cycle and activation of a subset of Wnt/β-catenin target genes (Feng et al. 2012). Using RNA from stable Axin deleted and control bile-duct organoids grown in EM and DM, RT-qPCR assays were carried out to assess Axin, Wnt targets and G2/M cell cycle gene expression using the same panel of genes as used for *in vivo* studies.

The panel of genes was first assessed in Control organoids. Like the loss of *Lgr5* already observed in control organoids grown in DM, expression of *Axin2* was lost. Results also showed a 3-fold increase in *c-Myc* and *Cdc25a* expression. This is most likely due to the addition of the TGF-β inhibitor A83-01 to the differentiation media. No changes were seen in the expression to Axin and Wnt targets *Axin1*, β-*catenin*, *Tiam1*, *Caspase-3*, *c-Jun*, *CD44*, *p53* and *CyclinD1*. Expression of G2/M cell cycle genes *cyclins A2, B1, B2, Cdk1, Cdca3, Cdc20, Ki-67, Mastl* and *FoxM1* remained unchanged in organoids grown in DM relative to EM (Figure 5.19).

Stably induced AhCreER^{T} Axin1$^{\Delta/\Delta}$ organoids in EM showed an 85% reduced level of Axin1 transcripts containing exon 2 as expected from the levels of recombination previously quantified. Furthermore, these organoids had a 3-fold increase in *Axin2* expression, 2.3-fold increase in *c-Myc* expression and 2.6-fold increase in *CyclinD1* expression suggesting elevated Wnt/β-catenin pathway activation. No significant changes in expression were seen to other Wnt targets or G2/M cell cycle genes (Figure 5.20A). Stably induced AhCreER^{T} Axin2$^{\Delta/\Delta}$ organoids in EM lost expression (362-fold decrease) of Axin2 transcripts containing exon 2 as would be expected following significant levels of recombination. This loss was not associated with increases to expression of Axin2 transcripts without exon 2. Expression of Axin1 increased 2.5-fold, similar to what was seen in the liver following Axin2 loss. No changes were seen in expression of Wnt targets or G2/M cell cycle genes (Figure 5.20B). Stably induced AhCreER^{T} Axin1$^{\Delta/\Delta}$, Axin2$^{\Delta/\Delta}$ organoids in EM had similar loss of expression of transcripts containing exon 2 of Axin1 and Axin2 as in the single mutants. This resulted in 3- and 5-fold increase in expression of Axin1 and Axin2 transcripts using primers targeting the c-terminal region that should not have been affected by recombination. Double Axin deleted organoids also showed 2.6-fold

increase in c-Myc expression, comparable to Axin1 deleted organoids. However, there were no significant increases to any other Wnt targets or G2/M cell cycle genes assessed (Figure 5.20C).

In contrast to control organoids in DM, AhCreER^{T} Axin1$^{\Delta/\Delta}$ organoids showed a 15-fold increase in the expression of Axin2 and a 2.3-fold increase in the expression of Tiam1. As in EM, Axin1 transcripts containing exon 2 were down 85%. No change in expression was observed in any other Wnt targets or G2/M cell cycle genes (Figure 5.21A) Besides the expected loss of transcripts of Axin2 containing exon 2, no other changes were seen in AhCreER^{T} Axin2$^{\Delta/\Delta}$ organoids in DM compared to controls (Figure 5.21B). Stably induced AhCreER^{T} Axin1$^{\Delta/\Delta}$, Axin2$^{\Delta/\Delta}$ organoids in DM showed reduced expression of transcripts of Axin1 and Axin2 containing exon 2 as expected. Expression of transcripts of Axin1 without exon 2, using primers targeting the c-terminal were unaltered. However, using primers targeting the c-terminal of Axin2 results showed a 78-fold increase compared to control, suggesting the loss of exon 2 of both Axins synergizes to increase the expression of the remaining exons of the Wnt target Axin2. However, no changes were seen to any other Wnt targets or to the panel of G2/M cell cycle genes assessed (Figure 5.21C).

Elevated expression of *Axin2* and *c-Myc* were also observed in Axin1 deleted livers at 1 year post induction (Figure 3.26A). However, it was surprising that the loss of Axin1 in DM conditions did not replicate the increase of G2/M cell cycle genes as observed by Offergeld (2015 PhD thesis) using AhCre mediated dynamic induction of bile-duct organoids. It was previously hypothesized that the reduced levels of recombination using AhCreER in the liver was the reason that this G2/M signature was not observed however, the 93% levels of recombination in culture (Figure 5.14B) brings this into question. *Axin1* expression was elevated in Axin2 deleted livers at 1 year post induction (Figure 3.26B) and was seen in Axin2 deleted organoids in EM. No other changes in expression matched the RT-qPCR results found in Axin2 deleted livers. Double Axin deleted organoids grown in EM replicated the increase in *Axin1* and *Axin2* expression using primers targeting c-terminal (Figure 3.2C, D) and *c-Myc* (Figure 3.26C) in the liver at 1 year post induction. However, the trends in the increase in G2/M phase cell cycle genes at day 6 post induction (Figure 3.13C) or the significant increases at 1 year post induction (Figure 3.26C) in the liver were not observed in bile-duct organoids in EM or DM.

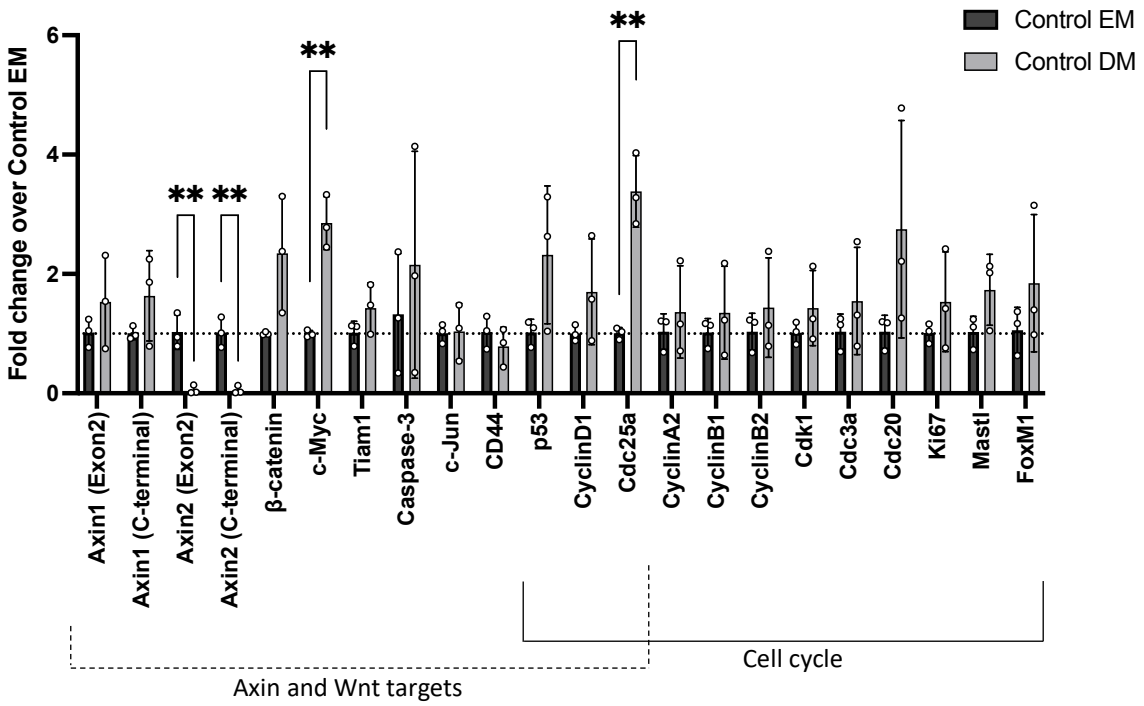

Figure 5.19 Axin, Wnt targets and cell cycle expression in control bile duct organoids following differentiation.

Changes in gene expression of control bile duct organoids grown in EM and DM. Data represents mean ±s.d. n = 3 biological replicates. Data was normalised to B2M and is shown as the relative fold change to AhCreER^{+}, Axin1$^{+/+}$, Axin2$^{+/+}$ (Control) grown in EM. Significance was calculated using unpaired t-test **p<0.01

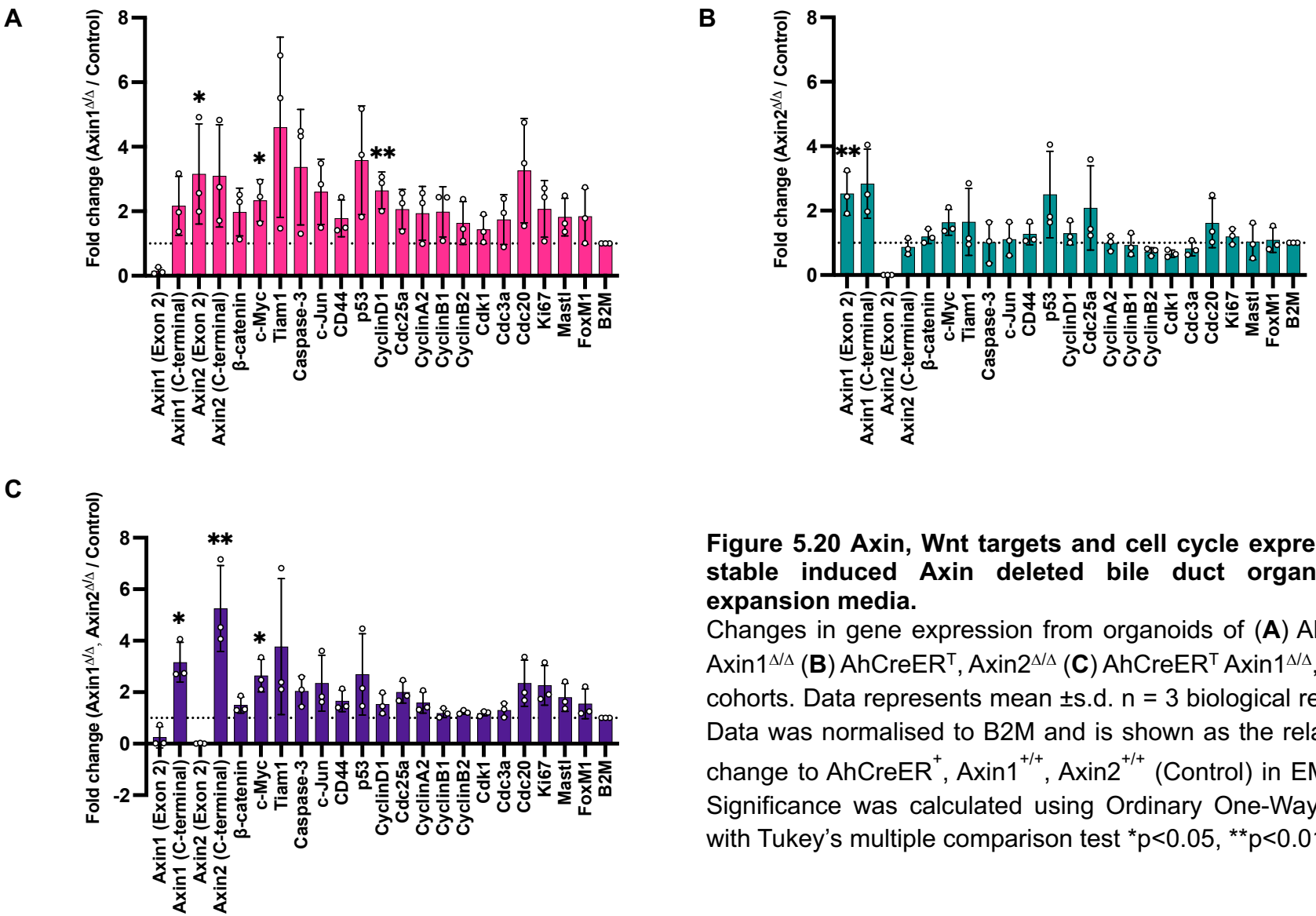

Figure 5.20 Axin, Wnt targets and cell cycle expression in stable induced Axin deleted bile duct organoids in expansion media.

Changes in gene expression from organoids of (**A**) AhCreER^{T} Axin1$^{\Delta/\Delta}$ (**B**) AhCreER^{T}, Axin2$^{\Delta/\Delta}$ (**C**) AhCreER^{T} Axin1$^{\Delta/\Delta}$, Axin2$^{\Delta/\Delta}$ cohorts. Data represents mean ±s.d. n = 3 biological replicates. Data was normalised to B2M and is shown as the relative fold change to AhCreER^{+}, Axin1$^{+/+}$, Axin2$^{+/+}$ (Control) in EM media. Significance was calculated using Ordinary One-Way ANOVA with Tukey's multiple comparison test *p<0.05, **p<0.01

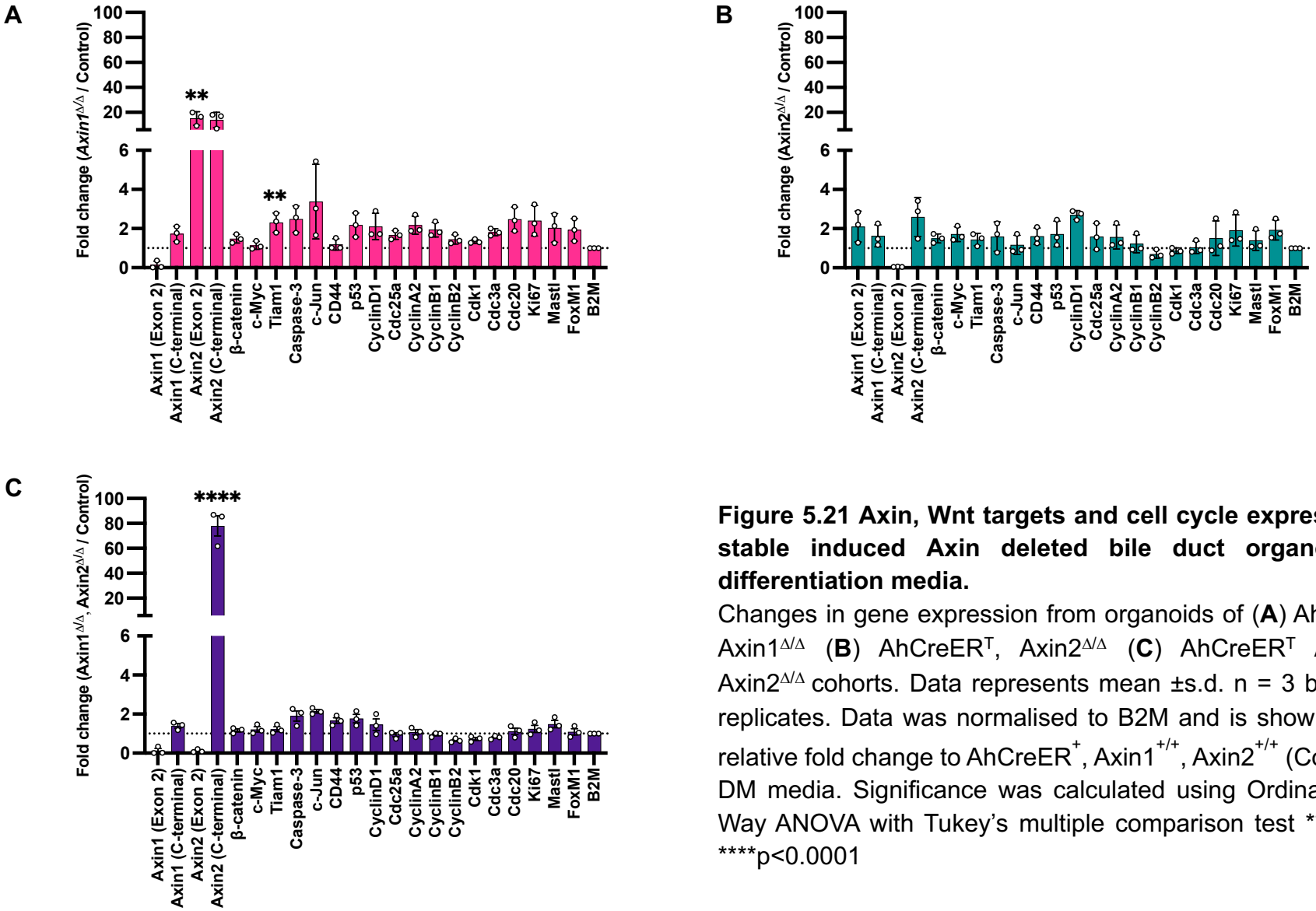

Figure 5.21 Axin, Wnt targets and cell cycle expression in stable induced Axin deleted bile duct organoids in differentiation media.

Changes in gene expression from organoids of (**A**) AhCreER^{T} Axin1$^{\Delta/\Delta}$ (**B**) AhCreER^{T}, Axin2$^{\Delta/\Delta}$ (**C**) AhCreER^{T} Axin1$^{\Delta/\Delta}$, Axin2$^{\Delta/\Delta}$ cohorts. Data represents mean ±s.d. n = 3 biological replicates. Data was normalised to B2M and is shown as the relative fold change to AhCreER^{+}, Axin1$^{+/+}$, Axin2$^{+/+}$ (Control) in DM media. Significance was calculated using Ordinary One-Way ANOVA with Tukey's multiple comparison test **p<0.01, ****p<0.0001

5.5.7 β-catenin localization in Axin deleted organoids.

AhCreER^T mediated deletion of Axin1, Axin2 or both Axin1 and Axin2 in the mouse liver at 6 days post induction did not result in aberrant nuclear β-catenin staining (Figure 3.11A). Elevated expression of Wnt/β-catenin targets Lgr5 and Axin2 (using primers targeting the c-terminal) in AhCreER^T Axin1$^{\Delta/\Delta}$ and even more so in AhCreER^T Axin1$^{\Delta/\Delta}$, Axin2$^{\Delta/\Delta}$ stably induced BD organoids may suggest elevated and mis-localised β-catenin. To assess localization of β-catenin, Axin deleted stably induced BD organoid cohorts grown in EM and DM were whole mount fixed and stained for β-catenin.

Immunofluorescence staining for β-catenin revealed strong membrane staining as expected in all cohorts grown in EM and DM (Figure 5.22). However, no clear nuclear β-catenin could be observed making this finding consistent with the observations seen at day 6 post induction in the mouse liver. Some cytoplasmic staining could be observed in AhCreER^T Axin1$^{\Delta/\Delta}$, Axin2$^{\Delta/\Delta}$ BD organoids in DM however, this was not consistent.

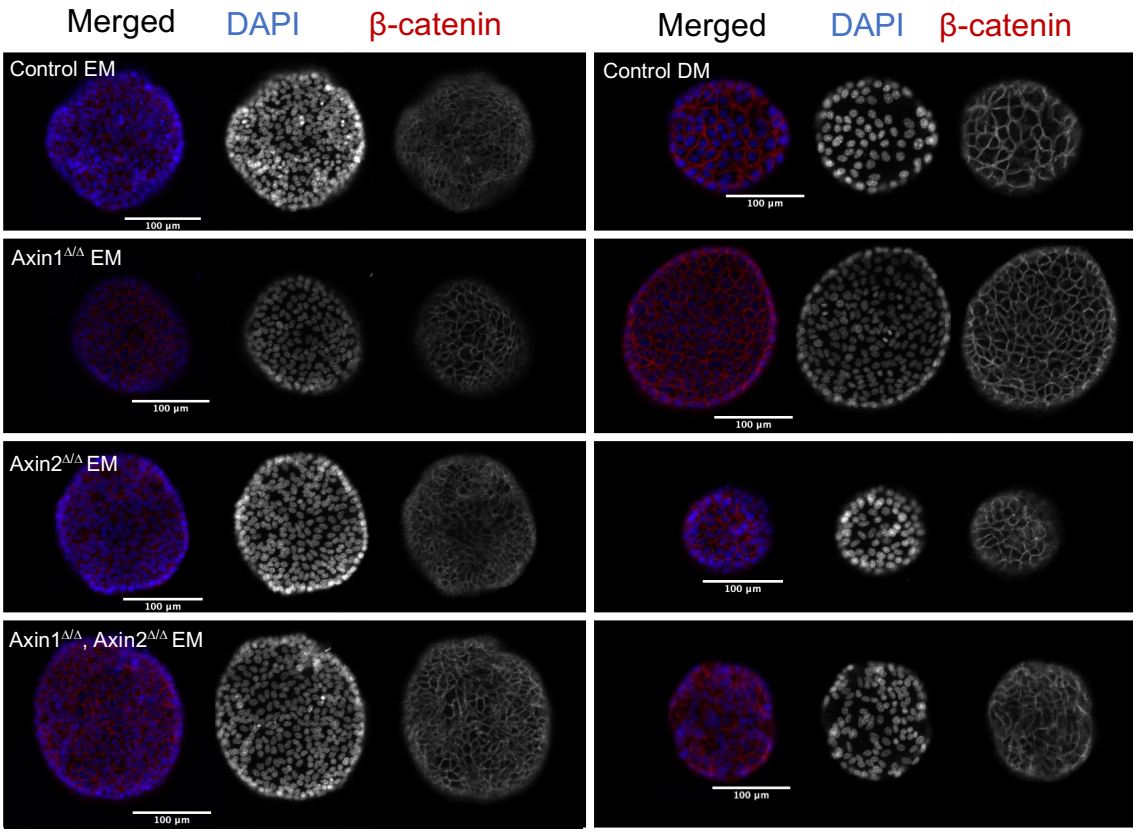

Figure 5.22 β-catenin localization in bile-duct organoids following Axin deletion using stable induction in EM and DM

Representative images of control and Axin deleted bile-duct organoids grown in EM and DM stained for β-catenin. Scale bar 100 μm

5.5.8 Ki67 staining in Axin deleted organoids.

Deletion of Axin1 and combined deletion of both Axin1 and Axin2 resulted in increased staining of Ki67 in the mouse liver 6 days post induction. To assess if this phenotype is replicated in the BD organoid system, stably induced Axin deleted BD organoids were stained for Ki67 (Figure 5.23A).

AhCreER^{T} Axin1$^{\Delta/\Delta}$ organoids grown in EM and DM showed a significantly higher percentage of cells stained positive for Ki67 (Figure 5.23B). Surprisingly, no differences in Ki67 staining were seen in AhCreER^{T} Axin1$^{\Delta/\Delta}$, Axin2$^{\Delta/\Delta}$ organoids. It was expected that the Ki67 counts for AhCreER^{T} Axin2$^{\Delta/\Delta}$ organoids grown in DM would be reduced. However, these organoids were generally much smaller, and it was difficult to find organoids to count that were comparable in size to other cohorts which may explain why no difference was seen.

AhCreER^{T} Axin1 deleted organoids have been shown to have an increase in Ki67 positive stained cells but without a G2/M signature. Additional deletion of Axin2 did not perturb Ki67 staining levels even though the combined loss of genes did result in the expression of higher levels of *Lgr5* and *Axin2* (transcripts without exon 2).

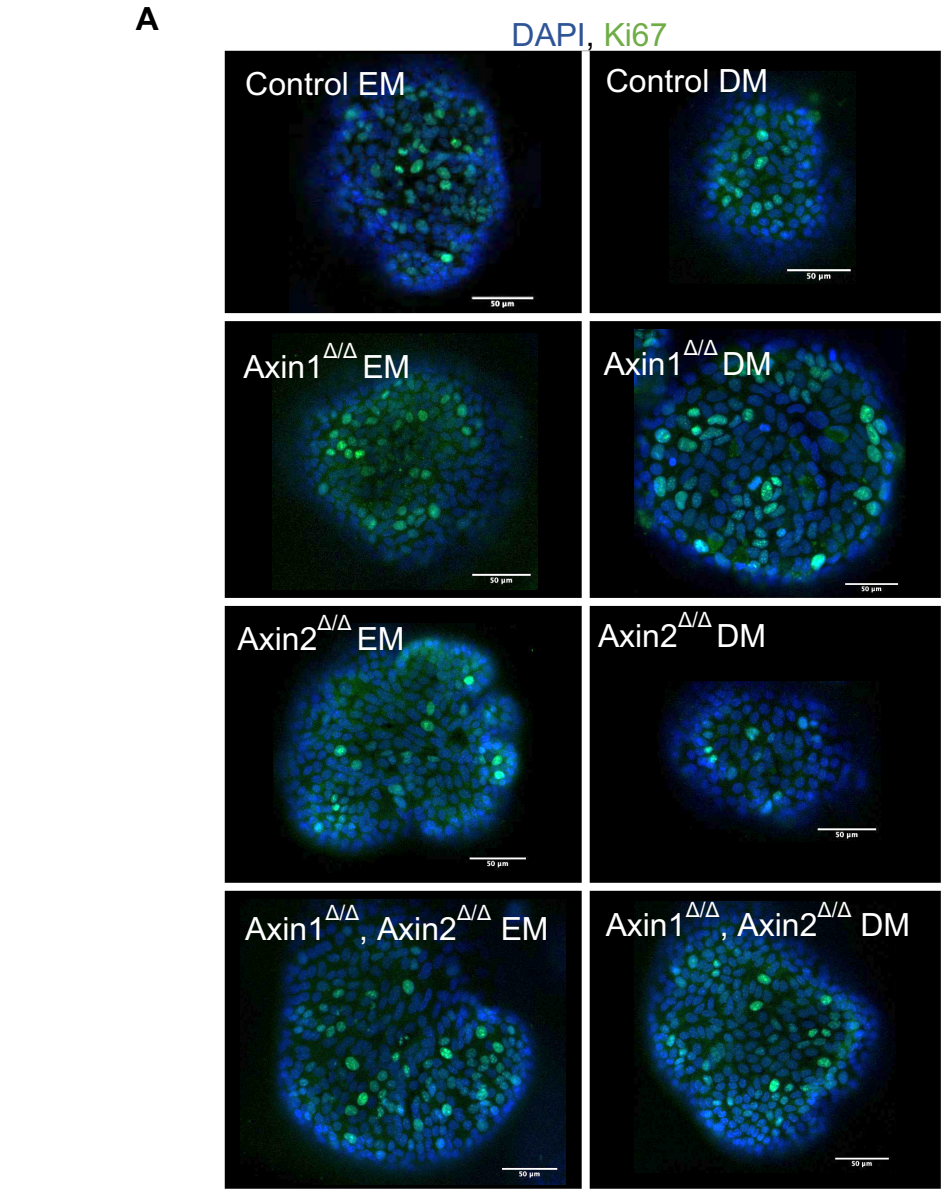

Figure 5.23 Immunofluorescence analysis of Ki67 staining of organoids grown in EM and DM.
(A) Representative images of Ki67 staining of organoid lines grown in EM and DM. Scale bar 50 μm **(B)** Quantification of Ki67 staining in organoids lines. Data represents n = 3 biological replicates and 3-4 technical replicates (organoids per organoid line). Significance was calculated using Ordinary One-Way ANOVA with Tukey's multiple comparison test *p<0.05, **p<0.01

5.5.9 γH2AX staining in Axin deleted organoids.

Increased levels of γH2AX, a marker of double strand breaks, were observed in AhCreER^{T} Axin1$^{\Delta/\Delta}$ and AhCreER^{T} Axin1$^{\Delta/\Delta}$, Axin2$^{\Delta/\Delta}$ mouse livers at 6 days post induction. To further evaluate the use of the BD organoid system to evaluate Axin loss, stably induced organoids were stained for γH2AX (Figure 5.24A). Counts were automated by use of CellProfiler open-source software. Masks were created for each nucleus in an organoid with further masks for each individual foci of γH2AX staining (see appendix for details).

No differences were seen in the levels of γH2AX staining between any of the cohorts grown in EM or DM (Figure 5.24B).

5.5.10 Yap, Wwtr1 and Yap target expression in Axin deleted organoids.

The Hippo pathway, in particular Yap expression and downstream targets, were looked at as an alternative link to the increases in proliferation seen in Axin deleted livers. AhCreER^{T} Axin1$^{\Delta/\Delta}$, Axin2$^{\Delta/\Delta}$ mouse livers at 6 days and at 1 month post induction showed a trend for increases in the expression of *Birc5* and *Hmmr* from the panel of Yap, Wwtr1 and Yap target genes. The same panel was used to directly compare expression in stably induced Axin deleted organoids with the *in vivo* scenario.

No significant differences were seen in the expression of *Yap*, *Wwtr1*, *Cyr61*, *Ctgf*, *Gpc3*, *Birc5*, *Fas*, *Sfrp1* and *Hmmr* in Axin deleted organoids grown in EM or DM (Figure 5.25A, B). Some trends for increases were observed for *Sfrp1* in EM and DM however, these were not significant due to variation between different lines within in each cohort.

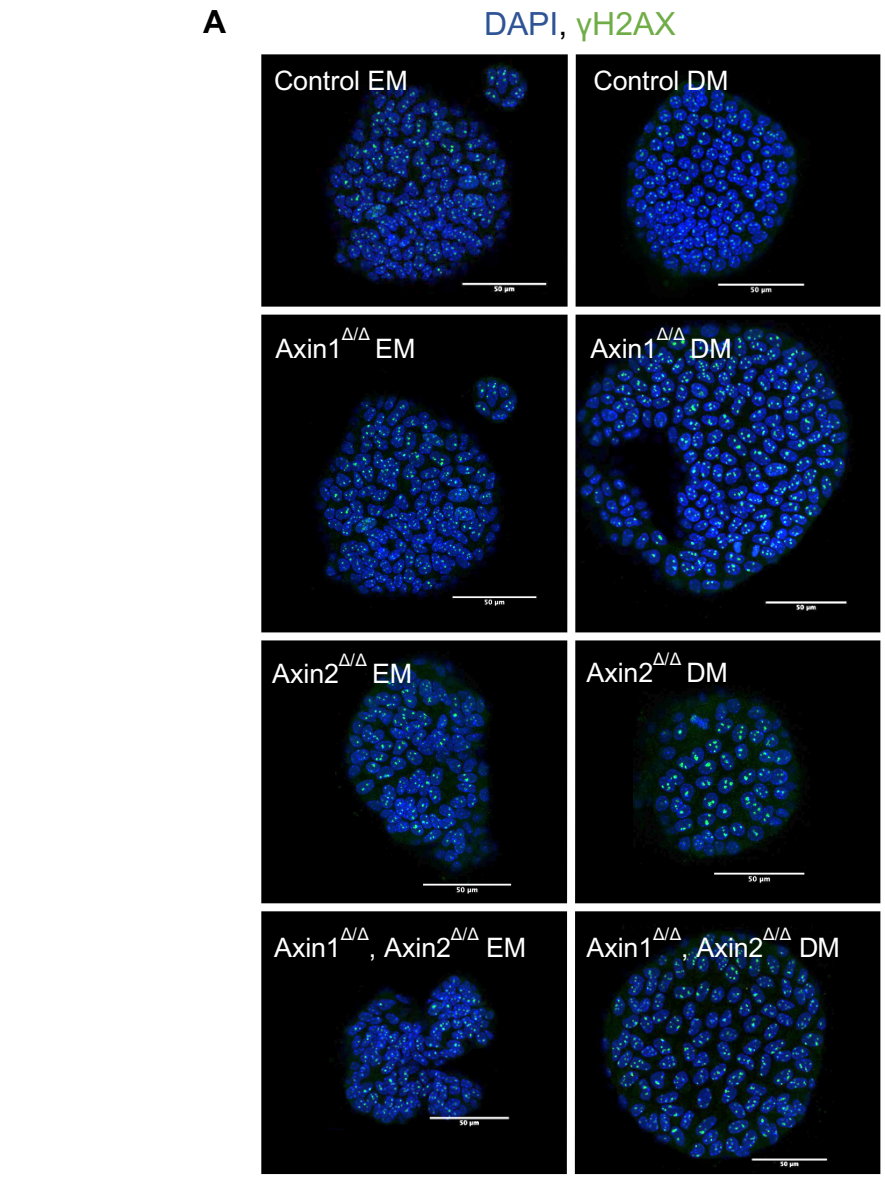

Figure 5.24 No difference in γH2AX foci in Axin deleted BD organoids grown in EM or DM.
(A) Representative images of γH2AX staining in organoid lines grown in EM or DM. Scale bar 50 μm **(B)** Quantification of staining in organoids n = 3 biological replicates and 3-4 technical replicates (organoids per organoid line). Counts represent the average number of γH2AX foci per nucleus, averaged per organoid. 3-4 organoids were scored for each biological replicate.

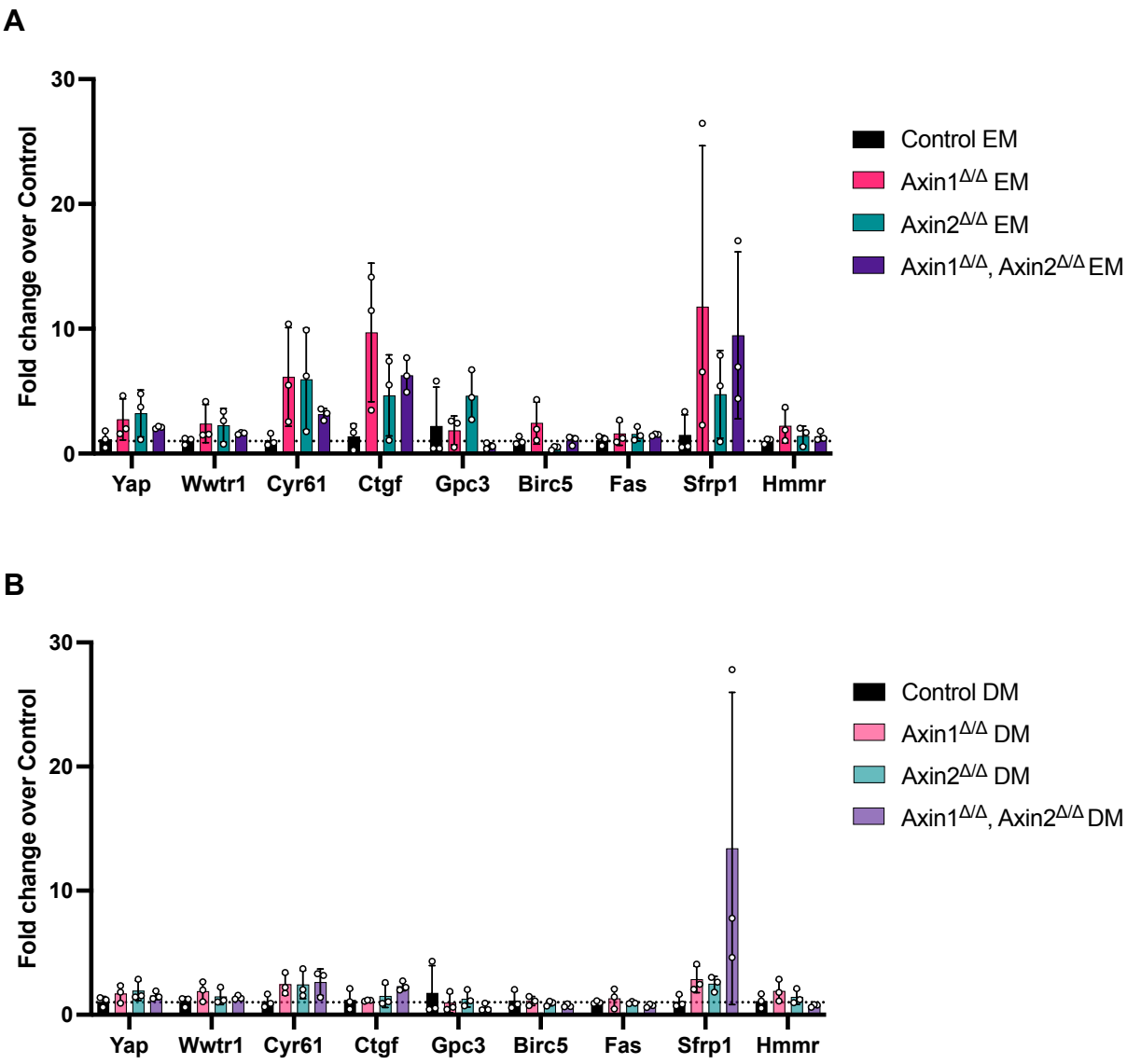

Figure 5.25 RT-qPCR analysis of Yap, Wwtr1 and Yap downstream target expression levels in Axin deleted BD organoids grown in EM and DM

Changes in gene expression of Axin deleted organoids grown in expansion media (EM) **(A)** and in differentiation media (DM) **(B).** Data represents mean ±s.d. n = 3 biological replicates. Data was normalised to B2M and is shown as the relative fold change to AhCreER^{+}, Axin1$^{+/+}$, Axin2$^{+/+}$ (Control) in EM media **(A)** or DM media **(B).**

5.5.11 Alternative stable induction strategy using CAG-Cre:GFP.

To mitigate the possibility that the observed results were due an adaptation to BNF in culture at the induction stage, an alternative stable induction strategy that used CAG-Cre-GFP was used to compare key results observed in AhCreER^{T} Axin1$^{\Delta/\Delta}$, Axin2$^{\Delta/\Delta}$ organoids. Liver fragments from three AhCreER^{T} negative but Axin1$^{fl/fl}$, Axin2$^{fl/fl}$ mice were used to establish BD organoids. Organoids were transiently transfected with a CAG-Cre:GFP fused plasmid (Matsuda and Cepko 2007) based on the transfection protocol outlined in (Broutier et al. 2016). Transfected cells were allowed 3 days to recover in culture before being dissociated to single cell and FACS sorted for GFP+ cells. GFP+ cells would have been exposed to Cre and therefore should have undergone recombination. Sorted cells were expanded as necessary before being seeded for expansion and differentiation and subsequent analysis (Figure 5.26). Unfortunately, only 2 lines were able to be established after FACS sorting from the 3 transfected lines. Cohorts of control, AhCreER^{T} Axin1$^{\Delta/\Delta}$, Axin2$^{\Delta/\Delta}$ stably induced with BNF and 4-OHT and AhCreER^{T} Axin1$^{\Delta/\Delta}$, Axin2$^{\Delta/\Delta}$ stably induced with CAG-Cre:GFP were set up to assess recombination, viability and key RT-qPCR results, Lgr5, Axin2 and Albumin. The hypothesis being that stable induction using either method would have the same outcome.

Levels of the unrecombined Axin1$^{fl/fl}$ allele using primer pair A (Figure 5.14A) were reduced by 97% and 99.8% in Axin1$^{\Delta/\Delta}$, Axin2$^{\Delta/\Delta}$ samples grown in EM using stable induction with BNF, 4-OHT, and GAG-Cre:GFP induction protocols respectively (Figure 5.27A). The expected increases in levels of the shorter recombined Axin1$^{\Delta/\Delta}$ allele using primer pair B (Figure 5.14A) were detected in both induction strategies (Figure 5.27B).

Viability as assessed by CellTiter-Glo 3D was equivalent between both cohorts of Axin deleted organoids grown in EM and DM (Figure 5.27C). Organoid size was not observed to be different between either Axin deleted organoids in EM or DM, but this was not quantified (Figure 5.27D).

As seen previously, *Lgr5* expression was greatly increased in Axin1$^{\Delta/\Delta}$, Axin2$^{\Delta/\Delta}$ organoids grown in DM using either stable induction method. Expression of *Axin2* using primers targeting the c-terminal of the transcript were significantly higher in Axin1$^{\Delta/\Delta}$, Axin2$^{\Delta/\Delta}$ organoids in EM. In DM conditions, *Axin2* expression of the remaining exons was found to be 156 and 198-fold higher in AhCreER^{T} and CAG-

Cre:GFP induced organoids respectively. Expression of transcripts containing exon 2 of *Axin2* in Axin deleted BD organoids was down by 99-100% (data not shown) suggesting near complete recombination thus the increase in expression of *Axin2* is from recombined cells that results in transcripts that do not contain exon 2. Albumin expression was found to be significantly lower in DM conditions in $Axin1^{\Delta/\Delta}$, $Axin2^{\Delta/\Delta}$ organoids using both induction methods (Figure 5.28).

Overall, these results suggest that the increases in *Lgr5* and *Axin2* (transcripts without exon 2), and the decrease in *Albumin* expression in combined Axin1 and Axin2 deleted BD organoids are independent of the induction method used. This increased stem cell like phenotype may in part contribute to the tumourigenesis seen in double Axin deleted liver.

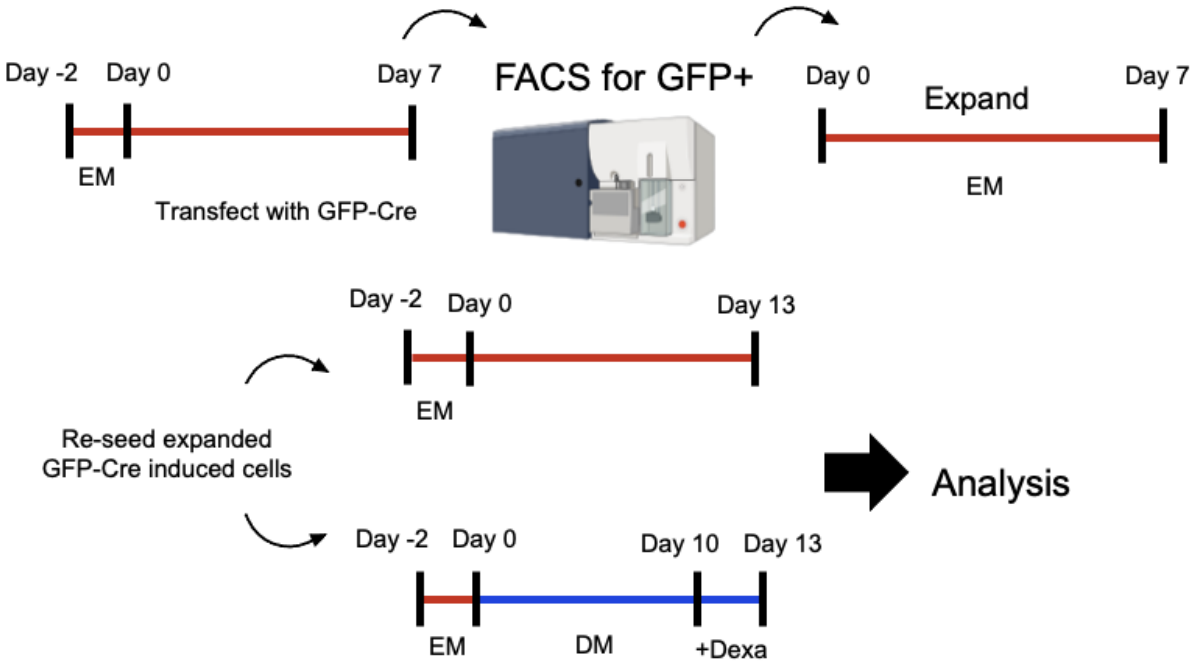

Figure 5.26 GFP-Cre Bile Duct organoid induction strategy.
Schematic for stable transfection induction strategy. Organoids were transfected with GFP-Cre then sorted for GFP+ cells which would indicate cells that have been exposed to Cre and undergone recombination. Collected GFP+ cells were expanded until enough were generated for seeding for the differentiation protocol and any subsequent analysis.

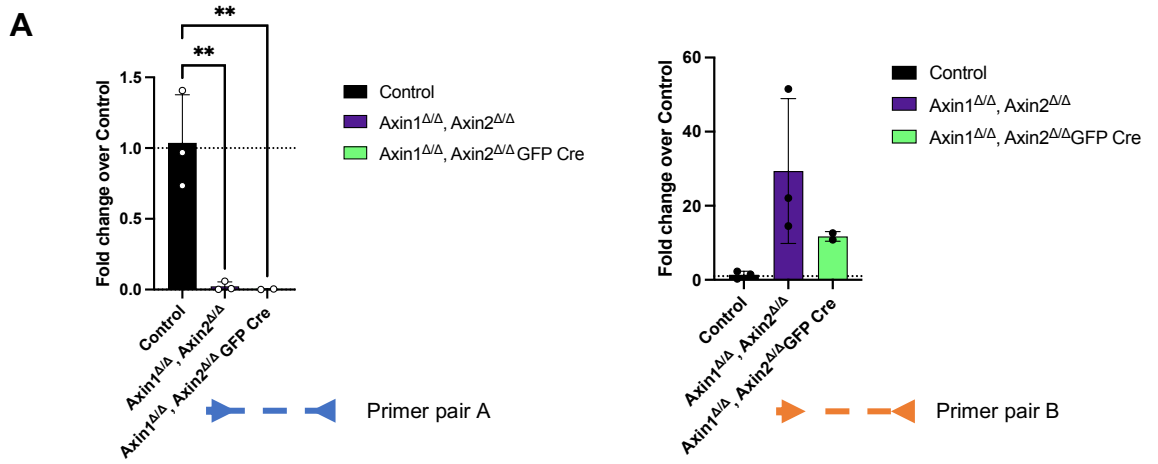
A
**
**
Fold change over Control
1.5
1.0
0.5
0.0
Control
Axin1Δ/Δ, Axin2Δ/Δ
Axin1Δ/Δ, Axin2Δ/Δ GFP Cre
Control
Axin1Δ/Δ, Axin2Δ/Δ
Axin1Δ/Δ, Axin2Δ/Δ GFP Cre
Primer pair A
Fold change over Control
60
40
20
0
Control
Axin1Δ/Δ, Axin2Δ/Δ
Axin1Δ/Δ, Axin2Δ/Δ GFP Cre
Primer pair B

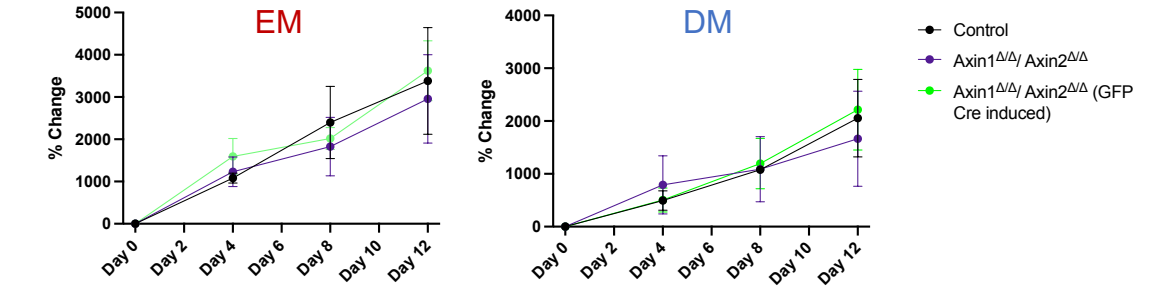
B
EM
% Change
5000
4000
3000
2000
1000
0
Day 0
Day 2
Day 4
Day 6
Day 8
Day 10
Day 12
DM
% Change
4000
3000
2000
1000
0
Day 0
Day 2
Day 4
Day 6
Day 8
Day 10
Day 12
Control
Axin1Δ/Δ/ Axin2Δ/Δ
Axin1Δ/Δ/ Axin2Δ/Δ (GFP Cre induced)

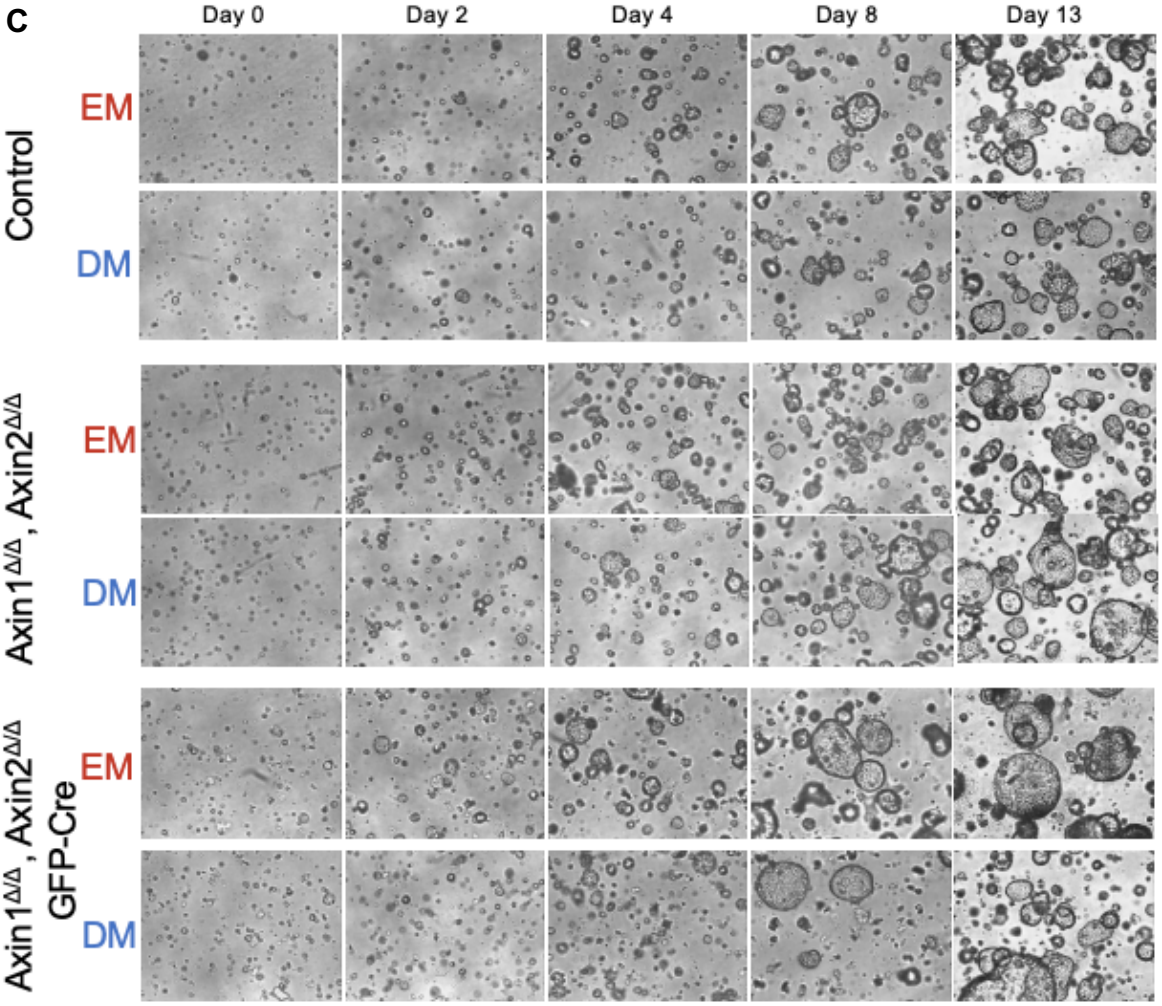
C
Day 0
Day 2
Day 4
Day 8
Day 13
Control
EM
DM
Axin1Δ/Δ, Axin2Δ/Δ
EM
DM
Axin1Δ/Δ, Axin2Δ/Δ GFP-Cre
EM
DM

Figure 5.27 Comparison of recombination and viability using alternative stable induction strategies.
(A) qPCR results using primer pair A showed comparable recombination levels of 97% and 99.8% of Axin1 in Axin1 and Axin1, Axin2 deleted bile-duct organoids using Stable induction strategies with BNF/4-OHT and CAG-Cre:GFP. **(B)** qPCR results using primer pair B showed between high increases of the recombined allele in Axin1 and Axin1, Axin2 deleted bile-duct organoids for both induction strategies. DNA was collected from organoids grown in EM. Data was normalised to *ApoB* and is shown as the relative fold change to Control organoids. n=2-3, error bars: SD. Significance was calculated using One-Way ANOVA with Tukey's multiple comparison test. **p<0.01 **(C)** CellTiter-Glo viability analysis of control and Axin deleted organoids induced with BNF/4-OHT and CAG-Cre:GFP in expansion and differentiation media n = 2-3 done in triplicate **(D)** Representative images of stably induced organoids grown in EM and DM at varying time-points. Scale bar 100 μm

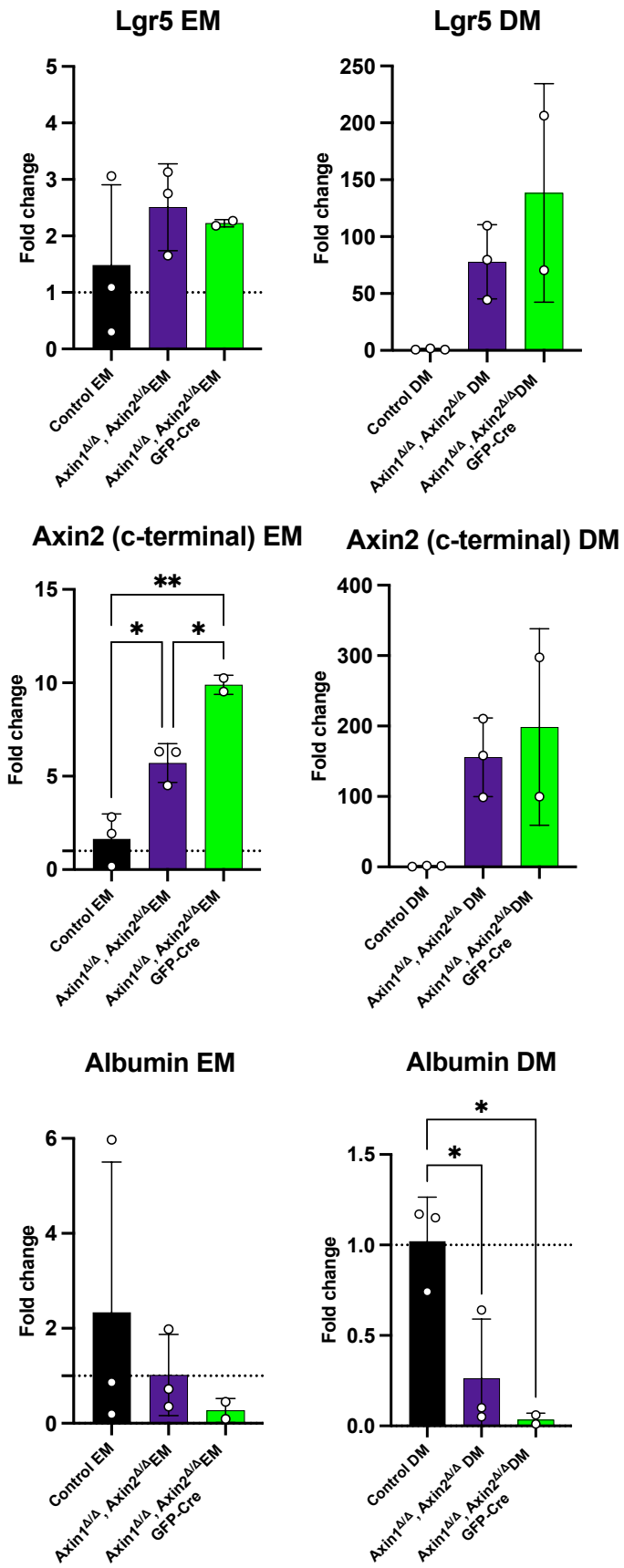

Figure 5.28 RT-qPCR analysis of key expression changes comparing induction strategies showed comparable results.
Changes in *Lgr5*, *Axin2* (C-terminal), and *Albumin* expression in organoids of AhCreER^{T} Axin1$^{\Delta/\Delta}$, Axin2$^{\Delta/\Delta}$ cohorts using different induction methods in EM and DM. Data represents mean ±s.d. n = 2-3 biological replicates. Data was normalised to B2M and is shown as the relative fold change to AhCreER^{+}, Axin1$^{+/+}$, Axin2$^{+/+}$ (Control). Significance was calculated using Ordinary One-Way ANOVA with Tukey's multiple comparison test *p<0.05, **p<0.01

Chapter 6: Discussion

6.1 Combined Axin1 and Axin2 deletion results in liver tumourigenesis

This thesis has described the deletion of Axin1, Axin2, and the combined deletion of both Axin1 and Axin2 in the mouse liver and BD organoids. *In vivo*, it was observed that AhCreER^{T} Axin1$^{\Delta/\Delta}$, Axin2$^{\Delta/\Delta}$ mice (hereafter referred to as DAX - Double Axin deleted) became moribund due to the presence of liver tumours as early as 8 months post induction.

Although not common, combined *AXIN1* and *AXIN2* mutations in human HCC have a Log2 odds ratio of 1.353 with a tendency to co-occur (C-Bio Portal data see Introduction section 1.5) arguing for the physiological relevance of this study as a model of cancers that display alterations to the expression or function of all four Axin alleles.

The classical two-hit model of cancer proposes the development or progression of cancers results from the combination of two distinct genetic alterations or "hits" in a cell's DNA for a single gene. The first hit, typically a germline mutation, creates a predisposition for the cell to acquire further mutations in the second allele, but is usually not enough to cause cancer alone. The second hit is typically a somatic mutation that occurs in the same cell as the first hit, and together with the first hit, results in the development of cancer. The second hit is thought to be the critical event that ultimately triggers the cancerous transformation of the cell. The two-hit model applies to many different types of cancers and suggests that at least two mutations are necessary for cancer to develop (Chernoff 2021). Some types of cancer may require more than two hits, while others may require only one hit if the mutation affects a critical gene or pathway. Axin1 deletion alone using the same floxed allele previously resulted in late onset of HCC (Feng et al. 2012). However, it has also been reported that loss of Axin1 alone is not sufficient for liver tumourigenesis (Qiao et al. 2019). Results in this thesis may be used to argue for an extension of the classical two hit model of cancer to include multiple alleles of closely related genes. Axin1 and Axin2 have previously been shown to be functionally equivalent in mouse development following the replacement of the coding region of Axin1 with sequences from Axin2 (Chia and Costantini 2005). In the context of Axin1 deleted HCC, the resulting increased expression of *Axin2* could

thus initially be acting in a partially functionally compensatory manner but may subsequently predispose to mutations in *Axin2*.

In some cases, the second hit may be caused by exposure to environmental factors such as chemicals or radiation. Alternatively, it may be a result of errors in DNA replication or repair. Axin1 has been shown to be important in mitotic fidelity (Poulton et al. 2013). Here we showed that Axin1 deletion significantly increased levels of γH2AX thus creating an environment in which additional mutations are more likely to occur.

While the two-hit model was originally formulated to describe the genetic basis of tumour suppressor gene inactivation, it has been expanded to include other mechanisms of inactivation or loss of function of these genes. For example, epigenetic alterations such as DNA methylation, histone modifications, and changes in chromatin structure can result in the silencing of tumour suppressor genes without altering the DNA sequence. Methylation of *Axin2* has been suggested to be a marker of poor prognosis and recurrence in colon cancer (Kandimalla et al. 2017) and has been found to be present in 16% of cases of non-small cell lung carcinoma (Paschidis et al. 2022). Methylation of secreted frizzled related protein (SFRP) is frequently found in HCC cell lines and primary cases (Takagi et al. 2008). The second hit may thus be associated with aberrant suppression of Axin2 through methylation. Alternatively, as *Axin2* expression is found to be zonated (Halpern et al. 2017) within the normal liver, functional compensation may be zonally constrained.

In a previous study using the same *Axin1* allele (Feng et al. 2012), 55% of mice developed liver tumours with features of HCC at 1 year post AhCre mediated induction. In this thesis, despite our data recapitulating the initial increase in proliferation following Axin1 deletion, the AhCreER^T directed deletion of Axin1 alone did not lead to macroscopic signs of HCC after 1 year of age (total 8 animals). Several reasons could explain this including i) Lower levels of recombination: AhCreER^T mediated recombination was associated with slightly lower levels of recombination compared to AhCre (66% for AhCreER^T at day 6 and 90% AhCre and day 4 for Axin1 in the liver (Figure 3.3)) which may have resulted in an insufficient number of recombined cells required for tumourigenesis. ii). Founder effects on ‘outbred’ diversity. Mice generated for use in this thesis were kept on an outbred background to more closely resemble the genetic diversity found in human populations. Though this is an advantage in one sense, the genetic variability in an outbred population can make it more difficult to

detect associations of the genetic variation of one gene and the disease being studied, Axin1 and HCC in this case. In a recent study, (Benegiamo et al. 2023) the genetic background of mice was shown to vary in response to metabolic challenge and in a review by (Maronpot 2009), inbred strains were reported to have varying susceptibility to hepatocarcinogenesis. Factors such as founder effect from the original AhCreER^T mouse used to establish the colony or genetic drift may have played a part in the observed lack of HCC development in Axin1 deleted mice in this thesis. In a study by Qiao (Qiao et al. 2019), CRISPR-Cas9-mediated gene editing to delete Axin1 in mouse hepatocytes *in vivo* did not result in tumourigenesis (although this was only up to 20 weeks post induction) and tumour formation required the additional activation of c-Met. iii). Differences in local mouse environment. Mouse hepatitis virus (MHV) was endemic within the facility at the time of the original Axin1 studies. Different MHV strains have varying effects on the mouse liver and depends on the strain of mouse (Hefler et al. 2021). The outbred background of mice used in this study may also have conferred some protection or variability in response to the local environment. Repeating deletion of Axin1 with the original Cre-drivers in a clean animal unit may be helpful in identifying these possible confounding effects.

The development of HCC during the studies described in this work required both Axin1 and Axin2 deletion. Four animals becoming moribund before 1 year due to liver tumours and although 55% of all DAX mice developed liver tumours, 4 out of 8 females had to be culled, prior to the detection of HCC, due to growth of mammary tumours. AhCreER^T drives efficient recombination in the epithelial cells of the GI tract such as the liver and small intestine however, recombination using the Ah promoter has also been observed in the bladder, seminiferous vesicles, (Ireland et al. 2004) heart and kidney (Kemp et al. 2004) and it has been suggested that the Ah promoter may be promiscuously active in some tissues during development. Whether the dual induction protocol using BNF and Tamoxifen efficiently activated Cyp1a1 expression in mouse mammary tissue was not assessed in this thesis however it is interesting to note that up to 90% of breast cancers have been found to constitutively express Cyp1a1 (Murray et al. 2010; Rodriguez and Potter 2013). Furthermore, *AXIN2* germline mutations and polymorphisms are associated with increased risk of breast cancer (Marvin et al. 2011; Aristizabal-Pachon et al. 2015). Combined *AXIN1* and *AXIN2* deep deletion is also found in approximately 9% of breast cancer tumours (cBioPortal, The Metastatic Breast Cancer Project). Recombination of Axin1 and Axin2 might later be assessed in

the archived tumour material generated in the work described here to give an indication whether their deletion may be playing a role. Later studies could then combine the Axin alleles with a more appropriate mammary-specific Cre such Blg Cre (Selbert et al. 1998), WAP-Cre (Wagner et al. 1997a) or MMTV Cre (Wagner et al. 1997) in future breast cancer studies.

A possible concern is whether the effects of Axin deletion in the liver are cell intrinsic or whether the phenotypes result from changes in other tissues in which Axin was deleted. In the AhCre strain, the activation of Cre expression is governed by the rat cytochrome P450 1A1 (CYP1A1) promoter, which undergoes transcriptional up-regulation in response to β-naphthoflavone. Notably this is most strongly induced in the liver and intestinal epithelium as demonstrated in a study by Ireland et al. in 2004. AhCreER^{T} is regulated transcriptionally through the CYP1A1 promoter, similar to AhCre. However, the activation of the Cre-ER fusion protein depends on the additional binding of tamoxifen, minimizing background recombination observed with AhCre. Preliminary assessment of AhCre and AhCreER^{T}; Axin1 deleted small intestine in the Dale lab did not show significant changes to proliferation or apoptosis at early or late timepoints (data not shown). This is supported in the study by Sanson et al. 2023, where Axin1 was found to be dispensable for normal homeostasis of the intestinal epithelium. However, their data suggests that Axin1 deficiency rendered mice more susceptible to chemically induced carcinogenesis, but reduced DSS induced colitis. They indicate that Axin1 plays a role in promoting an inflammatory response with tumor-suppressing capabilities in intestinal epithelial cells and that this response is characterized with an IFNγ/Th1 proinflammatory immune program. Whether *Axin* deletion in this study altered the immune response in the liver was not assessed however, an immune infiltrate phenotype was not noted during assessment of Axin deleted livers. There is also the possibility that the gene deletion strategy used in this study also results in the deletion of Axin in immune cells. To explore the potential impact of Axin loss in immune cells on tumor progression, one could conduct experiments using immune cell specific Cre deletion, hepatocyte specific Cre deletion, and combined immune/hepatocyte deletion.

Importantly, the DAX liver tumours appeared similar to those previously generated by Axin1 deletion by Feng (2012), having a similar phenotype including high levels of proliferation, high levels of expression of AFP and a histological trabecular pattern with pleomorphic hepatocytes. These features are also associated with the

hyperproliferative subset of HCC tumours (Cluster A (Lee et al. 2006), G1-G2-G3 class (Boyault et al. 2007), S1, S2 class (Hoshida et al. 2009)) making them relevant to human disease. Additionally, this study found an oncogenic Yap signature appeared in tumours emerging in the background studied, consistent with the findings from (Abitbol et al. 2018) in human and mouse *AXIN1/Axin1* mutant tumours.

Approximately half of the tumours from DAX mouse livers showed nuclear accumulation of β-catenin. This contrasts with the tumours generated in the study by Feng (2012) with just Axin1 deletion, where they observed only very few cells with nuclear β-catenin within tumours. Aberrant β-catenin staining was observed in 80% of tumours with activating β-catenin mutations suggesting that the combination of gene deletions present in the DAX genotype may predispose to the activation of the canonical Wnt/β-catenin pathway, although not with the same frequency as that observed in β-catenin mutants (Abitbol et al. 2018). Importantly however, β-catenin mutation led to the early stabilisation of β-catenin levels in mutant animals while the immediate early consequences of deletion in DAX livers did not result in a clear strong Wnt ON phenotype. This suggests that tumours generated in this study required additional mutational events prior to the stabilisation of β-catenin and its nuclear accumulation. Multi-step tumorigenesis is the process by which cancer develops through a series of genetic and cellular changes. The complex and multifactorial processes involving the accumulation of multiple genetic mutations and epigenetic alterations that ultimately result in tumours in the livers of DAX mice may have started with the proliferative advantage the Axin1 deleted cells gained following induction. In conjunction with the observed increased levels of γH2AX, a marker for double strand breaks, over time, additional mutations and genetic alterations likely accumulated in these abnormal cells, which would have led to further changes in their growth and behaviour. At some point in this process, it is likely Axin2 loss will have generated an additional growth advantage. As these tumours did not arise quickly after induction it would seem they needed time to acquire additional alterations in the expression of oncogenes and tumour suppressor genes, changes in DNA methylation patterns and alterations in the structure and organization of chromosomes. Sequence analysis of the Axin tumours looking for mutations and gene expression patterns in the future would provide valuable information to identify the mutations and changes involved.

The hypothesis at the start of the studies described was that Axin2 compensated for Axin1 loss at early times following deletion. This led to the prediction that dual

deletion of Axin1 and Axin2 would lead to the stabilisation of β-catenin. This acute deregulation of β-catenin levels was not observed. Interestingly, numerous mouse models have reported that the excessive expression of β-catenin in the liver or the presence of mutated, constitutively active β-catenin alone does not increase proliferation or lead to the development of HCC, indicating the requirement for cooperation with other pathways (Cadoret et al. 2002; Harada et al. 2002; Nejak-Bowen et al. 2010; Tao et al. 2016). Tumourigenesis in mouse models expressing β-catenin mutant proteins required the further expression of other tumour oncogenes / activation of other molecular pathways. DAX livers did not result in the expected strong Wnt ON phenotype at the early timepoint at 6 days post induction as seen with Apc deletion (Benhamouche et al. 2006; Reed et al. 2008). Despite no noticeable changes to levels or the localization of β-catenin or alteration to zonation as assessed with GS staining, DAX livers still developed tumours. The question as to whether the mechanism linking the loss of both alleles in DAX mice involves altered canonical Wnt/β-catenin signalling therefore remains unclear. It is possible that some Wnt/β-catenin signalling is involved in the early tumourigenic phenotype if the levels of pathway activation are not regarded as either 'on or off'. Perhaps then, Wnt/β-catenin signalling pathway in the context of Axin1 and Axin2 deletion, and more specifically in the liver, is governed by a regulatory mechanism that corresponds to 'just right' levels of Wnt/β-catenin pathway activation as originally proposed in (Albuquerque et al. 2002). The 'just right' hypothesis, was based on work carried out using APC mutations resulting in various truncations of the protein and suggested that the oncogenic truncations of APC conferred a sub-maximal level of Wnt signalling that was sufficient for cell transformation, but which does not lead to cytotoxicity. Levels of Wnt/β-catenin pathway activation that exceed a certain threshold are hypothesized to lead to a toxic environment where the levels of apoptosis counter-act the tumourigenic phenotype. This was nicely demonstrated in a study with the over stimulation of the Wnt/β-catenin pathway in a mouse model of intestinal tumourigenesis (Méniel et al. 2013). Expression of the Wnt target gene *Cited1* increases following Apc loss in intestinal epithelial cells and was found to be increased in human colorectal tumours. Combined Apc loss and Cited1 deficiency was shown to increase aspects associated with Apc loss alone such as Wnt pathway deregulation and cell death. However, this turned out to be protective and increased survival, in part due to the enhanced apoptotic phenotype observed after Apc loss alone. The 'just right' hypothesis of canonical Wnt

pathway activation has also previously linked distinct levels of Wnt/β-catenin signalling to distinct physiological outcomes in different tissues, with studies of Apc alleles in multiple tissues suggesting that the liver requiring lower levels of Wnt/β-catenin activation for tumour formation compared to the intestine (Buchert et al. 2010). The majority of APC mutations may result in too high a level of Wnt/β-catein pathway activation in the liver and could be part of the reason why so few cases of HCC present with APC mutations compared to CRC.

Differences between Apc deleted liver (Benhamouche et al. 2006; Reed et al. 2008) and DAX liver included a lack of nuclear β-catenin and no change to zonation as assessed by GS expression in the DAX liver. This leaves the possibility that total loss of both Axin alleles in the liver only leads to partial activation of Wnt/β-catenin signalling. This could be because there may be some additional yet-to-be discovered mechanism that could minimize β-catenin levels such as alterations in synthesis of mRNA (proven mechanism), or via some other mechanistic difference in the tissue that hasn't been identified yet. This could include the activation of unknown negative feedback loop, deacetylation of β-catenin (Chen et al. 2019), interference of β-catenin transcriptional co-activators or upregulation of miRNAs that can post-transcriptionally regulate β-catenin by inhibiting translation or promoting degradation (Lei et al. 2020).

However, observations in recent study by (Sanson et al. 2023) using alternative Axin alleles showed that the combined ablation of Axin1 and Axin2 in hepatocytes did result in aberrant activation of Wnt/β-catenin signalling, as assessed by GS staining, in the entire liver lobule. This phenocopied Apc deficient hepatocytes and the predicted DAX phenotype prior to the work described in this thesis. One possibility to explain the differences between the studies described here and the Sanson data could be whether the alleles under study functioned as null alleles in the liver. The next section will consider this evidence and how this matters for liver tumourigenesis.

6.2 Mechanisms linking Axin allele genotype and phenotypes.

The conditional *Axin1* allele that was used in this thesis, was generated within this laboratory (Feng et al. 2012; Offergeld 2015 Phd Thesis) and involved the insertion of loxP sites either side of exon 2 which contains the AUG start codon and RGS domain. Immunoprecipitation and western blot analysis of liver extracts from Axin1$^{\Delta/\Delta}$

mice using a polyclonal antibody raised against a peptide corresponding to the last 10 amino acids of the mouse Axin1 protein showed that a ≈ 120kd protein present in $Axin1^{WT/WT}$ liver was absent from liver tissue from $Axin1^{\Delta/\Delta}$ mice. Additionally, the CMV-Cre mediated recombination of the $Axin1^{fl/fl}$ allele in embryos, phenocopied the classic $Axin1^{Tg1/Tg1}$ allele, a transgene insertion into the locus, that has widely been assumed to be a true null (Perry et al. 1995; Zeng et al. 1997). This allele showed embryonic lethality at E 9.5 and was associated with a variety of defects such as forebrain truncation and axis duplication.

No indication of a truncated form of Axin1 that was expressed in the $Axin1^{\Delta/\Delta}$ livers was detected however, the expression of low levels of a truncated protein at levels below the detection limit of the Western technique used could not be excluded. A search for alternative start codons in alternatively spliced Axin mRNAs (lacking exon 2) raised the possibility that a fragment might be generated that lacked the RGS/APC/tankyrase binding domain but did contain the central GSK-3 / β-catenin binding sites and the C-terminal DIX domain (Offergeld 2015 PhD thesis). In more recent work (Offergeld; unpublished), Axin1 immunoprecipitation and concentration of Axin1 in $Axin1^{\Delta/\Delta}$ ES cell lysates identified a band, which corresponded to the expected length of a possible deleted Axin1 protein, suggesting that the exon 2 deleted allele might be produced in particular cellular contexts. Whether this gene product would retain any functionality is not known.

The conditional *Axin2* allele was generated by Gui Jie Feng using similar methodology to that for *Axin1*, with loxP sites being inserted that flanked exon 2, which also contains the start codon and RGS domain. Unfortunately, and by contrast with the human protein, there are no good anti-mouse Axin2 antibodies, that bind to sequences outside exon 2. Sequence analysis of the $Axin2^{\Delta/\Delta}$ protein by Anika Offergeld predicted 4 potential ORFs with protein sequences that contained β-catenin binding region and DIX domain (Offergeld 2015 PhD thesis). It therefore remains possible that the $Axin2^{\Delta/\Delta}$ allele might be able to generate a truncated protein that retains some residual function.

As it could not be determined whether an Axin2 protein was being made, Anika Offergeld compared the allele to a commercially available Axin2 deleted mouse line (Lustig et al. 2002a). The $Axin2^{lacZ/lacZ}$ has the LacZ gene inserted into exon 2, replacing most of the exon. It is presumed null, but there is little evidence that confirms or disproves this. The $Axin2^{lacZ/lacZ}$ mouse has been shown to be viable and fertile and shows only minor defects in embryonic skull formation (Yu et al. 2005). When the

embryonically active CMV-Cre was used to delete the floxed *Axin2* allele studied here, the embryos generated were found to be greatly reduced in size and died at E 9.5. The more severe phenotype of the $Axin2^{\Delta/\Delta}$ allele compared to the $Axin2^{lacZ/lacZ}$ allele might mean that $Axin2^{\Delta/\Delta}$ function is first essential during embryogenesis but could also mean that a deleted protein is expressed from the allele that is embryonically lethal. Heterozygous embryos were found to have a range of phenotypes ranging from no observable phenotype to major reductions in head size and head development. The differences in phenotype may have been down to varying levels of recombination and presence of wild type Axin2 protein. These phenotypes in head development were similar to previously described anterior-posterior (A-P) embryonic defects that have been linked to aberrant Wnt pathway activation (Petersen and Reddien 2009). In particular, the phenotypes of $Axin2^{\Delta/\Delta}$ and $Axin2^{\Delta/WT}$ resembled the range of phenotypes presented in (Fossat et al. 2011) with the increasing levels of β-catenin/TCF hyperactivation leading to increased head truncation. Taken together, the data suggests that $Axin2^{\Delta/\Delta}$ allele in the embryo activates Wnt/β-catenin regulatory function. Interestingly, $Axin2^{lacZ/lacZ}$ adult animals have shorter noses, a characteristic that has also been linked to with overactive embryonic Wnt/β-catenin pathway activity. These data contrast with the results from the liver where deletion of the $Axin2^{\Delta/\Delta}$ allele appeared to be linked to lower than expected Wnt pathway activity.

As a marker of Wnt pathway activity, reduced GS is seen in livers infected with the adenoviral vectors expressing the canonical Wnt pathway inhibitor Dkk1 (Benhamouche et al. 2006) or following liver specific deletion of β-catenin (Sekine et al. 2006). The reduced GS staining surrounding the CV and lower expression of *Lgr5* in $Axin2^{\Delta/\Delta}$ livers suggests that deletion inhibits Wnt/β-catenin signalling. The simplest explanation for this is that a truncated Axin2 protein is expressed in the liver from the $Axin2^{\Delta/\Delta}$ allele that has a greater inhibitory effect than WT Axin2.

There is some precedent for the idea that a mutant or truncated Axin2 protein could have greater inhibitory effects on β-catenin/TCF outputs compared to the WT protein. Investigations carried out on the more stable Axin2 mutant protein ($Axin2^{canp}$) resulting from a V26D substitution within the evolutionarily conserved N-terminal Tankyrase binding motif (Qian et al., 2011) showed that this mutant was lethal during mid-gestation, manifesting aberrations in cardiac, caudal, and primitive streak morphogenesis. However, $Axin2^{canp}$ mutants showed reduced levels of TCF-reporter

activity, the apparent opposite of the phenotype suggested by our preliminary studies of the CMV-Cre, Axin2$^{fl/fl}$ embryos (Offergeld 2015 PhD thesis). In most tissues, a reduction in Wnt signalling activity has been linked to increased expression of Axin2 or a more stable Axin2 protein. This suggests that Axin function and phenotypes may be very dependent on context and that additional studies in both the liver and embryo may be required to identify the mechanisms driving the phenotypes observed.

The hypothesis that a truncated Axin2 protein missing exon 2, more specifically the RGS domain, results in a greater inhibitory effect of β-catenin, is supported with the data from the study by (Bernkopf et al. 2019). The study identified an aggregon (aggregation) site within the RGS domain of Axin2 (Q188, V189) that reduces Axin protein polymerization mediated by the C-terminal DIX domain. The formation of the β-catenin destruction complex and the subsequent degradation of β-catenin requires the polymerization of Axin and is associated with the formation of distinct puncta. Axin2 is less efficient in forming puncta than Axin1 and is as a consequence thought to be less efficient in degrading β-catenin (Bernkopf et al. 2015). Bernkopf used multiple methods to show that Axin2 puncta formation was more efficient if the function of the N-terminus of the protein including the aggregon site was blocked. These included the removal of the Axin2 RGS domain (similar to the Axin2$^{\Delta/\Delta}$ allele), mutation of the aggregon site (Q188P;V189S), swapping the Axin2 RGS domain with the Axin1 RGS domain and saturation with a peptide to mask the site. Taken together, this functional data suggests that a truncated protein, were it to be expressed, may be more effective in the degradation of β-catenin.

This leaves the open question of why, if the Axin2$^{\Delta/\Delta}$ allele is more effective in the degradation of β-catenin, do we see an increased and accelerated rise in HCC when compared to Axin1$^{\Delta/\Delta}$ alone. In the study by Bernkopf, transient expression of Axin2 QP-VS mutant protein was shown to be as efficient as Axin1 in degrading β-catenin as measured by staining intensity, and reduced proliferation in SW480 cells. However, the QP-VS protein was still able to bind APC whereas, a truncated Axin2$^{\Delta/\Delta}$ protein is missing the whole of exon 2 and thus not only does it not have the aggregon sites preventing polymerisation, neither does it have the RGS domain that binds APC as part of the β-catenin turnover mechanism. It is therefore possible that a truncated Axin2 protein might not be able to fully compensate for the increased proliferation following Axin1 deletion.

The results in this thesis showed that loss of both *Axin1* and *Axin2* alleles in DAX livers was associated with reduced cell proliferation, lower *Lgr5* expression and lower levels of γH2AX compared to Axin1$^{\Delta/\Delta}$ alone at day 6 post induction, which was not associated with increased apoptosis. Though not looked at over a time course, these acute phenotypes may in theory have attenuated tumourigenesis in DAX liver.

Axin2 expression is normally most strongly found surrounding the central vein. The loss of GS expression in Axin2$^{\Delta/\Delta}$ livers may be attributed to an increased capacity for β-catenin degradation. It may be presumed that there is sufficient GS expression remaining or is compensated by other methods to maintain normal liver function and that where *Axin2* expression is not normally present it may not have an effect. However, in the context of acute damage such as PHx, Axin2$^{\Delta/\Delta}$ livers may have a reduced capacity for regeneration as seen in β-catenin deleted livers (Sekine et al. 2006). Therefore, it is possible that in the context of DAX liver, Axin1$^{\Delta/\Delta}$ results in slightly higher levels of β-catenin, this in turn increases expression of Axin2$^{\Delta/\Delta}$, presumably throughout the liver. This creates a combination of enhanced β-catenin degradation, via a more efficient Axin2$^{\Delta/\Delta}$ protein on a background of elevated pathway activation from *Axin1* deletion. This does not result in nuclear β-catenin accumulation or expanded GS expression as predicted. Instead, it creates a chronic low level of β-catenin that impairs the livers' ability to maintain homeostasis. DAX liver also shows elevated expression of *Birc5*, an anti-apoptotic protein expressed in many cancers, including HCC (Su 2016). Alternatively, the combined mutations could lead to changes in other cellular processes beyond the Wnt pathway. This will be considered later in the section.

The *Axin1* deleted allele in the (Sanson et al. 2023) study relied on the removal of exons 4 and 5 that contain the GSK-3 and β-catenin binding regions as described in (Abitbol et al. 2018). Both the *Axin1* allele used by Feng et al (2012) and the one used in the Abitbol study resulted in HCC formation without clear β-catenin activation (Feng et al. 2012; Abitbol et al. 2018). Both systems involved highly efficient deletion. AhCre in a mixed background in the Feng study and TTR-Cre-Tam in a C57/Bl6 background in the Abitbol study, which expresses the Cre recombinase specifically in hepatocytes after tamoxifen injection. The Cre recombinases can achieve between 80-100% recombination in hepatocytes (Tannour-Louet et al. 2002; Ireland et al. 2004). However, no increase in hepatocyte proliferation was observed following Axin1

deletion in the Abitbol study whereas increased proliferation was seen at day 4 post induction and persisted for at least 3 months in the Feng study. This discrepancy may be because of the background of the mouse models used, the *Axin1* construct or the Cre recombinase as AhCre expression is not limited to the liver in the Feng study.

The $Axin2^{lacz/lacz}$ allele (Lustig et al. 2002a) was shown not to result in changes to GS expression in the liver (Sanson et al. 2023). $Axin2^{lacz/lacz}$ mice aged to one year in this laboratory also showed no changes to GS expression (data not shown). This contrasts with our $Axin2^{\Delta/\Delta}$ mice in which a reduction in GS expression was observed. In the Sanson study, the combined deletion of Axin1, using Ad Cre, with the $Axin2^{lacz/lacz}$ allele resulted in the expansion of GS, replicating the expansion of GS in Apc KO (Sanson et al. 2023). This is in stark contrast to DAX liver that does not result in GS changes at day 6 post induction.

If we consider both Abitbol and Feng Axin1 alleles as comparable (null) as they both result in liver tumourigenesis, then based on the phenotypes in combination with $Axin2^{\Delta/\Delta}$ or $Axin2^{lacz/lacz}$ it is likely that the $Axin2^{lacz/lacz}$ is the true null as it results in the expected phenotype as seen with Apc deletion. If this is the case, then it could be expected that deletion of $Axin1^{\Delta/\Delta}$ (exon 2 deleted) in the livers of $Axin2^{lacZ/lacZ}$ mice may phenocopy the expansion of GS as seen by Sanson (2023). Initial matings set up by Victoria Marsh Durban and later attempts by myself with multiple breeding pairs and trios to generate a combined AhCre; $Axin1^{fl/fl}$; $Axin2^{lacZ/lacZ}$ mouse were unsuccessful in this laboratory. This was possibly due to the leakiness of the Cre resulting in embryonic lethality however, this was not fully investigated. Future attempts might be able to generate $Axin1^{\Delta/\Delta}$, $Axin2^{lacz/lacz}$ livers through the use of the $AhCreER^{T}$ promoter to reduce background recombination.

Further evidence to suggest that $Axin2^{\Delta/\Delta}$ is not a null comes from the study by (Moshkovsky and Kirschner 2022). They show that shRNA knockdown of *Axin1* and *Axin2* results in similar levels of β-catenin protein to shRNA knockdown of *APC* in RKO cells. shRNA knockdown of *Axin1* alone results in less than half the amount of β-catenin protein as seen with shRNA knockdown of *APC*. shRNA knockdown of *Axin2* alone was comparable to controls. The weaker increase in the levels of β-catenin protein in Axin1 shRNA cells (compared to APC shRNA) was interpreted as being due to the Wnt/β-catenin induction of *Axin2* transcription and the subsequent increase of Axin2 protein levels to compensate for Axin1 loss. This weaker increase in the levels

of β-catenin may explain the lack of a strong Wnt ON phenotype seen in Axin1$^{\Delta/\Delta}$ livers as we see slight elevation in the expression of *Axin2* (see Figure 3.23).

Whether the Axin alleles used in this thesis are truly null does not detract from the observation that the recombination of exon 2 of both genes in the DKO liver enhances liver tumourigenesis. Cancer genome sequencing reveals a more intricate scenario where tumor suppressor gene mutations frequently exhibit mutational heterogeneity in which tumourigenesis is associated with alleles that are not always 'null' in function. The alleles that are observed in cancer are not always adequately modelled by knockout models. For example, the presence of specific mutations in different regions of the *APC* gene is connected to distinct β-catenin transcriptional activity and varying susceptibility to tumourigenesis (Gaspar and Fodde 2004). More recently, using CRISPR/Cas9 genome editing to investigate the consequences of incremental APC truncations, Novellasdemunt et al. found that the loss of the β-catenin inhibitory domain (CID) within APC, acts as a critical threshold controlling the pathological levels of Wnt activation and facilitating tumor transformation (Novellasdemunt et al. 2017). Further truncation resulted in incremental increases in Wnt signalling. In the case of the AXIN human mutational landscape, a review revealed a high prevalence of missense mutations ≈50% for AXIN1 and ≈65% for AXIN2 in comparison to deletions and truncations 45% and 30% respectively (Bugter et al. 2021). A study by Anvarian et al. using fluorescence-based thermal denaturation in HEK293 cells, attributed AXIN1 mutant tumourigenic properties to its acquired destabilisation rather than loss of tumour-suppressor function (Anvarian et al. 2016). It may therefore be speculated that the Axin alleles and resulting truncated proteins provide a just right level of tumour pathway deregulation needed for tumourigenesis in the liver. Interestingly, gain of function (GOF) mutations in β-catenin (Tao et al. 2016) and loss of function (LOF) deletion of Apc (Zhang et al. 2021) were insufficient for liver tumourigenesis although strong levels of Wnt β-catenin signalling were induced by both. Conversely, Axin1 and Axin1/Axin2 LOF models had enhanced rates of tumourigenesis but less evidence of strong Wnt pathway deregulation. Whether tumourigenesis in the DAX model described here requires Wnt/β-catenin pathway activity still needs to be definitively resolved and is considered further in section 6.4 Future directions. Similarly, the strong Wnt/β-catenin ON phenotype observed by (Sanson et al. 2023) in the Axin1$^{\Delta/\Delta}$, Axin2$^{lacz/lacz}$ model needs to be followed over time

to determine whether the strong Wnt/β-catenin deregulation observed leads onto HCC formation.

In addition to its role in Wnt/β-catenin signalling, it is possible that tumourigenesis in the DAX animals and in human *AXIN* mutant HCCs is in part played by disruption to other Axin interaction partners. One key Axin interaction partner is GSK3 which itself has near 100 substrates (Sutherland 2011). Axin increases β-catenin phosphorylation by glycogen synthase kinase 3β (GSK3β) but also reduces GSK-3 phosphorylation of other targets. A study by Gavagan et al. investigated this with experiments using a minimal, biochemically reconstituted system to measure the reaction rates of GSK3β with multiple substrates (Gavagan et al. 2020). Interestingly, the researchers found that Axin had a modest effect on the reaction between GSK3β and β-catenin when measured in isolation. However, in the presence of both β-catenin and non-Wnt pathway substrates, Axin played a significant role by preventing competition with alternative substrates. In physiological settings with multiple GSK3β substrates, Axin suppressed interactions with competing substrates, resulting in a greater than 10-fold rate increase in the reaction. It is likely that this mechanism allows Axin to promote signalling specificity by controlling substrate competition for GSK3β. In addition, Axin may directly increase the phosphorylation of substrates, other than β-catenin, that have been shown to bind directly to Axin (e.g. SMAD3 (Guo et al. 2008)). Higher levels of total β-catenin in Axin DKO (using $Axin2^{LacZ}$ allele) and $GSK3^{\Delta/\Delta}$ ES cells when compared to WT were found by Anika Offergeld suggesting dysregulation of the β-catenin degradation and the Wnt signalling pathway. Proteins targeted by GSK3, excluding those involved in the core Wnt/β-catenin signalling pathway, include proteins associated with glycogen biogenesis, cell cycle regulation, inflammation response, and microtubule stability (Hoffmeister et al. 2020; Hajka et al. 2021). The function of Axin in relation to GSK3 and these other substrates will need to be further investigated to determine whether Axin loss might directly or indirectly alter the rates of phosphorylation of non-β-catenin target proteins involved in tumourigenesis.

Wnt regulation involves Axin in the formation of a receptor complex which is required for formation of signalosomes. Recruitment of GSK-3 to multivesicular bodies might be dependent on Axin in receptor complexes. This could be distinct from the formation of β-catenin turnover complexes, which requires Axin to negatively regulate the pathway. In this context, the Niehrs group showed that Wnt signalling operated via a β-catenin independent, but GSK3 dependent WntSTOP (STabilisation Of Protein)

pathway to regulate the proteolysis of multiple proteins in the G2/M phase of the cell cycle (Acebron et al. 2014). The activation of this β-catenin-independent Wnt/Lrp6 cascade prevents the phosphorylation and polyubiquitination of multiple target proteins which includes c-Myc, thereby increasing protein stability and cell size in preparation for cell mitosis. Evidence has also indicated that Axin plays a crucial role outside of the Wnt pathway in the maintenance of genome integrity by facilitating centrosome separation during mitosis (Poulton et al. 2013). Consistent with these observations we see double strand breaks as marked by γH2AX and nuclear atypia in Axin deleted cohorts indicating a genomic instability phenotype.

The heightened expression of myc proto-oncogenes has been linked to the initiation of numerous human tumors (Paglia et al. 2020) and it is additionally recognized as a key factor driving cell competition (Johnston 2014). Thus, cells exhibiting increased Myc expression may display a super-competitor phenotype, potentially playing a role, at least in theory, in promoting neoplastic behaviour. Notably, significantly elevated expression of *c-Myc* was found in DAX liver at 1 year post induction and even more so in DAX liver tumours. Studies in Drosophila models have shown that elevated Wnt/Wg signalling due to mutations in *Axin* or *APC* exhibit super competitor behaviour, actively outcompeting and eliminating neighbouring wild-type cells however this was independent of Myc (Vincent et al. 2011). Instead the process relied on the Wnt antagonist Notum. It may therefore be of interest to assess expression and localization of Notum in the Axin deleted livers.

Axin has been indicated to be involved in multiple other pathways (Luo and Lin 2004). In the study by Azzolin et al, Yap was found to bind to Axin1 and associate with the β-catenin destruction complex in a Wnt off state (Azzolin et al. 2014). A Wnt ON state leads to the release of Yap leading to its accumulation and the activation of YAP/TAZ/TEAD-dependent transcription. It was predicted that the loss of Axin1 would lead to expression of Yap targets. Unsupervised gene set enrichment analysis (GSEA) revealed a significant enrichment of a YAP/TAZ and Notch signature in the profile of mouse Axin1 deleted tumors vs.non-tumour (Abitbol et al. 2018). In support of the findings in Abitbol et al, DAX tumours were found to have nuclear accumulation of Yap and increased expression of a number of Yap downstream targets. However, early timepoints at day 6 and 1 month after *Axin1* and *Axin2* deletion in the studies here showed little evidence for increase in Yap expression or induction of downstream targets. This suggests that mutations accrued in the tumour resulted in the Yap

signature seen and was not immediately driving tumourigenesis following Axin deletion. Whole genome sequencing would have been interesting to perform on the tumours to identify potential driver mutations for these observations. The study by Abitbol also identified an activated Notch signature in Axin deficient HCC. In the future it may be worthwhile to examine whether the DKO tumours also display this elevated Notch signature to further show relevance of this model to study HCC.

6.3 Context specific differences in Axin function

An unresolved question that remains from the *in vivo* studies is the origin of the tumours. The simplest and most likely origin is that the tumours arise from hepatocytes. The tumour cells look like hepatocytes and there does not appear to be an obvious ductular reaction after deletion of Axin. However, the data here does not rule out the possibility that a small number of Axin deleted hepatocytes transitioned into a biliary / hepatocyte intermediate state or that biliary-derived cells, following Axin loss, formed tumours. However, this cannot be formally ruled out as this study did not perform lineage tracing after Axin deletion. As biliary organoids are able to partially differentiate towards a hepatocyte-like state, biliary-derived organoids provide an opportunity to be to study Axin disruption in a relevant or related functional context.

Induction of differentiation using DM conditions towards a hepatocyte like fate in Axin1$^{\Delta/\Delta}$ organoids resulted in the elevated expression of *Lgr5* that was even more evident in double mutant DAX organoids. This contrasts with *in vivo* data that showed *Lgr5* expression was slightly down in the DAX liver compared to control at day 6 post induction. It is possible the increase in *Lgr5* expression in bile duct or intermediary cells was masked by lower expression in the overall liver caused by the inhibitory effects observed with Axin2 deletion, suggesting phenotypes following deletion of Axin may be cell type specific. Elevated expression of *Lgr5* has previously been linked with liver injury (Huch et al. 2013). Additionally, *LGR5* expression has been shown to be elevated in human HCC and mouse liver tumours (Cao et al. 2020). The Cao et al. study also showed that Lgr5+ cells were superior in their capacity for tumour organoid formation. The BD organoid experiments described in this theis suggested that Axin1 deleted and particularly DAX organoids had an increase in stem like biology that has previously been linked to chronic injury in the liver (Khan et al. 2017). The cells in the DAX liver that gained this elevated, “just right,” stem like phenotype may in part explain

why tumourigenesis is only seen in DAX livers and not Axin1$^{\Delta/\Delta}$ livers when using AhCreER^{T}. This could suggest that select Lgr5+ cells in DAX livers could be the cells of origin of the tumours generated. If this is the case, then why do DAX tumours fall into two distinct β-catenin phenotypes? It is possible that the location of the initiating cell plays a part. The study by Ang et al. 2019 shows Lgr5+ cells surrounding the central vein are the main cellular origin of DEN induced HCC. They suppose that the Lgr5+ identity of the cells is in part due to the local niche generated by the endothelial cells of the central vein. This niche may drive tumourigenesis on a more Wnt activated path. DAX livers also showed patchy expression of GS that was not associated with the central vein. HCC that originates from these cells may not have the same niche but still maintain an intrinsic proliferative and competitive advantage and therefore result in tumours without nuclear β-catenin as observed in Axin1 deficient tumours (Feng et al. 2012, Abitbol et al. 2018).

Deletion of Axin using the same alleles in BD organoids and ES cells (Offergeld 2015 PhD Thesis) impeded differentiation down hepatocyte/biliary pathways and towards ES-cell derived, differentiated cell types respectively. Although the BD and ES systems showed some similarity, there were differences, particularly in respect to the loss of Axin2. Using DM (differentiating) conditions, WT BD organoids express some hepatocyte markers like Albumin (Huch et al. 2013). In Axin1$^{\Delta/\Delta}$ and DAX BD organoids in DM, Albumin expression was found to be up to 97% lower than WT organoids suggesting a failure to differentiate. It did not appear that Axin2$^{\Delta/\Delta}$ in combination with Axin1$^{\Delta/\Delta}$ exacerbated this phenotype. Whereas in ES cells, combined Axin1$^{\Delta/\Delta}$, Axin2$^{\Delta/\Delta}$ mutants were shown to impede expression of alkaline phosphatase under differentiation conditions (Offergeld 2015 PhD Thesis). Interestingly, in the work by Anika Offergeld, Axin2$^{\Delta/\Delta}$ and Axin2$^{lacz/lacz}$ ES cells failed to form cardiomyocytes in an embryoid body assay, suggested to be due to Wnt pathway hyperactivation. In contrast, Axin2$^{\Delta/\Delta}$ BD organoids showed no signs of Wnt pathway activation and had comparable levels of Albumin expression to WT organoids in DM conditions suggesting they did not fail to differentiate. Furthermore, Axin2$^{\Delta/\Delta}$ livers appeared to have a suppressive effect on the Wnt/β-catenin pathway and when combined with Axin1$^{\Delta/\Delta}$ had an opposing effect to Axin1 deletion alone, rather than cumulative as seen in the BD organoids and ES cells. The Axin2$^{lacz/lacz}$ allele in ES cells appeared to hyperactivate the Wnt pathway whereas this does not appear to be the case in the liver

when assessing GS staining (Sanson et al. 2023). These observations would suggest that the effects of the Axin alleles varies based on the system that they are used in. It is therefore very important to understand the exact cell type in which Axin alleles are lost during the tumourigenesis pathway. Lineage tracing may help in identifying the potential cancer cell of origin.

There are however limitations with the BD organoid system used in this thesis. For the system to be useful, it needs to recapitulate the phenotypes seen *in vivo*. A G2/M signature was not observed in any of the Axin mutant organoids grown in EM or DM despite one being present in DAX livers. For organoids grown in EM this is understandable as the RSPO in the media will be driving Wnt pathway activation and may therefore be masking the effects of Axin loss as the differences between mutants may only be very subtle. Axin1$^{\Delta/\Delta}$ BD organoids in DM were previously shown by Anika Offergeld (PhD Thesis 2015) to recapitulate the G2/M signature that was seen in the Axin1$^{\Delta/\Delta}$ liver by Feng (2012). This BD organoid phenotype was not observed here. The discrepancy is unlikely to be due to levels of recombination as AhCreER^{T}, Axin1$^{\Delta/\Delta}$ BD organoids saw levels of around 97% recombination. A G2/M signature wasn't seen in the AhCreER^{T}, Axin1$^{\Delta/\Delta}$ so it is possible that the phenotype may also have been dependent on the background of the mouse line. While ex vivo experiments can provide valuable insights into cellular responses to Axin deletion, they may not fully recapitulate the complexity of in vivo consequences. Chronic inflammation is a well-established risk factor for the initiation and progression of liver cancer. Wnt signalling has been implicated in modulating inflammation and immune responses (Li et al. 2019). Axin deletion may affect these processes in vivo, leading to altered immune cell functions and potentially contributing to inflammatory conditions. Inflammation in the liver is associated with the release of inflammatory cytokines, such as IL-6 and TNF-α (Tanaka et al. 2014). These cytokines contribute to the activation of signalling pathways that promote cell survival, proliferation, and angiogenesis. It is therefore possible that the proliferative phenotype seen following Axin deletion is in part fuelled by an inflammatory response.

Ideally, the organoid system used to study the effects of Axin deletion should be derived from definitive hepatocytes with an induction protocol that does not interfere with the cultured cells. The hepatocyte organoid system needs some further development, and this will be explored further in section 6.4.

The context specificity of Axin allele deletion in non-liver tissues *in vivo* might later be studied using the alleles described. Some aspects of Axin function will certainly be accessible using the specific lines of animal described since the Ah promoter induces high levels of recombination in the liver and in the gastrointestinal (GI) tract. Lower levels of deletion have been described in the gall bladder, the bladder and seminiferous vesicles and proximal esophagus (Ireland et al. 2004). Axin2 deleted cohorts presented with several abnormalities that were not found to occur in control mice. In aged $Axin2^{\Delta/\Delta}$ mice this included cases of an enlarged spleen, a mammary tumour, a stomach tumour, and one mouse presented with seizures. These cases may have just been down to the greater numbers in the aged $Axin2^{\Delta/\Delta}$ cohort compared to control. More notably, 3 males were found to have enlarged seminal vesicles, but this was not investigated further. However, a *pry-1* (*C. elegans* Axin homolog) mutant was found to be involved in reproductive structure development (Mallick et al. 2022) and disruption of the Wnt pathway in germ cell development in developed adult mice caused interference to spermatogenesis (Kerr et al. 2014). The Axin alleles may be of interest for future studies in reproductive organ development.

Mutations in Axin have been implicated in CRC (Mazzoni and Fearon 2014) and germline mutations of *AXIN2* are associated with familial adenomatous polyposis (FAP) syndrome (Lammi et al. 2004; Marvin et al. 2011; Rivera et al. 2014). The location of germline and somatic *AXIN2* variants implicated in GI cancers are predominately found in exon 7 resulting in an early stop codon. The germline *AXIN2* mutations are heterozygous, indicating a potential link between *AXIN2* mutation and cancer susceptibility following the classical tumor suppressor model with the second allele of AXIN2 likely being deactivated during tumor development via LOH. However, despite deletion of Axin in the intestinal tract following BNF and Tamoxifen induction (data not shown), only one colon polyp was identified at dissection in one aged $AhCreER^{T}$ $Axin1^{\Delta/\Delta}$, $Axin2^{\Delta/\Delta}$ mouse. As stated previously, HCC development requires lower levels of Wnt/β-catenin activation compared to CRC (Buchert et al. 2010). As we do not see a strong Wnt ON phenotype in the liver with the current Axin alleles, it would suggest that in the context of the intestine, this is generally not sufficient for tumour development. In contrast, the deletion of both Axins in the study by Sanson et al., phenocopied the loss of Apc in the intestine (Sanson et al. 2023).

6.4 Future directions

Due to the limited availability of reliable antibodies capable of accurately detecting Axin protein lacking the RGS domain, it was challenging to definitively confirm the absence of Axin protein in either of the $Axin1^{\Delta/\Delta}$ or $Axin2^{\Delta/\Delta}$ alleles. However, immunoprecipitation followed by Western analysis by Anika Offergeld using ES cells did identify a protein band that was consistent with a predicted truncated protein fragment of Axin1 that was absent in liver extracts (Feng et al. 2012). As argued above, the $Axin2^{\Delta/\Delta}$ allele likely encodes a protein that, when it is expressed, degrades β-catenin more effectively and may even be resistant to downregulation by upstream signals (Bernkopf et al. 2019). Lastly, double Axin deletion in the liver did not result in the predicted strong Wnt ON phenotype whereas, the study by (Sanson et al. 2023) using alternative Axin alleles resulted in the expansion of GS expression replicating what was seen following Apc deletion. Collectively these results suggest that the Axin alleles used in this thesis may not produce nulls. This confounds interpretation of the mechanisms underlying the acute and long-term tumour phenotypes.

Future long-term tumour studies could combine the use of the $AhCreER^{T}$; $Axin1^{fl/fl}$ alleles with the $Axin2^{lacz/lacz}$ allele (Lustig et al. 2002a) to generate double Axin knockouts that would be predicted to replicate the phenotype seen in (Sanson et al. 2023). A major drawback with this method is that it still leaves open the question as to whether any Axin proteins are expressed from the remaining Axin coding sequences within the alleles involved. Without definitive nulls it will make it difficult to derive clear mechanistic conclusions. In future experiments, further attempts could be made to generate definitive Axin1, Axin2 double null mutants as was attempted as part of this study. This could be done by re-engineering loxP sites from scratch prior to the first and last coding exons of Axin1 and Axin2 in ES cells prior to embryo transfer. Alternatively, further attempts could be taken to those described here to engineer a 3rd loxP site at the end of the coding regions of both Axin1 and Axin2 using CRSIPR/Cas9 technology in order to produce definitive nulls. Results showed that the strategy used was successful for the integration of the 3rd LoxP site and subsequent deletion of *Axin2*. However, it was not possible to determine why both alleles of *Axin1* ES cells could not have the 3rd LoxP site inserted. One possibility is that the integration site chosen was very close to the downstream gene *Pdia2* and that this may have resulted in some interference. Future attempts could use alternative sites at the 3' end of *Axin1* that

does not disturb *Pdia2*. Technical optimisations such as custom-made targeting constructs already in a vector and using an updated version of the Cas9 nickase vector (Ran et al. 2013) may aid in achieving the desired outcome. Once all newly Axin fully floxed ES cells are generated they can be directly compared to exon 2 floxed ES cells and any differences ascertained both in acute and long-term phenotypes.

One key question remaining unanswered is whether the deletion of exon 2 of both Axin genes leads to tumour development in a Wnt/β-Catenin dependent manner. As Axin1 and Axin2 are crucial mediators in Wnt signalling regulation, it was hypothesized that the acute effects of Axin1 and Axin1, Axin2 deletions in the liver were mediated by the subsequent stabilisation of β-catenin. However, β-catenin was not found to be aberrantly expressed and excluding a mild 1.3-fold increase in *Lgr5* expression in AhCreER^{T} Axin1$^{\Delta/\Delta}$ liver at day 6 post induction, gene expression analysis conducted on various Axin acute deletions did not show significant activation of Wnt target genes *in vivo*. However, this analysis provides limited insight into intracellular processes, as some cells may exhibit increased Wnt signalling while others show decreased or no signalling, potentially balancing each other out. Consequently, these changes may not be observable in the overall gene expression profile. It however remains possible that activation of Wnt signalling below the detection threshold in a small subset of cells could eventually trigger tumorigenesis.

To determine the dependence of Axin mutant phenotypes on β-Catenin, mice with floxed Axin1 and/or Axin2 alleles can be bred with a conditional loss-of-function β-catenin allele (Brault et al. 2001). Similar experiments conducted with conditional Apc alleles have shown that loss of β-catenin rescues the acute effects of Apc loss (Reed et al. 2008). There is evidence to suggest that Axin loss does require intact β-catenin for liver tumourigenesis. In a mouse study with Axin1 deletion with c-Met activation, ablation of β-catenin prevented hepatocarcinogenesis (Qiao et al. 2019). This study however can only be applied for the need of intact β-catenin in mutant Axin1 and activated c-Met tumours. If complete loss of β-catenin mitigates Axin mutant phenotypes, a subsequent set of assays could be performed using a mutant allele of β-catenin lacking the ability to bind TCF and therefore to regulate transcription. A double mutant β-catenin allele generated in the lab of Konrad Balser which lacks the ability to bind N-terminal and C-terminal coactivators (BCL9 and TBP/Brg1/CBP/MED12/Parafibromin respectively) but retains β-catenin's structural

role by binding to E-cadherin could be used. (Valenta et al. 2011). This will help determine whether β-catenin's transcriptional activity is essential for Axin-mediated phenotypes or whether β-catenin's ability to interact with E-cadherin for its adhesive role is sufficient to rescue function in the absence of TCF-dependent transcription.

Bile duct derived organoids used in Chapter 5 to study Axin loss provided evidence of Wnt pathway activation with elevated *Lgr5* expression and hints of restricted differentiation potential as evidenced by reduced *Albumin* expression. However, they failed to replicate the G2/M signature seen in Feng (2012). The stable induction strategy used to induce Axin deletion in these organoids meant that cells had 22 days since their first exposure to the inducing agents – 7 days induction in culture, disassociation and seeding, 2 days recovery, then 13 days in expansion or differentiation media before being analysed. This delay may mean that cells have already partly adapted to the initial loss of Axin. Improvements to the induction of the organoids is essential to **a)** remove the effects of the inducing agent (BNF) and **b)** allow the study of the immediate effects of Axin deletion in established organoids to allow time course analyses that would help in the delineation of signal events. Lentiviral transfection of BD organoids with the Tamoxifen inducible Lenti-CMV-$ER^{T2}CreER^{T2}$ construct was found to be feasible in the work done by Anika Offergeld (2015 PhD Thesis) and, if suitably rapid and efficient, may be a better system.

As stated previously, tumourigenesis most likely started in hepatocytes and therefore a definitive hepatocyte model may be better to study tumourigenic potential *in vitro*. To this end, Chapter 5 also introduced an attempt at an improved 3D definitive hepatocyte culture system that could ultimately be used to investigate the impact of Axin loss in hepatocytes. Using published media compositions (Hu et al. 2018; Peng et al. 2018), a combination of the two and with alternative Wnt pathway activating components, I was unable to establish hepatic organoids from cryopreserved human hepatocytes. One possibility for this could be the exchange of the homemade RSPO1 conditioned media used in the study by Hu (2018) with recombinant RSPO1 protein that was not the right level for correct Wnt pathway activation required. Conditioned media also contains 10% FBS and we have no way of knowing the exact concentration of RSPO1 this media. Mouse hepatic organoids were able to be established in the lab by Eider Valle-Encinas using the published protocol in (Peng et al. 2018). However, despite claims that cryopreserved organoids could be re-established, I was unable to

do so using the published method or additional various recovery media compositions. This precluded them from being a useful tool for the studies needed.

The culture and expansion of primary hepatocytes (PH) and PH organoids with sustained hepatic functions are crucial for studying liver physiology, drug metabolism, toxicity testing, and developing cell-based therapies. However, achieving a stable and functional PH culture system that can be expanded rapidly remains a challenge. Wnt agonists, or the inflammatory cytokine TNFα, have been shown to be important for the generation of murine PH organoids (Hu et al. 2018; Peng et al. 2018). Some combination of the two media compositions will likely provide a more optimal setting for hepatic organoids. Other groups are finding additional mitogens that may also help contribute to PH organoid growth, most recently neurotrophin-3 has been shown to induce hepatocyte proliferation (Trinh et al. 2023). Alternately, it may be possible to generate robust PH organoids cultures without the addition of mitogenic components. In a study by (Atanasova et al. 2023), using a co-culture technique, colorectal cancer organoids were able to be grown without the addition of classical niche factors such as noggin, EGF, inhibitor of TGF-β signalling (A-8301) or p38 inhibitor (SB202190). Instead, factors such as EGF family members, FGF7, HGF, TGF-β1/2 Noggin, RSPO1/2, Wnt2/5a and IL6 were secreted by fibroblasts or cancer associated fibroblasts (CAFs). Additionally, organoids grown with CAFs were better able to replicate the tumour heterogeneity seen in the original tumour. It would be interesting to assess whether this could be replicated with hepatocytes co-cultured with fibroblasts or perhaps biliary epithelial cells if they can be prevented from overgrowing. It may be further necessary to supplement cultures with endothelial cells from central veins, known to secrete RSPO3, Wnt2 and Wnt9b (Rocha et al. 2015; Preziosi et al. 2018) or Kupffer cells for TNFα secretion (Nguyen-Lefebvre and Horuzsko 2015). By utilizing the co-culture technique involving patient HCC samples alongside CAFs, endothelial cells, and immune cells derived from the same individual, we may be able to create organoids that faithfully preserve the inherent characteristics of primary tumors and that includes an immune response. This approach may eliminate the necessity of altering culture conditions for each patient separately, significantly accelerating the advancement of personalized medicine. Moreover, the utilization of these HCC-derived organoids in drug screening could enable the identification of the most suitable treatment options for individual patients.

Once robust hepatic organoid cultures are established that allow for a more faithful recapitulation of the hepatic microenvironment, Axin's role in hepatic tumorigenesis can be further elucidated within a more relevant and physiologically representative system. While a comprehensive exploration of Axin's function would be facilitated by complete deletion of the gene, it is crucial to note that a major fraction of HCC in human cancer results from point mutations within the Axin gene (Anvarian et al. 2016). To establish a platform for investigating cancer progression *in vitro*, base editing to introduce point mutations (Zafra et al. 2018) observed in human cancer cases could be adopted. This strategy could enable the emulation of multiple relevant genetic alterations found in HCC, thereby facilitating a more accurate and insightful study of cancer development. Furthermore, it will allow for a more relevant evaluation of possible therapies of direct relevance. This includes Tankyrase inhibitors that have been shown to stabilise Axin protein and reduce colony formation capacity in HCC cell lines (Wang et al. 2021). Interestingly, this observation seemed to indicate an apparent independence from the modulation of β-catenin signalling in some cases. This could possibly be to Tankyrases being associated with various other cellular processes, including Hippo signalling, mitosis, and repair of double strand breaks (Nagy et al. 2016; Jia et al. 2017).

The novel aspects of this work include the molecular examination of a conditional *Axin2* allele that was investigated alone and in combination with a previously published *Axin1* allele *in vivo* in the liver and *in vitro,* using a liver biliary duct derived organoid system. The *in vivo* analysis showed accelerated hepatocarcinogenesis in DAX livers compared to the previous Feng study using the *Axin1* allele alone. Despite deletion of both Axins, a clear strong ‘Wnt ON’ phenotype was not observed as hypothesized. The *in vivo* data suggests that the *Axin2* allele may result in a protein that has enhanced β-catenin turnover capabilities. For publication it may be necessary to demonstrate that the conditional deletion of *Axin2* results in the formation of puncta as observed in the study by Bernkopf et al. 2015 to verify this hypothesis. This thesis also demonstrated that the resulting phenotypes following deletion of the Axin alleles was context specific, with the BD organoids showing a very significant increase in *Lgr5* expression in DM conditions. Transplantation and tracing of Axin deleted BD organoids could be carried out to show whether they have tumourigenic potential for greater impact. Additionally, sequencing of the DAX liver tumours may provide mechanistic insight.

The Axin mutants employed in this study have proven to be invaluable tools for investigating the intricate mechanisms underlying tumour formation. In combination with *in vitro* systems, they may be useful in exploring the development of potential therapeutic interventions.

List of References

Abdolahi, S., Ghazvinian, Z., Muhammadnejad, S., Saleh, M., Asadzadeh Aghdaei, H. and Baghaei, K. 2022. Patient-derived xenograft (PDX) models, applications and challenges in cancer research. *Journal of translational medicine* 20(1), p. 206. Available at: http://www.ncbi.nlm.nih.gov/pubmed/35538576.

Abitbol, S. et al. 2018. AXIN deficiency in human and mouse hepatocytes induces hepatocellular carcinoma in the absence of β-catenin activation. *Journal of Hepatology* 68(6), pp. 1203–1213. Available at: https://doi.org/10.1016/j.jhep.2017.12.018.

Acebron, S.P., Karaulanov, E., Berger, B.S., Huang, Y.L. and Niehrs, C. 2014. Mitotic Wnt Signaling Promotes Protein Stabilization and Regulates Cell Size. *Molecular Cell* 54(4), pp. 663–674. Available at: http://dx.doi.org/10.1016/j.molcel.2014.04.014.

Agostino, M. and Pohl, S.Ö.G. 2020. The structural biology of canonical Wnt signalling. *Biochemical Society Transactions* 48(4), pp. 1765–1780. doi: 10.1042/BST20200243.

Albuquerque, C. et al. 2002. The “just-right” signaling model: APC somatic mutations are selected based on a specific level of activation of the beta-catenin signaling cascade. *Human molecular genetics* 11(13), pp. 1549–60. Available at: http://www.ncbi.nlm.nih.gov/pubmed/12045208.

van Amerongen, R. 2012. Alternative Wnt pathways and receptors. *Cold Spring Harbor Perspectives in Biology* 4(10). doi: 10.1101/cshperspect.a007914.

An, Y.-Z., Cho, E., Ling, J. and Zhang, X. 2020. The Axin2-snail axis promotes bone invasion by activating cancer-associated fibroblasts in oral squamous cell carcinoma. *BMC cancer* 20(1), p. 987. Available at: http://www.ncbi.nlm.nih.gov/pubmed/33046030.

Ang, C.H. et al. 2019. Lgr5+ pericentral hepatocytes are self-maintained in normal liver regeneration and susceptible to hepatocarcinogenesis. *Proceedings of the National Academy of Sciences of the United States of America* 116(39), pp. 19530–19540. doi: 10.1073/pnas.1908099116.

Anvarian, Z. et al. 2016. Axin cancer mutants form nanoaggregates to rewire the Wnt signaling network. *Nature structural & molecular biology* 23(4), pp. 324–32. Available at: http://www.ncbi.nlm.nih.gov/pubmed/26974125.

Aristizabal-Pachon, A.F., Carvalho, T.I., Carrara, H.H., Andrade, J. and Takahashi, C.S. 2015. AXIN2 Polymorphisms, the β-Catenin Destruction Complex Expression Profile and Breast Cancer Susceptibility. *Asian Pacific journal of cancer prevention : APJCP* 16(16), pp. 7277–84. doi: 10.7314/apjcp.2015.16.16.7277.

Atanasova, V.S. et al. 2023. Mimicking tumor cell heterogeneity of colorectal cancer in a patient-derived organoid-fibroblast model. *Cellular and Molecular Gastroenterology and Hepatology*. doi: 10.1016/j.jcmgh.2023.02.014.

Austinat, M., Dunsch, R., Wittekind, C., Tannapfel, A., Gebhardt, R. and Gaunitz, F. 2008. Correlation between β-catenin mutations and expression of Wnt-signaling target genes in hepatocellular carcinoma. *Molecular Cancer* 7. doi: 10.1186/1476-4598-7-21.

Azzolin, L. et al. 2014. YAP/TAZ incorporation in the β-catenin destruction complex orchestrates the Wnt response. *Cell* 158(1), pp. 157–170. Available at: http://dx.doi.org/10.1016/j.cell.2014.06.013.

Barker, N. et al. 2007. Identification of stem cells in small intestine and colon by marker gene Lgr5. *Nature* 449(7165), pp. 1003–7. Available at: http://www.ncbi.nlm.nih.gov/pubmed/17934449

Barker, N. et al. 2009. Crypt stem cells as the cells-of-origin of intestinal cancer. *Nature* 457(7229), pp. 608–611. Available at: http://dx.doi.org/10.1038/nature07602.

Benedict, M. and Zhang, X. 2017. Non-alcoholic fatty liver disease: An expanded review. *World journal of hepatology* 9(16), pp. 715–732. Available at: http://www.ncbi.nlm.nih.gov/pubmed/28652891.

Benegiamo, G. et al. 2023. The genetic background shapes the susceptibility to mitochondrial dysfunction and NASH progression. *Journal of Experimental Medicine* 220(4). Available at: https://rupress.org/jem/article/220/4/e20221738/213867/The-genetic-background-shapes-the-susceptibility.

Benhamouche, S. et al. 2006. Apc tumor suppressor gene is the “zonation-keeper” of mouse liver. *Developmental cell* 10(6), pp. 759–70. Available at: http://linkinghub.elsevier.com/retrieve/pii/S1534580706001614

Ben-Moshe, S. and Itzkovitz, S. 2019. Spatial heterogeneity in the mammalian liver. *Nature Reviews Gastroenterology & Hepatology* 16(7), pp. 395–410. Available at: http://www.nature.com/articles/s41575-019-0134-x.

Bernkopf, D.B., Brückner, M., Hadjihannas, M. V. and Behrens, J. 2019. An aggregon in conductin/axin2 regulates Wnt/β-catenin signaling and holds potential for cancer therapy. *Nature Communications* 10(1). Available at: http://dx.doi.org/10.1038/s41467-019-12203-8.

Bernkopf, D.B., Hadjihannas, M. V and Behrens, J. 2015. Negative-feedback regulation of the Wnt pathway by conductin/axin2 involves insensitivity to upstream signalling. *Journal of cell science* 128(1), pp. 33–9. Available at: http://www.ncbi.nlm.nih.gov/pubmed/25380820.

Bisso, A. et al. 2020. Cooperation Between MYC and β-Catenin in Liver Tumorigenesis Requires Yap/Taz. *HEPATOLOGY* 72(4), p. 2020. Available at: https://www.komp.org.

Bosch, F.X., Ribes, J., Díaz, M. and Cléries, R. 2004. Primary liver cancer: Worldwide incidence and trends. In: *Gastroenterology*. W.B. Saunders. doi: 10.1053/j.gastro.2004.09.011.

Boyault, S. et al. 2007. Transcriptome classification of HCC is related to gene alterations and to new therapeutic targets. *Hepatology* 45(1), pp. 42–52. doi: 10.1002/hep.21467.

Boyer, J.L. 2013. Bile formation and secretion. *Comprehensive Physiology* 3(3), pp. 1035–1078. doi: 10.1002/cphy.c120027.

Brault, V. et al. 2001. Inactivation of the beta-catenin gene by Wnt1-Cre-mediated deletion results in dramatic brain malformation and failure of craniofacial development. *Development* (Cambridge, England) 128(8), pp. 1253–64. Available at: http://www.ncbi.nlm.nih.gov/pubmed/11262227.

Broutier, L. et al. 2017. Human primary liver cancer–derived organoid cultures for disease modeling and drug screening. *Nature Medicine* 23, pages 1424–1435. Available at: http://www.nature.com/doifinder/10.1038/nm.4438.

Broutier, L., Andersson-Rolf, A., Hindley, C.J., Boj, S.F., Clevers, H., Koo, B.K. and Huch, M. 2016. Culture and establishment of self-renewing human and mouse adult liver and pancreas 3D organoids and their genetic manipulation. *Nature protocols* 11(9), pp. 1724–1743. doi: 10.1038/nprot.2016.097.

Buchert, M. et al. 2010. Genetic dissection of differential signaling threshold requirements for the Wnt/β-catenin pathway in vivo. *PLoS Genetics* 6(1). doi: 10.1371/journal.pgen.1000816.

Bugter, J.M., Fenderico, N. and Maurice, M.M. 2021. Mutations and mechanisms of WNT pathway tumour suppressors in cancer. *Nature Reviews Cancer* 21(1), pp. 5–21. doi: 10.1038/s41568-020-00307-z.

Burke, Z.D., Reed, K.R., Phesse, T.J., Sansom, O.J., Clarke, A.R. and Tosh, D. 2009. Liver zonation occurs through a beta-catenin-dependent, c-Myc-independent mechanism. *Gastroenterology* 136(7), pp. 2316-2324.e1–3. Available at: http://www.ncbi.nlm.nih.gov/pubmed/19268669.

Burke, Z.D., Reed, K.R., Yeh, S.-W., Meniel, V., Sansom, O.J., Clarke, A.R. and Tosh, D. 2018. Spatiotemporal regulation of liver development by the Wnt/β-catenin pathway. *Scientific Reports* 8(1), p. 2735. Available at: https://www.nature.com/articles/s41598-018-20888-y.

Burm, R., Collignon, L., Mesalam, A.A. and Meuleman, P. 2018. Animal models to study hepatitis C virus infection. *Frontiers in Immunology* 9. doi: 10.3389/fimmu.2018.01032.

Cadoret, A. et al. 2002. New targets of beta-catenin signaling in the liver are involved in the glutamine metabolism. *Oncogene 21*(54), pp. 8293–301. Available at: http://www.ncbi.nlm.nih.gov/pubmed/12447692.

Calderaro, J. et al. 2017. Histological subtypes of hepatocellular carcinoma are related to gene mutations and molecular tumour classification. *Journal of Hepatology* 67(4), pp. 727–738. Available at: http://dx.doi.org/10.1016/j.jhep.2017.05.014.

Callow, M.G. et al. 2011. Ubiquitin ligase RNF146 regulates tankyrase and Axin to promote Wnt signaling. *PLoS ONE* 6(7). doi: 10.1371/journal.pone.0022595.

Camargo, F.D., Gokhale, S., Johnnidis, J.B., Fu, D., Bell, G.W., Jaenisch, R. and Brummelkamp, T.R. 2007. YAP1 Increases Organ Size and Expands Undifferentiated Progenitor Cells. *Current Biology* 17(23), pp. 2054–2060. doi: 10.1016/j.cub.2007.10.039.

Campani, C., Zucman-Rossi, J. and Nault, J.C. 2023. Genetics of Hepatocellular Carcinoma: From Tumor to Circulating DNA. *Cancers* 15(3). doi: 10.3390/cancers15030817.

Cao, L., Li, W.-J., Yang, J.-H., Wang, Y., Hua, Z.-J., Liu, D., Chen, Y.-Q., Zhang, H.-M., Zhang, R., Zhao, J.-S., Cheng, S.-J., & Zhang, Q. (2019). Inflammatory cytokine-induced expression of MASTL is involved in hepatocarcinogenesis by regulating cell cycle progression. *Oncology Letters* 17(3), 3163–3172. https://doi.org/10.3892/ol.2019.9983

Cao, W. et al. 2017. Dynamics of Proliferative and Quiescent Stem Cells in Liver Homeostasis and Injury. *Gastroenterology* 153(4), pp. 1133–1147. doi: 10.1053/j.gastro.2017.07.006.

Cao, W. et al. 2020. LGR5 marks targetable tumor-initiating cells in mouse liver cancer. *Nature Communications* 11(1), pp. 1–16. Available at: http://dx.doi.org/10.1038/s41467-020-15846-0.

Chandele, A., Prasad, V., Jagtap, J.C., Shukla, R. and Shastry, P.R. 2004. Upregulation of Survivin in G2/M Cells and Inhibition of Caspase 9 Activity Enhances Resistance in Staurosporine-Induced Apoptosis. *Neoplasia* 6(1):29-40

Chang, T.T. and Hughes-Fulford, M. 2014. Molecular mechanisms underlying the enhanced functions of three-dimensional hepatocyte aggregates. *Biomaterials* 35(7), pp. 2162–71. Available at: http://www.ncbi.nlm.nih.gov/pubmed/24332390.

Chen, F. et al. 2020. Broad Distribution of Hepatocyte Proliferation in Liver Homeostasis and Regeneration. *Cell Stem Cell* 26(1), pp. 27-33.e4. Available at: https://doi.org/10.1016/j.stem.2019.11.001.

Chen, X. et al. 2019. Deacetylation of β-catenin by SIRT1 regulates self-renewal and oncogenesis of liver cancer stem cells. *Cancer letters* 463, pp. 1–10. doi: 10.1016/j.canlet.2019.07.021.

Chernoff, J. 2021. The two-hit theory hits 50. *Molecular biology of the cell* 32(22), p. rt1. doi: 10.1091/mbc.E21-08-0407.

Chia, I. V and Costantini, F. 2005. Mouse axin and axin2/conductin proteins are functionally equivalent in vivo. *Molecular and cellular biology* 25(11), pp. 4371–6. Available at: http://mcb.asm.org/cgi/doi/10.1128/MCB.25.11.4371-4376.2005%0Ahttp://www.ncbi.nlm.nih.gov/pubmed/15899843%0Ahttp://www.pubmedcentral.nih.gov/articlerender.fcgi?artid=PMC1140612.

Chia, I. V, Kim, M.J., Itoh, K., Sokol, S.Y. and Costantini, F. 2009. Both the RGS domain and the six C-terminal amino acids of mouse Axin are required for normal embryogenesis. *Genetics* 181(4), pp. 1359–68. Available at: http://www.ncbi.nlm.nih.gov/pubmed/19204372.

Chiang, D.Y. et al. 2008. Focal gains of VEGFA and molecular classification of hepatocellular carcinoma. *Cancer Research* 68(16), pp. 6779–6788. doi: 10.1158/0008-5472.CAN-08-0742.

Colnot, S. et al. 2004. Liver-targeted disruption of Apc in mice activates β-catenin signaling and leads to hepatocellular carcinomas. *Proceedings of the National Academy of Sciences* 101(49), pp. 17216–17221. Available at: https://pnas.org/doi/full/10.1073/pnas.0404761101.

Corbett, J.L. and Duncan, S.A. 2019. iPSC-Derived Hepatocytes as a Platform for Disease Modeling and Drug Discovery. *Frontiers in Medicine* 6. Available at: https://www.frontiersin.org/article/10.3389/fmed.2019.00265/full.

Corda, G. and Sala, A. 2017. Non-canonical WNT/PCP signalling in cancer: Fzd6 takes centre stage. *Oncogenesis* 6(7), p. e364. doi: 10.1038/oncsis.2017.69.

Crauciuc, G. A., Iancu, M., Olah, P., Tripon, F., Anciuc, M., Gozar, L., Togănel, R., & Bănescu, C. (2020). Significant Associations between AXIN1 rs1805105, rs12921862, rs370681 Haplotypes and Variant Genotypes of AXIN2 rs2240308 with Risk of Congenital Heart Defects. *International Journal of Environmental Research and Public Health* 17(20). https://doi.org/10.3390/ijerph17207671

Cui, Y., Hu, X., Zhang, C., & Wang, K. (2022). The genetic polymorphisms of key genes in WNT pathway (LRP5 and AXIN1) was associated with osteoporosis susceptibility in Chinese Han population. *Endocrine* 75(2), 560–574. https://doi.org/10.1007/s12020-021-02866-z

Dahmen, R.P. et al. 2001. Deletions of AXIN1, a component of the WNT/wingless pathway, in sporadic medulloblastomas. *Cancer research* 61(19), pp. 7039–43. Available at: http://www.ncbi.nlm.nih.gov/pubmed/11585731.

Deharde, D. et al. 2016. Bile canaliculi formation and biliary transport in 3D sandwich-cultured hepatocytes in dependence of the extracellular matrix composition. *Archives of toxicology* 90(10), pp. 2497–511. Available at: http://www.ncbi.nlm.nih.gov/pubmed/27325308.

Dembowy, J., Adissu, H.A., Liu, J.C., Zacksenhaus, E. and Woodgett, J.R. 2015. Effect of glycogen synthase kinase-3 inactivation on mouse mammary gland development and oncogenesis. *Oncogene* 34(27), pp. 3514–3526. doi: 10.1038/onc.2014.279.

Deng, G.L., Zeng, S. and Shen, H. 2015. Chemotherapy and target therapy for hepatocellular carcinoma: New advances and challenges. *World Journal of Hepatology* 7(5), pp. 787–798. doi: 10.4254/wjh.v7.i5.787.

Du, Y., Broering, R., Li, X., Zhang, X., Liu, J., Yang, D. and Lu, M. 2021. In Vivo Mouse Models for Hepatitis B Virus Infection and Their Application. *Frontiers in Immunology* 12. doi: 10.3389/fimmu.2021.766534.

Dunn, J.C., Tompkins, R.G. and Yarmush, M.L. 1992. Hepatocytes in collagen sandwich: evidence for transcriptional and translational regulation. *The Journal of cell biology* 116(4), pp. 1043–53. Available at: http://www.ncbi.nlm.nih.gov/pubmed/1734019.

Fattovich, G., Stroffolini, T., Zagni, I. and Donato, F. 2004. Hepatocellular carcinoma in cirrhosis: Incidence and risk factors. *Gastroenterology* 127(5), pp. S35–S50. doi: 10.1053/j.gastro.2004.09.014.

Faux, M.C., Coates, J.L., Catimel, B., Cody, S., Clayton, A.H.A., Layton, M.J. and Burgess, A.W. 2008. Recruitment of adenomatous polyposis coli and beta-catenin to axin-puncta. *Oncogene* 27(44), pp. 5808–20. Available at: http://www.ncbi.nlm.nih.gov/pubmed/18591934.

Feng, G.J. et al. 2012. Conditional disruption of Axin1 leads to development of liver tumors in mice. *Gastroenterology* 143(6), pp. 1650–9. Available at: http://www.ncbi.nlm.nih.gov/pubmed/22960659.

Fickert, P. et al. 2007. A new xenobiotic-induced mouse model of sclerosing cholangitis and biliary fibrosis. *The American journal of pathology* 171(2), pp. 525–36. Available at: http://www.ncbi.nlm.nih.gov/pubmed/17600122.

Fiedler, M., Mendoza-Topaz, C., Rutherford, T.J., Mieszczanek, J. and Bienz, M. 2011. Dishevelled interacts with the DIX domain polymerization interface of Axin to interfere with its function in down-regulating β-catenin. *Proceedings of the National Academy of Sciences* 108(5), pp. 1937–1942. Available at: https://pnas.org/doi/full/10.1073/pnas.1017063108.

Fossat, N. et al. 2011. Stringent requirement of a proper level of canonical WNT signalling activity for head formation in mouse embryo. *Development* (Cambridge, England) 138(4), pp. 667–76. doi: 10.1242/dev.052803.

Frevert, C.W., Felgenhauer, J., Wygrecka, M., Nastase, M. V and Schaefer, L. 2018. Danger-Associated Molecular Patterns Derived From the Extracellular Matrix Provide Temporal Control of Innate Immunity. *The journal of histochemistry and cytochemistry : official journal of the Histochemistry Society* 66(4), pp. 213–227. doi: 10.1369/0022155417740880.

Furuhashi, M. et al. 2001. Axin Facilitates Smad3 Activation in the Transforming Growth Factor β Signaling Pathway. *Molecular and Cellular Biology* 21(15), pp. 5132–5141. doi: 10.1128/mcb.21.15.5132-5141.2001.

Galle, P.R. et al. 2018. EASL Clinical Practice Guidelines: Management of hepatocellular carcinoma. *Journal of Hepatology* 69(1), pp. 182–236. doi: 10.1016/j.jhep.2018.03.019.

Gammons, M. V., Renko, M., Johnson, C.M., Rutherford, T.J. and Bienz, M. 2016. Wnt Signalosome Assembly by DEP Domain Swapping of Dishevelled. *Molecular Cell* 64(1), pp. 92–104. doi: 10.1016/j.molcel.2016.08.026.

Ganne-Carrié, N. and Nahon, P. 2019. Hepatocellular carcinoma in the setting of alcohol-related liver disease. *Journal of Hepatology* 70(2), pp. 284–293. doi: 10.1016/j.jhep.2018.10.008.

Gaspar, C. and Fodde, R. 2004. APC dosage effects in tumorigenesis and stem cell differentiation. *The International Journal of Developmental Biology* 48(5–6), pp. 377–386. Available at: http://www.intjdevbiol.com/paper.php?doi=041807cg.

Gavagan, M., Fagnan, E., Speltz, E.B. and Zalatan, J.G. 2020. The Scaffold Protein Axin Promotes Signaling Specificity within the Wnt Pathway by Suppressing Competing Kinase Reactions. *Cell systems* 10(6), pp. 515-525.e5. Available at: http://www.ncbi.nlm.nih.gov/pubmed/32553184.

Gouas, D., Shi, H. and Hainaut, P. 2009. The aflatoxin-induced TP53 mutation at codon 249 (R249S): Biomarker of exposure, early detection and target for therapy. *Cancer Letters* 286(1), pp. 29–37. doi: 10.1016/j.canlet.2009.02.057.

Guichard, C. et al. 2012. Integrated analysis of somatic mutations and focal copy-number changes identifies key genes and pathways in hepatocellular carcinoma. *Nature Genetics* 44(6), pp. 694–698. doi: 10.1038/ng.2256.

Guo, X., Ramirez, A., Waddell, D.S., Li, Z., Liu, X. and Wang, X.F. 2008. Axin and GSK3-β control Smad3 protein stability and modulate TGF-β signaling. *Genes and Development* 22(1), pp. 106–120. doi: 10.1101/gad.1590908.

Hajka, D., Budziak, B., Pietras, Ł., Duda, P., McCubrey, J.A. and Gizak, A. 2021. GSK3 as a Regulator of Cytoskeleton Architecture: Consequences for Health and Disease. *Cells* 10(8). Available at: http://www.ncbi.nlm.nih.gov/pubmed/34440861.

Halpern, K.B. et al. 2017. Single-cell spatial reconstruction reveals global division of labour in the mammalian liver. *Nature*. 542(7641):352-356 Available at: http://www.nature.com/doifinder/10.1038/nature21065.

Hanahan, D. 2022. Hallmarks of Cancer: New Dimensions. *Cancer Discovery* 12(1), pp. 31–46. doi: 10.1158/2159-8290.CD-21-1059.

Harada, N., Miyoshi, H., Murai, N., Oshima, H., Tamai, Y., Oshima, M. and Taketo, M.M. 2002. Lack of tumorigenesis in the mouse liver after adenovirus-mediated expression of a dominant stable mutant of beta-catenin. *Cancer research* 62(7), pp. 1971–7. Available at: http://www.ncbi.nlm.nih.gov/pubmed/11929813.

Hart, M., Adams, S.D. and Draviam, V.M. 2021. Multinucleation associated DNA damage blocks proliferation in p53-compromised cells. *Communications Biology* 4(1). doi: 10.1038/s42003-021-01979-5.

Hart, M.J., De Los Santos, R., Albert, I.N., Rubinfeld, B. and Polakis, P. 1998. Downregulation of β-catenin by human Axin and its association with the APC tumor

suppressor, β-catenin and GSK3β. *Current Biology* 8(10), pp. 573–581. doi: 10.1016/s0960-9822(98)70226-x.

Haseeb, M., Pirzada, R.H., Ul Ain, Q. and Choi, S. 2019. Wnt signaling in the regulation of immune cell and cancer therapeutics. *Cells* 8(11). doi: 10.3390/cells8111380.

Hefler, J., Marfil-Garza, B.A., Pawlick, R.L., Freed, D.H., Karvellas, C.J., Bigam, D.L. and Shapiro, A.M.J. 2021. Preclinical models of acute liver failure: a comprehensive review. *PeerJ* 9, p. e12579. doi: 10.7717/peerj.12579.

Higashi, T., Friedman, S.L. and Hoshida, Y. 2017. Hepatic stellate cells as key target in liver fibrosis. *Advanced drug delivery reviews* 121, pp. 27–42. Available at: http://www.ncbi.nlm.nih.gov/pubmed/28506744.

Hofer, M. and Lutolf, M.P. 2021. Engineering organoids. *Nature Reviews Materials* 6(5), pp. 402–420. Available at: https://www.nature.com/articles/s41578-021-00279-y.

Hoffmeister, L., Diekmann, M., Brand, K. and Huber, R. 2020. GSK3: A Kinase Balancing Promotion and Resolution of Inflammation. *Cells* 9(4). Available at: http://www.ncbi.nlm.nih.gov/pubmed/32231133.

Hoshida, Y. et al. 2009. Integrative transcriptome analysis reveals common molecular subclasses of human hepatocellular carcinoma. *Cancer Research* 69(18), pp. 7385–7392. doi: 10.1158/0008-5472.CAN-09-1089.

Hu, H. et al. 2018. Long-Term Expansion of Functional Mouse and Human Hepatocytes as 3D Organoids. *Cell* 175(6), pp. 1591-1606.e19. Available at: http://www.ncbi.nlm.nih.gov/pubmed/30500538.

Huang, J., Ye, X., Guan, J., Chen, B., Li, Q., Zheng, X., Liu, L., Wang, S., Ding, Y., Ding, Y., & Chen, L. (2013). Tiam1 is associated with hepatocellular carcinoma metastasis. *International Journal of Cancer*, *132*(1), 90–100. https://doi.org/10.1002/ijc.27627

Huch, M. et al. 2013. In vitro expansion of single Lgr5+ liver stem cells induced by Wnt-driven regeneration. *Nature* 494(7436), pp. 247–50. Available at: http://www.ncbi.nlm.nih.gov/pubmed/23354049.

Huch, M. et al. 2015. Long-term culture of genome-stable bipotent stem cells from adult human liver. *Cell* 160(1–2), pp. 299–312. Available at: http://dx.doi.org/10.1016/j.cell.2014.11.050.

Hughes, D.M. et al. 2021. Serum Levels of α-Fetoprotein Increased More Than 10 Years Before Detection of Hepatocellular Carcinoma. *Clinical Gastroenterology and Hepatology* 19(1), pp. 162-170.e4. doi: 10.1016/j.cgh.2020.04.084.

Hughes, T.A. and Brady, H.J.M. 2005. Expression of Axin2 is regulated by the alternative 5′-untranslated regions of its mRNA. *Journal of Biological Chemistry* 280(9), pp. 8581–8588. doi: 10.1074/jbc.M410806200.

Ireland, H., Kemp, R., Houghton, C., Howard, L., Clarke, A.R., Sansom, O.J. and Winton, D.J. 2004. Inducible Cre-Mediated Control of Gene Expression in the Murine Gastrointestinal Tract: Effect of Loss of β-Catenin. *Gastroenterology* 126(5), pp. 1236–1246. doi: 10.1053/j.gastro.2004.03.020.

Johnston, L. A. (2014). Socializing with MYC: cell competition in development and as a model for premalignant cancer. *Cold Spring Harbor Perspectives in Medicine*, *4*(4), a014274. https://doi.org/10.1101/cshperspect.a014274

Jia, J. et al. 2017. Tankyrase inhibitors suppress hepatocellular carcinoma cell growth via modulating the Hippo cascade. *PloS one* 12(9), p. e0184068. doi: 10.1371/journal.pone.0184068.

Jiang, J.X. and Török, N.J. 2013. Liver Injury and the Activation of the Hepatic Myofibroblasts. Current pathobiology reports 1(3), pp. 215–223. doi: 10.1007/s40139-013-0019-6.

Jinek, M., Chylinski, K., Fonfara, I., Hauer, M., Doudna, J.A. and Charpentier, E. 2012. A programmable dual-RNA-guided DNA endonuclease in adaptive bacterial immunity. *Science* (New York, N.Y.) 337(6096), pp. 816–21. Available at: http://www.ncbi.nlm.nih.gov/pubmed/22745249.

Kamimoto, K., Kaneko, K., Kok, C.Y.-Y., Okada, H., Miyajima, A. and Itoh, T. 2016. Heterogeneity and stochastic growth regulation of biliary epithelial cells dictate dynamic epithelial tissue remodeling. *eLife* 5. Available at: https://elifesciences.org/articles/15034.

Kandimalla, R. et al. 2017. Methylation of WNT target genes AXIN2 and DKK1 as robust biomarkers for recurrence prediction in stage II colon cancer. *Oncogenesis* 6(4). doi: 10.1038/oncsis.2017.9.

Karkampouna, S., Ten Dijke, P., Dooley, S. and Kruithof-De Julio, M. 2012. TGF Signaling in Liver Regeneration. *Cell Tissue Res* 347(1):245-56

Katoh, H., Shibata, T., Kokubu, A., Ojima, H., Fukayama, M., Kanai, Y. and Hirohashi, S. 2006. Epigenetic instability and chromosomal instability in hepatocellular carcinoma. *American Journal of Pathology* 168(4), pp. 1375–1384. doi: 10.2353/ajpath.2006.050989.

Kaur, I., Vasudevan, A., Rawal, P., Tripathi, D., Ramakrishna, S., Kaur, S. and Sarin, S. 2023. Primary Hepatocyte Isolation and Cultures: Technical Aspects, Challenges and Advancements. *Bioengineering* 10(2), p. 131. doi: 10.3390/bioengineering10020131.

Kemp, R., Ireland, H., Clayton, E., Houghton, C., Howard, L. and Winton, D.J. 2004. Elimination of background recombination: somatic induction of Cre by combined transcriptional regulation and hormone binding affinity. *Nucleic acids research* 32(11), pp. e92–e92. Available at: http://www.pubmedcentral.nih.gov/articlerender.fcgi?artid=443557&tool=pmcentrez&rendertype=abstract.

Kerr, G.E., Young, J.C., Horvay, K., Abud, H.E. and Loveland, K.L. 2014. Regulated Wnt/Beta-Catenin Signaling Sustains Adult Spermatogenesis in Mice1. *Biology of Reproduction* 90(1). doi: 10.1095/biolreprod.112.105809.

Kersten, K., de Visser, K.E., van Miltenburg, M.H. and Jonkers, J. 2017. Genetically engineered mouse models in oncology research and cancer medicine. *EMBO molecular medicine* 9(2), pp. 137–153. Available at: http://www.ncbi.nlm.nih.gov/pubmed/28028012.

Khan, Z., Orr, A., Michalopoulos, G.K. and Ranganathan, S. 2017. Immunohistochemical Analysis of the Stem Cell Marker LGR5 in Pediatric Liver Disease. *Pediatric and developmental pathology : the official journal of the Society for Pediatric Pathology and the Paediatric Pathology Society* 20(1), pp. 16–27. doi: 10.1177/1093526616686244.

Kim, H., Kim, M., Im, S.-K. and Fang, S. 2018. Mouse Cre-LoxP system: general principles to determine tissue-specific roles of target genes. *Laboratory Animal Research* 34(4), p. 147. doi: 10.5625/lar.2018.34.4.147.

Kim, K.H. et al. 2004. Expression of connective tissue growth factor, a biomarker in senescence of human diploid fibroblasts, is up-regulated by a transforming growth factor-β-mediated signaling pathway. *Biochemical and Biophysical Research Communications* 318(4), pp. 819–825. doi: 10.1016/j.bbrc.2004.04.108.

Kin, M., Torimura, T., Ueno, T., Inuzuka, S. and Tanikawa, K. 1994. Sinusoidal capillarization in small hepatocellular carcinoma. Pathology international 44(10–11), pp. 771–8. doi: 10.1111/j.1440-1827.1994.tb02925.x.

Kinzler, K.W. and Vogelstein, B. 1996. Lessons from Hereditary Colorectal Cancer. *Cell* 87(2), pp. 159–170. Available at: https://linkinghub.elsevier.com/retrieve/pii/S0092867400813331.

Kitazawa, M., Hatta, T., Ogawa, K., Fukuda, E., Goshima, N. and Natsume, T. 2017. Determination of Rate-Limiting Factor for Formation of Beta-Catenin Destruction Complexes Using Absolute Protein Quantification. *Journal of proteome research* 16(10), pp. 3576–3584. Available at: http://www.ncbi.nlm.nih.gov/pubmed/28810742.

Knöfler, M., Haider, S., Saleh, L., Pollheimer, J., Gamage, T.K.J.B. and James, J. 2019. Human placenta and trophoblast development: key molecular mechanisms and model systems. *Cellular and Molecular Life Sciences* 76(18), pp. 3479–3496. doi: 10.1007/s00018-019-03104-6.

Krausova, M. and Korinek, V. 2014. Wnt signaling in adult intestinal stem cells and cancer. *Cellular Signalling*. 26(3):570-9 doi: 10.1016/j.cellsig.2013.11.032.

Lammi, L. et al. 2004. Mutations in AXIN2 Cause Familial Tooth Agenesis and Predispose to Colorectal Cancer. *American Journal of Human Genetics* 74(5), pp. 1043–1050. doi: 10.1086/386293.

de Lau, W., Peng, W.C., Gros, P. and Clevers, H. 2014. The R-spondin/Lgr5/Rnf43 module: Regulator of Wnt signal strength. *Genes and Development* 28(4), pp. 305–316. doi: 10.1101/gad.235473.113.

Lee, E., Salic, A., Krüger, R., Heinrich, R. and Kirschner, M.W. 2003. The Roles of APC and Axin Derived from Experimental and Theoretical Analysis of the Wnt Pathway. Roel Nusse ed. *PLoS Biology* 1(1), p. e10. Available at: https://dx.plos.org/10.1371/journal.pbio.0000010.

Lee, J.S. et al. 2006. A novel prognostic subtype of human hepatocellular carcinoma derived from hepatic progenitor cells. *Nature Medicine* 12(4), pp. 410–416. doi: 10.1038/nm1377.

Lefkowitch, J.H. 2021. Acute Viral Hepatitis. In: Scheuer's Liver Biopsy Interpretation. Elsevier, pp. 89–107. Available at: https://linkinghub.elsevier.com/retrieve/pii/B9780702075841000061.

Lei, Y. et al. 2020. MicroRNAs target the Wnt/β catenin signaling pathway to regulate epithelial mesenchymal transition in cancer (Review). *Oncology reports* 44(4), pp. 1299–1313. doi: 10.3892/or.2020.7703.

Li, Q. et al. 2009. Axin determines cell fate by controlling the p53 activation threshold after DNA damage. *Nature Cell Biology* 11(9), pp. 1128–1134. doi: 10.1038/ncb1927.

Li, S., Wang, C., Liu, X., Hua, S. and Liu, X. 2015. The roles of AXIN2 in tumorigenesis and epigenetic regulation. *Familial cancer* 14(2), pp. 325–31. Available at: http://www.ncbi.nlm.nih.gov/pubmed/25504512.

Liang, B. et al. 2022. Differential requirement of Hippo cascade during CTNNB1 or AXIN1 mutation-driven hepatocarcinogenesis. *Hepatology*. 77(6):1929-1942 doi: 10.1002/hep.32693.

Liko, D. et al. 2019. Brf1 loss and not overexpression disrupts tissues homeostasis in the intestine, liver and pancreas. *Cell Death and Differentiation* 26(12), pp. 2535–2550. doi: 10.1038/s41418-019-0316-7.

Limaye, P.B., Bowen, W.C., Orr, A. v., Luo, J., Tseng, G.C. and Michalopoulos, G.K. 2008. Mechanisms of hepatocyte growth factor-mediated and epidermal growth factor-mediated signaling in transdifferentiation of rat hepatocytes to biliary epithelium. *Hepatology* 47(5), pp. 1702–1713. doi: 10.1002/hep.22221.

Lin, S. et al. 2018. Distributed hepatocytes expressing telomerase repopulate the liver in homeostasis and injury. *Nature* 556(7700), pp. 244–248. Available at: http://www.nature.com/articles/s41586-018-0004-7.

Lipson, K.E., Wong, C., Teng, Y. and Spong, S. 2012. CTGF is a central mediator of tissue remodeling and fibrosis and its inhibition can reverse the process of fibrosis. *Fibrogenesis & Tissue Repair* 5(S1). doi: 10.1186/1755-1536-5-s1-s24.

Liu, J. et al. 2022. Wnt/β-catenin signalling: function, biological mechanisms, and therapeutic opportunities. *Signal Transduction and Targeted Therapy* 7(1). doi: 10.1038/s41392-021-00762-6.

Liu, W. et al. 2006. Axin is a scaffold protein in TGF-β signaling that promotes degradation of Smad7 by Arkadia. *EMBO Journal* 25(8), pp. 1646–1658. doi: 10.1038/sj.emboj.7601057.

Liu, Y. et al. 2014. Clinical significance of CTNNB1 mutation and Wnt pathway activation in endometrioid endometrial carcinoma. *Journal of the National Cancer Institute* 106(9). doi: 10.1093/jnci/dju245.

Liu, Y., Meyer, C., Xu, C., Weng, H., Hellerbrand, C., ten Dijke, P. and Dooley, S. 2013. Animal models of chronic liver diseases. *American Journal of Physiology-Gastrointestinal and Liver Physiology* 304(5), pp. G449–G468. Available at: https://www.physiology.org/doi/10.1152/ajpgi.00199.2012.

Livak, K.J. and Schmittgen, T.D. 2001. Analysis of Relative Gene Expression Data Using Real-Time Quantitative PCR and the 2−ΔΔCT Method. *Methods* 25(4), pp. 402–408. Available at: https://linkinghub.elsevier.com/retrieve/pii/S1046202301912629.

Llovet, J.M. et al. 2021. Hepatocellular carcinoma. *Nature reviews*. Disease primers 7(1), p. 6. Available at: http://www.ncbi.nlm.nih.gov/pubmed/33479224.

Llovet, J.M., Zucman-Rossi, J., Pikarsky, E., Sangro, B., Schwartz, M., Sherman, M. and Gores, G. 2016. Hepatocellular carcinoma. *Nature Reviews* Disease Primers 2. doi: 10.1038/nrdp.2016.18.

Loforese, G. et al. 2017. Impaired liver regeneration in aged mice can be rescued by silencing Hippo core kinases MST1 and MST2. *EMBO Molecular Medicine* 9(1), pp. 46–60. doi: 10.15252/emmm.201506089.

Lu, T. et al. 2021. High Expression of Hyaluronan-Mediated Motility Receptor Predicts Adverse Outcomes: A Potential Therapeutic Target for Head and Neck Squamous Cell Carcinoma. *Frontiers in Oncology* 11. doi: 10.3389/fonc.2021.608842.

Luo, W. and Lin, S.-C. 2004. Axin: a master scaffold for multiple signaling pathways. *Neuro-Signals* 13(3), pp. 99–113. doi: 10.1159/000076563.

Luo, W., Ng, W.W., Jin, L.H., Ye, Z., Han, J. and Lin, S.C. 2003. Axin utilizes distinct regions for competitive MEKK1 and MEKK4 binding and JNK activation. *Journal of Biological Chemistry* 278(39), pp. 37451–37458. doi: 10.1074/jbc.M305277200.

Lustig, B. et al. 2002a. Negative feedback loop of Wnt signaling through upregulation of conductin/axin2 in colorectal and liver tumors. *Molecular and cellular biology* 22(4), pp. 1184–93. Available at: http://www.ncbi.nlm.nih.gov/pubmed/11809809%5Cnhttp://www.pubmedcentral.nih.gov/articlerender.fcgi?artid=PMC134640.

Ly, T. et al. 2017. Proteomic analysis of cell cycle progression in asynchronous cultures, including mitotic subphases, using PRIMMUS. *eLife* 6. Available at: https://elifesciences.org/articles/27574.

Ma, J., Lu, W., Chen, D., Xu, B. and Li, Y. 2017. Role of Wnt Co-Receptor LRP6 in Triple Negative Breast Cancer Cell Migration and Invasion. *Journal of Cellular Biochemistry* 118(9), pp. 2968–2976. doi: 10.1002/jcb.25956.

Macfarlane, D.P. et al. 2011. Metabolic pathways promoting intrahepatic fatty acid accumulation in methionine and choline deficiency: implications for the pathogenesis of steatohepatitis. American journal of physiology. *Endocrinology and metabolism* 300(2), pp. E402-9. Available at: http://www.ncbi.nlm.nih.gov/pubmed/21119028.

Madison, B.B., Dunbar, L., Qiao, X.T., Braunstein, K., Braunstein, E. and Gumucio, D.L. 2002. Cis elements of the villin gene control expression in restricted domains of the vertical (crypt) and horizontal (duodenum, cecum) axes of the intestine. *The Journal of biological chemistry* 277(36), pp. 33275–83. doi: 10.1074/jbc.M204935200.

Mah, L.J., El-Osta, A. and Karagiannis, T.C. 2010. γh2AX: A sensitive molecular marker of DNA damage and repair. *Leukemia* 24(4), pp. 679–686. doi: 10.1038/leu.2010.6.

Mallick, A., Jhaveri, N., Jeon, J., Chang, Y., Shah, K., Hosein, H. and Gupta, B.P. 2022. Genetic analysis of Caenorhabditis elegans pry-1/Axin suppressors identifies genes involved in reproductive structure development, stress responses, and aging. *G3 (Bethesda, Md.)* 12(2). doi: 10.1093/g3journal/jkab430.

Maronpot, R.R. 2009. Biological Basis of Differential Susceptibility to Hepatocarcinogenesis among Mouse Strains. *Journal of toxicologic pathology* 22(1), pp. 11–33. Available at: http://www.ncbi.nlm.nih.gov/pubmed/22271974.

Martini, T., Naef, F. and Tchorz, J.S. 2023. Spatiotemporal Metabolic Liver Zonation and Consequences on Pathophysiology. *Annual Review of Pathology: Mechanisms of Disease* 18(1), pp. 439–466. Available at: https://www.annualreviews.org/doi/10.1146/annurev-pathmechdis-031521-024831.

Marvin, M.L., Mazzoni, S.M., Herron, C.M., Edwards, S., Gruber, S.B. and Petty, E.M. 2011. AXIN2-associated autosomal dominant ectodermal dysplasia and neoplastic syndrome. *American journal of medical genetics*. Part A 155A(4), pp. 898–902. Available at: http://www.ncbi.nlm.nih.gov/pubmed/21416598.

Matsuda, T. and Cepko, C.L. 2007. Controlled expression of transgenes introduced by in vivo electroporation. *PNAS* 104(3):1027-32 Available at: www.pnas.org/cgi/content/full/.

Matsumoto, T., Wakefield, L., Tarlow, B.D. and Grompe, M. 2020. In Vivo Lineage Tracing of Polyploid Hepatocytes Reveals Extensive Proliferation during Liver Regeneration. *Cell Stem Cell* 26(1), pp. 34-47.e3. doi: 10.1016/j.stem.2019.11.014.

May, S. et al. 2023. Absent expansion of AXIN2+ hepatocytes and altered physiology in Axin2CreERT2 mice challenges the role of pericentral hepatocytes in homeostatic liver regeneration. *Journal of Hepatology*. doi: 10.1016/j.jhep.2023.01.009.

Mazzoni, S.M. and Fearon, E.R. 2014. AXIN1 and AXIN2 variants in gastrointestinal cancers. *Cancer Letters* 355(1), pp. 1–8. doi: 10.1016/j.canlet.2014.09.018.

Méniel, V. et al. 2013. Cited1 Deficiency Suppresses Intestinal Tumorigenesis. Clurman, B. E. ed. *PLoS Genetics* 9(8), p. e1003638. Available at: http://dx.plos.org/10.1371/journal.pgen.1003638.

Méniel, V., Megges, M., Young, M.A., Cole, A., Sansom, O.J. and Clarke, A.R. 2015. Apc and p53 interaction in DNA damage and genomic instability in hepatocytes. *Oncogene* 34(31), pp. 4118–4129. Available at: http://www.nature.com/doifinder/10.1038/onc.2014.342.

Michalopoulos, G.K. 2010. Liver regeneration after partial hepatectomy: Critical analysis of mechanistic dilemmas. *American Journal of Pathology* 176(1), pp. 2–13. Available at: http://dx.doi.org/10.2353/ajpath.2010.090675.

Michalopoulos, G.K. and Bhushan, B. 2021. Liver regeneration: biological and pathological mechanisms and implications. *Nature Reviews Gastroenterology and Hepatology* 18(1), pp. 40–55. doi: 10.1038/s41575-020-0342-4.

Mikels, A.J. and Nusse, R. 2006. Wnts as ligands: Processing, secretion and reception. *Oncogene* 25(57), pp. 7461–7468. doi: 10.1038/sj.onc.1210053.

Mirabelli, Coppola and Salvatore. 2019. Cancer Cell Lines Are Useful Model Systems for Medical Research. *Cancers* 11(8), p. 1098. Available at: https://www.mdpi.com/2072-6694/11/8/1098.

Miyoshi, H. et al. 2009. Hepatocellular carcinoma development induced by conditional β-catenin activation in Lkb1+/- mice. *Cancer Science* 100(11), pp. 2046–2053. doi: 10.1111/j.1349-7006.2009.01284.x.

Mizuno, T. et al. 2012. YAP induces malignant mesothelioma cell proliferation by upregulating transcription of cell cycle-promoting genes. *Oncogene* 31(49), pp. 5117–5122. doi: 10.1038/onc.2012.5.

Monga, S.P.S. 2014. Role and regulation of β-catenin signaling during physiological liver growth. *Gene expression* 16(2), pp. 51–62. Available at: http://www.ncbi.nlm.nih.gov/pubmed/24801166.

Monga, S.P.S., Pediaditakis, P., Mule, K., Beer Stolz, D. and Michalopoulos, G.K. 2001. Changes in Wnt/β-Catenin Pathway During Regulated Growth in Rat Liver Regeneration. Hepatology 33(5): 1098–1109. doi: 10.1053/jhep.2001.23786

Morin, P.J., Sparks, A.B., Korinek, V., Barker, N., Clevers, H., Vogelstein, B. and Kinzler, K.W. 1997. Activation of beta-catenin-Tcf signaling in colon cancer by mutations in beta-catenin or APC. *Science* (New York, N.Y.) 275(5307), pp. 1787–90. Available at: http://www.ncbi.nlm.nih.gov/pubmed/9065402.

Morrone, S., Cheng, Z., Moon, R.T., Cong, F. and Xu, W. 2012. Crystal structure of a Tankyrase-Axin complex and its implications for Axin turnover and Tankyrase substrate recruitment. *Proceedings of the National Academy of Sciences* 109(5), pp. 1500–1505. Available at: https://pnas.org/doi/full/10.1073/pnas.1116618109.

Moshkovsky, A.R. and Kirschner, M.W. 2022. The nonredundant nature of the Axin2 regulatory network in the canonical Wnt signaling pathway. *Proceedings of the National Academy of Sciences of the United States of America* 119(9). doi: 10.1073/pnas.2108408119.

Murray, G.I., Patimalla, S., Stewart, K.N., Miller, I.D. and Heys, S.D. 2010. Profiling the expression of cytochrome P450 in breast cancer. *Histopathology* 57(2), pp. 202–11. Available at: http://www.ncbi.nlm.nih.gov/pubmed/20716162.

Nagy, Z., Kalousi, A., Furst, A., Koch, M., Fischer, B. and Soutoglou, E. 2016. Tankyrases Promote Homologous Recombination and Check Point Activation in Response to DSBs. *PLoS genetics* 12(2), p. e1005791. doi: 10.1371/journal.pgen.1005791.

Nault, J.C. et al. 2014. Telomerase reverse transcriptase promoter mutation is an early somatic genetic alteration in the transformation of premalignant nodules in hepatocellular carcinoma on cirrhosis. *Hepatology* 60(6), pp. 1983–1992. doi: 10.1002/hep.27372.

Nejak-Bowen, K.N. et al. 2010. Accelerated liver regeneration and hepatocarcinogenesis in mice overexpressing serine-45 mutant beta-catenin. *Hepatology* (Baltimore, Md.) 51(5), pp. 1603–13. Available at: http://www.ncbi.nlm.nih.gov/pubmed/20432254.

Nguyen, T.B., Roncalli, M., di Tommaso, L. and Kakar, S. 2016. Combined use of heat-shock protein 70 and glutamine synthetase is useful in the distinction of typical hepatocellular adenoma from atypical hepatocellular neoplasms and well-differentiated hepatocellular carcinoma. *Modern Pathology* 29(3), pp. 283–292. doi: 10.1038/modpathol.2015.162.

Nguyen-Lefebvre, A.T. and Horuzsko, A. 2015. Kupffer Cell Metabolism and Function. *Journal of enzymology and metabolism* 1(1).

Nong, J., Kang, K., Shi, Q., Zhu, X., Tao, Q. and Chen, Y. 2021. Phase separation of Axin organizes the β-catenin destruction complex. *Journal of Cell Biology* 220(4). Available at: https://rupress.org/jcb/article/doi/10.1083/jcb.202012112/211840/Phase-separation-of-Axin-organizes-the-catenin.

Novellasdemunt, L. et al. 2017. USP7 Is a Tumor-Specific WNT Activator for APC-Mutated Colorectal Cancer by Mediating β-Catenin Deubiquitination. *Cell reports* 21(3), pp. 612–627. Available at: http://www.ncbi.nlm.nih.gov/pubmed/29045831.

Nusse, R. and Clevers, H. 2017. Wnt/β-Catenin Signaling, Disease, and Emerging Therapeutic Modalities. *Cell* 169(6), pp. 985–999. Available at: http://dx.doi.org/10.1016/j.cell.2017.05.016.

Nusse, R. and Varmus, H.E. 1982. Many Tumors Induced by the Mouse Mammary Tumor Virus Contain a Provirus Integrated in the Same Region of the Host Genome. Ochoa, B. et al. 2010. Hedgehog signaling is critical for normal liver regeneration after partial hepatectomy in mice. *Hepatology* 51(5), pp. 1712–1723. doi: 10.1002/hep.23525.

Offergeld, A (2015) PhD Thesis Acute effects of Axin loss in the mouse liver and embryonic development.

Oji, A. et al. 2016. CRISPR/Cas9 mediated genome editing in ES cells and its application for chimeric analysis in mice. *Scientific Reports* 6. doi: 10.1038/srep31666.

Okada, S., Vaeteewoottacharn, K. and Kariya, R. 2019. Application of Highly Immunocompromised Mice for the Establishment of Patient-Derived Xenograft (PDX) Models. *Cells* 8(8). Available at: http://www.ncbi.nlm.nih.gov/pubmed/31412684.

Paglia, S., Sollazzo, M., Di Giacomo, S., Strocchi, S., & Grifoni, D. (2020). Exploring MYC relevance to cancer biology from the perspective of cell competition. *Seminars in Cancer Biology*, *63*, 49–59. https://doi.org/10.1016/j.semcancer.2019.05.009

Parsons, M.J., Tammela, T. and Dow, L.E. 2021. WNT as a driver and dependency in cancer. *Cancer Discovery* 11(10), pp. 2413–2429. doi: 10.1158/2159-8290.CD-21-0190.

Paschidis, K., Zougros, A., Chatziandreou, I., Tsikalakis, S., Korkolopoulou, P., Kavantzas, N. and Saetta, A.A. 2022. Methylation analysis of APC, AXIN2, DACT1, RASSF1A and MGMT gene promoters in non-small cell lung cancer. *Pathology, research and practice* 234, p. 153899. Available at: http://www.ncbi.nlm.nih.gov/pubmed/35489124.

Péneau, C. et al. 2022. Hepatitis B virus integrations promote local and distant oncogenic driver alterations in hepatocellular carcinoma. *Gut* 71(3), pp. 616–626. doi: 10.1136/gutjnl-2020-323153.

Peng, W.C. et al. 2018. Inflammatory Cytokine TNFα Promotes the Long-Term Expansion of Primary Hepatocytes in 3D Culture. *Cell* 175(6), pp. 1607-1619.e15. doi: 10.1016/j.cell.2018.11.012.

Perry, W.L. et al. 1995. Phenotypic and molecular analysis of a transgenic insertional allele of the mouse fused locus. *Genetics* 141(1), pp. 321–332. doi: 10.1093/genetics/141.1.321.

Petersen, C.P. and Reddien, P.W. 2009. Wnt signaling and the polarity of the primary body axis. *Cell* 139(6), pp. 1056–68. Available at: http://www.ncbi.nlm.nih.gov/pubmed/20005801.

Planas-Paz, L. et al. 2016. The RSPO-LGR4/5-ZNRF3/RNF43 module controls liver zonation and size. *Nature Cell Biology* 18(5), pp. 467–479. doi: 10.1038/ncb3337.

Poulton, J.S., Mu, F.W., Roberts, D.M. and Peifer, M. 2013. APC2 and Axin promote mitotic fidelity by facilitating centrosome separation and cytoskeletal regulation. *Development* (Cambridge) 140(20), pp. 4226–4236. doi: 10.1242/dev.094425.

Preziosi, M., Okabe, H., Poddar, M., Singh, S. and Monga, S.P. 2018. Endothelial Wnts regulate β-catenin signaling in murine liver zonation and regeneration: A sequel to the Wnt-Wnt situation. *Hepatology communications* 2(7), pp. 845–860. Available at: http://www.ncbi.nlm.nih.gov/pubmed/30027142.

Pronobis, M.I., Rusan, N.M. and Peifer, M. 2015. A novel GSK3-regulated APC:Axin interaction regulates Wnt signaling by driving a catalytic cycle of efficient βcatenin destruction. *eLife* 4. Available at: https://elifesciences.org/articles/08022.

Qiao, Y. et al. 2019. Axis inhibition protein 1 (Axin1) Deletion–Induced Hepatocarcinogenesis Requires Intact β-Catenin but Not Notch Cascade in Mice. *Hepatology* 70(6), pp. 2003–2017. Available at: https://onlinelibrary.wiley.com/doi/10.1002/hep.30556.

Quevedo, R. et al. 2020. Assessment of Genetic Drift in Large Pharmacogenomic Studies. *Cell Systems* 11(4), pp. 393-401.e2. doi: 10.1016/j.cels.2020.08.012.

Quinn, H.M. et al. 2021. YAP and β;-Catenin cooperate to drive oncogenesis in basal breast cancer. *Cancer Research* 81(8), pp. 2116–2127. doi: 10.1158/0008-5472.CAN-20-2801.

Rahman, S., Patel, Y., Murray, J., Patel, K. V, Sumathipala, R., Sobel, M. and Wijelath, E.S. 2005. Novel hepatocyte growth factor (HGF) binding domains on fibronectin and vitronectin coordinate a distinct and amplified Met-integrin induced signalling pathway in endothelial cells. BMC cell biology 6(1), p. 8. doi: 10.1186/1471-2121-6-8.

Ramadan, R., van Driel, M.S., Vermeulen, L. and van Neerven, S.M. 2022. Intestinal stem cell dynamics in homeostasis and cancer. *Trends in Cancer* 8(5), pp. 416–425. doi: 10.1016/j.trecan.2022.01.011.

Ran, F.A. et al. 2013. Double nicking by RNA-guided CRISPR Cas9 for enhanced genome editing specificity. *Cell* 154(6), pp. 1380–9. Available at: http://www.ncbi.nlm.nih.gov/pubmed/23992846.

Raven, A. et al. 2017. Cholangiocytes act as facultative liver stem cells during impaired hepatocyte regeneration. *Nature* 547(7663), pp. 350–354. Available at: http://dx.doi.org/10.1038/nature23015.

Ravichandra, A. and Schwabe, R.F. 2021. Mouse Models of Liver Fibrosis. pp. 339–356. Available at: https://link.springer.com/10.1007/978-1-0716-1382-5_23.

Rebouissou, S. and Nault, J.-C. 2020. Advances in molecular classification and precision oncology in hepatocellular carcinoma. *Journal of hepatology* 72(2), pp. 215–229. Available at: http://www.ncbi.nlm.nih.gov/pubmed/31954487.

Reed, K.R. et al. 2008. B-catenin deficiency, but not Myc deletion, suppresses the immediate phenotypes of APC loss in the liver. *Proceedings of the National Academy of Sciences of the United States of America* 105(48), pp. 18919–18923. doi: 10.1073/pnas.0805778105.

Reig, M. et al. 2022. BCLC strategy for prognosis prediction and treatment recommendation: The 2022 update. *Journal of Hepatology* 76(3), pp. 681–693. doi: 10.1016/j.jhep.2021.11.018.

Rekha, R.D. et al. 2008. Thioacetamide accelerates steatohepatitis, cirrhosis and HCC by expressing HCV core protein in transgenic zebrafish Danio rerio. Toxicology 243(1–2), pp. 11–22. Available at: http://www.ncbi.nlm.nih.gov/pubmed/17997003.

Rim, E.Y., Clevers, H. and Nusse, R. 2022. The Wnt Pathway: From Signaling Mechanisms to Synthetic Modulators. *Annual review of biochemistry* 91, pp. 571–598. Available at: http://www.ncbi.nlm.nih.gov/pubmed/35303793.

Rinella, M.E. and Green, R.M. 2004. The methionine-choline deficient dietary model of steatohepatitis does not exhibit insulin resistance. *Journal of hepatology* 40(1), pp. 47–51. Available at: http://www.ncbi.nlm.nih.gov/pubmed/14672613.

Rivera, B. et al. 2014. A novel AXIN2 germline variant associated with attenuated FAP without signs of oligondontia or ectodermal dysplasia. *European Journal of Human Genetics* 22(3), pp. 423–426. doi: 10.1038/ejhg.2013.146.

Rocha, A.S., Vidal, V., Mertz, M., Kendall, T.J., Charlet, A., Okamoto, H. and Schedl, A. 2015. The Angiocrine Factor Rspondin3 Is a Key Determinant of Liver Zonation. *Cell Reports* 13(9), pp. 1757–1764. Available at: http://dx.doi.org/10.1016/j.celrep.2015.10.049.

Rodriguez, M. and Potter, D.A. 2013. CYP1A1 regulates breast cancer proliferation and survival. *Molecular cancer research* : MCR 11(7), pp. 780–92. doi: 10.1158/1541-7786.MCR-12-0675.

Rosso, S.B. and Inestrosa, N.C. 2013. WNT signalling in neuronal maturation and synaptogenesis. *Frontiers in Cellular Neuroscience* 4;7:103 doi: 10.3389/fncel.2013.00103.

Royle, S.R., Tabin, C.J. and Young, J.J. 2021. Limb positioning and initiation: An evolutionary context of pattern and formation. *Developmental Dynamics* 250(9), pp. 1264–1279. doi: 10.1002/dvdy.308.

Rui, H.L., Fan, E., Zhou, H.M., Xu, Z., Zhang, Y. and Lin, S.C. 2002. SUMO-1 modification of the C-terminal KVEKVD of axin is required for JNK activation but has no effect on Wnt signaling. *Journal of Biological Chemistry* 277(45), pp. 42981–42986. doi: 10.1074/jbc.M208099200.

Rui, Y. et al. 2004. Axin stimulates p53 functions by activation of HIPK2 kinase through multimeric complex formation. *EMBO Journal* 23(23), pp. 4583–4594. doi: 10.1038/sj.emboj.7600475.

Russell, J.O. and Monga, S.P. 2018. Wnt/β-Catenin Signaling in Liver Development, Homeostasis, and Pathobiology. *Annual review of pathology* 13(1), pp. 351–378. Available at: http://www.ncbi.nlm.nih.gov/pubmed/29125798.

Sadasivam, N., Kim, Y.-J., Radhakrishnan, K. and Kim, D.-K. 2022. Oxidative Stress, Genomic Integrity, and Liver Diseases. Molecules 27(10), p. 3159. doi: 10.3390/molecules27103159.

Salamov, A.A., Nishikawa, T. and Swindells, M.B. 1998. Assessing protein coding region integrity in cDNA sequencing projects. *Bioinformatics* 14(5), pp. 384–390. doi: 10.1093/bioinformatics/14.5.384.

Sanson, R. et al. 2023. Axin1 Protects Colon Carcinogenesis by an Immune-Mediated Effect. *CMGH* 15(3), pp. 689–715. doi: 10.1016/j.jcmgh.2022.10.017.

Sarin, K.Y. et al. 2005. Conditional telomerase induction causes proliferation of hair follicle stem cells. *Nature* 436(7053), pp. 1048–52. Available at: http://www.ncbi.nlm.nih.gov/pubmed/16107853.

Sato, K., Tanaka, M., Kusaba, T., Fukuda, H. and Tanikawa, K. 1998. Immunohistochemical demonstration of alpha-fetoprotein in small hepatocellular carcinoma. *Oncology Reports* 5, pp. 355–358. Available at: http://www.spandidos-publications.com/10.3892/or.5.2.355.

Sauer, B. and Henderson, N. 1988. Site-specific DNA recombination in mammalian cells by the Cre recombinase of bacteriophage P1. *Proceedings of the National Academy of Sciences* 85(14), pp. 5166–5170. Available at: https://pnas.org/doi/full/10.1073/pnas.85.14.5166.

Saydé, T., Hamoui, O. El, Alies, B., Gaudin, K., Lespes, G. and Battu, S. 2021. Biomaterials for three-dimensional cell culture: From applications in oncology to nanotechnology. *Nanomaterials* 11(2), pp. 1–29. doi: 10.3390/nano11020481.

Schaefer, K.N., Bonello, T.T., Zhang, S., Williams, C.E., Roberts, D.M., McKay, D.J. and Peifer, M. 2018. Supramolecular assembly of the beta-catenin destruction complex and the effect of Wnt signaling on its localization, molecular size, and activity in vivo. *PLoS genetics* 14(4), p. e1007339. Available at: http://www.ncbi.nlm.nih.gov/pubmed/29641560.

Schaefer, K.N. and Peifer, M. 2019. Wnt/Beta-Catenin Signaling Regulation and a Role for Biomolecular Condensates. *Developmental cell* 48(4), pp. 429–444. Available at: http://www.ncbi.nlm.nih.gov/pubmed/30782412.

Sekine, S., Lan, B.Y.-A., Bedolli, M., Feng, S. and Hebrok, M. 2006. Liver-specific loss of beta-catenin blocks glutamine synthesis pathway activity and cytochrome p450 expression in mice. *Hepatology* (Baltimore, Md.) 43(4), pp. 817–25. doi: 10.1002/hep.21131.

Selbert, S., Bentley, D.J., Melton, D.W., Rannie, D., Lourenço, P., Watson, C.J. and Clarke, A.R. 1998. Efficient BLG-Cre mediated gene deletion in the mammary gland. *Transgenic research* 7(5), pp. 387–96. doi: 10.1023/a:1008848304391.

Shi, J., Li, Y., Jia, R. and Fan, X. 2020. The fidelity of cancer cells in PDX models: Characteristics, mechanism and clinical significance. *International journal of cancer* 146(8), pp. 2078–2088. Available at: http://www.ncbi.nlm.nih.gov/pubmed/31479514.

Shibata, H. et al. 1997. Rapid colorectal adenoma formation initiated by conditional targeting of the APC gene. *Science* 278(5335), pp. 120–133. doi: 10.1126/science.278.5335.120.

So, J., Kim, A., Lee, S.H. and Shin, D. 2020. Liver progenitor cell-driven liver regeneration. *Experimental and Molecular Medicine* 52(8), pp. 1230–1238. doi: 10.1038/s12276-020-0483-0.

Sodhi, D., Micsenyi, A., Bowen, W.C., Monga, D.K., Talavera, J.-C.L. and Monga, S.P.S. 2005. Morpholino oligonucleotide-triggered beta-catenin knockdown compromises normal liver regeneration. *Journal of hepatology* 43(1), pp. 132–41. Available at: http://www.ncbi.nlm.nih.gov/pubmed/15893845.

Soriano, P. 1999. Generalized lacZ expression with the ROSA26 Cre reporter strain. *Nature Genetics* 21(1), pp. 70–71. doi: 10.1038/5007.

Spit, M. et al. 2020. RNF 43 truncations trap CK 1 to drive niche-independent self-renewal in cancer . The EMBO Journal 39(18). doi: 10.15252/embj.2019103932.
Stamos, J.L. and Weis, W.I. 2013. The β-catenin destruction complex. *Cold Spring Harbor perspectives in biology* 5(1), p. a007898. Available at: http://www.ncbi.nlm.nih.gov/pubmed/23169527.

Stauffer, J.K. et al. 2011. Coactivation of AKT and β-catenin in mice rapidly induces formation of lipogenic liver tumors. *Cancer research* 71(7), pp. 2718–27. Available at: http://www.ncbi.nlm.nih.gov/pubmed/21324921.

ter Steege, E.J. and Bakker, E.R.M. 2021. The role of R-spondin proteins in cancer biology. *Oncogene* 40(47), pp. 6469–6478. doi: 10.1038/s41388-021-02059-y.

Steinhart, Z. and Angers, S. 2018. Wnt signaling in development and tissue homeostasis. *Development* (Cambridge, England) 145(11). doi: 10.1242/dev.146589.

Su, C. 2016. Survivin in survival of hepatocellular carcinoma. *Cancer letters* 379(2), pp. 184–90. Available at: http://www.ncbi.nlm.nih.gov/pubmed/26118774.

Sun, T. et al. 2020. AXIN2+ Pericentral Hepatocytes Have Limited Contributions to Liver Homeostasis and Regeneration. *Cell Stem Cell* 26(1), pp. 97-107.e6. Available at: https://doi.org/10.1016/j.stem.2019.10.011.

Sun, Y., Wang, W. and Zhao, C. 2021. Frizzled receptors in tumors, focusing on signaling, roles, modulation mechanisms, and targeted therapies. *Oncology Research* 28(6), pp. 661–674. doi: 10.3727/096504020X16014648664459.

Sung, H., Ferlay, J., Siegel, R.L., Laversanne, M., Soerjomataram, I., Jemal, A. and Bray, F. 2021. Global Cancer Statistics 2020: GLOBOCAN Estimates of Incidence

and Mortality Worldwide for 36 Cancers in 185 Countries. CA: A Cancer Journal for Clinicians 71(3), pp. 209–249. doi: 10.3322/caac.21660.

Sutherland, C. 2011. What Are the bona fide GSK3 Substrates. *International journal of Alzheimer's disease* 2011, p. 505607. Available at: http://www.ncbi.nlm.nih.gov/pubmed/21629754.

Takagi, H. et al. 2008. Frequent epigenetic inactivation of SFRP genes in hepatocellular carcinoma. *Journal of gastroenterology* 43(5), pp. 378–89. Available at: http://www.ncbi.nlm.nih.gov/pubmed/18592156.

Tan, X., Behari, J., Cieply, B., Michalopoulos, G.K. and Monga, S.P.S. 2006. Conditional Deletion of β-Catenin Reveals Its Role in Liver Growth and Regeneration. *Gastroenterology* 131(5), pp. 1561–1572. doi: 10.1053/j.gastro.2006.08.042.

Tannour-Louet, M., Porteu, A., Vaulont, S., Kahn, A. and Vasseur-Cognet, M. 2002. A tamoxifen-inducible chimeric Cre recombinase specifically effective in the fetal and adult mouse liver. *Hepatology* (Baltimore, Md.) 35(5), pp. 1072–81. doi: 10.1053/jhep.2002.33164.

Tao, J. et al. 2014. Activation of β-catenin and Yap1 in human hepatoblastoma and induction of hepatocarcinogenesis in mice. *Gastroenterology* 147(3), pp. 690–701. Available at: http://www.ncbi.nlm.nih.gov/pubmed/24837480.

Tao, J. et al. 2016. Modeling a human hepatocellular carcinoma subset in mice through coexpression of met and point-mutant β-catenin. *Hepatology* (Baltimore, Md.) 64(5), pp. 1587–1605. Available at: http://www.ncbi.nlm.nih.gov/pubmed/27097116.

Tapia, N. and Schöler, H.R. 2016. Molecular Obstacles to Clinical Translation of iPSCs. *Cell stem cell* 19(3), pp. 298–309. Available at: http://www.ncbi.nlm.nih.gov/pubmed/27452174.

Tarlow, B.D., Pelz, C., Naugler, W.E., Wakefield, L., Wilson, E.M., Finegold, M.J. and Grompe, M. 2014. Bipotential adult liver progenitors are derived from chronically injured mature hepatocytes. *Cell Stem Cell* 15(5), pp. 605–618. doi: 10.1016/j.stem.2014.09.008.

Taub, R. 2004. Liver regeneration: From myth to mechanism. *Nature Reviews Molecular Cell Biology* 5(10), pp. 836–847. doi: 10.1038/nrm1489.

Tejeda-Muñoz, N., Albrecht, L. V., Bui, M.H. and De Robertis, E.M. 2019. Wnt canonical pathway activates macropinocytosis and lysosomal degradation of extracellular proteins. *Proceedings of the National Academy of Sciences of the United States of America* 116(21), pp. 10402–10411. doi: 10.1073/pnas.1903506116.

Trefts, E., Gannon, M. and Wasserman, D.H. 2017. The liver. *Current biology : CB* 27(21), pp. R1147–R1151. Available at: http://www.ncbi.nlm.nih.gov/pubmed/29112863.

Trevisani, F. et al. 2001. Serum alpha-fetoprotein for diagnosis of hepatocellular carcinoma in patients with chronic liver disease: influence of HBsAg and anti-HCV status. *Journal of hepatology* 34(4), pp. 570–5. Available at: http://www.ncbi.nlm.nih.gov/pubmed/11394657.

Trinh, V.Q.-H. et al. 2023. Hepatic stellate cells maintain liver homeostasis through paracrine neurotrophin-3 signaling that induces hepatocyte proliferation. *Science Signaling* 16(787). Available at: https://www.science.org/doi/10.1126/scisignal.adf6696.

Valenta, T. et al. 2011. Probing transcription-specific outputs of β-catenin in vivo. *Genes & development* 25(24), pp. 2631–43. Available at: http://www.ncbi.nlm.nih.gov/pubmed/22190459.

Villanueva, A. 2019. Hepatocellular Carcinoma. Longo, D. L. ed. *New England Journal of Medicine* 380(15), pp. 1450–1462. Available at: https://linkinghub.elsevier.com/retrieve/pii/S0140673612612835.

Vinken, M. 2021. Primary hepatocyte cultures for liver disease modeling. *Current Opinion in Toxicology* 25, pp. 1–5. Available at: https://linkinghub.elsevier.com/retrieve/pii/S2468202020300516.

Wagner, K.U. et al. 1997a. Cre-mediated gene deletion in the mammary gland. *Nucleic acids research* 25(21), pp. 4323–30. doi: 10.1093/nar/25.21.4323.

Wallace, M.C., Hamesch, K., Lunova, M., Kim, Y., Weiskirchen, R., Strnad, P. and Friedman, S.L. 2015. Standard operating procedures in experimental liver research: thioacetamide model in mice and rats. *Laboratory animals* 49(1 Suppl), pp. 21–9. Available at: http://www.ncbi.nlm.nih.gov/pubmed/25835735.

Wang, B., Zhao, L., Fish, M., Logan, C.Y. and Nusse, R. 2015. Self-renewing diploid Axin2(+) cells fuel homeostatic renewal of the liver. *Nature* 524(7564), pp. 180–5. Available at: http://www.ncbi.nlm.nih.gov/pubmed/26245375.

Wang, W. et al. 2021. Evaluation of AXIN1 and AXIN2 as targets of tankyrase inhibition in hepatocellular carcinoma cell lines. *Scientific Reports* 11(1). Available at: https://doi.org/10.1038/s41598-021-87091-4.

Wen, Y., Lambrecht, J., Ju, C. and Tacke, F. 2021. Hepatic macrophages in liver homeostasis and diseases-diversity, plasticity and therapeutic opportunities. Cellular & Molecular Immunology 18(1), pp. 45–56. doi: 10.1038/s41423-020-00558-8.

Wenzel, J. et al. 2020. Loss of the nuclear Wnt pathway effector TCF7L2 promotes migration and invasion of human colorectal cancer cells. *Oncogene* 39(19), pp. 3893–3909. doi: 10.1038/s41388-020-1259-7.

West, J., Card, T.R., Aithal, G.P. and Fleming, K.M. 2017. Risk of hepatocellular carcinoma among individuals with different aetiologies of cirrhosis: a population-based cohort study. *Alimentary Pharmacology and Therapeutics* 45(7), pp. 983–990. doi: 10.1111/apt.13961.

Wiese, K.E., Nusse, R. and van Amerongen, R. 2018. Wnt signalling: Conquering complexity. *Development* (Cambridge) 145(12). doi: 10.1242/dev.165902.

Wong, G.L.-H. 2014. Prediction of fibrosis progression in chronic viral hepatitis. *Clinical and molecular hepatology* 20(3), pp. 228–36. Available at: http://www.ncbi.nlm.nih.gov/pubmed/25320725.

Wu, Z.Q., Brabletz, T., Fearon, E., Willis, A.L., Hu, C.Y., Li, X.Y. and Weiss, S.J. 2012. Canonical Wnt suppressor, Axin2, promotes colon carcinoma oncogenic activity. *Proceedings of the National Academy of Sciences of the United States of America* 109(28), pp. 11312–11317. doi: 10.1073/pnas.1203015109.

Xu, J. et al. 2017. The Role of Human Cytochrome P450 2E1 in Liver Inflammation and Fibrosis. *Hepatology Communications* 1, pp. 1043–1057. Available at: https://aasldpubs.onlinelibrary.wiley.com/doi/10.1002/hep4.1115.

Xu, R. et al. 2021. Identification of prognostic markers for hepatocellular carcinoma based on the epithelial-mesenchymal transition-related gene BIRC5. *BMC Cancer* 21(1). doi: 10.1186/s12885-021-08390-7.

Yaeger, R. et al. 2018. Clinical Sequencing Defines the Genomic Landscape of Metastatic Colorectal Cancer. *Cancer Cell* 33(1), pp. 125-136.e3. doi: 10.1016/j.ccell.2017.12.004.

Yamamoto, H., Kishida, S., Uochi, T., Ikeda, S., Koyama, S., Asashima, M. and Kikuchi, A. 1998. Axil, a member of the Axin family, interacts with both glycogen synthase kinase 3beta and beta-catenin and inhibits axis formation of Xenopus embryos. *Molecular and cellular biology* 18(5), pp. 2867–75. Available at: http://www.ncbi.nlm.nih.gov/pubmed/9566905.

Yamanishi, K., Fiedler, M., Terawaki, S., Higuchi, Y., Bienz, M. and Shibata, N. 2019. A direct heterotypic interaction between the DIX domains of Dishevelled and Axin mediates signaling to β-catenin. *Science Signaling* 12(611), p. 5505. Available at: https://www.science.org/doi/10.1126/scisignal.aaw5505.

Yang, J.D., Hainaut, P., Gores, G.J., Amadou, A., Plymoth, A. and Roberts, L.R. 2019. A global view of hepatocellular carcinoma: trends, risk, prevention and management. *Nature Reviews Gastroenterology and Hepatology* 16(10), pp. 589–604. doi: 10.1038/s41575-019-0186-y.

Young, M.A., Daly, C.S., Taylor, E., James, R., Clarke, A.R. and Reed, K.R. 2018. Subtle Deregulation of the Wnt-Signaling Pathway Through Loss of Apc2 Reduces the Fitness of Intestinal Stem Cells. *Stem cells* (Dayton, Ohio) 36(1), pp. 114–122. Available at: http://www.ncbi.nlm.nih.gov/pubmed/29027285.

Yu, H.M.I. et al. 2005. The role of Axin2 in calvarial morphogenesis and craniosynostosis. *Development* 132(8), pp. 1995–2005. doi: 10.1242/dev.01786.

Zafra, M.P. et al. 2018. Optimized base editors enable efficient editing in cells, organoids and mice. *Nature Biotechnology* 36(9), pp. 888–896. doi: 10.1038/nbt.4194.

Zanotti, S. et al. 2022. The Role of Chronic Liver Diseases in the Emergence and Recurrence of Hepatocellular Carcinoma: An Omics Perspective. Frontiers in medicine 9, p. 888850. doi: 10.3389/fmed.2022.888850.

Zeng, L. et al. 1997. The Mouse Fused Locus Encodes Axin, an Inhibitor of the Wnt Signaling Pathway That Regulates Embryonic Axis Formation. Cell 90, pp. 181–192. Zhan, T., Rindtorff, N. and Boutros, M. 2017. Wnt signaling in cancer. *Oncogene* 36(11), pp. 1461–1473. doi: 10.1038/onc.2016.304.

Zhang, J.P. et al. 2017. Efficient precise knockin with a double cut HDR donor after CRISPR/Cas9-mediated double-stranded DNA cleavage. *Genome Biology* 18(1). doi: 10.1186/s13059-017-1164-8.

Zhang, M. et al. 2018. Cumulative evidence for relationships between multiple variants in the VTI1A and TCF7L2 genes and cancer incidence. *International Journal of Cancer* 142(3), pp. 498–513. doi: 10.1002/ijc.31074.

Zhang, S. and Zhou, D. 2019. Role of the transcriptional coactivators YAP/TAZ in liver cancer. *Current Opinion in Cell Biology* 61, pp. 64–71. doi: 10.1016/j.ceb.2019.07.006.

Zhang, T., Otevrel, T., Gao, Z., Gao, Z., Ehrlich, S.M., Fields, J.Z. and Boman, B.M. 2001. Evidence that APC regulates survivin expression: a possible mechanism contributing to the stem cell origin of colon cancer. *Cancer research* 61(24), pp. 8664–7. Available at: http://www.ncbi.nlm.nih.gov/pubmed/11751382.

Zhang, X.H., Tee, L.Y., Wang, X.G., Huang, Q.S. and Yang, S.H. 2015. Off-target effects in CRISPR/Cas9-mediated genome engineering. *Molecular Therapy - Nucleic Acids* 4(11), p. e264. doi: 10.1038/mtna.2015.37.

Zhang, Y. et al. 2021. Loss of Apc Cooperates with Activated Oncogenes to Induce Liver Tumor Formation in Mice. *The American journal of pathology* 191(5), pp. 930–946. Available at: http://www.ncbi.nlm.nih.gov/pubmed/33545120.

Zhang, Y., Riesterer, C., Ayrall, A.-M., Sablitzky, F., Littlewood, T.D. and Reth, M. 1996. Inducible Site-Directed Recombination in Mouse Embryonic Stem Cells. *Nucleic Acids Research* 24(4), pp. 543–548. doi: 10.1093/nar/24.4.543.

Zhang, Y.L. et al. 2013. AMP as a low-energy charge signal autonomously initiates assembly of axin-ampk-lkb1 complex for AMPK activation. *Cell Metabolism* 18(4), pp. 546–555. doi: 10.1016/j.cmet.2013.09.005.

Zhao, H., Wu, L., Yan, G., Chen, Y., Zhou, M., Wu, Y. and Li, Y. 2021. Inflammation and tumor progression: signaling pathways and targeted intervention. Signal Transduction and Targeted Therapy 6(1), p. 263. doi: 10.1038/s41392-021-00658-5.

Zhong, Z. and Virshup, D.M. 2020. Wnt signaling and drug resistance in cancer. *Molecular Pharmacology* 97(2), pp. 72–89. doi: 10.1124/MOL.119.117978.

Zucman-Rossi, J. et al. 2007. Differential effects of inactivated Axin1 and activated β-catenin mutations in human hepatocellular carcinomas. *Oncogene* 26(5), pp. 774–780. doi: 10.1038/sj.onc.1209824.

Appendices

Appendix I Table of mice in aged cohorts

Genotype	Sex	Days PI	Reason for being culled	Liver Tumour	Dissection Notes
Control	Male	235	Found dead - No signs of ill health before death	No	No obvious abnormalities noted
Control	Male	1 Year	1 Year PI cohort	No	No abnormalities noted
Control	Male	1 Year	1 Year PI cohort	No	No abnormalities noted
Control	Female	1 Year	1 Year PI cohort	No	No abnormalities noted
Control	Female	1 Year	1 Year PI cohort	No	No abnormalities noted
Control	Male	1 Year	1 Year PI cohort	No	No abnormalities noted
Control	Female	640	End-point	No	No abnormalities noted
Control	Female	640	End-point	No	No abnormalities noted
Control	Male	640	End-point	No	No abnormalities noted
$Axin1^{\Delta/\Delta}$	Male	1 Year	1 Year PI cohort	No	No abnormalities noted
$Axin1^{\Delta/\Delta}$	Male	1 Year	1 Year PI cohort	No	No abnormalities noted
$Axin1^{\Delta/\Delta}$	Female	1 Year	1 Year PI cohort	No	No abnormalities noted
$Axin1^{\Delta/\Delta}$	Male	1 Year	1 Year PI cohort	No	No abnormalities noted
$Axin1^{\Delta/\Delta}$	Male	1 Year	1 Year PI cohort	No	No abnormalities noted
$Axin1^{\Delta/\Delta}$	Female	640	End-point	No	No abnormalities noted
$Axin1^{\Delta/\Delta}$	Female	640	End-point	No	No abnormalities noted
$Axin1^{\Delta/\Delta}$	Male	640	End-point	No	No abnormalities noted
$Axin2^{\Delta/\Delta}$	Female	36	Found dead - No signs of ill health before death	No	No obvious abnormalities noted
$Axin2^{\Delta/\Delta}$	Female	99	Bloated abdomen, walking on tiptoes	No	Enlarged spleen and kidneys
$Axin2^{\Delta/\Delta}$	Female	270	Mouse very thin	No	Intestines empty, possibly not eating
$Axin2^{\Delta/\Delta}$	Male	1 Year	1 Year PI cohort	No	No abnormalities noted
$Axin2^{\Delta/\Delta}$	Male	1 Year	1 Year PI cohort	No	No abnormalities noted
$Axin2^{\Delta/\Delta}$	Female	1 Year	1 Year PI cohort	No	No abnormalities noted
$Axin2^{\Delta/\Delta}$	Male	1 Year	1 Year PI cohort	No	No abnormalities noted
$Axin2^{\Delta/\Delta}$	Male	1 Year	1 Year PI cohort	No	No abnormalities noted
$Axin2^{\Delta/\Delta}$	Male	455	Sore eye and lump behind eye	No	Enlarged seminal vesicles
$Axin2^{\Delta/\Delta}$	Male	470	Cyst on abdomen	No	Enlarged testicle and seminal vesicles
$Axin2^{\Delta/\Delta}$	Female	554	Seizures	No	No other abnormalities noted
$Axin2^{\Delta/\Delta}$	Male	594	Found dead - No signs of ill health before death	No	Mass seen in chest cavity
$Axin2^{\Delta/\Delta}$	Female	610	Lump on neck increasing in size	No	No other abnormalities noted
$Axin2^{\Delta/\Delta}$	Male	640	End-point	No	No abnormalities noted
$Axin2^{\Delta/\Delta}$	Female	640	End-point	No	No abnormalities noted
$Axin2^{\Delta/\Delta}$	Female	640	End-point	No	No abnormalities noted
$Axin2^{\Delta/\Delta}$	Male	640	End-point	No	No abnormalities noted
$Axin2^{\Delta/\Delta}$	Male	640	End-point	No	No abnormalities noted
$Axin2^{\Delta/\Delta}$	Male	640	End-point	No	No abnormalities noted
$Axin2^{\Delta/\Delta}$	Female	640	End-point	No	No abnormalities noted
$Axin2^{\Delta/\Delta}$	Female	640	End-point	No	No abnormalities noted
$Axin2^{\Delta/\Delta}$	Male	640	End-point	No	No abnormalities noted
$Axin2^{\Delta/\Delta}$	Male	640	End-point	No	Enlarged spleen
$Axin2^{\Delta/\Delta}$	Male	640	End-point	No	No abnormalities noted
$Axin2^{\Delta/\Delta}$	Female	640	End-Point	No	No abnormalities noted
$Axin1^{\Delta/\Delta}$, $Axin2^{\Delta/\Delta}$	Male	12	Hunched and bumblebee posture	No	Thickened intestines
$Axin1^{\Delta/\Delta}$, $Axin2^{\Delta/\Delta}$	Female	87	Large lump on chest	No	No other abnormalities noted
$Axin1^{\Delta/\Delta}$, $Axin2^{\Delta/\Delta}$	Male	241	Distended abdomen	Yes	Large liver tumour mass x2
$Axin1^{\Delta/\Delta}$, $Axin2^{\Delta/\Delta}$	Female	279	Distended abdomen and pinched in posture	Yes	Large liver tumour mass, part of tumour cystic and filled with fluid
$Axin1^{\Delta/\Delta}$, $Axin2^{\Delta/\Delta}$	Male	286	Distended abdomen, rapid breathing	Yes	Large liver tumour mass
$Axin1^{\Delta/\Delta}$, $Axin2^{\Delta/\Delta}$	Female	346	Growing lump by vagina effecting movement	No	Lump possibly mammary tumour Liver appeared normal
$Axin1^{\Delta/\Delta}$, $Axin2^{\Delta/\Delta}$	Female	358	Scabby tail - began to ulcerate	No	Mass on right flank - possible mammary tumour
$Axin1^{\Delta/\Delta}$, $Axin2^{\Delta/\Delta}$	Male	358	Distended abdomen and pinched posture	Yes	Large liver tumour mass
$Axin1^{\Delta/\Delta}$, $Axin2^{\Delta/\Delta}$	Male	1 Year	1 Year PI cohort	Yes	Large liver tumour mass
$Axin1^{\Delta/\Delta}$, $Axin2^{\Delta/\Delta}$	Female	1 Year	1 Year PI cohort	Yes	Large liver tumour mass
$Axin1^{\Delta/\Delta}$, $Axin2^{\Delta/\Delta}$	Female	1 Year	1 Year PI cohort	No	No abnormalities noted
$Axin1^{\Delta/\Delta}$, $Axin2^{\Delta/\Delta}$	Male	1 Year	1 Year PI cohort	No	No abnormalities noted
$Axin1^{\Delta/\Delta}$, $Axin2^{\Delta/\Delta}$	Female	1 Year	1 Year PI cohort	No	No abnormalities noted
$Axin1^{\Delta/\Delta}$, $Axin2^{\Delta/\Delta}$	Male	374	Distended abdomen	Yes	Large liver tumour mass
$Axin1^{\Delta/\Delta}$, $Axin2^{\Delta/\Delta}$	Male	401	Hunched posture and thin	Yes	Large liver tumour mass
$Axin1^{\Delta/\Delta}$, $Axin2^{\Delta/\Delta}$	Female	428	Lump by vagina began to ulcerate	No	Liver appeared pale. Lump by vagina possibly mammary tumour. Ovaries were cystic. Scabby tail
$Axin1^{\Delta/\Delta}$, $Axin2^{\Delta/\Delta}$	Male	438	Distended abdomen and reduced mobility	Yes	Small tumours throughout liver
$Axin1^{\Delta/\Delta}$, $Axin2^{\Delta/\Delta}$	Male	455	Distended abdomen and pinched posture	Yes	Large liver tumour mass
$Axin1^{\Delta/\Delta}$, $Axin2^{\Delta/\Delta}$	Male	542	Distended abdomen	Yes	Distended abdomen and pinched posture difficult to identify normal liver tissue
$Axin1^{\Delta/\Delta}$, $Axin2^{\Delta/\Delta}$	Male	542	Prolaspse	No	Liver appeared normal. Colon polyp

Appendix II Varying GS staining patterns in AhCreER^{T} Axin1$^{\Delta/\Delta}$, Axin2$^{\Delta/\Delta}$ aged mice

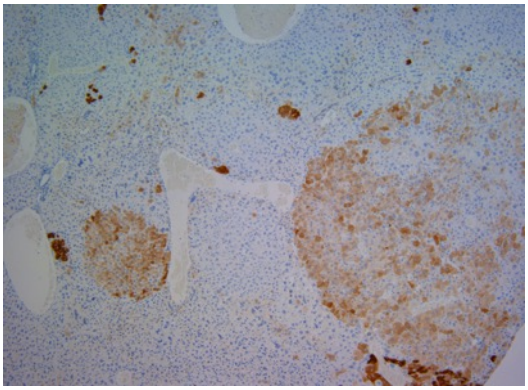
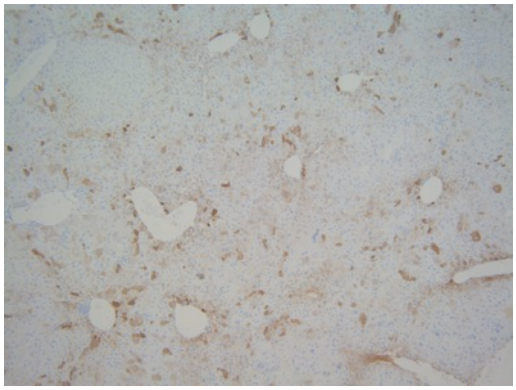
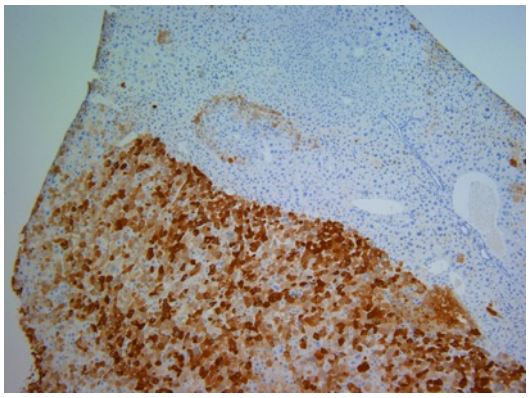
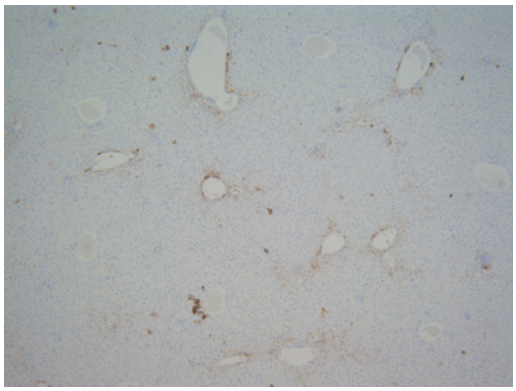

Appendix III Plasmid map of pCAGGS-Cre-IRESpuro

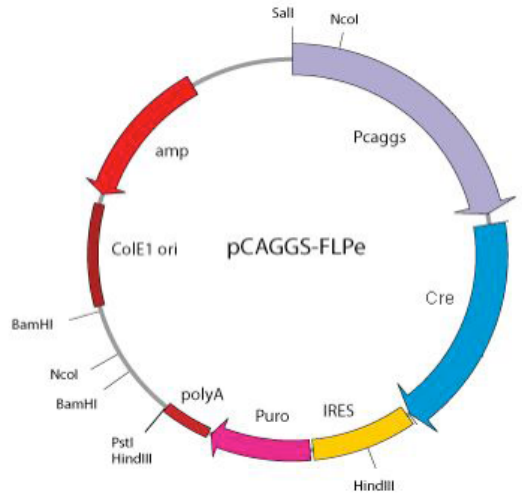

Expression of Cre recombinase under the control of the chicken-beta-actin promoter and an hCMV immediate early enhancer. The recombinase is linked to a puromycin resistance gene by an internal ribosomal entry site (IRES). This vector was used to achieve Cre recombination in culture (Schnütgen et al. 2006).

Appendix IV

Representative images of Lonza hepatocytes plated on collagen with Matrigel overlay and Lonza HCM™ Hepatocyte Culture Medium

At plating

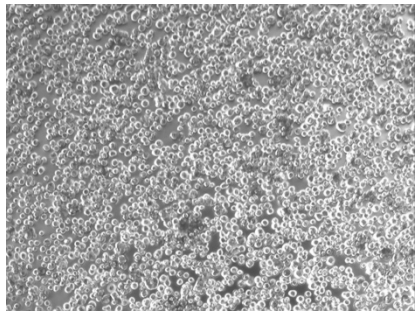

Day 1

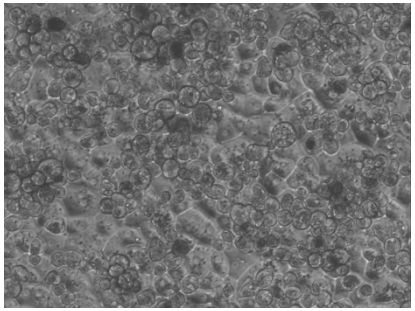

Day 3

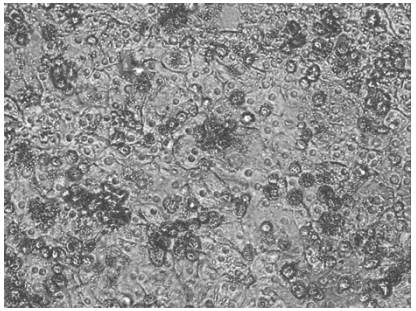

Day 5

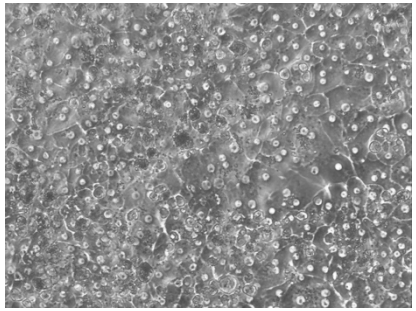

Day 9

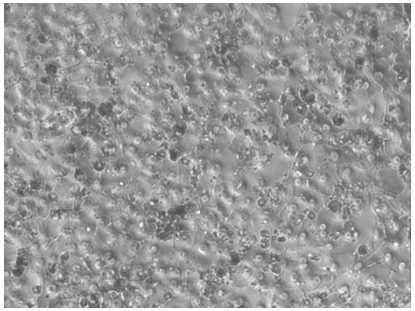

Day 20

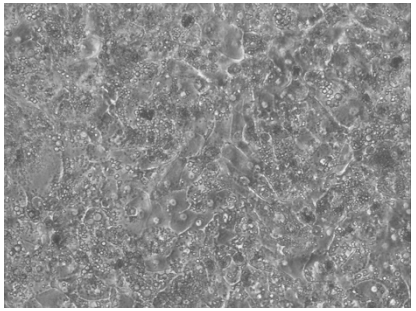

Day 30

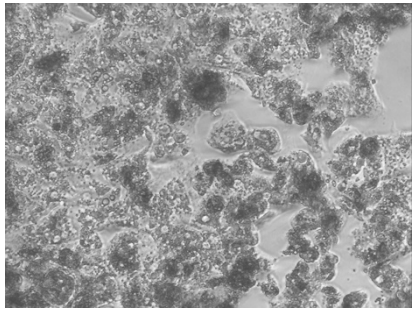

Appendix V PDX lot info used for organoid establishment

Patient & Tumor Profile	
Tumor type	Hepatocellular carcinoma
Tumor subtype	N/A
Tumor status	Primary
ER/PR/HER2 status	N/A
TNBC subtype	N/A
Harvest site	Liver
Histology	Carcinoma
Tumor grade	Poorly differentiated
Diagnosis	First diagnosis
Treatment history	Naive
Disease stage	Not available
Smoking history	Former smoker
Age	60
Gender	Male
Ethnicity	Asian
HPV16/HPV18 status	N/A
HBV/HCV status	HBV+

Mutations from NGS			
AKAP9	p.S1065G	SNV	NON_SYNONYMOUS_CODING
ARID1A	p.P1618S	SNV	NON_SYNONYMOUS_CODING
ATM	p.G2922S	SNV	NON_SYNONYMOUS_CODING
CD74		SNV	UTR_3_PRIME
CIC	p.S1104T	SNV	NON_SYNONYMOUS_CODING
CREBBP	p.Y1125del	Deletion	CODON_CHANGE_PLUS_CODON_DELETION
CTNNB1	p.S33F	SNV	NON_SYNONYMOUS_CODING
ECT2L		Deletion	SPLICE_SITE_DONOR
GATA2	p.S340S	SNV	SPLICE_SITE_REGION
KIT	p.T84M	SNV	NON_SYNONYMOUS_CODING
KMT2D	p.Q4557Q	SNV	SPLICE_SITE_REGION
LCP1	p.G451A	SNV	NON_SYNONYMOUS_CODING
NOTCH2		SNV	SPLICE_SITE_REGION
PBX1		Deletion	UTR_3_PRIME
PDE4DIP	p.A272T	SNV	NON_SYNONYMOUS_CODING
POT1	p.H393R	SNV	NON_SYNONYMOUS_CODING
PRDM1	p.E80V	SNV	NON_SYNONYMOUS_CODING
RET	p.T278N	SNV	NON_SYNONYMOUS_CODING
SBDS		SNV	SPLICE_SITE_DONOR
SETD2	p.N719D	SNV	NON_SYNONYMOUS_CODING
TP53	p.R273H	SNV	NON_SYNONYMOUS_CODING
TRAF7	p.R29G	SNV	NON_SYNONYMOUS_CODING
TRAF7		SNV	UTR_3_PRIME
TSC2	p.Y1250*	SNV	STOP_GAINED
USP6	p.F327L	SNV	NON_SYNONYMOUS_CODING

PD-L1 (P3)

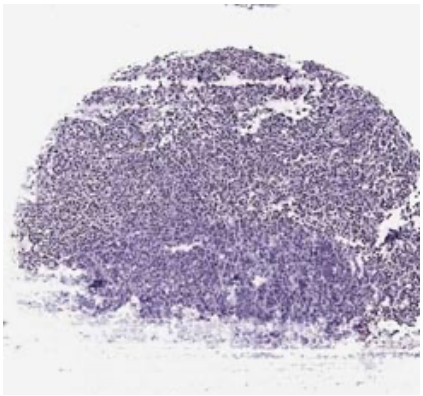

Appendix VI Nucleus and γH2AX foci masking generated by CellProfiler for counts.